JAN 31 1949

THE PHYSICAL REVIEW

VOLUME 75 Second Series NUMBER 2

JANUARY 15, 1949

Published for the

AMERICAN PHYSICAL SOCIETY

by the

AMERICAN INSTITUTE OF PHYSICS

Lancaster, Pa., and New York, N. Y.

[illegible] REVIEW

A journal of exp[illegible] *[illegible] physics established by E. L. Nichols in 1893*

Published by the American Institute of Phy[illegible]
for the

AMERICAN PHYSICAL SOCIE[illegible]

Officers

President

J. R. OPPENHEIMER
Institute for Advanced Study
Princeton, New Jersey

Vice-President

F. W. LOOMIS
University of Illinois
Urbana, Illinois

Secretary

K. K. DARROW
Bell Telephone Laboratories
Office:
Columbia University
New York 27, New York

Treasurer

G. B. PEGRAM
Columbia University
New York 27, New York

Local Secretary
for the Pacific Coast

J. KAPLAN
University of California at [illegible]
Angeles
Los Angeles, California

Managing Editor

JOHN T. TATE
University of Minnesota
Minneapolis, Minnesota

The Physical Review is pu[illegible] Prince and Lemon Streets, Lancaster, Pennsylvania.
Entered as second-class matter Mon[illegible] Post Office at Lancaster, Pennsylvania, under the Act of March 3, [illegible]
Acceptance for mailing at special rate of [illegible] provided for in paragraph (d), section 538, P. L. & R., authorized January [illegible]

BOARD OF EDITORS

[illegible]

Associate Editors

H. A. BETHE — S. A. [illegible]
L. A. RIDENOUR — R. M. [illegible]
W. H. ZACHARIASEN — F. [illegible]

[illegible] for publication should be submitted to John T. Tate, University of Minnesota, Minneapolis, Minnesota.

[illegible] all correspondence concerning papers in the process of [illegible] addressed to the Publication Manager, American Institute of [illegible] East 53rd Street, New York 22, New York.

Subscription Price

[illegible] States and Canada.....$[illegible]
[illegible]pers.....$[illegible]

Back Numbers

[illegible] Series 2: Vol. 1, 1913–Vol. 74, 1948—$[illegible]
[illegible] $[illegible]
[illegible] each, prior to July, 1929;
[illegible] each, July, 1929–December, 1941;
[illegible] each, January, 1942–December, 1946.
[illegible]: $1.00 each.

[illegible] and orders for back numbers should be addressed [illegible] Street, Lancaster, Pennsylvania, or to the American [illegible] East 53rd Street, New York 22, New York.

[illegible] subscriptions in the case of members of the American [illegible] by the Treasurer; in the case of other subscriptions, [illegible] Manager, American Institute of Physics.

[illegible] Member Department, Cornell University, Ithaca, New [illegible]

THE
PHYSICAL REVIEW

A journal of experimental and theoretical physics established by E. L. Nichols in 1893

SECOND SERIES, VOL. 75, NO. 2 JANUARY 15, 1949

The Effect of Crystal Orientation on the Scattering of Slow Neutrons*

G. P. ARNOLD, V. W. MYERS, AND A. H. WEBER**
Argonne National Laboratory, Chicago, Illinois
(Received September 15, 1948)

A simple theory is developed for taking into account non-random orientations in microcrystalline material of the hexagonal system. The transmission of slow neutrons through extruded and through powdered graphite is measured experimentally and compared with the theory.

INTRODUCTION

THE transmission of slow neutrons through microcrystalline materials has been the subject of several investigations.[1-4] However, a theoretical treatment of the effect of non-random orientations of the microcrystals on neutron scattering has not been considered in detail. A simplified scheme is developed for taking account of the orientation effect when a single symmetry axis only needs to be considered. A comparison is made with the measurements of the transmission of slow neutrons through randomly oriented and through extruded graphite. It is possible to obtain an estimate of the amount of crystal orientation in this instance.

THEORETICAL

If ψ is the angle between the direction of extrusion and the symmetry axis of a given microcrystal, the probability of finding a crystal oriented in the solid angle $d(\cos\psi)d\beta$ is assumed to be

$$P(\cos\psi)d(\cos\psi)d\beta. \quad (1)$$

If $\mathbf{b}$ denotes the product of the order of the Bragg reflection and the reciprocal lattice vector and the symmetry axis of the crystal is taken in the direction of one of the basic reciprocal lattice vectors $\mathbf{b}_3$, then

$$\mathbf{b}=l\mathbf{b}_1+m\mathbf{b}_2+n\mathbf{b}_3, \quad (2)$$

where l, m, n are the products of the order of the

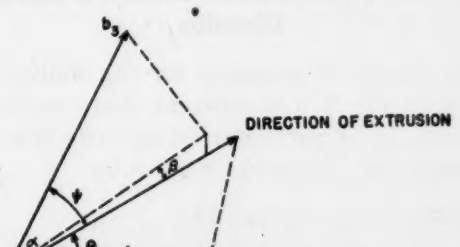

FIG. 1. Angles used in calculating the orientation effect. ϕ is generated perpendicular to a plane through $\mathbf{b}$ and $\mathbf{b}_3$, β is generated perpendicular to a plane through $\mathbf{b}_3$ and the extrusion direction.

* This document is based on work performed under Contract No. W-31-109-eng-38 for the Atomic Energy Project at the Argonne National Laboratory.
** Present addresses: G.P.A., California Institute of Technology; V.W.M., Pennsylvania State College; A.H.W., Saint Louis University.
[1] Halpern, Hammermesh, and Johnson, Phys. Rev. **59**, 981 (1941).
[2] Robert Weinstock, Phys. Rev. **65**, 1 (1944).
[3] Fermi, Sturm, and Sachs, Phys. Rev. **71**, 589 (1947).
[4] G. Arnold and A. H. Weber, Phys. Rev. **73**, 1385 (1948).

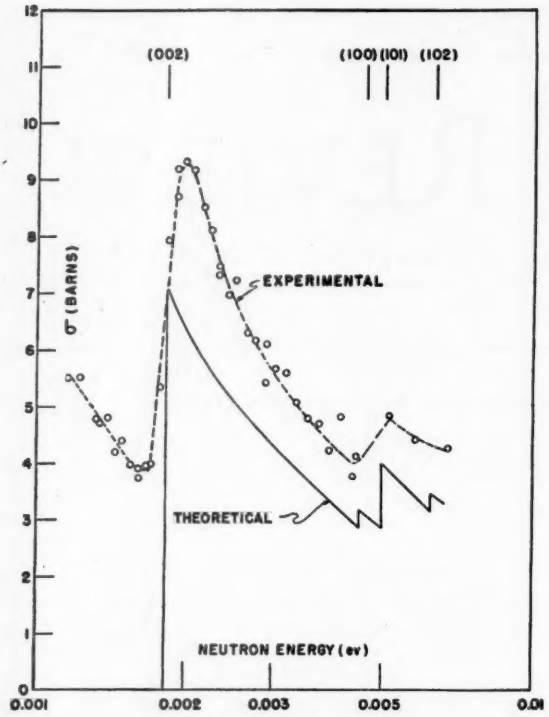

FIG. 2. Total cross section *vs.* neutron energy for randomly oriented (powdered) graphite. The positions of the various Bragg low energy limits are shown by the vertical lines with Miller indices above the curves.

reflection and the Miller indices for the particular Bragg reflection under consideration.

It is sufficient to consider the incident neutron beam either parallel or perpendicular to the extrusion direction since the experimental measurements have been made for these two cases for which it is possible to estimate separately the amount of microcrystalline orientation.

A. Incident Neutron Beam Parallel to Extrusion Direction

The details of geometry for the analysis are shown by Fig. 1. The coherent elastic scattering intensity for a particular Bragg reflection into the solid angle $d(\cos\psi)d\beta$ is given by[3]

$$\sigma_b d(\cos\psi)d\beta=(FN\lambda^2/2\pi b^2\Delta\lambda)\times\exp(-\omega b^2)P(\cos\psi)d(\cos\psi)d\beta, \quad (3)$$

where σ_b is the coherent elastic scattering cross section per unit cell for the Bragg reflection b, N is the number of unit cells per unit volume, $\Delta\lambda$ gives the spread in the wave-length of the incident neutron beam, $\exp(-\omega b^2)$ is the Debye-Waller temperature function,[2] and F, the *form factor* per unit cell of the graphite crystal, is calculated by

$$F=(4\sigma_{\text{free}}/\mu^2\{1+(-1)^n\cos^2 2\pi(l/3+2m/3)+[1+(-1)^n]\cos 2\pi(l/3+2m/3)\}, \quad (4)$$

in which*** σ_{free} is the free atom elastic scattering cross section and μ is the reduced mass of the carbon nucleus in units of the neutron mass.

Transforming to the variables θ, ϕ it follows from elementary analysis that

$$\cos\psi=\cos\theta\cos\alpha+\sin\theta\sin\alpha\cos\phi=(nb_3/b)\cos\theta+[1-(n^2b_3^2/b^2)]^{\frac{1}{2}}\sin\theta\cos\phi, \quad (5)$$

and $d(\cos\psi)d\beta=d(\cos\theta)d\phi$. Whence from the Bragg relation $\cos\theta=b\lambda/2$ and $\Delta\lambda$ small, Eq. (3) becomes

$$\int\sigma_b d(\cos\psi)d\beta=(FN\lambda^2/4\pi b)\exp(-\omega b^2)\times\int_0^{2\pi}P(\theta,\phi)d\phi. \quad (6)$$

In order to proceed further, it is necessary to make some specific assumptions concerning the function $P(\cos\psi)$. Consider a distribution function with two parameters, namely,

$$P(\cos\psi)=(1/4\pi)+x(\cos^2\psi-\tfrac{1}{3})+y(\cos^4\psi-\tfrac{1}{5}). \quad (7)$$

The quantities x and y give a measure of the degree of correlation in orientation among the microcrystals and are subject to the limitation that $P(\cos\psi)$ shall remain positive for all values of ψ. The factors $\frac{1}{3}$ and $\frac{1}{5}$ in Eq. (7) are necessary in order that P shall be normalized to unity. Substituting the above expression for P in Eq. (6) yields

$$\begin{aligned}\int\sigma_b d(\cos\psi)d\beta=&(FN\lambda^2/4\pi b)\exp(-\omega b^2)\\&\times\{[\tfrac{1}{2}-(2\pi x/3)-(2\pi y/5)]\\&+2\pi x[(b^2\lambda^2/4)\cdot(n^2b_3^2/b^2)\\&+\tfrac{1}{2}(1-(b^2\lambda^2/4))(1-(n^2b_3^2/b^2))]\\&+2\pi y[(b^4\lambda^4/16)\cdot(n^4b_3^4/b^4)\\&+2(b^2\lambda^2/4)(1-(b^2\lambda^2/4))(n^2b_3^2/b^2)\\&\times(1-(n^2b_3^2/b^2))+\tfrac{3}{8}(1-(b^2\lambda^2/4))^2\\&\times(1-n^2b_3^2/b^2)^2]\}. \quad (8)\end{aligned}$$

*** The quantity enclosed by the braces of Eq. (4) is the x-ray *crystal structure factor* squared.

Equation (8) now must be summed over all possible Bragg reflections. Transforming from neutron wave-length to energy via the relationship $E_b/E=\lambda^2b^2/4$ yields

$$\sigma_c=\sum_{E_b\leq E}(FNE_b/2\pi b^3E)\exp(-\omega b^2)$$
$$\times\{[1-(4\pi x/3)-(4\pi y/5)]$$
$$+4\pi x[(E_b/E)\cdot(n^2b_3^2/b^2)$$
$$+\tfrac{1}{2}(1-(E_b/E)(1-(n^2b_3^2/b^2))]$$
$$+4\pi y[(E_b^2/E^2)\cdot(n^4b_3^4/b^4)$$
$$+2(E_b/E)(1-(E_b/E))(n^2b_3^2/b^2)$$
$$\times(1-(n^2b_3^2/b^2))+\tfrac{3}{8}(1-(E_b/E))^2$$
$$\times(1-(n^2b_3^2/b^2))^2]\},\quad(9)$$

where σ_c is the total coherent elastic scattering cross section at the neutron energy E and E_b is the neutron energy at a particular Bragg long wave-length limit.

B. Incident Neutron Beam Perpendicular to Extrusion Direction

If the incident neutron beam is perpendicular to the direction of extrusion, the previous analysis must be modified slightly. It is necessary to rotate the direction of the incident beam through 90°. Therefore, Eq. (5) has the form

$$\cos\psi=(nb_3/b)\cos\theta'$$
$$+[1-(n^2b_3^2/b^2)]^{\frac{1}{2}}\sin\theta'\cos\phi,\quad(10)$$

where $\theta'=\theta-90°$. Hence, corresponding to Eq. (9),

$$\sigma_c=\sum_{E_b\leq E}(FNE_b/2\pi b^3E)\exp(-\omega b^2)$$
$$\times\{[1-(4\pi x/3)-(4\pi y/5)]$$
$$+4\pi x[(1-(E_b/E))(n^2b_3^2/b^2)$$
$$+\tfrac{1}{2}(E_b/E)(1-(n^2b_3^2/b^2))]$$
$$+4\pi y[(1-(E_b/E))^2(n^4b_3^4/b^4)$$
$$+2(E_b/E)(1-(E_b/E))(n^2b_3^2/b^2)$$
$$\times(1-(n^2b_3^2/b^2))+\tfrac{3}{8}(E_b^2/E^2)$$
$$\times(1-(n^2b_3^2/b^2))^2]\}.\quad(11)$$

EXPERIMENTAL

A mechanical velocity selector[5] in conjunction with the heavy water pile at the Argonne Laboratory was used to measure the cross sections for randomly oriented (powdered) and extruded graphite. The results are shown in Figs. 2–4. All of the experimental curves exhibit a fairly large amount of scattering for energies below the region of Bragg effects (the (002) plane is the lower limit). This effect probably is due mainly to inelastic scattering of the "cool" neutrons by the crystal lattice. Graphite has an extremely low absorption cross section, 0.005 barn at thermal energy,[6] so that neutron capture should play an unimportant part. Scattering and absorption by adsorbed gases is a probable contributing factor also in the observed low energy scattering.

In the computation of the theoretical curves, a free atom cross section of 4.5 barns was used and the Debye temperature of graphite was estimated to be 1500°K from specific heat data.[7]

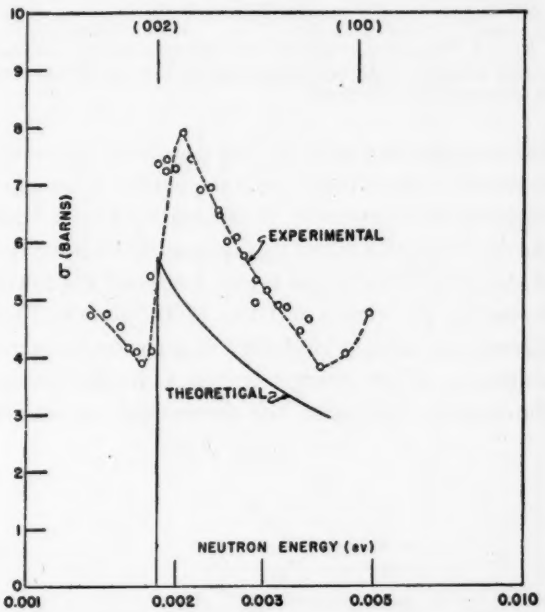

FIG. 3. Total cross section *vs.* neutron energy for extruded graphite with neutron beam incident *parallel* to the extrusion direction.

[5] T. Brill and H. V. Lichtenberger, Phys. Rev. **72**, 585 (1947).
[6] C. Goodman *et al.*, *The Science and Engineering of Nuclear Power* (Addison-Wesley Press, Inc., Cambridge, Massachusetts, 1947), p. 189.
[7] Walther Nernst, Ann. d. Physik **36**, 395 (1911).

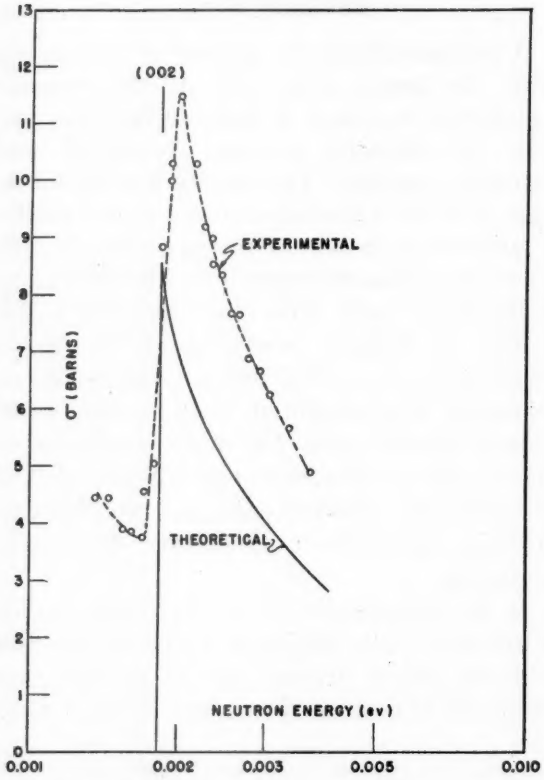

FIG. 4. Total cross section *vs.* neutron energy for extruded graphite with neutron beam incident *perpendicular* to the extrusion direction.

The theoretical curve for the powdered material (random orientation) is, of course, that corresponding to $x=y=0$. It is seen by Fig. 2 that the experimental curve lies appreciably above the theoretical curve in the region between the lower limits for the (002) and the (100) planes. This discrepancy also is probably due to the inelastic scattering of low energy neutrons. In the case of the extruded graphite, the theoretical curves are fairly sensitive to the choice of the parameters x and y. The values $x=-0.07$, $y=0.04$ yielded about the best agreement with the empirical data, and these are used in Figs. 3 and 4. Hence, the orientation function Eq. (7) becomes

$$P(\cos\psi)=1/4\pi-0.07(\cos^2\psi-\tfrac{1}{3})+0.04(\cos^4\psi-\tfrac{1}{5})$$
$$=1/4\pi(1.2-0.9\cos^2\psi+0.5\cos^4\psi). \quad (12)$$

It is seen that $P(1)<P(0)$. This means that the sixfold symmetry axis of graphite tends to be perpendicular to the direction of extrusion so that the hexagonal basal planes show a preferential alignment along or nearly along the extrusion direction. This may be noted also in the experimental curves. The coherent cross section at the Bragg low energy limit for the (002) hexagonal plane is about twice greater for the neutron beam perpendicular (Fig. 4) than for parallel (Fig. 3) to the extrusion direction. Figure 2, for random orientation, has the (002) plane maximum properly between these two limits. These results have been confirmed by W. H. Zachariasen[8] who, by x-ray analyses of the same graphite samples, found the same approximate ratio 2:1, for coherent scattering of x-rays perpendicular and parallel to the extrusion direction.

In conclusion, it is seen that the effect of crystal orientations on the Bragg scattering of slow neutrons may be considerable and that measurement by neutron scattering affords a means of estimating the amount of microcrystalline orientation. The authors wish to thank Dr. R. G. Sachs for suggesting this problem and for his helpful comments.

[8] William H. Zachariasen, Argonne National Laboratory unpublished report.

Radiations from Cd^{115}, $*In^{115}$, and Hf^{181}†

C. E. MANDEVILLE, M. V. SCHERB,†† AND W. B. KEIGHTON†††
Bartol Research Foundation of the Franklin Institute, Swarthmore, Pennsylvania

(Received October 8, 1948)

The characteristic radiations of Cd^{115}, $*In^{115}$, and Hf^{181} have been measured by absorption and coincidence methods. The beta-gamma-coincidence rate of Cd^{115} indicates the presence of an inner beta-ray group at 0.46 Mev. Coincidence measurements show that the 4-hour isomer of indium (115) decays with the emission of a single partially converted gamma-ray. Hf^{181} was found to emit 0.52 Mev beta-rays (aluminum absorption) and 0.17- and 0.47-Mev gamma-rays (lead absorption). Beta-gamma-coincidence data indicate that the beta-ray spectrum of Hf^{181} could be complex. Beta-beta- and gamma-gamma-coincidence data were also obtained.

INTRODUCTION

THE disintegration schemes of Cd^{115}, $*In^{115}$, and Hf^{181} have been investigated by absorption and coincidence methods which have been previously described.[1]

The 2.5-day period of Cd^{115} and its 4-hour daughter activity, $*In^{115}$, were induced in metallic cadmium irradiated by slow neutrons in the Oak Ridge pile. The time of exposure was only one hour, so that little of the 43-day cadmium was present. Chemical separations were carried out for the removal of iron, calcium, and phosphorous as possible impurities. All measurements on the cadmium fraction were completed within four days after removal of the irradiated cadmium from the pile.

The 46-day period was induced in Hf_2O_3 by pile neutrons. Chemical separations should have removed any Cu, Fe, Ag, Ni, Pb, Sn, and Zn. A spectrographic analysis indicated that zirconium was present with an abundance of two-tenths of one percent by weight. Since the chemistry of zirconium is identical with that of hafnium, the elements could not be separated. However, the characteristic radiations and coincidence rates of Zr^{95} have been previously investigated in this laboratory.[2] Those data show that the present measurements on Hf^{181} are uninfluenced by the presence of any zirconium.

Cd^{115}

The energies of the beta-rays and gamma-rays of Cd^{115} and its daughter element, the 4-hour isomer of indium (115), have been previously studied in considerable detail.[3–6] The beta-rays have been reported to have an energy as high as 1.25 Mev.[6] Lawson and Cork[4] have found a maximum beta-ray energy of 1.13 ± 0.03 Mev for the beta-rays of Cd^{115}. Their spectrogram also gave evidence of an inner spectrum having a maximum energy of about 0.6 Mev. Those au-

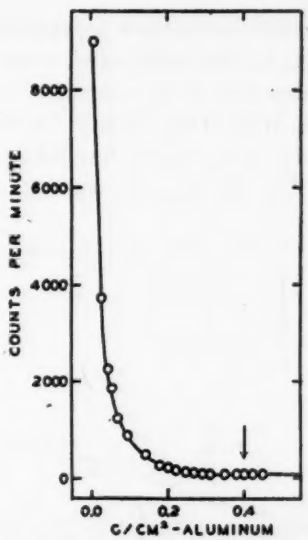

FIG. 1. Absorption in aluminum of the beta-rays of Cd^{115}.

† Assisted by the Joint Program of the Office of Naval Research and the Atomic Energy Commission.
†† Now at Princeton University.
††† Also of the Department of Chemistry, Swarthmore College.

[1] C. E. Mandeville and M. V. Scherb, Phys. Rev. **73**, 143 (1948).
[2] C. E. Mandeville and M. V. Scherb, Phys. Rev. **73**, 1434 (1948).
[3] J. M. Cork and J. L. Lawson, Phys. Rev. **56**, 241 (1939).
[4] J. L. Lawson and J. M. Cork, Phys. Rev. **57**, 982 (1940). References 3 and 4 contain a complete list of all papers published in 1940 and prior to that year relating to Cd^{115} and In^{115}.
[5] C. E. Mandeville and H. W. Fulbright, Phys. Rev. **64**, 265 (1943).
[6] R. P. Metcalf, MDDC—614GG.

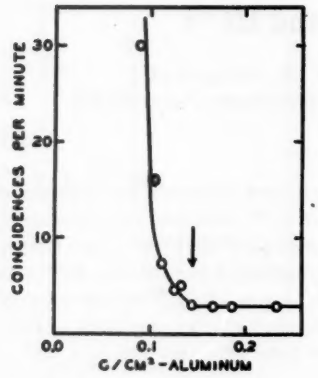

FIG. 2. Coincidence absorption of the Compton electrons of the gamma-rays of Cd^{115}.

thors also reported a gamma-ray energy of 0.54 Mev, measured by lead absorption. Mandeville and Fulbright[5] have reported 0.65 Mev as the energy of this gamma-ray.

The beta-ray and gamma-ray energies of Cd^{115} have been remeasured in the course of the present experiments. An absorption curve in aluminum of the beta-rays of the 2.5-day cadmium is shown in Fig. 1. The end point shown at 0.40 g/cm² in aluminum corresponds to a maximum energy of 1.03 Mev.

A coincidence absorption experiment gave the curve of Fig. 2. The end point of the Compton recoils corresponds to a quantum energy of the order of 0.6 Mev. This estimate is not particularly accurate, since the calibration of the coincidence counting set used in the coincidence absorption measurements has not been extended below 0.75 Mev.[2]

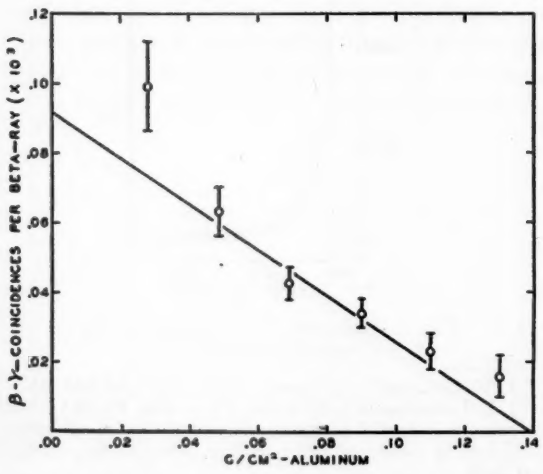

FIG. 3. The beta-gamma-coincidence rate of Cd^{115} as a function of the surface density of aluminum placed before the beta-ray counter.

The curves of Figs. 1 and 2 do indicate that after chemical separation the cadmium was free of impurities.

A source of Cd^{115}, freshly separated from the 4-hour indium daughter activity, was placed between two counters in coincidence (resolving time 0.10 microsecond), and beta-gamma-coincidences were observed as a function of the surface density of the aluminum placed before the beta-ray counter. The data thus obtained are plotted in Fig. 3, where the beta-gamma-coincidence rate is seen to decrease from an extrapolated value of 0.093×10^{-3} coincidence per beta-ray at zero absorber thickness to zero at 0.14 g/cm², corresponding to a beta-ray energy of 0.46 Mev.[7] The level diagram given by Lawson and Cork[4] is thus confirmed.‡

A small gamma-gamma-coincidence rate, 0.08×10^{-3} coincidence per gamma-ray recorded in the gamma-ray counter, was measured, suggesting cascade emission of gamma-rays in the cadmium fraction. No gamma-rays, other than the 0.54-Mev gamma-ray, have been reported. A search was made for beta-beta-coincidences, but none were found in the cadmium fraction.

$^{*}In^{115}$

Absorption and coincidence measurements were carried out on the conversion electrons of

[7] L. E. Glendenin, Nucleonics 2, No. 1, 12 (1948).

‡ In a note added in proof in their 1940 paper, Lawson and Cork remark that the beta-gamma-coincidences shown in Fig. 3 of this paper were not observed by Mitchell and Langer of Indiana University.

Although no data are given in the note concerning the value of the coincidence resolving time of their circuit, the published literature of that period indicates that a resolving time of about 3.2×10^{-6} second was employed by the Indiana group. It seems probable that for almost any reasonable counting rates in either counter, the relatively small beta-gamma-coincidence rate of Cd^{115} would be partially obscured by accidentals. A considerable advantage was held by the writers in that the coincidence resolving time of their circuit was only 0.10×10^{-6} second.

Calibration of the gamma-ray counter gave a beta-gamma-coincidence rate of 2.61×10^{-3} coincidence per beta-ray for Sc^{46}. Were each beta-ray of Cd^{115} followed by the 0.54 Mev gamma-ray, the coincidence rate would have been 0.7×10^{-3} coincidence per beta-ray. Thus, 0.093×10^{-3} coincidence per beta-ray at zero absorber thickness suggests that the soft spectrum has an intensity about one eighth as great as that of the 1.03 Mev beta-rays. This is a lower limit of the intensity, since no correction has been made for the fact that the soft spectrum is more heavily absorbed and scattered in the thin window of the beta-ray counter.

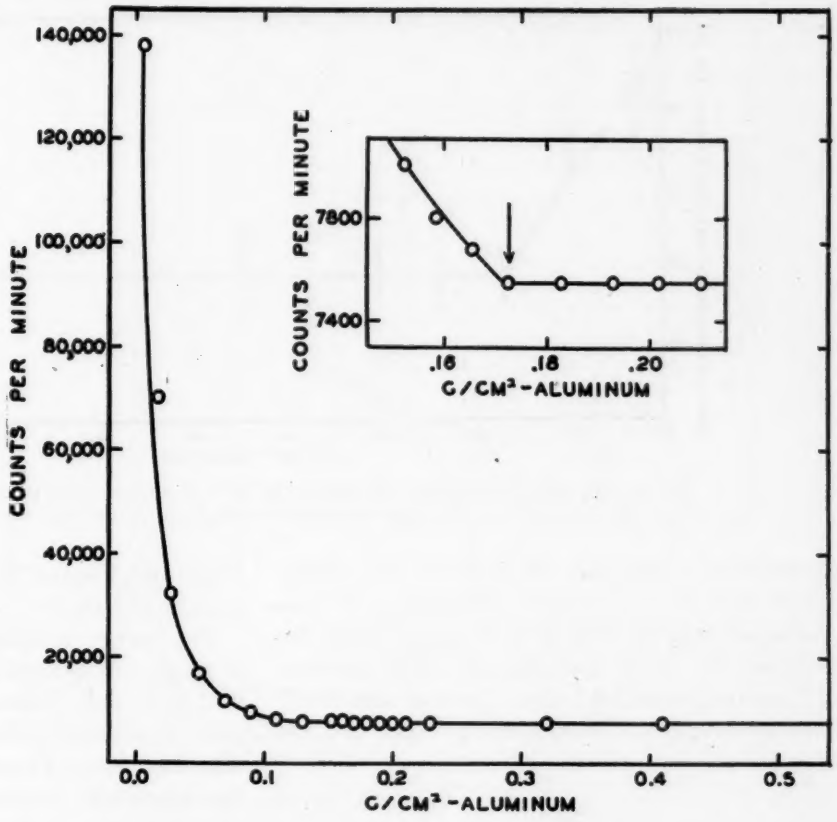

FIG. 4. Absorption in aluminum of the beta-rays of Hf^{181}.

the 4-hour $*In^{115}$, separated from its cadmium parent. Conversion electron-gamma- and gamma-gamma-coincidences were observed, but all coincidence rates could be accounted for by the

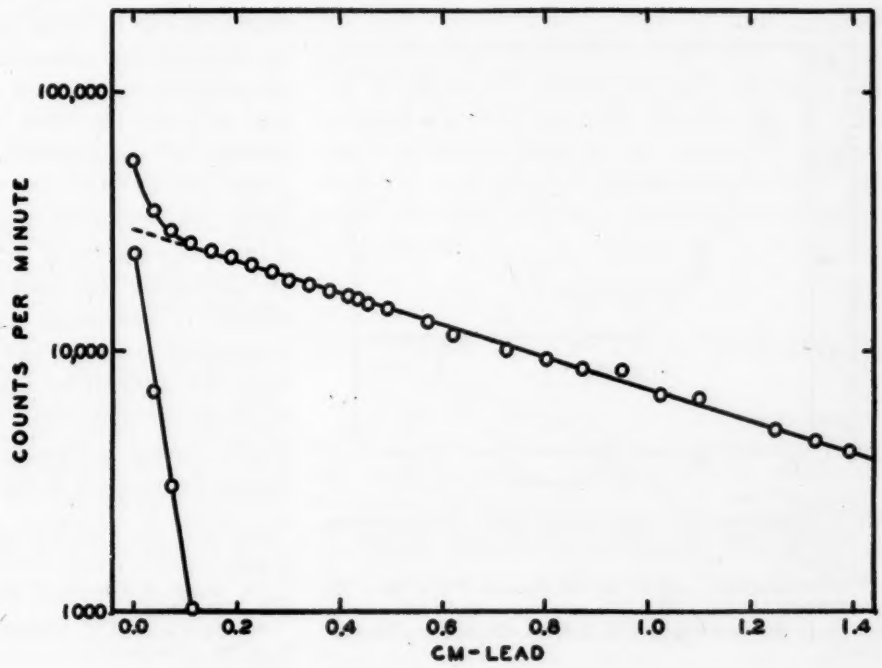

FIG. 5. Absorption in lead of the gamma-rays of Hf^{181}.

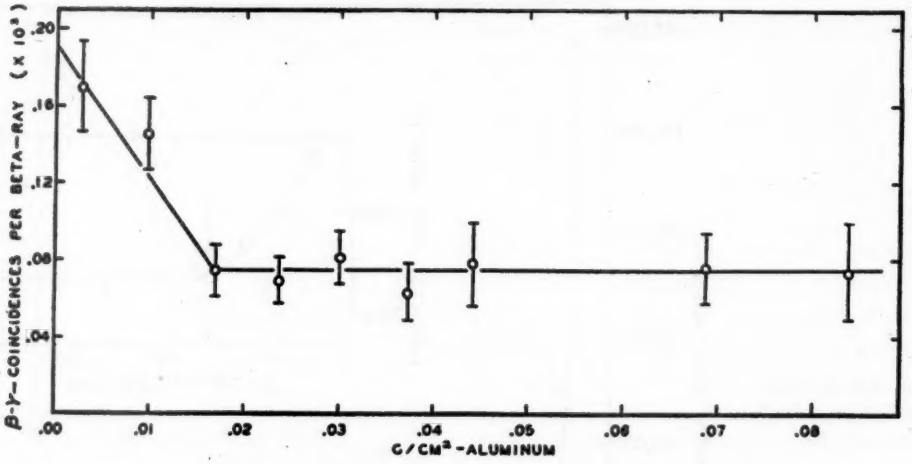

FIG. 6. The beta-gamma-coincidence rate of Hf^{181} as a function of the surface density of aluminum placed before the beta-ray counter.

presence of conversion electron-(x-ray) coincidences and (x-ray)-(x-ray) coincidences. It was concluded that the 4-hour level decays with the emission of a single partially converted gamma-ray and its associated x-rays. Lawson and Cork[4] have given a spectrometric energy value of 0.338 Mev for this gamma-ray.

Hf^{181}

The radiations of the 46-day hafnium (181) have been previously investigated by DeBenedetti and McGowan,[8] Wiedenbeck and Chu,[9] Voigt and Thamer,[10] and by Beněs, Ghosh, Hedgran, and Hole.[11]

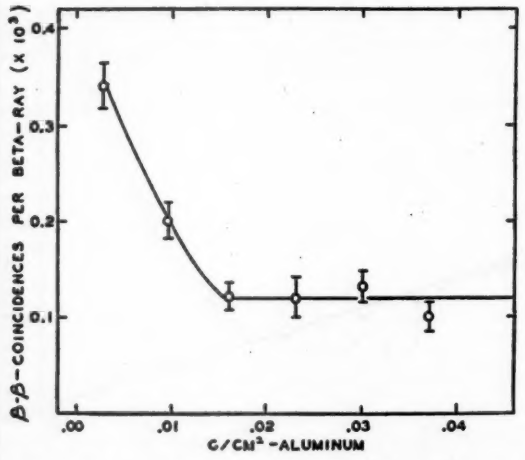

FIG. 7. Beta-beta coincidence rate of Hf^{181}. The aluminum absorbers were placed before both beta-ray counters.

The energy of the beta-rays of Hf^{181}, absorbed in aluminum as shown in Fig. 4, was found to be 0.52 Mev. Absorption in lead of the gamma-rays gave two components having energies of 0.17 and 0.47 Mev. These data are given in Fig. 5. Spectrometric measurements[10–12] have shown gamma-rays present having energies of 0.128, 0.342, and 0.472 Mev. The beta-gamma-coincidence rate as a function of aluminum absorber thickness inserted before the beta-ray counter is shown in Fig. 6. From the curve, it is clear that the beta-gamma-coincidence rate decreases from an extrapolated value of 0.192×10^{-3} coincidence per beta-ray at zero absorber thickness to 0.075×10^{-3} coincidence per beta-ray at 0.017 g/cm² or 0.11 Mev[5] and remains constant thereafter. The curve of Fig. 6 was taken with a coincidence resolving time of 0.10 microsecond. On increasing the resolving time to one microsecond, it was noted that the curve remained unchanged in shape and absolute magnitude. It was very difficult to attain any high statistical accuracy beyond 0.05 g/cm², because the relatively strong gamma-gamma-coincidence rate begins to interfere with the beta-gamma-meas-

[8] S. DeBenedetti and F. K. McGowan, Phys. Rev. **70**, 569 (1946).
[9] M. L. Wiedenbeck and K. Y. Chu, Phys. Rev. **72**, 1164 (1947).
[10] A. F. Voigt and B. J. Thamer, Phys. Rev. **74**, 1264 (1948).
[11] J. Beneš, A. Ghosh, A. Hedgran, and N. Hole, Nature **162**, 262 (1948).
[12] J. M. Cork, R. G. Shreffler, and C. M. Fowler, Phys. Rev. **72**, 1209 (1947).

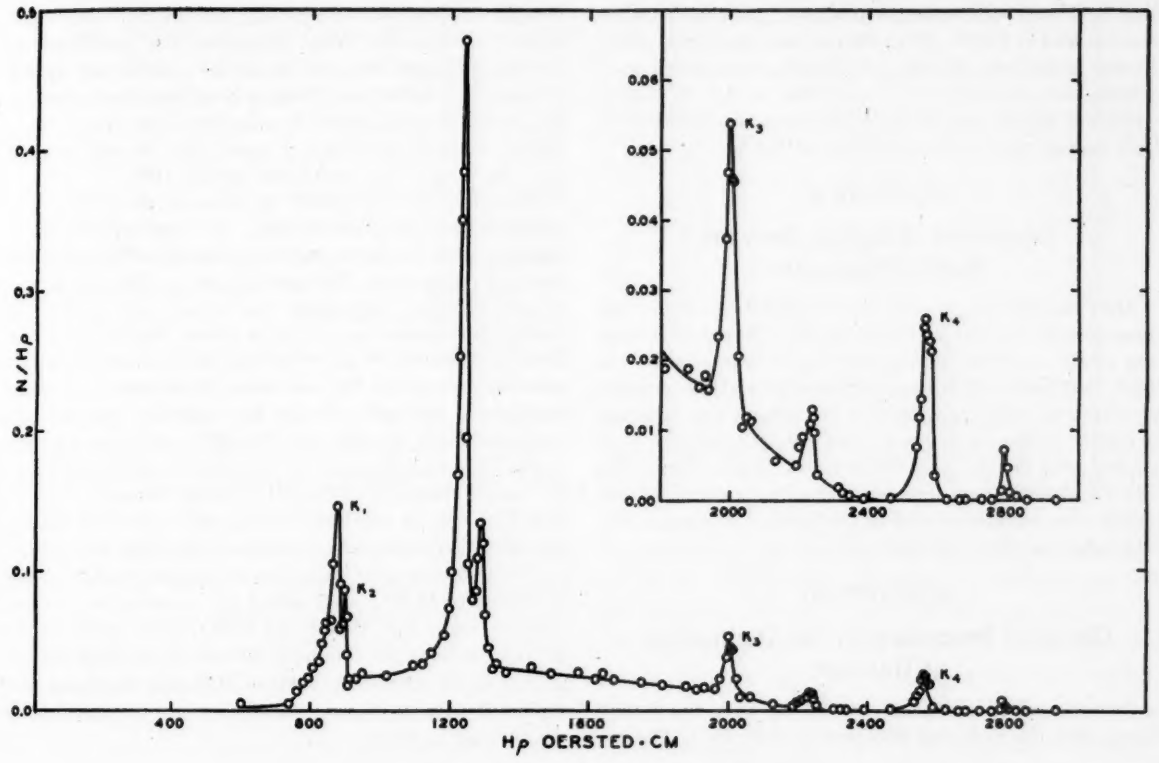

FIG. 8. Beta-ray spectrum of Hf^{181}.

urements. The curve of Fig. 6 shows that the beta-ray spectrum of Hf^{181} may be complex.

The beta-beta-coincidence rate measured in two "bubble" counters (bubble thickness 2.5 mg/cm²) is plotted in Fig. 7. The coincidence rate did not decrease to zero but remained roughly constant beyond 0.016 g/cm². This was interpreted as showing that some of the higher energy gamma-rays are to some extent converted. As in the case of the beta-gamma-coincidence rate of Fig. 6, the beta-beta-coincidence rate of Fig. 7 remained unchanged in shape and absolute magnitude when the resolving time was changed from 0.10 microsecond to 1.0 microsecond.

At this point, it should be remarked that Wiedenbeck and Chu[9] have published a beta-gamma-coincidence curve for Hf^{181} which rises from a relatively low value at zero absorber thickness to a plateau in the vicinity of 0.05 g/cm². Since their data differed so markedly from those of Fig. 6, the writers communicated to them their results and learned that they had independently resumed their investigation of Hf^{181}. They have now obtained a beta-gamma-curve substantially in agreement with the measurements of Fig. 6. Their newly obtained data on Hf^{181} are given in the paper following this one. They have also kindly observed the beta-ray spectrum and associated conversion lines of Hf^{181} in their spectrometer, using a portion of the material purified and used by the writers. The spectrogram is shown in Fig. 8. Since it is identical with that of their sample, the purity of the materials used by both groups of investigators is confirmed.

APPENDIX I

Chemical Procedure for the Purification of Cadmium

One gram of irradiated cadmium metal with about 50 mg of Ag, 50 mg of Pb, and 50 mg of Cu, added as carriers for possible impurities in the cadmium, were dissolved in nitric acid and the solution was diluted with water. The silver was precipitated and filtered out by adding NH_4Cl. The sulfides of lead, copper, and cadmium were precipitated with H_2S from a solution 0.3*N* in H. The filtrate, which would contain any In, Fe, Ca, or P, was rejected.

Cadmium sulfide was dissolved from the precipitate by dilute (1:2) HCl, and the solution was evaporated with

H_2SO_4, diluted with water, and allowed to stand to separate out lead as $PbSO_4$. After filtering out the $PbSO_4$, about 50 mg of indium, dissolved in H_2SO_4, was added as a carrier, and the acidity was adjusted to $1N$ in H_2SO_4. Cadmium sulfide was precipitated from this solution by H_2S, washed with water, and dried at 105°C.

APPENDIX II

Separation of Indium from the Purified Cadmium

After completion of the measurements on CdS, this same precipitate was dissolved in HCl; 30 mg of indium was added, and the acid concentration was adjusted to $0.3N$. Cadmium sulfide was precipitated with H_2S, removed by filtration, and the acidity of the filtrate was adjusted to $0.05N$. Indium sulfide was then precipitated with H_2S, washed with water, and dissolved in HNO_3. From this solution, $In(OH)_3$ was precipitated with an excess of ammonia. The precipitate was washed with a 2 percent NH_4NO_3 solution, dried, and ignited to In_2O_3.

APPENDIX III

Chemical Procedure for the Purification of Hafnium

Three hundred milligrams of Hf_2O_3 were fused with borax, and the melt was dissolved in $2N$−HCl. The hydroxide was precipitated with ammonia in slight excess and washed with water. After dissolving the precipitate in N−H_2SO_4, about 20 mg of copper (as a carrier for Ag, Sn, Pb, and Cu) and about 20 mg of iron (as a carrier for Fe, Ni, and Zn) were added in solution. The solution was diluted to $0.3N$, and H_2S was passed into the cold solution until the copper was completely precipitated.

Tartaric acid was added to prevent precipitation of hafnium and, without filtering, the solution was made alkaline, with ammonia and saturated with H_2S, until the iron was precipitated. This precipitate was filtered out and discarded. After neutralizing the filtrate with H_2SO_4, 10 percent by volume was added in excess, and the H_2S was boiled off. About 20 mg of erbium were added, in H_2SO_4 solution, as a carrier for rare earths. Hafnium was precipitated from the cold solution by cupferron reagent; the precipitate was washed with N−HCl and ignited to the oxide. This was dissolved in hydrafluoric acid, evaporated to a small volume, and diluted with ten volumes of water. The hafnium, in solution, was separated by decantation and filtration from carbon and fluorides of the rare earths.

To the filtrate containing the hafnium was added a few milliliters of H_2SO_4, after which the solution was evaporated to expel HF. Water and H_2SO_4 were added to the solution to bring the volume to 300 ml and the acid concentration to 10 percent by volume. Hafnium was again precipitated with cupferron. After washing, the precipitate was ignited to HfO_2.

PHYSICAL REVIEW VOLUME 75, NUMBER 2 JANUARY 15, 1949

The Radiations from Hf^{181}

K. Y. Chu* and M. L. Wiedenbeck
Department of Physics, University of Michigan, Ann Arbor, Michigan

(Received October 8, 1948)

The beta-spectrum and photoelectron spectrum of Hf^{181} have been studied with a semicircular focusing beta-ray spectrograph of 2 percent resolving power. In addition to the continuous beta-spectrum, four partially converted gamma-rays were found. An estimate of the relative intensities of the two higher energy gamma-rays can be made from the Compton and photoelectron intensities. Data have also been obtained from $\beta-\gamma$- and $\beta-e^-$-coincidence measurements. An energy level diagram is discussed.

INTRODUCTION

THE beta- and conversion electron spectrum of Hf^{181} has previously been studied by Cork, Shreffler, and Fowler,[1] Voigt and Thamer,[2] and by Beneš, Ghosh, Hedgran, and Hole.[3] Coincidence work on the radiations of Hf^{181} is also discussed in the preceding paper by Mandeville, Scherb, and Keighton.

BETA-SPECTRUM OF Hf^{181}

We have studied the beta-spectrum of Hf^{181}, using a semicircular focusing spectrograph of 2 percent resolving power. The spectrograph was calibrated from the 0.400-Mev line[4] of Au^{198}. The

* Rackham Predoctoral Fellow, 1948–49.

[1] J. M. Cork, R. G. Shreffler, and C. M. Fowler, Phys. Rev. 72, 1209 (1947).

[2] A. F. Voigt and B. J. Thamer. Phys. Rev. 74, 1254 (1948).

[3] J. Beneš, A. Ghosh, A. Hedgran, and N. Hole, Nature 162, 261 (1948).

[4] K. Siegbahn, Proc. Roy. Soc. 187, 527 (1947).

sources were of hafnium oxide mounted on 0.2-mil sheet Nylon. A Geiger counter was used as a detector. Two types of counter windows were used, one of mica which transmitted electrons of energies above 38 kev; the second was of Nylon which had a cut-off at about 12 kev.

A typical spectrum obtained with a Nylon window is shown in Fig. 1. This spectrum is not corrected for window absorption. It is seen that conversion lines from four distinct gamma-rays are superimposed on the continuous beta-spectrum. The energies of the gamma-rays giving rise to these lines are 0.130, 0.134, 0.337, and 0.471 Mev. The two lowest energy lines are clearly shown in the enlarged section of Fig. 1. (Some of the experimental points have been omitted from the main diagram to avoid overlapping.) These two lines had first been observed on a photographic plate by Cork *et al.*,[1] and ascribed to conversion electrons and photoelectrons arising from a single gamma-ray. From a study of the intensity of this group we feel that two separate gamma-rays of nearly the same energy are emitted in the decay of Hf^{181}. In fact, the total conversion coefficient in the low energy groups (i.e., $N_{K_1+K_2+L_1+L_2+M_1+M_2}/N_\beta$) is found to be 0.7, even if no correction is made for window absorption. If the number of conversion electrons is corrected for window absorption and the number of beta-particles is obtained by extrapolating the Fermi plot to zero energy, the total conversion coefficient for the low energy

TABLE I. The conversion coefficients listed are the ratio of the number of conversion electrons in the group to the total number of beta-particles.

Line	Energy in Mev	Conversion coefficient
K_1	0.130	~0.56
K_2	0.134	~0.22
L_1+L_2		~0.425
M_1+M_2		~0.089
K_3	0.337	0.019
L_3		0.0053
K_4	0.471	0.021
L_4		0.0071

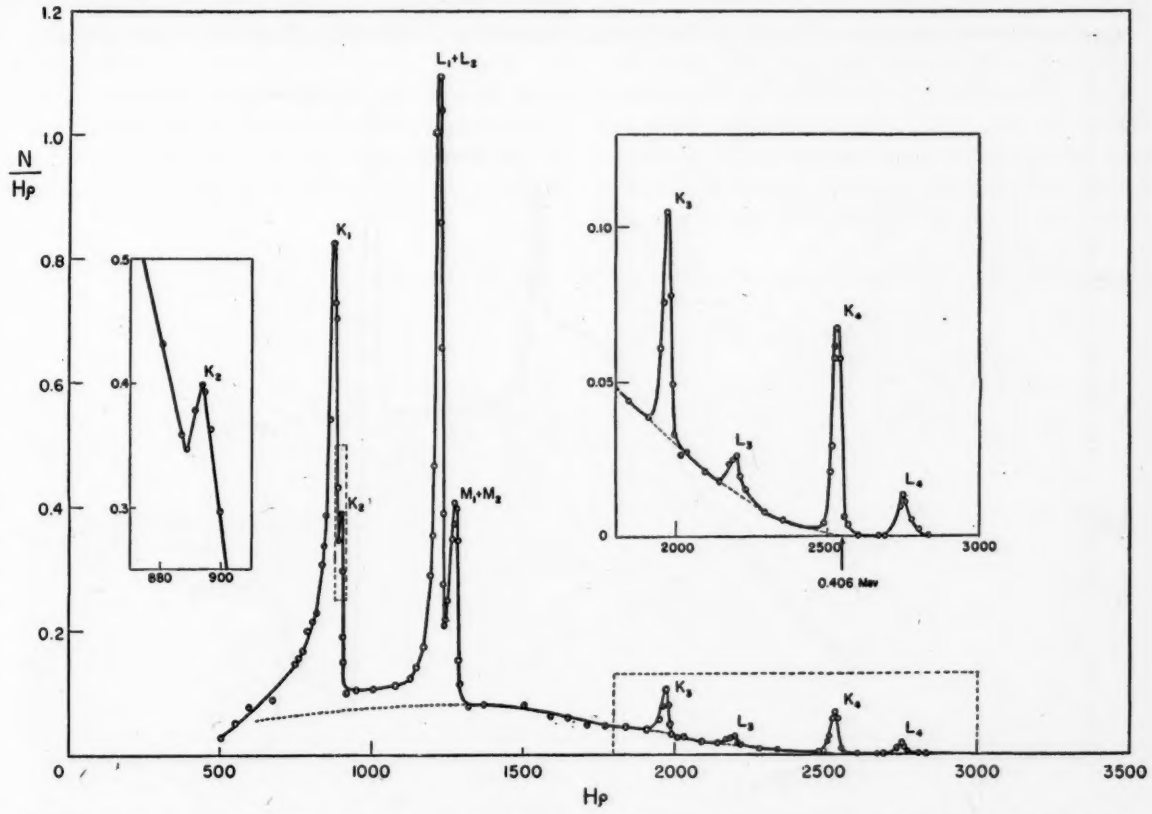

FIG. 1. Beta-spectrum of Hf^{181}. The K conversion lines of the low energy components can be clearly distinguished.

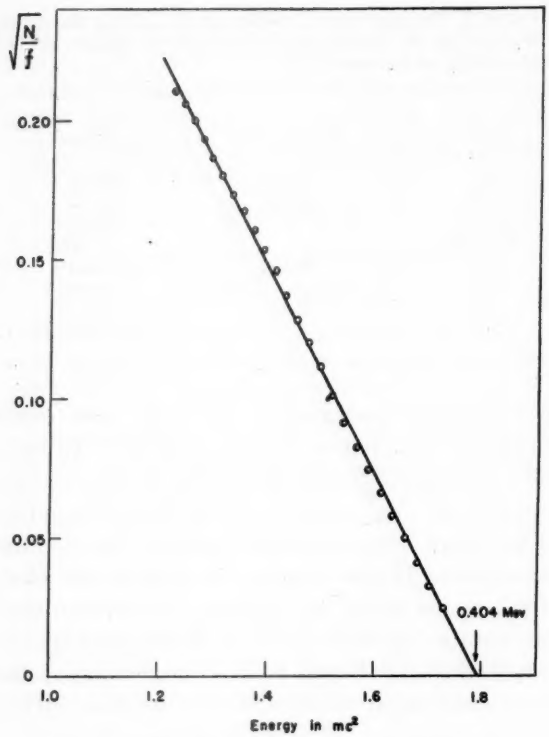

FIG. 2. Fermi plot of the Hf^{181} beta-spectrum.

groups is ~1.3. Therefore, it seems clear that two distinct gamma-rays are present.**

The conversion coefficients for the various lines are listed in Table I.

A Fermi plot obtained from the continuous spectrum is shown in Fig. 2. It appears to be linear down to energies at which window absorption becomes appreciable. The end point of the beta-spectrum is 0.404 Mev.

The decay of a Hf^{181} source was followed in the spectrograph over a period of sixty days. Within the experimental uncertainties, all components decayed with the same lifetime.

PHOTOELECTRON SPECTRUM OF Hf^{181}

The photoelectron spectrum obtained by using a lead radiator is shown in Fig. 3. It is seen that the photo-lines of the two higher energy gamma-

** *Note added in proof:* The beta-spectrum has been studied using a source which consisted of 50 percent active hafnium oxide mixed with 50 percent non-active hafnium oxide. The ratio of the peaks of K_1 and K_2 remained unchanged thus indicating conclusively that the photo effect plays no important role in the production of these peaks.

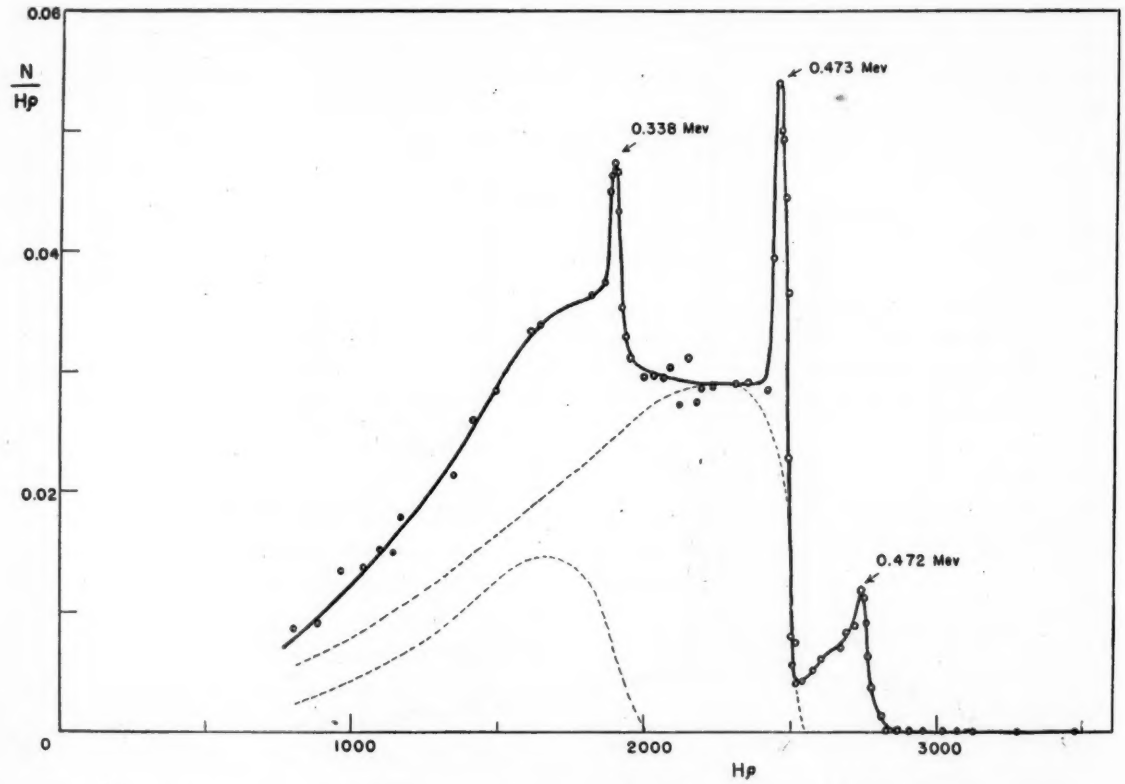

FIG. 3. Photoelectron spectrum of Hf^{181}, using lead as a radiator. The shapes of the Compton components were made to match that obtained for gold with the same spectrograph.

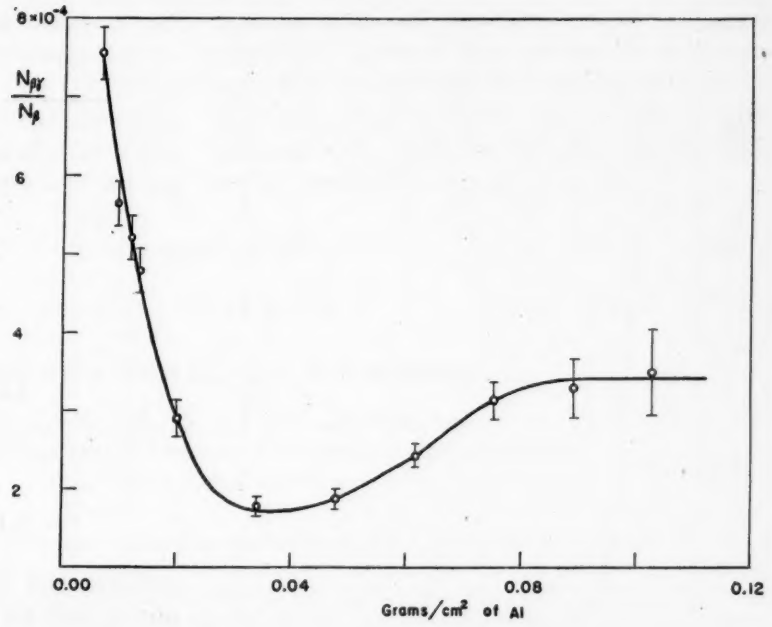

FIG. 4. Beta-gamma-coincidence rate as a function of beta-absorber thickness. The source used in obtaining this curve had been chemically separated.

rays are present, superimposed on the Compton spectra. There is no indication of a photo-line arising from the lowest energy gamma-ray, thus giving further evidence that the lines K_1 and K_2 in the beta-spectrum arise from highly converted gamma-rays.

The Compton spectra have been broken into two components as indicated. The shapes were made to match that of the spectrum of Au^{198}, which has a strong gamma-ray of energy 0.400 Mev.

From the intensities of the Compton components, one obtains a ratio of gamma-intensities $\gamma_3:\gamma_4=1:2$. The corresponding value as obtained from the K photo-lines (following the procedure of Deutsch, Elliot, and Evans[5]) is $\gamma_3:\gamma_4=1:2.8$.

It may also be noted that no additional lines occur in the photoelectron spectrum which had not been observed in the beta- and conversion spectrum. The photoelectron spectrum has been checked up to 0.8 Mev but has given no indication of activity beyond that of the L_4 photo-line.

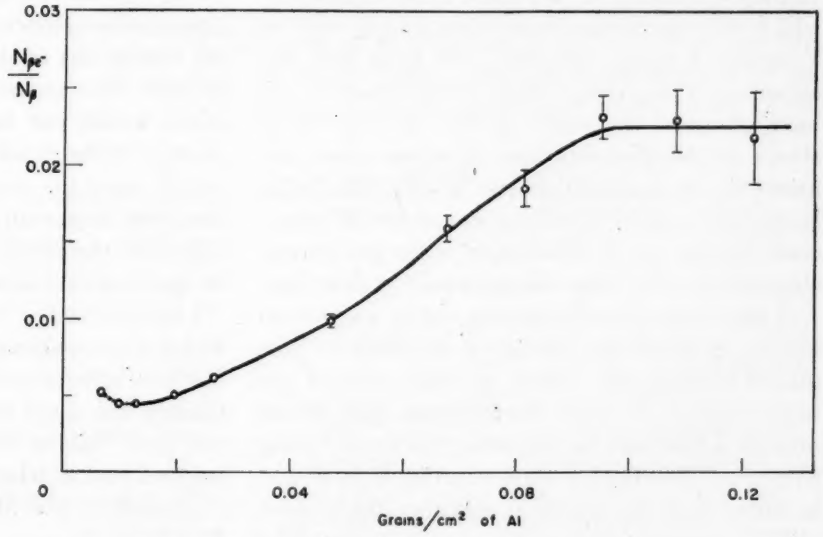

FIG. 5. Beta-beta-coincidence rate using a single absorber.

[5] M. Deutsch, L. G. Elliot, and R. D. Evans, Rev. Sci. Inst. 15, 178 (1944).

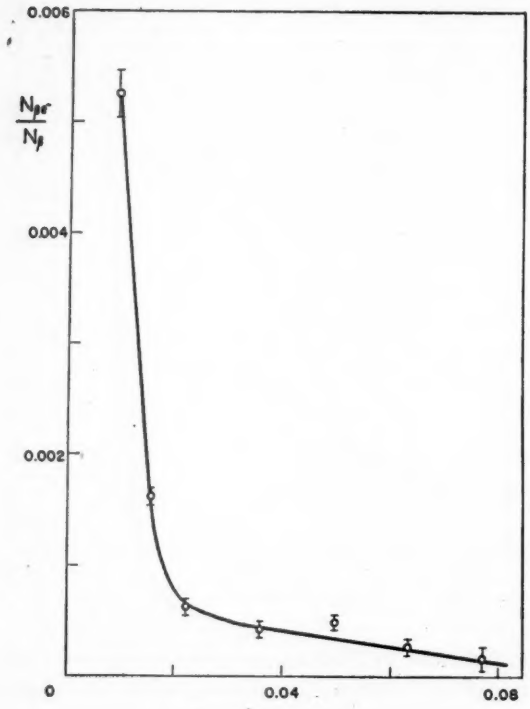

FIG. 6. Beta-beta-coincidence rate using absorbers before each counter.

COINCIDENCE MEASUREMENTS

Coincidence measurements on Hf^{181} can be extremely treacherous because of the complicated nature of the decay and the abundance of low energy electrons and gamma-rays. We have previously published a β-γ-coincidence curve[6] in which the coincidence rate was found to rise by a factor of three. Recently, we have had the opportunity to repeat these measurements and have obtained the curve in Fig. 4. This curve shows an initial sharp drop to a low value, followed by an appreciable rise which appears to be real. The sharp drop was not observed previously because of the absorption of the low energy electrons in the counter windows used at that time.

A beta-beta-coincidence rate curve is shown in Fig. 5. In obtaining this curve, an absorber was placed between the source and only one of the beta-counters. A curve showing the coincidence rate as a function of absorber thickness, using two equal absorbers, is shown in Fig. 6. It should be noted that the points at absorber thicknesses

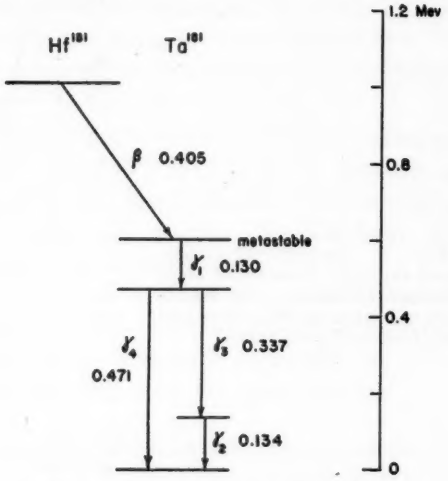

FIG. 7. Proposed energy level scheme.

greater than 0.05 gram/cm² are difficult to obtain both for the beta-gamma- and beta-beta-coincidences with two absorbers.

PROPOSED LEVEL SCHEME

Two energy level schemes have been proposed thus far.[1,3] The cascade arrangement of Beneš *et al.*[3] does not take into account the presence of the two low energy gamma-rays. In addition, the photoelectron and Compton spectrum (Fig. 3) indicates that the 0.471-Mev gamma-ray is considerably more abundant than the 0.337-Mev gamma-ray. It would therefore seem that a level scheme similar to that shown in Fig. 7 might account for most of the observed facts. The beta-gamma-coincidence curve (including the apparent minimum) could clearly be fitted by such a scheme. The shape and magnitude of the β-γ-curve would not be appreciably affected by a change in the resolving time of the coincidence circuit since the conversion electrons would play the most important role, even at high energies. Likewise, the beta-beta-coincidence curves could be qualitatively accounted for by this scheme.

Unfortunately, coincidence measurements which are capable of distinguishing among various level schemes are extremely difficult to make. Clearly the level scheme proposed here should not give rise to coincidences between a non-delayed and a delayed gamma-ray. The work of DeBenedetti and McGowan[7] indicates that such

[6] M. L. Wiedenbeck and K. Y. Chu, Phys. Rev. 72, 1164 (1947).

[7] S. DeBenedetti and F. K. McGowan, Phys. Rev. 70, 569 (1946).

coincidences do not occur, while Beněs *et al.*[3] report a small number of this type of coincidence. A second test would occur in the beta-beta-coincidence rate obtained with two absorbers. That portion of the curve *at great absorber thicknesses* should be due to coincidences between the beta-ray and delayed high energy conversion electrons, therefore this portion of the curve should be sensitive to the resolving time of the coincidence circuit. That portion of the curve obtained with small absorber thicknesses should not be sensitive to the resolving time.

PHYSICAL REVIEW VOLUME 75, NUMBER 2 JANUARY 15, 1949

Evidence for a New Isotope of Potassium*

ROY OVERSTREET,** LOUIS JACOBSON,*** AND P. R. STOUT†
Agricultural Experiment Station, University of California, Berkeley, California

(Received September 13, 1948)

A study of the potassium isotopes produced by the bombardment of argon with helium ions reveals the presence of a hitherto unknown isotope with a 22.4 hour half-life. The new potassium isotope has two beta-components of approximately 0.25-Mev and 0.8-Mev maximum energies. A gamma-component is present of roughly 0.4-Mev energy. The evidence strongly suggests that the isotope in question is K^{43} produced by the reaction $A^{40}(\alpha, p)K^{43}$.

I. INTRODUCTION

IN a recent communication by two of the authors[1] it was shown that bombardment of argon with 40-Mev helium ions resulted in the production of radio-potassium in exceptionally high yields (about one millicurie per microampere-hour). This bombardment subsequently has proven to be a very satisfactory method for the production of radioactive carrier free potassium, particularly for use as a tracer in the biological and agricultural sciences. Moreover, the apparatus used (See Fig. 1) which was designed by M. T. Webb of the Crocker Radiation Laboratory may be employed for the bombardment of other gases with protons, deuterons or helium ions. The reaction is carried out in a bell-jar constructed of 2*S* commercially pure aluminum so as to contain the beam and through which a slow stream of argon gas continuously flows. The outlet tube for the gas is approximately 20 feet in length and the end of the tube is immersed in a beaker of water. Also the outlet tube contains a glass wool plug adjacent to the bell-jar. The rate of gas flow and length of outlet tube are adjusted so as to prevent air being sucked back into the bell-jar as a result of cooling caused by momentary interruptions in the beam from sparking of the deflector, etc. The major portion of the radio-potassium settles out on the walls of the

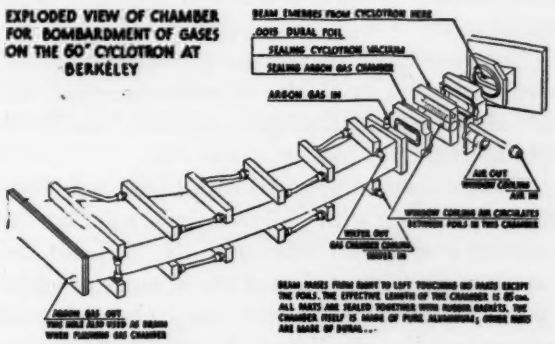

FIG. 1. Exploded diagram of aluminum bell-jar used for bombardment of gases with protons, deuterons, or alpha-particles.

* This paper is based on work performed under contract No. W-7405-eng.-48-A with the Atomic Energy Commission, in connection with the Radiation Laboratory, University of California, Berkeley, California.
The authors are indebted to the staff of the 60-inch Cyclotron, University of California, for performing the bombardments with helium ions.
** Associate Professor of Soil Chemistry and Associate Soil Chemist in the Agricultural Experiment Station, University of California.
*** Assistant Professor of Plant Nutrition and Assistant Plant Biochemist in the Agricultural Experiment Station, University of California.
† Associate Professor of Plant Nutrition and Associate Chemist in the Agricultural Experiment Station, University of California.
[1] Roy Overstreet and Louis Jacobson, Phys. Rev. **72**, 349 (1947).

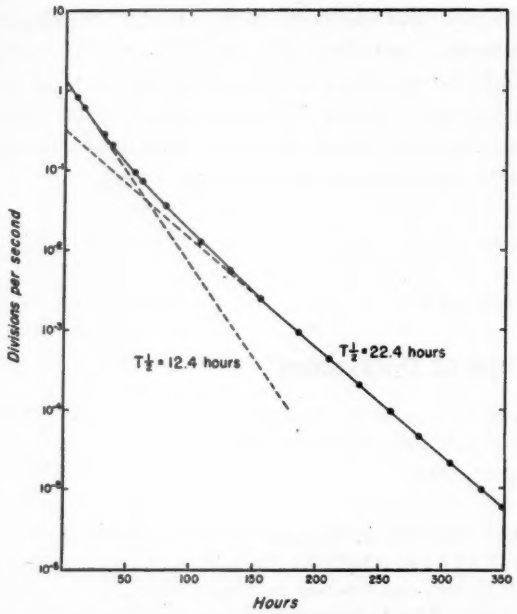

FIG. 2. Decay curve for potassium isotopes produced by the bombardment of argon gas with 40-Mev helium ions.

bell-jar and the remainder is caught in the glass wool plug in the gas outlet. Following the bombardment, the walls of the bell-jar and the glass wool plug are treated with warm distilled water. In this manner an essentially pure preparation of carrier free radio-potassium is obtained that can be used without further purification in most instances. However, it will be shown in the following sections that this preparation contains more than one long-lived isotope of potassium.

II. PURIFICATION OF RADIO-POTASSIUM

In order to identify chemically the radioactivity produced by the above method the preparation was carried through a series of chemical separations.

To a water solution of the potassium preparation 10 mg each of the following carriers was added in the form of soluble salts: Zn, Cu, Na, K, Rb, Cs, Ca, Ba, and Sr.

The Cu was precipitated with H_2S in acid solution and the Zn with H_2S in neutral solution. No activity was carried down with the CuS and ZnS precipitates. This indicated the absence of essentially all elements except those behaving as anions and the alkali and alkaline earth groups.

The elements K, Rb and Cs were precipitated as the perchlorates. Only a trace of activity was found in the filtrate which probably was due to the slight solubility of $KClO_4$. The perchlorate precipitate was recrystallized 15 times in the presence of Na, Ca, Ba and Sr carriers. There was no detectable change in the specific activity of the perchlorate precipitate. It was, therefore, evident that all of the activity was associated with the K, Rb and Cs fraction.

The perchlorates of K, Rb and Cs were then converted to the nitrites by precipitation of the elements with cobaltinitrite, fusing with $NaNO_2$, and filtering off the cobalt oxides. Rb and Cs were separated from K in the nitrite solution by precipitation with bismuth subnitrate. The Rb and Cs were subsequently separated from each other by precipitation of the Cs with antimony chloride.[2] Each of the three fractions were examined for activity. The Cs fraction was inactive. Approximately 97 percent of the activity was associated with the *K* fraction. The remainder of the activity was in the Rb fraction. However, since the decay rate and energy distribution of this activity was identical to that of the activity in the K fraction, and also since the separation of Rb from K is known to be not entirely complete, we can definitely attribute the small Rb activity to co-precipitated K.

The above chemical separations were carried out both on a newly bombarded sample and on an aged sample (200 hours). The distribution of activity was identical in both cases. The chemical separations indicate that no detectable activity of half-life more than a few minutes other than potassium is deposited on the walls of the bell-jar in this bombardment, or arose from the bombarded areas of the bell-jar itself.

FIG. 3. Beta-spectrogram of the energy groups of radioactive potassium formed by helium ion bombardment of argon. Spectrogram taken approximately 24 hours after bombardment.

[2] A. A. Noyes and W C. Bray, *Qualitative Analysis for the Rare Elements* (The Macmillan Company, New York, 1927), pp. 260–267.

III. DECAY MEASUREMENTS

Although the potassium preparation has been shown to be very pure chemically, the decay curve does not show the 12.4-hour period characteristic of K^{42}.[3] For example, the activity, when purified as described above, has at 5.5 hours after bombardment a half-life of 14.8 hours and at 150 to 350 hours after bombardment a half-life of 22.4 hours. The decay curve for the purified preparation is given in Fig. 2.

An analysis of the curve of Fig. 2 clearly indicates the existence of an unknown isotope of K with a half-life of 22.4 hours in addition to the 12.4 hour period of K^{42}. The new isotope accounts for approximately 22 percent of the total initial potassium activity as measured with a Lauritsen electroscope. The air gap plus the electroscope window was equivalent to 5 milligrams per square centimeter of aluminum.

IV. MAGNETIC SPECTROGRAPH MEASUREMENTS

Examination of the purified potassium preparation in a magnetic spectrograph with a field strength of 2400 gauss showed no evidence of positron emission. Three beta-components of the following maximum energies were obtained: 0.24 Mev, 0.81 Mev, and 3.5 Mev. The 3.5-Mev component evidently corresponds to the 3.58-Mev beta-particles reported for K^{42}.[3] On standing, this component disappeared in a manner consistent with a 12.4-hour half-life, leaving the 0.25-Mev and the 0.81-Mev components. A magnetic spectrogram taken approximately 24 hours after bombardment is given in Fig. 3.

V. Al AND Pb ABSORPTION CURVES

The Al and Pb absorption curves for the purified preparation taken 210 hours after bombardment are given in Fig. 4. The Al curve shows a soft beta-component with a range of about 60 mg/cm² which is equivalent to a maximum energy of 0.24 Mev. The curve also shows a beta-component with a range of roughly 300 mg/cm² or a maximum energy in the neighborhood of 0.8 Mev.

[3] Kai Siegbahn, Ark. f. mat., astr. o. fysik **34B**, No. 4, 1 (1947).

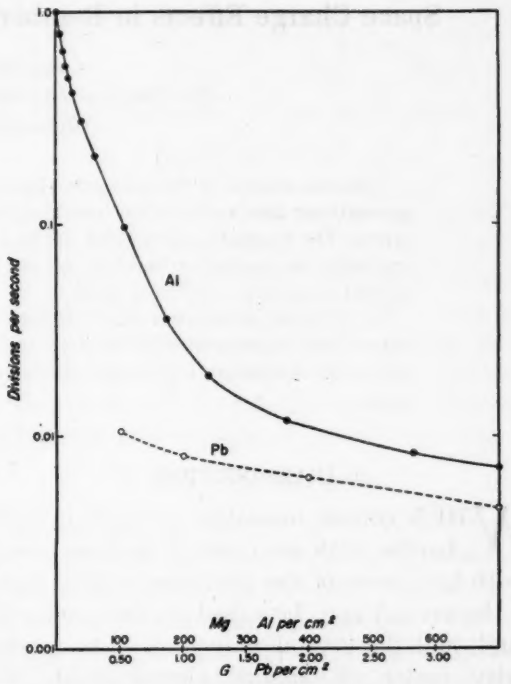

FIG. 4. Aluminum and lead absorption curves for potassium isotopes produced by the bombardment of argon gas with 40-Mev helium ions. Measurements made 210 hours after bombardment.

The Pb absorption curve, although it does not permit an accurate estimation, indicates a gamma-component with a half-value thickness of about 3.5 g/cm² or an energy of 0.4 Mev. A comparison of the beta- to gamma-ratio taken for a sample 5.5 hours after bombardment with that calculated from Fig. 4 (210 hours after bombardment) indicates that this gamma-component must be due to the new isotope.

VI. ISOTOPE ASSIGNMENT

A study of the possible isotopes resulting from the bombardment of argon with alpha-particles favors the assignment of K^{43} to the 22.4 hour potassium isotope. The reaction would be $A^{40}(\alpha, p)K^{43}$. This choice is further substantiated by the fact that the new isotope is a beta-emitter.

VII. ACKNOWLEDGMENTS

The authors wish to thank Professors J. G. Hamilton and Glenn T. Seaborg for valuable criticism and suggestions.

Space Charge Effects in Bombardment Conductivity through Diamond

ROBERT R. NEWTON*
Bell Telephone Laboratories, Murray Hill, New Jersey
(Received August 23, 1948)

Electrons excited to the conduction band of an insulator under electron bombardment are, in general, not able to leave the insulator, but become trapped at imperfections in the crystal lattice. The trapped electrons give rise to a space charge which modifies the motion of electrons excited to the conduction band subsequent to the trapping. In this way, the current through the crystal becomes a function of time.

In this paper, a tentative theory of such space charge effects is presented and compared with experiment. Agreement with the data which exist at present is reasonably good. Some predictions and suggestions for future experiments, which arise as consequences of the theory, are made.

I. INTRODUCTION

WHEN certain insulating crystals are bombarded with electrons of medium energy (~10 kv), some of the electrons in filled bands of the crystal may be raised to the conduction band, and the crystal may then show conductivity under an applied electric field. This phenomenon, which we shall call electron bombardment conductivity, or, more briefly, bombardment conductivity, is similar in many respects to the effects involved in crystal counters. Crystal counters which depend upon induced conductivity rather than upon observation of scintillations[1] have been made from various materials: silver chloride at liquid air temperature,[2] diamond,[3] zinc sulfide,[4] a mixture of thallous halides,[5] and cadmium sulfide.[6] In the work with electron bombardment, however, what is sought is the response to a beam of particles rather than response to isolated particles. Hence, the situation is perhaps more analogous to the photo-conductivity of an insulator when illuminated in its fundamental absorption band.[7]

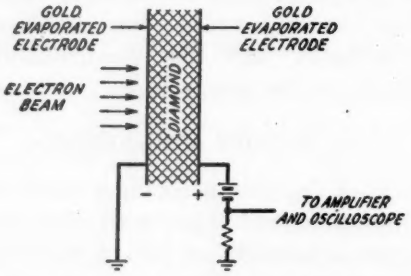

FIG. 1. Experimental arrangement for observing bombardment conductivity.

Bombardment conductivity has been observed by Dr. K. G. McKay in diamond.[8] The experimental arrangement which he used is shown in Fig. 1. The diamond used was in the form of a plate about 0.05 cm thick, with gold electrodes evaporated onto the faces. A collimated electron beam of variable energy, and of diameter $\frac{1}{32}''$ (~0.08 cm) impinged upon one face, which we shall call the front face of the diamond. The geometry of the system is a fair approximation to infinite plane-parallel geometry.

The impinging electrons penetrate the diamond and produce ionization; the ionization range is about 3×10^{-4} cm, which is less than 1 percent of the thickness of the diamond. With the voltage as shown, the positive holes left by the ionization travel to the front face, and can make no appreciable contribution to the observed current. The observed current is that carried by the electrons which travel toward the back face. Experiments were also performed in which the

* Now at The University of Tennessee, Knoxville, Tennessee.

[1] R. J. Moon, Phys. Rev. 73, 1210 (1948).

[2] P. J. Van Heerden, *The Crystal Counter* (thesis) (Utrecht, 1945); R. Hofstadter, Phys. Rev. 72, 747 (1947); R Hofstadter, J. C. D. Milton, and S. L. Ridgway, Phys. Rev. 72, 977 (1947).

[3] D. E. Wooldridge, A. J. Ahearn, and J. A. Burton, Phys. Rev. 71, 913 (1947); L. F. Curtiss and B. W. Brown, Phys. Rev. 72, 643 (1947); W. Jentschke, Phys. Rev. 73, 77 (1947); G. Stetter, Verh. d. D. Phys. Ges. 22, 13 (1941).

[4] A. J. Ahearn, Phys. Rev. 73, 524 (1948).

[5] R. Hofstadter, Phys. Rev. 72, 1120 (1947).

[6] R. Frerichs, Phys. Rev. 72, 594 (1947).

[7] See J. H. De Boer, *Electron Emission and Adsorption Phenomena* (Cambridge University Press, London, 1935), p. 305.

[8] Reported verbally at the symposium of Division of Electron Physics, New York, Jan. 31, 1948, Phys. Rev. 73, 1238 (1948).

back face was negative, so that the current is carried by positive holes.

We shall assume that there are no qualitative differences in behavior between electrons and positive holes, although their characteristic parameters (mobility, etc.) may have different values. Our discussion will then hold equally well for either type of current carrier; for convenience, however, we shall always speak of electrons as carriers, so that we are referring to the voltage arrangement of Fig. 1.

The diamond used is not a perfect crystal, but contains flaws or impurities which can act as electron traps. Thus some of the electrons which start across are trapped in the interior of the crystal, giving rise to a space charge which impedes the further flow of electrons. The current through the crystal will, as a consequence, vary with time; the purpose of this paper is to study this time variation.

In order to observe the time variation of the current, McKay pulsed the bombarding electron beam, using pulses lasting for the order of 10^{-6} sec., and repeated 60 times per second. Between pulses, he subjected the crystal to a treatment designed to neutralize the space charge deposited during the preceding pulse, so that the beginning of each pulse would find the crystal free of space charge.

Typical curves for the variation of current during a pulse are shown in Fig. 2. For a particular voltage, at some high current density, the curve is everywhere concave upward. With the same voltage, if the current density is lowered sufficiently, the curve is at first concave downward, and then becomes and remains concave upward. We believe that qualitatively different mechanisms are responsible for the different portions of the curve at low current densities, and that both portions are actually present in all the curves. At high current densities, however, the first portion is of such short duration that it is lost in the finite rise time of the pulse and the finite response of the amplifier.

As we mentioned before, the ionization range of the bombarding electrons is about 3×10^{-4} cm. Within the layer extending to this depth from the front face, which we shall call the plasma layer, both positive holes and electrons are to be found. We therefore expect different behavior in

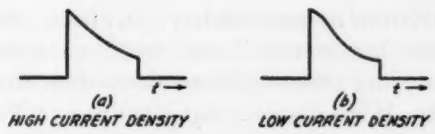

FIG. 2. Typical current-time curves.

this plasma layer from the rest of the diamond, in which only electrons are to be found. In the next section we shall discuss the plasma layer; the remainder of the paper will deal with the part of the diamond between the plasma layer and the back face. At the end of the next section, we shall be in a position to discuss the differences between the two portions of the curves in Fig. 2.

II. THE PLASMA LAYER

Each impinging electron penetrates the diamond a certain distance before losing its ability to produce ions, and, in this distance, produces on the average a number of electrons which we shall denote by δ_∞. If an infinite field were applied to the crystal, all of these electrons would be collected by the electrodes. Hence we call δ_∞ the yield for infinite field strength. We shall assume that the points of origin on these δ_∞ electrons are distributed uniformly along the ionizing range of the impinging electron.

Within the plasma layer are high concentrations of electrons and positive holes. This situation is comparable to that which exists when the diamond is illuminated in its fundamental ultraviolet band, when little or no photo-conductivity exists, presumably because most of the photo-electrons recombine with the holes.[7] Our first question is then: How many electrons escape from the plasma layer to enter the main body of the diamond?

We expect the number of recombinations of electrons and holes per cm³ per second to be of the form:

$$Kn_+n_-, \tag{1}$$

where n_+ and n_- are the volume densities of holes and electrons, respectively, and K is a constant. K can be estimated to order of magnitude; if we neglect the velocity of the holes compared with that of the electrons and let v be the average velocity of an electron in its Brownian path, and σ the cross section for recombination:

$$K=v\sigma.$$

The electrons in question have just been knocked into the conduction band by the impinging electron, and probably have more than thermal velocity. If we assume that they have 0.5 ev of kinetic energy, and that $\sigma=10^{-15}$ cm^2, we get $K=6\times10^{-8}$.

We now wish to show that recombination is negligible unless the field is quite low, probably of the order of 20 volt/cm or less. With one of the largest bombarding currents and the highest δ_∞ which McKay has used, the number of electrons and holes created per sec. per cm^2 cross section of the plasma layer is 6×10^{16}. The lowest field used is about 2000 volts per cm; if the mobility of holes is 30 cm/sec. per volt/cm, the longest time required for a hole to traverse the plasma layer is

$$3\times10^{-4}/(30\times2000)=5\times10^{-9}\text{ sec.}$$

After this length of time, the number of holes and electrons which have been created per cm^2 of plasma is

$$6\times10^{16}\times5\times10^{-9}=3\times10^{8},$$

and the density is certainly not greater than 10^{12} electrons or holes per cm^3 of plasma. The number of recombinations per cm^3 per sec., according to Eq. (1), is not greater than

$$Kn_+n_-=6\times10^{-8}\times10^{24}=6\times10^{16}.$$

In 5×10^{-9} sec. then, per cm^2 cross section of plasma layer, we would have

$$6\times10^{16}\times5\times10^{-9}\times3\times10^{-4}=9\times10^{4}$$

recombinations. Since, in the same time and the same volume, 3×10^8 electrons and holes have been created, the reader can readily convince himself that recombination is negligible under the conditions assumed, and is probably not important unless the field in the plasma falls below the order of 20 volts/cm.

We now wish to discuss the time and space variation of the densities of holes and electrons within the plasma. Let i_0 = bombarding current density in electrons/cm^2/sec., let l = thickness of the plasma layer, and let v_+ and v_- be the mobilities of holes and electrons, respectively. Then the equations of continuity for holes and electrons read

$$(\partial n_-/\partial t)=-v_-F(\partial n_-/\partial x)+(i_0\delta_\infty/l)-Kn_+n_-, \quad (2)$$

$$(\partial n_+/\partial t)=v_+F(\partial n_+/\partial x)+(i_0\delta_\infty/l)-Kn_+n_-. \quad (3)$$

The x coordinate is taken to be zero at the front face, and increases as we go into the crystal, while the field F is taken positive if in the direction of decreasing x. In Eqs. (2) and (3), the first term on the right in each represents the transport, the second the creation by the bombarding electrons, and the third the loss by recombination. We neglect trapping of holes or electrons within the plasma layer. Equations (2) and (3) are subject to the conditions that $n_+=n_-=0$ at $t=0$ for all x, and that $n_+=0$, $x=l$, $n_-=0$, $x=0$, for all t.

We shall first assume that F does not change appreciably across the plasma layer. Unless the field F is quite small, the recombination is negligible, and Eqs. (2) and (3) are independent. The solutions for n_+ and n_- are similar; that for n_+ can be readily verified to be

$$n_+=(i_0\delta_\infty/l)[t-\text{max.}(t+(x-l)/v_+F,\,0)]. \quad (4)$$

By the symbol max.(A, B), we mean the larger of A or B. At any position x, this becomes independent of t when $t=(l-x)/v_+F$. For $t\geq l/v_+F$, n_+ is everywhere independent of t, and is given by

$$n_+=(i_0\delta_\infty/l)(l-x)/v_+F. \quad (5)$$

We now verify that the change in F across the plasma layer is small. If ΔF is the change in F, ϵ the electronic charge, and κ the dielectric constant, we have, neglecting the electrons in the plasma,

$$\Delta F=(4\pi\epsilon/\kappa)(i_0\delta_\infty/2v_+F)l.$$

Using the figures we used to estimate the recombination, $\Delta F/F=2$ percent, or the field varies from its average value by about 1 percent. If the electrons are included in the computation, the result is multiplied by $1-2(v_+/v_-)$, as may be readily verified.

We should also make some statements about the possibility of electrons being trapped in the plasma layer. Using material to be presented in the next several sections, we can conclude that trapping in the plasma layer is negligible unless the field in the plasma falls below about 25 volts/cm.

The solution of Eqs. (2) and (3), when recombination, trapping, and variation of F are included, is a more formidable task which we shall

not undertake here. From the calculations which we have just made, however, we can draw two conclusions: (a) Unless the field is below, say, 200 volts/cm, the field across the plasma is fairly constant, and the charge contained in the plasma can be neglected in computing the space charge effects. (b) Unless the field in the plasma is below, say, 25 volts/cm, all of the electrons liberated by the bombarding electrons escape from the plasma layer into the main portion of the crystal. If the field is lower than this value, electrons may be lost either by recombination or trapping.

The significance of these conclusions is that, during the early part of the bombardment, when the field is 2000 volts/cm or higher, we can neglect the plasma and the positive holes, and assume that all of the electrons leave the plasma and start across the crystal. Some or all of these electrons are trapped in the crystal; their space charge lowers the field at the front face, so that electrons can be trapped more readily, and so on. This period of operation corresponds to the first portion of the curves in Fig. 2. Unless the trapped electrons are released too quickly, at some time the field at the front face must become nearly zero. When this occurs, the number of electrons leaving the plasma layer is substantially reduced. The current now falls to a steady value which is determined by this consideration: The field in the plasma layer is held by the trapped electrons (i.e., trapped in the main part of the crystal) at such a value that the number of electrons leaving the plasma layer just balances the number of electrons lost from the crystal by thermal release from traps and subsequent drift out of the crystal.

Qualitatively, this picture leads to a negative second time derivative of the current (current curve concave downward) as long as all electrons leave the plasma, at least for small thermal release rates. That is, a trapping of electrons, which means a decrease in current, so alters the field conditions that trapping, and hence the decrease in current, becomes more rapid. We shall give a semiquantitative discussion of this point in Section VI.

If the thermal release rate is large, a different condition of equilibrium from that just discussed may obtain. This condition will be discussed in Section VII. If this condition can be achieved, it affords a method of obtaining information about the plasma layer, which is at present inaccessible to study.

The point of inflection of the curve in Fig. 2 must then occur near the time when the field in the plasma layer becomes small. We can readily estimate the time at which this occurs, as follows: Until the point of inflection is reached, almost all of the electrons freed by the ionization leave the plasma, but are trapped in the body of the diamond. Hence, at time t, the number of electrons trapped per unit cross section of the diamond is approximately

$$i_0\delta_\infty t.$$

The change ΔF in F as we traverse the crystal is

$$\Delta F=(4\pi\epsilon/\kappa)i_0\delta_\infty t.$$

Since the voltage across the diamond is held constant, the average field must always equal the originally applied field F_0. Hence, if the field at the front face is to be approximately zero, ΔF approximately equals $2F_0$, and the time t at which the point of inflection occurs is approximately

$$t=2\kappa F_0/4\pi\epsilon i_0\delta_\infty. \tag{6}$$

Equation (6) was derived before any curves were observed which showed a point of inflection. Using this equation, conditions under which a point of inflection should be observable were computed, and the points of inflection were then discovered. Figure 3 shows the agreement between the observed values of t at the inflection point, and the values predicted by Eq. (6). The agreement is good only to order of magnitude, and the observed values are always greater than the predicted ones.

In the derivation of Eq. (6), we neglected the electrons which are released thermally from traps, and also those which cross the crystal without being trapped. In Section VI, we give a computation which includes these electrons. The results of these calculations are also shown in Fig. 3. The curves labeled $B(1-f)=0$ include the electrons which are not trapped, and the curves $B(1-f)=0.03\times10^6$ include, in addition, those released thermally, with a particular assumption about the thermal release rate. These latter curves are discussed in Section VI.

The hypothesis underlying Eq. (6) is in line with another observation. If we consider what should happen to the shape of the pulse as we vary the amount of space charge neutralization, we see that, if negative charge is left in the crystal, the field in the plasma layer is already small at the beginning of the pulse, and the entire pulse should be concave upward. The portion which is concave downward should not appear until the space charge neutralization is almost complete. This is the observed behavior.

III. TYPES OF TRAPS, THE TRAPPING LAW

Experiments which have been performed indicate that there is more than one type of electron trap in a diamond. Dr. A. J. Ahearn has performed some interesting experiments in this connection, which we shall describe briefly.

Ahearn was studying the properties of diamond as a counter of α-rays.[3] He first determined the counting efficiency of a particular diamond as a function of the electric field applied to it, when the bombardment lasts too short a time for space charge to be significant, for conduction either by holes or electrons. He then bombarded this diamond with α-particles at the rate of 500 per min., over a circle of 0.06-in. diameter, with 4000 volts per cm applied to the crystal in such a direction that electrons conduct, for one minute, and then removed the applied field. The space charge field then became the dominant field; it is in a direction such as to make the crystal conduct by means of holes. The counting rate immediately after removal of the applied field corresponded to a field of 320 volts per cm. When the bombardment time was increased to 2 min., the initial counting rate under the space charge field corresponded to 480 volts per cm.

As we shall show in the next section, most electrons released by the α-particles are trapped in the diamond. Assuming 5×10^5 ion pairs per α-particle, we find that, after 1-min. bombardment, there have been approximately 1.4×10^{10} electrons per cm^2 cross section trapped in the diamond. To produce a field of 320 volts per cm, however, requires only 1.8×10^9 electrons per cm^2. Hence we compute that a fraction,

$$1.8\times10^9/1.4\times10^{10}=13 \text{ percent},$$

remain trapped for the order of a minute. Similarly, when the bombardment with applied field continued for 2 min., about 10 percent were still trapped at the end of the bombardment.

We conclude, then, that of all the traps in the diamond, about 10 percent are deep enough that the half-life for thermal release is of the order of a minute. This measurement was made on only one diamond. Most of the other traps must be substantially shallower than this 10 percent.

It is of some interest at this point to estimate what depth of trap, expressed in volts, is actually required to produce the observed lifetime, and to see if the depth agrees with a reasonable mechanism for producing traps.

Mott and Gurney[9] give an approximate relation between the half-life and trap depth,

$$B/\sigma=2\pi m(kT)^2h^{-3}(6\pi)^{\frac{1}{2}}\exp(-E/kT), \quad (7)$$

in which B is the probability per second that an electron escapes from the trap, σ is the capture cross section of the trap for thermal electrons, and E the depth of the trap (below the conduction band). With $B\sim10^{-2}$ (half-life of 100 sec.), $\sigma\sim10^{-16}$ cm^2, we get $E=0.75$ ev. On the other hand, if $B=10^6$ (half-life of 1 μsec.), $E=0.25$ ev. Hence, we need assume only that the traps with which we are dealing lie at depths between one-fourth and three-fourths of a volt.

Regarding mechanisms, an obvious suggestion is that a foreign singly charged ion is placed at one of the many normally unoccupied lattice sites in the crystal. An electron could be caught in the field of this ion. The presence of such a foreign ion is not in itself sufficient to produce a trap, because, in an otherwise normal lattice, the ion would have to be neutralized. Dr. C. Herring has suggested to the author that a trap could be produced if the diamond contained both an interstitial foreign atom, and a trivalent atom in place of one of the carbons. Such a configuration would be electrically neutral; there would, however, be an unpaired electron on one carbon atom. Either of two things could conceivably occur: A valence electron from the foreign atom could pair off with the excess electron from a carbon, leaving the atom ionized, or the foreign atom could remain neutral, but an electron

[9] N. F. Mott and R. W. Gurney, *Electronic Processes in Ionic Crystals* (Oxford University Press, London, 1940), p. 108.

could be trapped by forming a bond between the trivalent atom and the unsaturated carbon. For the latter process, the foreign atom is not necessary. No calculations have been made of the trap depths to be expected from such a model, but depths of the order of 1/2 volt do not seem unreasonable. A hydrogenic trap in a medium of dielectric constant = 5 has a depth of 13.5/25 $\approx 1/2$ volt. If the shallow traps are produced by interstitial alkali atoms or trivalent substituted atoms, deeper traps could be produced by divalent atoms at interstitial and lattice positions.

For later work, we wish to know a function $G(x, x')$, which is defined by saying that $G(x, x')dx$ is to be the probability that an electron set free at a depth x' in the crystal will be trapped at a depth between x and $x+dx$. We assume that the lines of force are straight, although not necessarily of uniform density, and that x is measured in the direction of drift of electrons. For reasons discussed by Mott and Gurney,[10] the probability that an electron has not been trapped depends on the time since it was released, and this probability is

$$\exp(-t/T),$$

where T is a constant which depends upon the density of traps and their capture cross section. This implies that the drift velocity of electrons is less than their thermal velocity. If the electron is traveling in a field which is a function of position, t is clearly given by

$$t = \int_{x'}^{x} dx/vF.$$

Hence the probability that an electron is still free after traveling from x' to x is

$$\exp\left(-\int_{x'}^{x} dx/vTF\right).$$

The function $G(x, x')$ is the negative derivative of this quantity with respect to x, or

$$G(x, x') = (vTF)^{-1} \exp\left(-\int_{x'}^{x} dx/vTF\right). \quad (8)$$

Equation (8) assumes $x \geq x'$. If $x < x'$, $G(x, x') = 0$.

[10] See reference 9, p. 122.

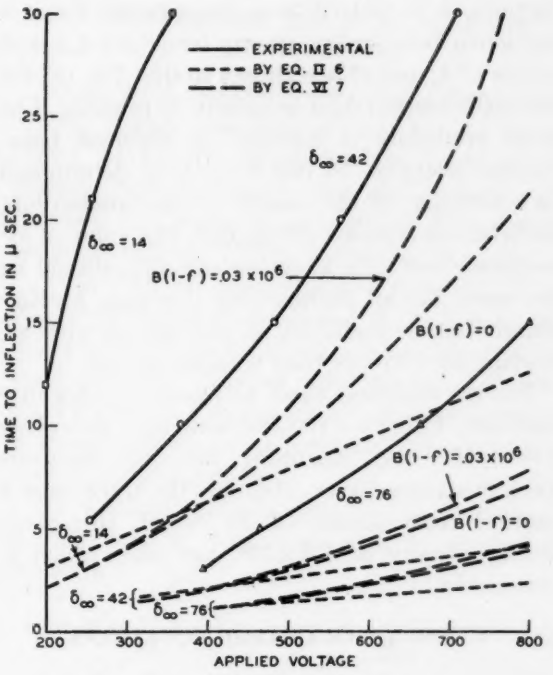

FIG. 3. Time to inflection *vs.* applied voltage.

$G(x, x')$ gives the probability of capture into some trap. The probability of capture into some particular type of trap is $G(x, x')$ times the relative number of traps of this type.

IV. EXPERIMENTAL DETERMINATION OF THE TRAPPING CONSTANT T

The trapping function $G(x, x')$ contains the unknown constant, T, which is to be interpreted as the mean life of an electron in the conduction band. McKay has measured T for the diamond which he is studying; we shall review his method briefly.

McKay defines a quantity δ, called the yield, which is the ratio of the current carried by conduction electrons to the bombarding current, when measured in a crystal free of space charge. δ should be given by the following formula, which was first derived by Hecht[11] in connection with photo-conductivity, and whose application to the present problem will be examined critically by McKay in his forthcoming paper:

$$(\delta/\delta_\infty) = (vTF/l)[1-\exp(-l/vTF)]. \quad (9)$$

l is the thickness of the crystal. In applying this

[11] K. Hecht, Zeits. f. Physik **77**, 235 (1932). Also, see Mott and Gurney, reference 9, p. 122.

formula, δ is plotted as a function of F for a particular bombarding energy (constant δ_∞), and values of δ_∞ and vT are chosen so that Eq. (9) fits the experimental data as closely as possible. The same procedure is followed at different bombarding energies. In this way, δ_∞ is determined as a function of the energy of the bombarding electrons. If formula (9) applies, the value of vT necessary to fit the experimental data should be the same for all bombarding energies. McKay found that he could fit all the curves with vT varying by no more than a factor of two.

For the diamond used, he found $vT \sim 6\times10^{-6}$ cm²/volt. Using $v=100$ cm²/volt sec., this gives $T=6\times10^{-8}$ sec. Assuming that the electrons have thermal velocity, and that the traps have a capture cross section of 10^{-16} cm², this gives a trap density of 1.7×10^{16} per cm³, which is reasonable.

V. THE SPACE CHARGE EQUATIONS

We are now in a position to set up the equations governing the accumulation of space charge in the diamond, and the current through it. We assume infinite plane-parallel geometry, so that we need only one space coordinate x. We take the origin of x to be at the boundary between the plasma layer and the rest of the crystal, and increasing as we go to the back face, which lies at $x=L$. As in Section III, we take the field F to be positive if it points in the negative x direction. We let n_s = density of electrons in shallow traps, with a probability B of thermal release per second, and let n_d = density of electrons in deep traps, with negligible probability of release. Let f be the ratio of the density of deep traps to the total trap density, and let j_0 = number of electrons leaving the plasma layer per cm² per sec. At equilibrium, j_0 is also the current measured externally.

We saw in the last section that the mean life T of an electron in the conduction band is about 6×10^{-8} sec. Since this is somewhat smaller than the times of observation, we make the crude but simplifying assumption that the elapsed time between the release and the trapping of an electron is negligible.

Consider now the quantities $(\partial/\partial t)n_s(x, t)dxdt$ and $(\partial/\partial t)n_d(x, t)dxdt$, which are the changes in time dt of the numbers of electrons in shallow and deep traps, respectively, contained in the distance dx at x. These quantities consist of three parts:

(a) Loss by thermal agitation. This equals $-Bn_s(x, t)dxdt$ for shallow traps, and zero for deep traps.

(b) Capture in dx of electrons released elsewhere by thermal agitation. In time dt, $Bn_s(x', t)dtdx'$ electrons are released from the interval dx'. Of these, $G(x, x')dx$ are captured in dx. Hence, the total number of such electrons caught in dx in time dt is

$$Bdxdt\int_0^x G(x, x')n_s(x', t)dx'. \tag{10}$$

The contribution by this mechanism for shallow traps is $(1-f)$ times expression (10), and for deep traps is f times (10).

(c) Trapping of electrons entering from the plasma layer. In time dt, j_0dt electrons enter the crystal, and the fraction trapped in dx is $G(x, 0)dx$. Hence, the contribution for shallow traps from this source is $(1-f)j_0G(x, 0)dxdt$, and for deep traps is $fj_0G(x, 0)dxdt$.

If we equate $(\partial/\partial t)n_s(x, t)dxdt$ and $(\partial/\partial t)\times n_d(x, t)dxdt$ to the sum of contributions 1, 2, and 3, and divide through by $dxdt$, we get the pair of integral-differential equations:

$$(\partial/\partial t)n_s(x, t) = -Bn_s(x, t)+(1-f)B\times\int_0^x G(x, x')n_s(x', t)dx' +(1-f)j_0G(x, 0); \tag{11}$$

$$(\partial/\partial t)n_d(x, t) = fB\int_0^x G(x, x')n_s(x', t)dx' +fj_0G(x, 0). \tag{12}$$

The function $G(x, x')$ is defined by Eq. (8), and involves, in addition to x and x', the field strength F at all points between x' and x. In addition to Eqs. (11) and (12), the quantities F, n_s, and n_d are further related by Poisson's equation:

$$\partial F/\partial x = (4\pi\epsilon/\kappa)(n_s+n_d). \tag{13}$$

Poisson's equation is subject to the restriction that the potential difference across the diamond

is fixed:

$$\int_0^L F dx = F_0 L, \tag{14}$$

where F_0 is the applied field. In other words, the mean value of the field is constant in time. The whole system of Eqs. (11) through (14) is subject to the initial conditions:

$$n_s(x, 0) = n_d(x, 0) = 0. \tag{15}$$

From $n_s(x, t)$ and $n_d(x, t)$, we wish to determine the current density $j(t)$ through the diamond. To do this, we observe that, in time dt, $j_0 dt$ electrons/cm² start across the crystal. Letting $n = n_s + n_d$, the number of electrons/cm² which travel the distance dx from x to $x+dx$ is

$$j_0 dt - dt \int_0^x (\partial/\partial t) n(y, t) dy.$$

Their contribution to the charge transferred in time dt is dx/L times this, so that the externally measured current density j is

$$j = \int_0^L \left[j_0 dt - dt \int_0^x (\partial/\partial t) n(y, t) dy \right] dx/L dt.$$

Canceling dt and reversing the order of integration gives

$$j = j_0 - L^{-1} \int_0^L (\partial/\partial t) n(x, t)(L - x) dx, \tag{16}$$

in electronic charges/cm²/sec.

The system of equations which we have just derived holds for either portion of the current curves shown in Fig. 2. From the viewpoint of these equations, the difference between the two portions of the curves arises from the behavior of j_0, the current density. During the first portion of the curve, when the field in the plasma layer is high, j_0 is a constant and equals $i_0 \delta_\infty$. When the field in the plasma layer becomes small, j_0 becomes dependent on the strength of this field. In principle, we could calculate the dependence of j_0 on field by solving for conditions in the plasma layer, but, in view of the diversity of possible mechanisms and the mathematical difficulties of solution, it is unlikely that the results would be reliable.

VI. THE CURRENT FOR HIGH FIELDS IN THE PLASMA

This section deals with the current through the crystal during the first portion of the curves shown in Fig. 2, which, on the basis of our present picture, means that the current j_0 is constant and equal to $i_0 \delta_\infty$, the total number of electrons released by the impinging electrons.

Even with the assumption of constant j_0, the system of equations developed in the last section is too complicated to admit simple solutions. We can, however, develop approximate solutions good for small t by assuming analytic solutions and using power series methods. The procedure is quite straightforward.

We assume that the densities of electrons in shallow and in deep traps can be written in the form:

$$n_s(x, t) = \sum_{i=1}^{\infty} a_i(x) t^i, \quad n_d(x, t) = \sum_{i=1}^{\infty} b_i(x) t^i. \tag{17}$$

The summations start at $i=1$ rather than at $i=0$ because both densities are initially zero, by (15). Substituting (17) into (13) and using (14), we find that $F(x, t)$ can be written as

$$F(x, t) = F_0 (1 + \sum_1^{\infty} f_i(x) t^i), \tag{18a}$$

where

$$f_i(x) = (4\pi\epsilon/\kappa F_0) \left(\int_0^x [a_i(y) + b_i(y)] dy - \int_0^L L^{-1} dx \int_0^x [a_i(y) + b_i(y)] dy \right). \tag{18b}$$

$F(x, t)$ occurs only as the reciprocal, so we must divide (18a) into unity. Upon doing so, we may write $F^{-1}(x, t)$ as

$$F^{-1}(x, t) = F_0^{-1} (1 + \sum_1^{\infty} f_i^{(-1)}(x) t^i), \tag{19}$$

where $f_1^{(-1)}(x) = -f_1(x)$, $f_2^{(-1)}(x) = f_1^2(x) - f_2(x)$, etc. It is next convenient to write $G(x, x')$ as a power series in t:

$$G(x, x') = (vTF_0)^{-1} \exp[-(x - x')/vTF_0] \times (1 + \sum_1^{\infty} g_i(x, x') t^i). \tag{20}$$

The $g_i(x, x')$ are evaluated by substituting series

(19) into Eq. (8), and expanding the resulting exponential. The first two of the $g_i(x, x')$ are:

$$g_1(x, x') = f_1^{(-1)}(x) - (vTF_0)^{-1} \int_{x'}^{x} f_1^{(-1)}(y)dy;$$

$$g_2(x, x') = f_2^{(-1)}(x) - (vTF_0)^{-1} \int_{x'}^{x} f_2^{(-1)}(y)dy + \tfrac{1}{2}(vTF_0)^{-2}\left[\int_{x'}^{x} f_1^{(-1)}(y)dy\right]^2 - (vTF_0)^{-1} f_1^{(-1)}(x) \int_{x'}^{x} f_1^{(-1)}(y)dy.$$

We have thus developed the function $G(x, x')$ as a power series whose coefficients are related in a known manner to the coefficients in series (17). Substituting, then, series (17) and (20) into Eqs. (11) and (12) gives us a recurrence relation for the coefficients $a_i(x)$ and $b_i(x)$. The series whose coefficients are thus obtained satisfies formally Eqs. (11) through (15). The first few coefficients are:

$$a_1(x) = (1-f)j_0(vTF_0)^{-1} \exp(-x/vTF_0),$$

$$b_1(x) = fj_0(vTF_0)^{-1} \exp(-x/vTF_0),$$

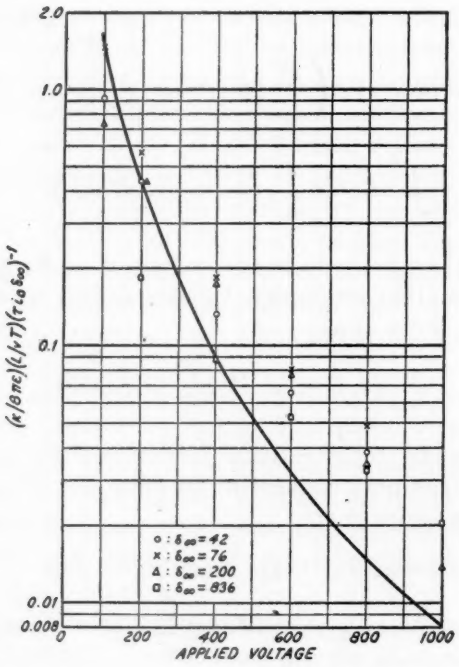

FIG. 4. Reduced half-life *vs.* applied voltage.

$$a_2(x) = -\tfrac{1}{2}Ba_1(x) + \tfrac{1}{2}(1-f)B(vTF_0)^{-1} \times \exp(-x/vTF_0) \times \int_0^x \exp(x'/vTF_0)a_1(x')dx' + \tfrac{1}{2}(1-f)j_0(vTF_0)^{-1} \times \exp(-x/vTF_0)g_1(x, 0),$$

$$b_2(x) = \tfrac{1}{2}fB(vTF_0)^{-1} \exp(-x/vTF_0) \times \int_0^x \exp(x'/vTF_0)a_1(x')dx' + \tfrac{1}{2}fj_0(vTF_0)^{-1} \exp(-x/vTF_0)g_1(x, 0).$$

Finally, the current j can be expanded in a series of the form

$$j = \sum_0^\infty J_i t^i. \tag{21}$$

The coefficients J_i are obtained in an obvious manner by substituting series (17) into Eq. (16). The first two of these coefficients are:

$$J_0 = j_0\lambda^{-1}(1-e^{-\lambda}),$$

$$J_1 = B(1-f)j_0[\lambda^{-1}(1-e^{-\lambda}) - e^{-\lambda}] - (4\pi\epsilon/\kappa) \times (j_0^2 vT/L)[\tfrac{1}{2}(1-e^{-2\lambda}) - \lambda^{-1}(1-e^{-\lambda})^2], \tag{22}$$

where $\lambda = L/vTF_0$. Both quantities in square brackets, for a given diamond, are functions only of the applied field, and are further non-negative.

We are also interested in computing $F(0, t)$, the electric field in the plasma layer. The reader can readily verify that it is given by

$$F(0, t) = F_0 - (4\pi\epsilon/\kappa)(j_0 - J_0)t + (2\pi\epsilon/\kappa)J_1 t^2 + \cdots. \tag{23}$$

By equating this to zero, we should obtain the time at which $F(0, t)$ becomes zero more accurately than we do from Eq. (6). We note from inspection of J_1 that the effect of thermal release of trapped electrons ($B>0$) is to increase this time, and, in fact, that if B is large enough, the field does not become zero in any time for which $F(0, t)$ is given accurately by three terms. However, if the initial derivative of the current is negative ($J_1<0$), we see that Eq. (23) has a root which is of the same order as that given by Eq. (6).

We can now get a rough comparison with

experiment by the use of Eqs. (22). If the current continued to decrease at its initial rate, we readily find that the time τ at which the current would have fallen to half of its initial value is found from

$$\tau^{-1} = -2J_1/J_0. \tag{24}$$

Values of τ have been estimated by McKay, from oscilloscope traces.

If we neglect B, we see that τ^{-1} is given by

$$\tau^{-1} = (8\pi\epsilon/\kappa) i_0 \delta_\infty (vT/L) \times [e^{-\lambda} - 1 + \tfrac{1}{2}\lambda(1+e^{-\lambda})] \tag{25}$$

from Eqs. (22). In other words, the quantity $(\kappa/8\pi\epsilon)(L/vT)(\tau i_0\delta_\infty)^{-1}$ should depend only upon λ, which in turn depends only on field strength for a particular diamond, and should not depend upon the energy of the bombarding electrons. This is tested in Fig. 4, in which the quantity in square brackets is plotted against applied voltage. If $vT = 5\times10^{-6}$ cm²/volt, and $L = 0.05$ cm, the relation between λ and V is $\lambda V = 500$ volts. The experimental values of $(\kappa/8\pi\epsilon)(L/vT)(\tau i_0\delta_\infty)^{-1}$ are also plotted for several values of the bombarding energy. The agreement is perhaps as good as could be expected, but it should be pointed out that for no values of the bombarding energy do the experimental values change as rapidly with V as is predicted.

An attempt was made to estimate a value for $B(1-f)$ by making the experimental points in Fig. 4 fit the theoretical curve as closely as possible. The required values of $B(1-f)$ turned out to be negative, and also to be roughly proportional to δ_∞, indicating a systematic discrepancy between experiment and the present theory.

We can, however, set an upper limit to $B(1-f)$ from the fact that the initial derivative of the current is negative in every situation which has yet been observed. If we compute the value of $B(1-f)$ in Eq. (22) which makes $J_1 = 0$, for various experimental conditions, we find that the smallest such value is 0.014×10^6 sec.$^{-1}$, or, in other words, the mean life for release of electrons from shallow traps by thermal agitation is of the order of 70 μsec. or greater.

Finally, we have also plotted in Fig. 3 the values of t at which $F(0,t)$ becomes zero, using Eq. (23), with $B(1-f) = 0$ and $B(1-f) = 0.03\times10^6$, using $j_0 = i_0\delta_\infty$. Since $B(1-f) < 0.014\times10^6$, the effect of thermal release upon this time is seen to be small. Most of the difference between Eqs. (6) and (23) does not come from the term quadratic in t, but from the fact that we have estimated the coefficient of t more accurately in (23) than in (6). The coefficient in (23) allows for electrons which cross the crystal without being trapped.

We mentioned in Section II that, if our theory is correct, it must lead to a negative second derivative for the current as long as the current density j_0 leaving the plasma is constant. To calculate the second derivative by extending the power series attack seems quite laborious and not justified at present. The following argument suggests strongly, however, that the second derivative is indeed negative, at least for small thermal release rates:

The current, according to Eq. (16), depends upon $\partial n/\partial t$, weighted by the factor $L-x$, and integrated over all x. Because of the weighting factor, what happens at the front face ($x=0$) is more important than what happens at the back ($x=L$). Accordingly, if $\partial^3 n/\partial t^3 > 0$ at $x=0$, we may expect that $\partial^2 j/\partial t^2 < 0$.

Neglecting thermal release, and adding Eqs. (11) and (12), we have

$$(\partial/\partial t) n(0,t) = j_0/vTF(0,t).$$

Differentiating twice with respect to t,

$$(\partial^3/\partial t^3) n(0,t) = (2j_0/vTF^3(0,t))(\partial F(0,t)/\partial t)^2 - (j_0/vTF^2(0,t))(\partial^2 F(0,t)/\partial t^2).$$

The first term of this is positive, since $F(0,t)$ is positive. By Eq. (23), $\partial^2 F(0,t)/\partial t^2 \approx (4\pi\epsilon/\kappa)J_1$ for small t, and is therefore negative whenever the initial derivative of the current is. Hence the second term above is also positive, and the second derivative of the current is probably negative for small t.

VII. CONDITIONS AFTER A LONG TIME

We are not in any position to discuss the approach of the current to equilibrium, having discovered no way to solve the necessary equations except numerically. Accordingly, we proceed at once to discuss equilibrium conditions.

Unless the fraction of traps which are deep is fairly large, we expect the crystal to approach

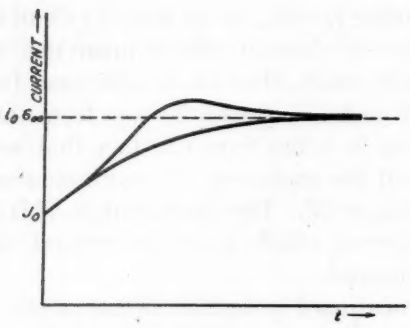

FIG. 5. Possible forms of the current if the thermal release rate is large. The current might also oscillate about the value $i_0\delta_\infty$.

in a fraction of a second a condition in which the loss of entering electrons by trapping is just balanced by thermal release from shallow traps. As the time increases, the number of electrons in deep traps increases, and finally becomes the dominating factor. On a time scale such that this effect is important, the electrons in shallow traps are released in negligible times, so that we may say that the final equilibrium is the balance between capture in and release from deep traps. We shall discuss only the first situation in which the deeply trapped electrons are negligible. That is, we assume that the behavior of all trapped electrons can be represented adequately by ascribing to them a probability $B(1-f)$ of release per second.

We take, then, Eq. (11), with $n_s=n$, and with $\partial/\partial t=0$. Solving Eq. (11) for j_0 under these conditions, using γ for the equivalent release rate $B(1-f)$, gives

$$j_0=\gamma vTF(x)n(x)\exp\left(\int_0^x dy/vTF(y)\right)$$
$$-\gamma\int_0^x n(x')\exp\left(\int_0^{x'} dy/vTF(y)\right)dx'.$$

Differentiating with respect to x shows that

$$(dF/dx)n+F(dn/dx)=0,$$

whence the product of F and n is a constant, which we write in the form $C/\gamma vT$:

$$F(x)n(x)=C/\gamma vT. \tag{26}$$

Inserting this back into the equation for j_0, we find that $C=j_0$.

Using Eqs. (13) and (14), and performing the necessary manipulations, we finally obtain

$$F_0L=\gamma(\kappa/12\pi\epsilon)(vT/j_0)([F^2(0)+(8\pi\epsilon/\kappa)\times(j_0/\gamma vT)L]^{\frac{3}{2}}-F^3(0)). \tag{27}$$

When j_0 is known as a function of $F(0)$, this can be solved numerically for $F(0)$, and other quantities of interest can be found by using the relations in Section V. For example, F can be computed as a function of x from Eq. (13), into which $n(x)$ is substituted from Eq. (26). $n(x)$ can then be computed by coming back to Eq. (26).

There are two general methods by which equilibrium may be attained, depending upon the size of γ. The first is the one which we discussed in Section II, in which $F(0)$ falls almost to zero, and j_0 becomes much smaller than $i_0\delta_\infty$. This is the only behavior which has yet been observed.

We see from Eq. (23), however, that if $J_1>0$ and is sufficiently large, $F(0,t)$ not only does not fall to zero, but begins to increase after a short period of decreasing. As long as deeply trapped electrons are negligible then, it seems unlikely that $F(0,t)$ will fall to zero at any later time. Therefore, j_0 always remains substantially equal to $i_0\delta_\infty$, and, since j_0 is the equilibrium current, there should be a second type of equilibrium in which the equilibrium current must equal $i_0\delta_\infty$. Further, the initial current must equal $i_0\delta_\infty\lambda^{-1}(1-e^{-\lambda})$, by Eq. (22), and hence the equilibrium current will be larger than the initial current.[12]

If this happens, the current *vs.* time curve must be like one of the forms sketched in Fig. 5. We cannot yet say which form it will follow; we can only say that, from conservation of charge,

$$\int_0^t jdt=i_0\delta_\infty t-\int_0^L n(x)dx, \tag{28}$$

for a value of t such that equilibrium is attained. $n(x)$ is evaluated by using Eq. (26).

VIII. TRAPPING AT THE ELECTRODES

A possibility which we have not yet discussed is that the space charge effects which cause the

[12] Compare with the discussion by F. Seitz in *Modern Theory of Solids* (McGraw-Hill Book Company, Inc., New York, 1940), p. 569.

current through the diamond to vary with time come from electrons (and/or holes) trapped at the boundary between the crystal and the electrode, rather than within the diamond. If the contact between the diamond and the electrode is not intimate, trapping at the surfaces may well be a dominant factor. With the gold-evaporated electrodes which have been used in all of the experiments witnessed by the author, we believe that surface trapping is unimportant compared with trapping in the volume. This conclusion is supported by at least two considerations:

(a) Enormous surface charges, or, alternatively, enormous times, would be required to produce appreciable space charge. If the field in the diamond is reduced to zero, all of the potential drop (called F_0L in the previous sections) is across the gap between the electrodes and the diamond. Calling the width of this gap D, the field E in the gap is $E=F_0L/D$. Assuming that all electrons released by the bombardment are trapped at the surface, the surface density of charge is $i_0\delta_\infty t$ electrons/cm^2, which must be equated to $E/4\pi\epsilon$. Hence:

$$t=F_0L/4\pi\epsilon D i_0\delta_\infty. \tag{29}$$

Taking typical values such as were used in Section II ($F_0=10$ e.s.u./cm, $L=0.05$ cm, $i_0\delta_\infty=6\times10^{16}$ electrons/cm^2/sec.), with D as large as 10^{-6} cm, gives $t\approx10^{-3}$ sec. In 1 μsec., which is of the order of the observed half-lives, space charge would change the field in the diamond by only about 0.1 percent.

(b) The hypothesis of surface trapping is incompatible with the conclusion reached in Section II, namely, that all the liberated electrons leave the plasma layer unless the field there is below 200 volts/cm. For, combining Section II with surface trapping would mean that the current would stay constant until the field in the plasma becomes small, and then would fall rapidly to a steady-state value. Further, the yield *vs.* voltage curves would not agree with Eq. (9), as they do, but would saturate at a quite low voltage.

Should occasion arise, one can construct a theory based on surface trapping as follows: The measured curve of initial yield *vs.* voltage is to be interpreted as giving the variation of j_0, the current leaving the plasma, with field at the front face. That is, the curve gives

$$j_0=j_0(F). \tag{30}$$

F is no longer a function of x.

If a surface charge of density σ is collected on one or both faces of the crystal, F and σ are related at any time by an equation of the form

$$F=aF_0-b\sigma, \tag{31}$$

where a and b are constants, and F_0 is the applied field. σ and j_0 are further related; if release of trapped charge is negligible, for example,

$$\sigma=\int_0^t j_0 dt. \tag{32}$$

Differentiating (31) and substituting for σ from (32), we get

$$dF/dt=(dF/dj_0)(dj_0/dt)=bj_0. \tag{33}$$

In view of (30), this can be integrated at once to give j_0 as a function of t.

IX. CONCLUSIONS AND SUGGESTIONS

There is at least qualitative agreement between the experimental results of McKay and the theory presented in the present paper. In assessing the success of the theory, it should be borne in mind that the theory contains no adjustable constants. All constants occurring are measured by methods independent of a space charge hypothesis. The theory was able to predict one result which was later confirmed experimentally, and it yields reasonable values for two independently measured physical quantities, namely, the initial slope and the time of inflection.

The calculations of Section II, which led to the conclusion that recombination and trapping in the plasma layer are negligible except at low fields, were based on certain assumptions about mobilities and cross sections. If these quantities, when measured, should be found to differ substantially from the assumed values, it might be necessary to revise the entire theory.

The postulation of the second type of equilibrium suggests an interesting experiment. The quantity γ depends exponentially upon temperature, so, by increasing the temperature, it may

be possible to achieve this type of equilibrium. This gives us first, a method of measuring δ_∞ which does not depend upon having an initially space charge free crystal. Second, by applying low fields to the crystal, we can measure directly the dependence of j_0 (at equilibrium) upon field strength. This same dependence may not hold, of course, for the ordinary temperatures at which the crystal is usually operated, but the information should none the less be theoretically valuable.

Finally, at ordinary temperatures, j_0 can be measured as a function of F_0, and the results used in Eq. (27) to determine j_0 as a function of $F(0)$. This is not a direct measure of $F(0)$, however, and should preferably be supplemented by other measurements.

We have emphasized the determination of j_0 as a function of $F(0)$ because it seems to us a good way of getting some information as to what goes on inside the plasma layer.

We are considerably indebted to various of our colleagues, particularly to Dr. R. W. Hamming, for a discussion of mathematical methods, and to Drs. McKay and Ahearn for extensive discussions of their experiments, and the bearing of the present theory upon them.

The data which we used in preparing Figs. 3 and 4 are from McKay's preliminary data, and are being carefully checked by him for later publication. It is thought that these data, although preliminary, are nearly enough correct so that use of the final data will not appreciably alter the theory or the conclusions drawn from it.

PHYSICAL REVIEW VOLUME 75, NUMBER 2 JANUARY 15, 1949

Absolute Voltage Determination of Three Nuclear Reactions

R. G. HERB, S. C. SNOWDON, AND O. SALA
University of Wisconsin, Madison, Wisconsin

(Received September 23, 1948)

A large electrostatic analyzer was used in conjunction with the Wisconsin electrostatic generator for an absolute voltage determination of the $Li^7(pn)Be^7$ threshold, an $Al^{27}(p\gamma)Si^{28}$ resonance, and a $F^{19}(p\alpha', \gamma)O^{16}$ resonance. Using absolute volts the values found are 1.882 Mev, 0.9933 Mev, and 0.8735 Mev, respectively. The uncertainties in the measurements appear to be about ± 0.1 percent.

INTRODUCTION

AN absolute measurement of the proton energy at the $Li(p\gamma)$ resonance was carried out by Hafstad *et al.*[1], using a calibrated resistor stack made up of I.R.C. metalized resistors. Parkinson *et al.*[2] checked this measurement and agree on a value of 0.440 Mev for the resonance energy with an estimated error of about two percent. Based on this determination, work at a number of laboratories lead to a number of secondary fixed points (i.e., $F(p\gamma)$ at 0.862 Mev and $Li(pn)$ at 1.856 Mev), which are used widely as reference voltages. Recently Tangen[3] has measured the $Li(p\gamma)$ resonance by the method used in reference (1) and has obtained 0.440 Mev with an estimated uncertainty of $\frac{1}{2}$ percent.

If one attempts to establish absolute voltage values above 1 Mv, the resistor method becomes difficult. In this case some form of electrostatic analyzer can be used to scale down the voltage to be measured by a factor of about 100. Hanson and Benedict[4] used an electrostatic analyzer, calibrated by an electron beam, to determine the following reaction energies: $Li(pn)$ at 1.883 Mev, $Be(pn)$ at 2.058 Mev, $F(p\gamma)$ at 0.877 Mev, and $Li(p\gamma)$ at 0.4465 Mev. An absolute calibration by direct calculation from the geometry was also

[1] L. R. Hafstad, N. P. Heydenburg, and M. A. Tuve, Phys. Rev. 50, 504 (1936).
[2] Parkinson, Herb, Bernet and McKibben, Phys. Rev. 53, 642 (1938).
[3] R. Tangen, Kgl. Norske Vid. Sels. Skrifter (1946) NRI.
[4] A. O. Hanson and D. L. Benedict, Phys. Rev. 65, 33 (1944).

used as a check. The absolute accuracy was thought to be about 0.3 percent.

At the University of Wisconsin a large 90° electrostatic analyzer was constructed in 1946[5] and has been in use for about two years. During this time excellent stability of equipment and reproducibility of results have been obtained. In this analyzer the plate separation is relatively large; therefore, an accurate measurement of the gap width is possible. Also, since the path length of the ion beam in the analyzer is about 1½ meters, the end corrections are small. Finally, since the geometrical measurements depend only on a ratio of two distances, the analyzer is self-compensating for temperature variations.

Although the consistency of Hanson's work was quite satisfactory, the departure of 1½ percent from the old values was disturbing. It was felt that another independent check should be made before shifting from the old Li 0.440-Mev standard. For the reasons indicated the Wisconsin equipment seemed well adapted for this purpose and hence was used to measure the Li($p n$) threshold, the Al($p\gamma$) resonance which on the old scale was at 0.985 Mev, and the F($p\gamma$) resonance. Measurement of the analyzer voltage together with the analyzer geometry gives an absolute determination of the proton energy at these points. As a check on the dependability of the results, the analyzer geometry was changed substantially after one series of runs and all the measurements were repeated.

MEASUREMENT OF VOLTAGE ON ANALYZER PLATES

From Fig. 2 it is seen that the aperture limiting slit and the exit slit, which are located in such a way as to reduce the end corrections, are at ground potential. The outer radius plate is raised to a positive potential and the inner radius plate to an equal negative potential. To supply the required potentials (±15 kv with 0.01 percent stability), work on an electronically regulated supply was initiated. Development work was under way at the time of these experiments but the requirements on voltage steadiness had not been met. However, experience with stacks of dry cells for this purpose had shown that they were practical where the current drains were small (one or two microamperes). Figure 1 shows the arrangement of the dry cell stacks* used in this work. The 5000 volt boxes were adjustable through 20 volts and each of the other boxes were adjustable through 10 volts except for the lower 500 volt boxes which could be adjusted from 0–500 volts continuously. A fixed resistor divider of manganin was used to compare this 500 volt box against a potentiometer.

The procedure in selecting a given analyzer plate voltage is as follows: (a) Choose a combination of battery boxes that gives approximately the required voltage; (b) adjust the lower 500 volt box in each stack to 500 volts;** (c) compare and balance the next 500-volt boxes with these boxes and adjust for zero circulating current (0.2 μa was detectable); (d) add the two 500-volt boxes together and compare with the 1000-volt box and so on until the stacks have been adjusted. The total voltage may be varied over a 500-volt range by resetting the potentiometer to

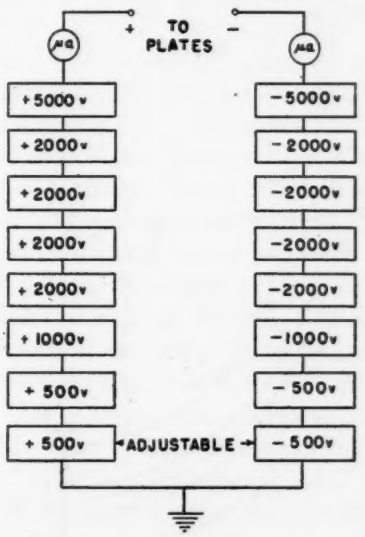

FIG. 1. Block diagram of battery stacks. Adjustable 500-volt boxes were set to any voltage below 500 volts by means of a potentiometer. The polarity of any of the boxes except the adjustable 500-volt box could be selected at will for comparison purposes.

[5] R. E. Warren, J. L. Powell, and R. G. Herb, Rev. Sci. Inst., **18**, 559 (1947).

* 5000 volt boxes used Eveready No. 493, 300 volt batteries. All other batteries were of the Burgess XX45, 67½ volt type except for several heavier duty batteries under continuous drain to provide continuous range of adjustments.

** The actual voltage is 504.08 Int. volts and is determined by the resistor divider ratio and the 1.50000 volt setting on the potentiometer.

a chosen value and then readjusting the lower 500-volt boxes for a balance.

The limitations on accuracy in the above procedure are discussed below.

1. Accuracy of balancing battery boxes. In each box used, an off-balance voltage of 0.01 percent was easily detected. The probable error in the total voltage introduced by imperfect balancing is therefore negligible.

2. The proton beam hitting the analyzer plates. This caused a current drain from the battery stacks of 1 μa or less during most of the measurements. The current was monitored continuously during each run and corrections to the battery voltages were computed from the measured internal resistance of the batteries.

In measuring the internal resistance of the batteries an unexpected difficulty was encountered. Even new batteries, recording full voltage when checked with a voltmeter draining about 50 μa, had resistances of about 100,000 ohms per kilovolt at current drains of less than 5 μa. Older batteries, in some cases, had many times this resistance. The resistance of each stack was measured several times during the course of the experiments by drawing 3 or 4 μa from each stack in turn through high voltage resistors, and determining the corresponding shift of the yield curves as plotted against potentiometer voltage. After the completion of the experiments the internal resistance of each box of batteries was determined by balancing two nearly equal boxes and measuring with a potentiometer the change in voltage caused by a drain of one or two microamperes from one of the units. Both methods of measurement gave consistent results. Therefore, in correcting for the current drain from the battery stacks, it is estimated that the uncertainty in battery resistance can cause an error no greater than 0.01 percent.

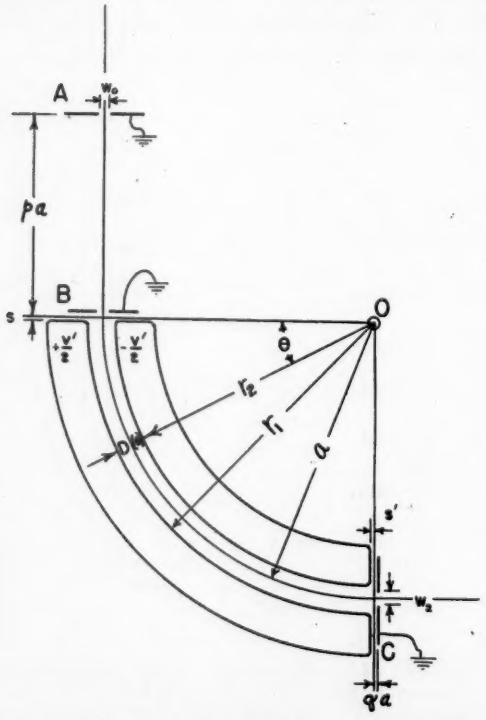

FIG. 2. Outline of electrostatic analyzer with plate separation highly exaggerated. Slits A, B, and C are the entrance slit, aperture limiting slit, and exit slit respectively. Note that p and q are dimensionless measures of the quantities they describe. Point O is the center of curvature. Distances S and S' are the distances to the effective entrance and exit planes of the analyzer from the ends of the analyzer. The angle Φ between these two planes is the total analyzer angle. Radius a is the geometric mean of r_1 and r_2. Magnetic fields are considered as positive if directed up from plane of paper.

3. Leakage currents from stacks to ground connections on battery boxes. This current was monitored with a suitably placed microammeter and at all times it was kept below $\frac{1}{2}$ μa. Taking the most unfavorable case of the first run on Li where several poor batteries were included in the stacks and the entire stack voltage ($\pm$15 kv) was used, the internal resistance amounted to about 5 megohms. This gives an error in the battery stack voltage of about 0.015 percent.

4. Drift of the battery voltage during run. This was accounted for by measuring the resulting off-balance currents in a recheck of the battery stacks after each run. The drifts were no greater than 0.01 percent and an attempt was made to correct for them by assuming a linear drift from the beginning of each run.

5. Standard cell used in potentiometer. A comparison intercheck of the standard cell used in these experiments with two auxiliary standard cells calibrated at the University of Wisconsin Standards Laboratory*** indicated that the value used was accurate to about 0.01 percent.

6. Potentiometer used to adjust variable 500-volt battery boxes. In setting up the battery stack, the two variable 500-volt boxes are first

*** Standard cells at the Wisconsin Standards Laboratory are regularly checked at the National Bureau of Standards.

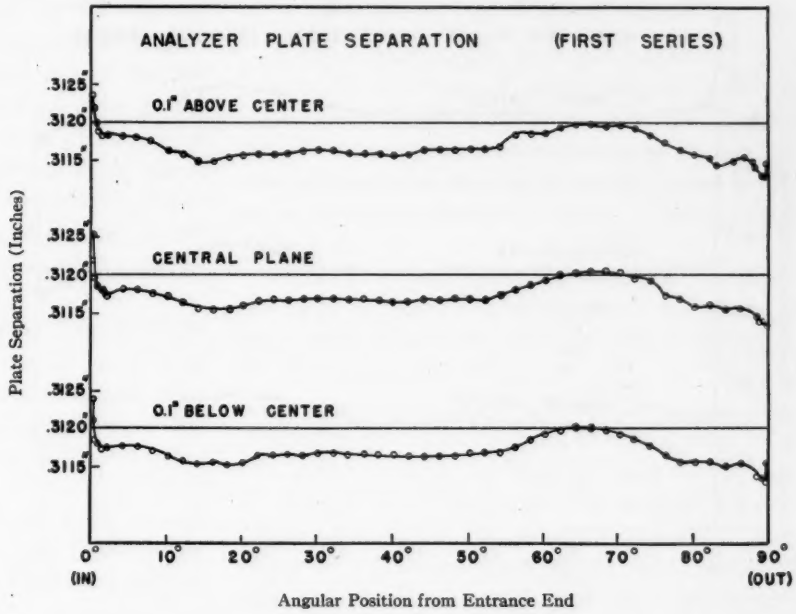

FIG. 3. Measurements of analyzer plate separation as a function of the angle θ from the analyzer entrance taken after first series of runs.

adjusted to 500 volts by means of a voltage divider and a potentiometer set at 1.50000 volts. These 500 volt values are then used as units in balancing against the other boxes; hence, any percentage error in the 1.50000 volt potentiometer setting causes the same percentage error to appear in the total battery voltage. All other settings of the potentiometer scale, which are used only to vary the two 500-volt boxes, need not be known as accurately as the 1.50000 volt point since large voltages are in series with the 500 volt boxes.

To insure the correctness of the 1.50000 volt setting, the Rubicon potentiometer used in the experiments was carefully interchecked with a Type K-1 Leeds-Northrup potentiometer. This included a check of the accuracy of transfer of the standard cell dial settings to the e.m.f. dial settings and a subsequent test of the linearity of the e.m.f. readings through the zero setting. It was concluded from these tests that the Rubicon potentiometer gave correct voltage readings within ± 0.00001 volt for any setting from 0.00010 volt to 1.50000 volts. The interval, 0.00000 to 0.00010 volt, apparently had the correct total resistance but its variation with respect to the dial setting was in error; it indicated, for instance, that the zero voltage occured at a setting of 0.00005 volt. Since an error of ± 0.00001 volt at 1.50000 volts is a negligible percentage error the percentage error at this setting is given directly by the standard cell percentage error.

7. Resistor divider used to compare the variable 500 volt boxes with the standard cell. After the measurements were completed the resistor divider was sent to the National Bureau of Standards for calibration. There the divider was studied under varying conditions of humidity over the voltage range which had been used. A change in voltage from 100 volts to 500 volts changed the ratio from 336.061 to 336.046 or 0.0045 percent. A measurement of the ratio after 23 days in a desiccator and then after 32 days in an atmosphere of 83-percent humidity indicated a change in the ratio of 0.005 percent. The Bureau's estimate of error in the ratio was 0.015 percent. Since the percentage error of each of the above effects causes an equal percentage error in the total battery voltage the net uncertainty in the battery voltage may be found by taking the square root of the sum of the squares of the above percentage errors. This gives about 0.03 percent.

GEOMETRICAL MEASUREMENT ON ANALYZER

An examination of the electrostatic analyzer theory given by Warren *et al.*[5] shows that the quantities described below must be measured (see Fig. 1).

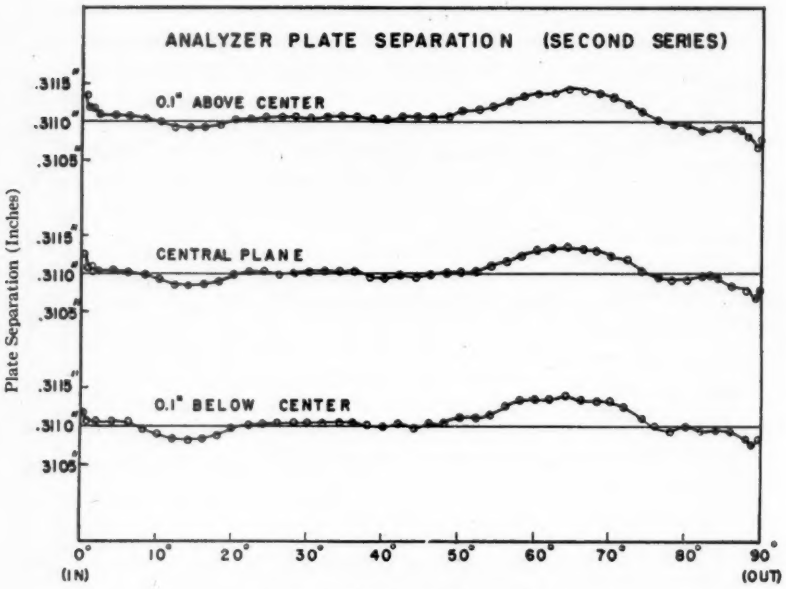

FIG. 4. Measurements of analyzer plate separation taken after second series of runs.

1. Radius of inner and outer plates. To measure the radius contour of each plate a reference gap constructed from gauge blocks was set up and aligned at the entrance end of the analyzer. Using an adjustable parallel and several combinations of gauge blocks for checking consistency, the distance between the near end of the reference gap and the pivot ("*O*" Fig. 2) was blocked out reproducibly to 0.002″ out of 40″ or to 0.005 percent. To measure the radius contour of each plate a dial gauge was mounted rigidly on a heavy bar. This bar was free to move about the central pivot "*O*" and was supported at its extremity by a wheel resting on the ground machinists' surface plate which supports the analyzer. Dial gauge readings were taken on each of the two surfaces as a function of angle at several different heights over the region of the central plane. Comparison readings on the surfaces of the reference gap were made repeatedly. These measurements were not used to determine the separation contours since a second series of measurements described below proved more dependable. They did serve as a rough check on the plate separation contours and were needed in work on the corrections to show that the effects of a tangential electric field were negligible.

2. Plate separation. A dial gauge with two contact points (something like a small inside micrometer) which directly measured the plate separation was used to measure the plate separation contours. Its mount was similar to the previous case except that it was held in a suspension which assured uniform contact pressure on both plates and measurement of the perpendicular distance between the plates. Reference gap readings were taken before and after each series of measurements at a given elevation in the analyzer gap. Figures 3 and 4 show the plate separation data taken in the central plane and 0.1″ above and below this plane for each of the two series of runs. It is seen that 0.0001″ was reproduced dependably. Since the gap was about 0.312″ the uncertainty in plate separation appears to be about 0.03 percent. There is a net reproducible fluctuation in the plate separation of about 0.0005″. This does not contribute to the error since a method of allowing for small variations in plate separation was used in the calculations.

3. Position of the centers of the entrance slit, aperture limiting slit, and exit slit. The position of the center of the entrance slit had to be known with respect to the intersection of the geometric mean plate radius and the effective plane defining the entrance to the analyzer (see Appendix I for definition of this effective plane). From (1) the geometric mean radius may be considered as known. Triangulation measurements then were made from this point and from the pivot point "*O*" to the center of the entrance slit. These

measurements were complicated by the slit container, but, after a series of careful measurements, the final uncertainty in the position of the entrance slit was estimated to give an error in the energy determination of about 0.01 percent.

The distance from the aperture limiting slit to the analyzer entrance could be measured to about 0.002″. An error in the location of this slit of this amount gives a corresponding error in the energy of 0.002 percent.

The distance from the exit slit to the exit of the analyzer plates affects the end correction in such a way as to change the magnification (see Appendix III). Since this only changes the amount of other corrections it is of second order importance.

4. Analyzer angle. The analyzer angle has an effect on the energy corrections only through the magnification, hence, as above, errors are only of second order importance.

5. Width of the opening of all slits. The slit openings, each of which could be measured to 0.001″, do not affect the mean energy determinations except in the case of the aperture limiting slit. Here an error of 0.001″ produces, through a change in the end correction, 0.0001 percent error in the energy. The effect of the opening of the slits is to give a triangular energy distribution to the proton beam at the exit of the analyzer, the total width of which is $4\cdot(300/8)\cdot(W_0/a)$ percent (see Eqs. (6) and (7)), where W_0 is the entrance slit width and a is the geometric mean radius. Thus the total energy spread is 0.075 percent of the mean energy since, in our case, $W_0=0.020''$ and $a=40''$.

6. Rounding of the corners at the ends of the analyzer plates. Since the radius of curvature of the corners (approximately $\frac{3}{16}''$) is about the same as the distance between the aperture limiting slit and the ends of the analyzer plates, it was felt that the effective position of the analyzer entrance plane might be calculated incorrectly if square corners were assumed. Appendix I gives briefly the details of the calculation, showing that the rounding effect results in a correction of only 0.001 percent.

The net uncertainty in the proton energy measurement due to the geometrical factors enumerated above is estimated to be about 0.04 percent.

MAGNETIC FIELD MEASUREMENTS

A small rectangular flip coil connected to a Leeds and Northrup Type R galvanometer was used to explore the magnetic field in the analyzer gap. Because of the low resistance of the flip coil the galvanometer was highly damped, and served as a sensitive fluxmeter (0.15 gauss per mm deflection).

Both the vertical and horizontal components of the magnetic field were measured as a function of angular position within the gap and as a function of distance between the entrance slit and the analyzer entrance. The analyzer plates were magnetized in a peculiar fashion, both components of the field reversing sign several times throughout the length of the analyzer. The average vertical component within the analyzer was 0.12 gauss upward and varied from about +0.3 gauss to −0.2 gauss. The average horizontal component was about 0.25 gauss but varied by as much as 9 gauss. The horizontal component was assumed to have no effect and the vertical component was treated as uniform, with a value equal to its average. Outside the analyzer the vertical component of the magnetic field averaged to 0.47 gauss downward. This varied from 0.35 gauss at the entrance slit to 0.61 gauss at the analyzer entrance. Again the average value was used and a uniform field was assumed. The horizontal component was less than 0.1 gauss and was also neglected.

From Eq. (2), the energy correction introduced by the magnetic field within the analyzer is about −0.008 percent for a 1 mv proton beam. Equation (4) gives +0.011 percent for the correction due to the magnetic field outside the analyzer. The total correction is then 0.003 percent and was neglected.

TARGET TECHNIQUES

In order to obtain reproducible results it was essential to maintain targets at elevated temperatures and to place a liquid air trap in the vicinity of the target.[6] In this work the targets were heated to 200°–250° Centigrade. The Li targets were prepared by evaporating lithium onto previously baked out tantalum backings. Exposure to air then permitted oxidation.

[6] R. S. Bender, F. C. Shoemaker, and J. L. Powell, Phys. Rev. 71, 905 (1947).

The thin Al targets were prepared by evaporating known quantities of aluminum onto prepared tantalum backings. They also were exposed to air before bombardment. Oxidation was probably complete for the target of 200 volts absorption thickness but the thicker targets probably were not completely oxidized.[7] Both the thin and thick Al targets were, in reality, composite targets and a knowledge of the thickness of each layer would be necessary to determine the true resonance position from the yield curves. No correction was made for the thick target because of the unknown amount of oxide. A correction was attempted for the thin targets since these targets were either completely or almost completely oxidized. The thin target measurements should then permit an estimate of the oxide on the thick target. The data were not sufficiently consistent to give this thickness; however, each set of runs on Al was consistent to a few hundredths of a percent so it was assumed that the oxide film on the thick target did not introduce uncertainties of more than 0.02 percent.

For the fluorine target, CaF_2 was evaporated onto the tantalum backings after previously fusing it in a beryllium oxide crucible. Exposure to air was permitted before bombardment but, presumably, this did not affect the target. A fine mesh platinum gauze covered the CaF_2 crystal which was used for the thick target. This prevents an accumulation of charge on the crystal which might give an erroneous resonance energy value.[8]

EVALUATION OF PROTON BEAM ENERGY

An elementary description of the ion dynamics in the present analyzer has been given by Warren *et al.*[5] Since we are concerned with an absolute calibration the details necessary to evaluate all the corrections will be given. First, the ideal analyzer, having infinitesimal slit widths and no fringing fields will be considered relativistically. Corrections to this theory caused by improper slit alignment, finite slit width, irregular contours of analyzer plates, fringing electric fields, and the presence of a small magnetic field both inside and outside the analyzer will be calculated nonrelativistically. The ideal analyzer is considered to have an electric field determined inside by the simple equations for concentric cylinders, and outside to have zero field (i.e., no end effects and perfect radial contours). Appendix II shows that, for the conditions present in this analyzer, the relation that holds for the ideal path (i.e., radius equal to geometric mean of inner and outer radii of analyzer plates) is

$$\tfrac{1}{2}V' = V_0(1-\gamma)\frac{d}{b}, \tag{1}$$

where

$\frac{1}{2}V'$ = positive battery stack voltage (negative stack is of same magnitude),
V_0 = proton energy in volts,
d = plate separation,
b = arithmetic mean of inner and outer radii,
$\gamma = V_0(\text{mv})/1880$.

For a given physical arrangement of the aperture limiting slit and exit slit, Appendix I shows that there exist effective planes at which the electric field inside the analyzer may be thought of as terminating. Outside these planes the electric field is zero and inside it has the value determined by a geometry of two concentric cylinders. The aperture limiting slit has no effect on the passage of an ion through the analyzer other than partially determining the position of the effective entrance plane and limiting the angular spread of the beam. On the other hand, the exit slit not only determines the position of the effective exit plane but its opening partially determines the energy spread of the emergent beam.

The first order focusing theory is concerned with the motion of the particles in the neighborhood of $r=a$ (paraxial rays in optical terminology). Appendix III shows that the effect of a small vertical component of a magnetic field inside the analyzer is to change Eq. (1) into:

$$\tfrac{1}{2}V' = V_0(1-\gamma)\cdot\left(1+\frac{eaB_i}{c(2emV_0)^{\frac{1}{2}}}\right)\cdot\frac{d}{b}, \tag{2}$$

where Gaussian units are used and e is the proton charge, B_i is the vertical (positive upwards in Fig. 2) component of the magnetic induction, c is the velocity of light, a is the geometric mean radius of the plates, and m is the proton mass.

[7] Private communication, F. C. Shoemaker.
[8] E. J. Bernet, R. G. Herb, and D. B. Parkinson, Phys. Rev. 54, 398 (1938).

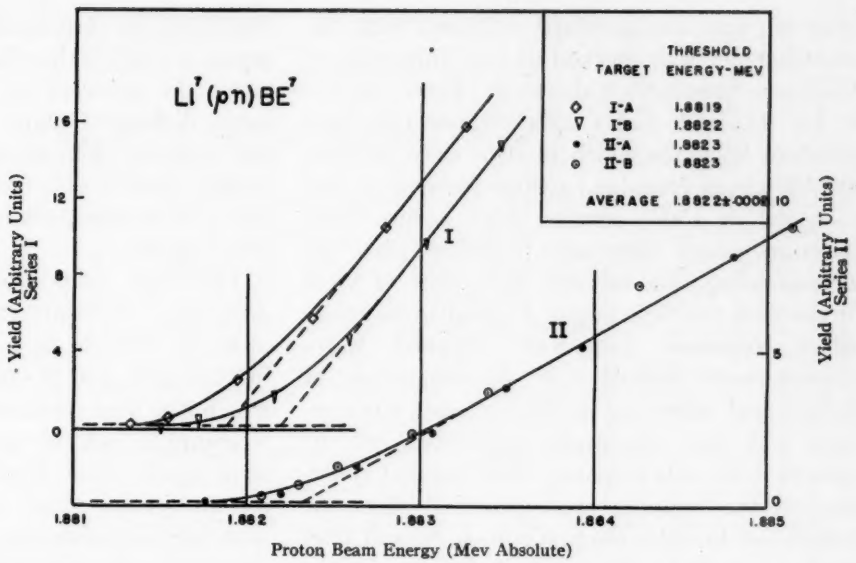

FIG. 5. Neutron yield curves for both series of measurements of Li(p,n) threshold reaction.

Appendix III also shows that ϵ, the fractional correction to the energy V_0 caused by improper location of the slits and presence of a small magnetic field exterior to the analyzer, is given by Eq. (37). This may be separated into part (a), the contribution due to the improper location of the slits,

$$\epsilon_s=(2/1-M)(x_2-Mx_0), \tag{3}$$

where x_0 and x_2 measure the perpendicular distances from the ideal path of an ion to the centers of the entrance and exit slits respectively. The ideal path is taken to be the circle of radius a within the analyzer and the straight lines tangent to this circle at the effective entrance and exit planes. x_0 and x_2 are measured in units of a and are positive if they correspond to an increase in radius over the ideal radius a. M is the analyzer magnification as explained in Appendix III. Part (b), the fractional energy shift caused by the presence of the external magnetic field B_0, is given by:

$$\epsilon_m=\frac{p}{1-M}\left(\frac{\partial M}{\partial\Phi}-pM\right)\frac{eaB_0}{c(2emV_0)^{\frac{1}{2}}}, \tag{4}$$

where p is the distance between the entrance slit and the effective entrance plane measured in units of a.

The conditions necessary for Eqs. (3) and (4) to hold are that the distance between the exit slit and the effective exit plane be very small, as is the case in the present analyzer, and that the plate separation d in Eq. (2) be taken as the following weighted mean:

$$d=\frac{\sqrt{2}}{1-\cos\sqrt{2}\Phi}\int_0^{\Phi}D(\theta)\sin\sqrt{2}(\Phi-\theta)d\theta. \tag{5}$$

The fact that x_0 and x_2 in Eq. (3) should be measured to the center of the slits can be seen by considering a plot of x_2 versus x_0 with ϵ_s as a parameter. From this plot and the assumption that the number of protons per unit energy range is constant over the range of energies accepted by the analyzer, it is evident that in the general case the energy distribution at the exit of the analyzer has the form of a symmetrical truncated triangle. If, as was approximately the case in the present analyzer, the relation between the entrance slit width W_0, and the exit slit width W_2 is

$$W_2=-MW_0, \tag{6}$$

where M is the magnification ($M\cong-0.60$), then the energy distribution at the exit of the analyzer has the form of an isosceles triangle. In this case the total energy spread is given by

$$\epsilon_t=-4(M/1-M)(W_0/a). \tag{7}$$

EXPERIMENTAL PROCEDURE

The electrostatic analyzer was opened up, cleaned, and geometrical measurements were taken to estimate the difficulty in making final precise measurements. Before starting the first

series of runs, the standard cell used with the potentiometer was checked at the University of Wisconsin Standards Laboratory. Fresh targets of Li, Al, and CaF_2 were evaporated onto tantalum backings which in turn were inserted into the target chamber; a thick piece of Al and a crystal of CaF_2 covered with a fine mesh platinum gauze were also inserted with the corresponding thin targets. A number of yield curves with the first target, Li, had to be taken before consistent data were obtained. Early measurements showed that the magnitude of the internal resistance of the batteries was very large and that continuous monitoring of the current drain was required. The internal resistance of the batteries was measured after the first run on Li, after the first run on Al, and after the last run on Li, the order of the experiments being Li, Al, and F for the first series and F, Al, and Li for the second series. Reasonable estimates then were made in order to get the internal battery resistance after each run.

After the first series of yield curves were obtained (Figs. 5, 6, 7) the analyzer was opened and accurate geometrical measurements were made. Because of preliminary difficulties, extensive running time was required for these first yield curves. The ion beam bombardment had caused the formation of a hard black tarnish or deposit on the plate surfaces in the plane of the ion beam. It was felt that this deposit might seriously affect the accuracy of the measurements. The outer deflecting plate then was removed and the working surfaces of both plates were thoroughly cleaned with crocus cloth. All the tarnish and a small thickness of metal were removed in this cleaning.

The outer plate then was replaced with no attempt to duplicate the previous separation, in order to provide as completely as possible an independent set of measurements. The slits, which had been removed, now were replaced and a complete set of geometrical measurements were again taken. Fresh targets were prepared for the second series of runs which were taken with but little difficulty (Figs. 5–7). The running time was approximately a factor of 10 shorter than for the first series. An examination of the plates after completion of this work showed very little deposit on the plates. The satisfactory check obtained between the two series of runs indicates, in particular, that the deposit on the plates did not cause serious inaccuracies.

In addition, a careful exploration of the magnetic field between the analyzer plates and along the path of the ion beam from the entrance slit to the entrance of the analyzer was made with a small flip coil. Finally, the potentiometer

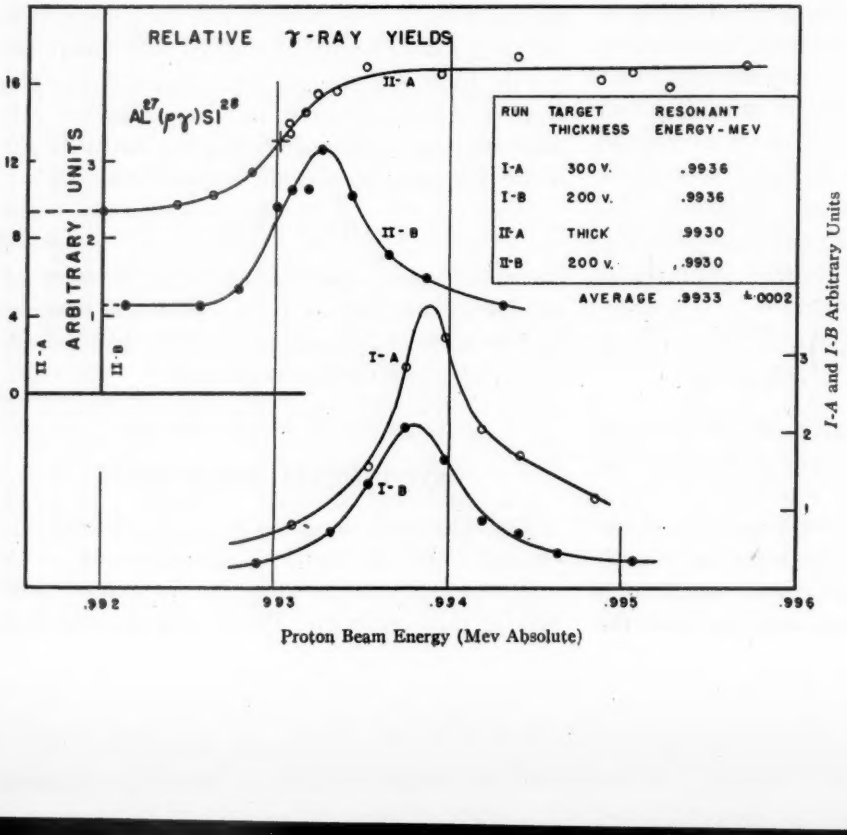

FIG. 6. γ-ray yield curves for both series of measurements of $Al(p\gamma)$ resonance reaction. Yield values are all on same relative scale.

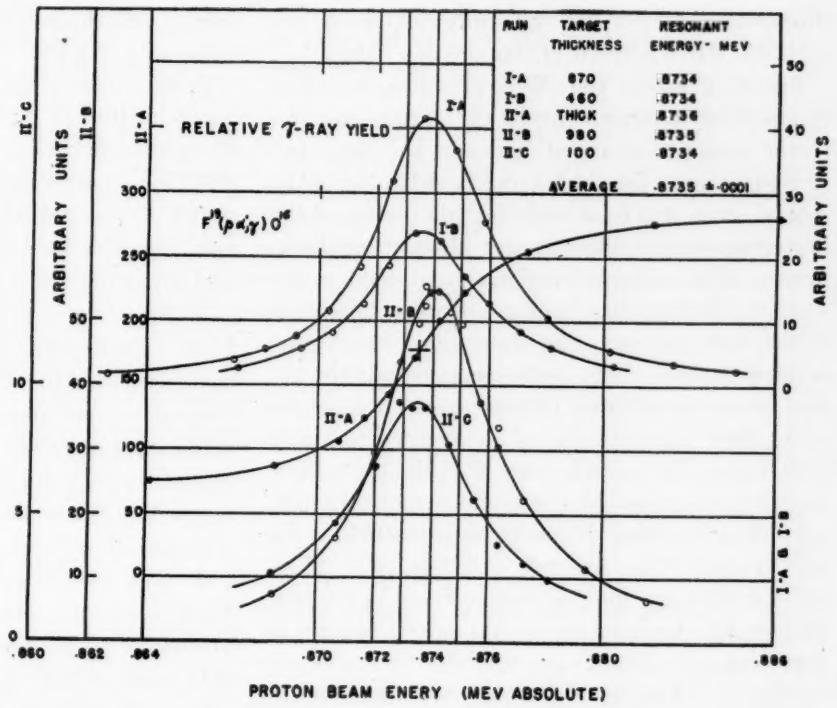

FIG. 7. γ-ray yield curves for both series of measurements of $F(p\gamma)$ resonance reaction. Yield values are all on same relative scale.

linearity was examined, the standard cell again was checked at the Wisconsin Standards Laboratory, the internal resistance of each battery box was measured at low drain, and the resistor divider was sent to the National Bureau of Standards for calibration.

EVALUATION OF DATA

The following corrections were applied to the experimental data: (1) correction for drift of the battery stack voltage, (2) correction for a change in the battery stack voltage caused by current drain from the stacks to the analyzer plates through the internal resistance in the battery stacks, and (3) correction for a shift in the resonance voltage of a thin target of finite voltage absorption thickness with respect to that of an ideally thin target of zero absorption thickness.

To convert potentiometer readings to battery stack voltages the resistor ratio for the lower 500-volt boxes as given by the Bureau of Standards was used in connection with the known number of additional battery boxes. Using the weighted mean plate separation (Eq. (5)) as found from Figs. 3 and 4 and the measured arithmetic mean radii of the plates, Eq. (1) gave the proton energies measured in volts corrected for relativistic effects and irregular contours of the plates. These voltages were then corrected for the measured deviations of the slit centers from their ideal positions (Eq. (3)) and for the magnetic fields both inside (Eq. (2)) and outside (Eq. (4)) the analyzer. Since the standard cell voltage was in international volts, all the values were increased by 0.033 percent to convert to absolute volts.

Both series of Li are shown in Fig. 5. The neutrons were counted by a BF_3 counter with about $\frac{1}{2}''$ of paraffin between the target and the counter. The finite energy spread of the proton beam accounts for the tails on the curves. If the cross section for the reaction were constant above the threshold, if the targets were uniform, and if the detector were energy insensitive, the yield curve would be linear after all the protons in the beam were energetic enough to cause the reaction. The curves do appear to have a reasonably linear portion and they were therefore extrapolated back to give the thresholds. Since the rounded tails of the curves extend over a region approximately equal to the total energy spread of the beam, this method appears to be justified. The average value of the threshold voltage for the four separate runs is 1.8822 mv where all

threshold voltages for the individual runs are within ±0.016 percent of the average value.

Figure 6 shows the $Al^{27}(p\gamma)$ resonance. The geometrical arrangement of the target and detector was not changed between the first and second series so the thick target yield curve of the second series was used with the thin targets of the first series to calculate target absorption thicknesses. With the reservations mentioned under Target Techniques, giving an uncertainty of about 0.02 percent, the data give four independent values of the resonance energy. For the first series of two thin targets these energies are very close together giving an average value of 0.9936 mv. The second series of a thin and a thick target gives resonance energies which are also very close together with a value of 0.9930 mv for the average. The average of these two values gives 0.9933 mv for the resonance energy where all individual values are within ±0.03 percent of this average.

Figure 7 shows the $F^{19}(p\gamma)$ resonance. In the first series two thin targets were used and in the second series a thick CaF_2 crystal was used in addition to two thin targets. Since the geometry of the detector and target was not changed between each series, the thick target was used to give the thin target absorption thicknesses for each series. The CaF_2 targets may be considered as simple targets as opposed to the composite targets of the previous case; therefore, the target absorption thickness may be calculated from much simpler considerations. The average value of the resonance energy for the five separate runs is 0.8735 mv where all individual values are within ±0.015 percent of this value.

DISCUSSION OF RESULTS

As a basis of comparison, several measurements of reaction energies in the voltage range considered are summarized as follows:

1. Based on Tangen's[3] value of 503 kv for a weak Al($p\gamma$) resonance which in turn was based on Tangen's absolute measurement of 440 kv for the Li($p\gamma$) reaction, Broström *et al.*[9], using a generating voltmeter whose linearity was checked with H^+, HH^+, and HHH^+ ions, obtained a value of 986 kv for a prominent Al($p\gamma$) resonance. A very strong doublet resonance occurred at a mean value of 1.375 mv.

2. Based on a value of 440 kv for the Li($p\gamma$) reaction, Bernet *et al.*[8] used a generating voltmeter whose linearity was checked with H^+, and HH^+ ions, and obtained a value of 862 kv for the strong F($p\gamma$) resonance. Care was taken to prevent the thick target crystal, CaF_2, from charging up by placing a fine mesh gauze over the crystal.

3. Based on a value of 862 kv for the strong F($p\gamma$) resonance where the CaF_2 crystal was covered with a nickel gauze, Plain *et al.*,[10] using a generating voltmeter, determined a secondary calibrating point of 1.368 mv at the strong Al($p\gamma$) resonance. A value of 505 kv was obtained for a weak Al($p\gamma$) resonance and a value of 985 kv for a strong Al($p\gamma$) resonance.

4. Based on a value of 862 kv for the strong F($p\gamma$) resonance, Haxby *et al.*,[11] using a generating voltmeter whose linearity was checked with H^+, HH^+, and HHH^+ ions, obtained a value of 1.856 mv for the Li(pn) threshold and a value of 2.028 mv for the Be(pn) threshold.

5. Hanson *et al.*,[4] using an electrostatic analyzer for an absolute calibration, find a value of 1.883 mv for the Li(pn) threshold. Using the electrostatic analyzer as a comparator they find a value of 2.058 mv for the Be(pn) threshold, a value of 877 kv for the strong F($p\gamma$) resonance, and a value of 446.5 kv for the Li($p\gamma$) resonance.

6. The present results give a value of 1.8816 mv for the Li(pn) threshold, a value of 873.2 kv for the strong F($p\gamma$) resonance, and a value of 993.0 kv for a prominent Al($p\gamma$) resonance. All the above values are given in international volts. Using absolute volts (1 international volt = 1.000330 absolute volt) the present results are 1.882 mv, 873.5 kv, and 993.3 kv for the Li, F, and Al reactions respectively.

An examination of the above results shows that there is a discrepancy of about 1.5±0.5 percent between the points based essentially on the resistor stack calibration and those based on the electrostatic analyzer calibration. It is suggested that target difficulties may be responsible for the

[9] K. J. Broström, T. Tuus, and R. Tangen, Phys. Rev. **71**, 661 (1947).

[10] Plain, Herb, Hudson, and Warren, Phys. Rev. **57**, 187 (1940).

[11] Haxby, Shoup, Stephens, and Wells, Phys. Rev. **58**, 1035 (1940).

±0.5 percent fluctuations; however, the 1.5 percent discrepancy remains unresolved.

The value of 440 kv for the Li($p\gamma$) resonance was given with an estimated uncertainty of 2 percent by Hafstad *et al.*,[1] and by Parkinson *et al.*,[2] while recently Tangen[3] has given the same value with an estimated uncertainty of about ½ percent. Hanson *et al.*,[4] felt that their uncertainties were about 0.3 percent, whereas, in view of the over-all consistency of the thin and thick target data and the reproducibility of the electrical and the geometrical measurements, it was felt that the uncertainties of the present work were about ±0.1 percent. However, some pertinent factor might have been overlooked, and another independent determination of these values would be desirable.

ACKNOWLEDGMENTS

The authors wish to acknowledge the generous assistance of Messrs. Dorr Ralph and Gerson Goldhaber in several phases of the work. One of us (O.S.) wishes to acknowledge the support given by the Rockefeller Foundation. The work was supported in part by the Atomic Energy Commission and in part by the Wisconsin Alumni Research Foundation.

APPENDIX I. DETERMINATION OF EFFECTIVE ENTRANCE AND EXIT PLANES OF ANALYZER

The factors influencing the position of the planes where the internal electric field may be thought of as terminating are: (a) The locations of the aperture limiting slit and exit slit, (b) the finite size of the opening in the slits, (c) the rounding of the corners of the analyzer plates, and (d) the radius of curvature of the analyzer plates. Herzog[12] has discussed effects (a) and (b). A slight but tedious modification using a rounded corner transformation[13] allows an estimate of the third effect. Since the above effects were estimated using plane parallel geometry for the analyzer plates, the effect of the radius of curvature was not investigated but probably only changes the above corrections by a fraction of the order of the plate separation divided by the radius of curvature (i.e., approximately 1 percent) and hence was neglected.

Referring to Figs. 2 and 8, let S_0 be the value of S when $r=0=w$ (i.e., for zero slit opening and no rounding of the corner). Herzog[12] then gives:

$$S_0=\frac{2d}{\pi}\tan^{-1}\frac{a}{2d}-\frac{a}{\pi}\ln\frac{2}{(1+(2d/a)^2)^{\frac{1}{2}}}. \tag{8}$$

[12] R. Herzog, Zeits. f. Physik 97, 596 (1935).
[13] W. R. Smythe *Static and Dynamic Electricity* (McGraw-Hill Book Company, Inc., New York, 1939), p. 97.

If ΔS_w is the correction to S_0 due to small opening of the slits, then Herzog[12] gives, after approximating his exact but implicit solution:

$$\Delta S_w=\frac{\pi}{16}\cdot\frac{w^2}{a}\cdot\frac{1}{1+(2d/a)^2}\ \text{(infinitely thin slit)}. \tag{9}$$

To determine the effect of the rounding of the corners the slit may be assumed to be closed. The transformation,[13] which takes the real axis in the Z_1-plane into the approximate boundary shown in the Z-plane, is given by

$$Z=jC\int\frac{[(Z_1-1+\epsilon)^{\frac{1}{2}}+\lambda(Z_1-1-\epsilon)^{\frac{1}{2}}]\cdot[(Z_1+1+\epsilon)^{\frac{1}{2}}+\lambda(Z_1+1-\epsilon)^{\frac{1}{2}}]}{Z_1^2-a_1^2}dZ_1. \tag{10}$$

The electrical problem in the Z_1-plane is two positive line charges at $Z_1=\pm a_1$. This gives the complex potential as

$$W=U+jV=-\frac{V_0}{2\pi}\ln\left[\left(\frac{Z_1}{a_1}\right)^2-1\right]+j\frac{V_0}{2}, \tag{11}$$

where U is the stream function, V is the potential function, and V_0 is the potential difference of the analyzer plates. The integral may be evaluated in terms of elementary transcendentals. However, an approximation is used to get a relation between the constants ϵ, λ, a_1, in the Z_1 plane and the corresponding constants r, d, a, in the Z plane. If the radius of curvature of the rounding is small then a sufficient approximation is to set $\lambda=1$ and to expand all terms containing ϵ, retaining terms up to ϵ^2. Following Herzog's procedure[12] we find that the effective position of entrance to the analyzer is given by

$$S=S_0+\frac{a}{12\pi}\epsilon^2\left[1+\frac{6}{5}\left(\frac{2d}{a}\right)^2\right], \tag{12}$$

where the term in ϵ represents the rounded corner effect. The relation between ϵ and r to the first approximation is given by

$$\epsilon^{\frac{1}{2}}=\tfrac{3}{4}\pi\cdot\frac{r}{a}\cdot\frac{(2d/a)^2}{1+(2d/a)^2}. \tag{13}$$

The details of the calculation are quite tedious and are not reproduced here. However, the algebraic correctness was insured by two independent calculations using different points in the Z_1-plane to find the corresponding points in the Z-plane. Thus S_0, given by Eq. (8), together with ΔS_w given by Eq. (9) and the ϵ^2 term in Eq. (12), when added together should give a good estimate of the effective position of the entrance to the analyzer. The position of the exit slit is not very critical since it only determines the total analyzer angle. This angle only enters the corrections and hence corrections to its value can be neglected. In designing the analyzer an attempt was made to set $S_0=0$ so all the corrections are expected to be small.

APPENDIX II: IDEAL ANALYZER RELATIONS

The electrostatic potential between the plates of two concentric cylinders with a charge per unit length $+Q$ on the outer plate of radius r_1 and $-Q$ on the inner plate of radius r_2 is

$$\Psi=2Q\ln(r/a), \tag{14}$$

where $a=(r_1r_2)^{\frac{1}{2}}$, the geometric mean of the plate radii. If the inner plate has a potential $-\frac{1}{2}V'$ and the outer plate

has a potential $\frac{1}{2}V'$ each with respect to ground, then

$$V'=2Q\ln(r_1/r_2). \tag{15}$$

To find the ideal path of the ions in the analyzer, balance the centripetal force $2Qe/r$ against the centrifugal force mv^2/r and note that the kinetic energy $(m-m_0)c^2$, plus the potential energy $e\Psi$ within the analyzer, is equal to the energy eV of the ions from the generator. Making use of the fact that $m=m_0/(1-v^2/c^2)^{\frac{1}{2}}$ or its equivalent $m^2v^2=(m^2-m_0^2)c^2$ it may be seen that:

$$Q=(V-\Psi)\frac{1+[e(V-\Psi)/2m_0c^2]}{1+[e(V-\Psi)/m_0c^2]}, \tag{16}$$

which is a constant for constant radius. Thus for an analyzer with a charge Q on the plates, in order to have a constant radius for the path of an ion that enters tangentially, it must have an energy eV that differs for different points of entry depending on the potential Ψ at that point. This may be thought of as due to a variable dipole layer at the ends of the analyzer which reduces the potential to zero outside in order that the ideal problem may represent its physical counterpart. The ideal path is chosen as the one for which $\Psi=0$ or, from Eq. (14), $r=a=(r_1r_2)^{\frac{1}{2}}$. Let the corresponding generator voltage be called V_0. Then:

$$Q=V_0(1+\gamma)/(1+2\gamma), \tag{17}$$

where

$$\gamma=\frac{eV_0}{2m_0c^2}=\frac{V_0(\text{mv})}{1880}. \tag{18}$$

Using this value of Q, Eq. (15) may be expanded in powers of the small numbers γ and d/b where b is the arithmetic mean of the plate radii and d is the plate separation. This gives:

$$V'=2V_0(1-\gamma+2\gamma^2+\cdots)\left(\frac{d}{b}+\frac{1}{12}\frac{d^3}{b^3}+\cdots\right). \tag{19}$$

Since $\gamma\sim0.001$ and $d/b\sim0.01$ it follows that the higher order terms may be neglected to an accuracy of 0.001 percent. Equation (1) of the text is the result.

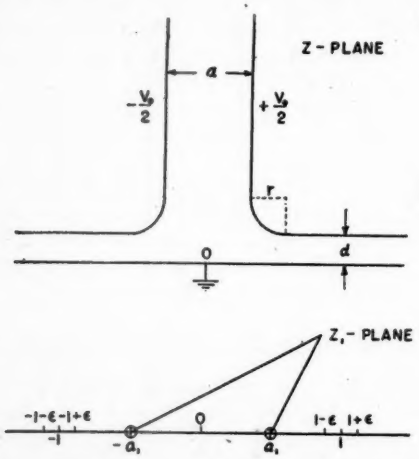

FIG. 8. Outline of quantities used in transformation of real axis of Z_1 plane into boundary shown in Z plane. Electrical problem in Z_1 plane corresponds to two positive line charges at $Z_1=\pm a_1$.

APPENDIX III: ION DYNAMICS

A non-relativistic discussion of the ion beam dynamics may be based on the following Lagrangian in polar coordinates and Gaussian units:

$$L=\tfrac{1}{2}m(\dot r^2+r^2\dot\theta^2)-e\Psi(r,\theta)+\frac{e}{c}r\dot\theta A_\theta(r), \tag{20}$$

where the potential of the ion between the analyzer plates is given by a function of the form:

$$\Psi(r,\theta)=C\ln\frac{r}{a}+\Sigma_\lambda\,(A_\lambda r^{n_\lambda}+B_\lambda r^{-n_\lambda})\cos(n_\lambda\theta+\alpha_\lambda). \tag{21}$$

The vertical uniform magnetic field is accounted for by the vector potential

$$A_\theta(r)=\tfrac{1}{2}B_ir. \tag{22}$$

Approximations will be introduced to enable the small higher order effects of the slightly non-radial contours of the analyzer plates represented by the summation to be determined. The constant C is determined from a knowledge of the ion beam energy eV_0 and the small magnetic field B_i. Since the magnetic field, the deviation of the path of the particle from $r=a$, and the angular dependence of the potential (i.e., deviation of the analyzer plates from constant radii) are all small, we may consider their effects separately.

First, consider only the effect of the small magnetic field. By Lagrange's equations, approximating for small A_θ:

$$m\ddot r-\frac{p^2}{mr^3}+\frac{eC}{r}=0, \tag{23}$$

where

$$mr^2\dot\theta+\frac{e}{c}rA_\theta=p=\text{constant}. \tag{24}$$

Since $r=a$ is to be an exact solution, then, from Eq. (23), the angular momentum that the incoming ion must have is determined by $p^2=ma^2eC$. However, the energy of a particle entering with this angular momentum is $eV_0=\frac{1}{2}ma^2\dot\theta^2$. Using Eqs. (22) and (24) with $r=a$, we see that

$$C=2V_0\left(1+\frac{eaB_i}{c(2emV_0)^{\frac{1}{2}}}\right). \tag{25}$$

Since the change in the angular momentum caused by the small magnetic field also causes a compensating change in the constant C in the electrostatic potential, the ion beam dynamics for the paraxial paths is unchanged. Therefore, the only effect of a small vertical magnetic field is to change Eq. (19) of the Appendix II into

$$V'=2V_0\left(1+\frac{eaB_i}{c(2emV_0)^{\frac{1}{2}}}\right)(1-\gamma)\frac{d}{b}. \tag{26}$$

The magnetic field effect inside the analyzer being accounted for, the path of a paraxial ion may now be calculated by setting $r=a(1+x)$ and $V=V_0(1+\epsilon)$. If the potential $\Psi(r,\theta)$ is expanded in the neighborhood of $r=a$ and third order terms are neglected, the result is

$$\Psi(x,\theta)=[2V_0+f_1(\theta)]x-V_0x^2+f_2(\theta). \tag{27}$$

To a first approximation $f_1(\theta)$ and $f_2(\theta)$ can be calculated by dropping the V_0x^2 term and requiring that $\Psi=\pm\frac{1}{2}V'$ on the plate surfaces. The torque $\partial L/\partial\theta$ may be set equal to zero for the following reasons based on its net effect: The

magnitude of the terms in θ in the potential Ψ is a measure of the gain in kinetic energy of the ions by tangential acceleration within the analyzer which is lost again as the ions pass out of the analyzer into a region of zero potential. This change in kinetic energy that occurs gradually throughout the analyzer produces a change in direction that cannot be compensated for by the opposite kinetic energy change at the exit of the analyzer. The magnitude of the terms in θ measure the amount of this deflection. A liberal estimate gives 0.005 percent for the possible energy error.

With the torque now set equal to zero, conservation of angular momentum follows and a simple differential equation of the path of the ion may be written down. If only first order effects are considered and the equation of conservation of energy is used to express the angular momentum p within the analyzer in terms of the total energy eV, the differential equation is

$$\frac{d^2x}{d\theta^2}+2x=\epsilon+\frac{D(\theta)}{d}-1. \tag{28}$$

Here,

$$D(\theta)=d-\frac{d}{2V_0}f_1(\theta) \tag{29}$$

is the actual plate separation as a function of angle and d is a weighted mean plate separation as yet to be determined. Noticing that $\alpha \cong dx/d\theta$ is the angle that the path of the ion makes with the tangent to a circle ($r=$const.) through the point and using x_1 and α_1 to denote the position and direction of the ion beam at $\theta=0$, the solution is

$$x=\tfrac{1}{2}\epsilon+\frac{1}{\sqrt{2}}\alpha_1\sin\sqrt{2}\theta+(x_1-\tfrac{1}{2}\epsilon)\cos\sqrt{2}\theta + \frac{1}{d\sqrt{2}}\int_0^\theta [D(\varphi)-d]\sin\sqrt{2}(\theta-\varphi)d\varphi. \tag{30}$$

This gives

$$\alpha=\alpha_1\cos\sqrt{2}\theta-\sqrt{2}(x_1-\tfrac{1}{2}\epsilon)\sin\sqrt{2}\theta + \frac{1}{d}\int_0^\theta [D(\varphi)-d]\cos\sqrt{2}(\theta-\varphi)d\varphi. \tag{31}$$

Since the exit slits are placed approximately at the exit of the analyzer plates, it is convenient to set the integral in Eq. (30) equal to zero for θ equal to the analyzer angle Φ. This gives:

$$d=\frac{\sqrt{2}}{1-\cos\sqrt{2}\Phi}\int_0^\Phi D(\varphi)\sin\sqrt{2}(\Phi-\varphi)d\varphi. \tag{32}$$

Thus, d is determined as a weighted mean of the separation contour data $D(\varphi)$.

Outside the analyzer, the earth's magnetic field causes the ion beam to deviate from a straight line. To a first approximation only the vertical component is effective in causing an apparent energy shift. Balancing the centripetal and centrifugal forces determines R, the radius of curvature of the ion. If the kinetic energy of the ion is expressed in terms of the beam voltage and the radius of curvature in units of a, the value of R is:

$$R=\frac{c}{eaB_0}(2emV_0)^{\frac{1}{2}} \text{ (Gaussian units).} \tag{33}$$

If an ion enters the entrance slit at a position x_0 and at an angle α_0 to the ideal path then, because of the external vertical magnetic field, it will enter the analyzer at a position

$$x_1=x_0+\alpha_0 p+\frac{p^2}{2R} \tag{34}$$

and will now be inclined at an angle

$$\alpha_1=\alpha_0+\frac{p}{R}, \tag{35}$$

where p is the distance from the effective entrance of the analyzer to the entrance slit measured in units of a. These values of x_1 and α_1 are then to be inserted in the equations for x and α. Since the exit slit is placed very close to the effective exit plane ($q \cong 0$), a straight line path for the emergent ion may be assumed. Following Herzog[14] we may then choose the relation between the entrance and exit slits to be

$$(p+q)\cos\sqrt{2}\Phi-\sqrt{2}pq\sin\sqrt{2}\Phi+\frac{\sqrt{2}}{2}\sin\sqrt{2}\Phi=0. \tag{36}$$

An ion entering the entrance slit at x_0 will leave the exit slit at x_2 where

$$x_2=\tfrac{1}{2}\epsilon-\left(\tfrac{1}{2}\epsilon-x_0-\frac{p^2}{2R}\right)M-\frac{p}{2R}\frac{\partial M}{\partial\Phi}, \tag{37}$$

and $M=-[q\sqrt{2}\sin\sqrt{2}\Phi-\cos\sqrt{2}\Phi]$, the lateral magnification of the analyzer. The integral in Eq. (31) does not appear in Eq. (37) since it would have occurred multiplied by q and was dropped since $q \cong 0$. Furthermore, the relation between x_0 and x_2 is independent of the angle α_0 of the entering beam.

[14] R. Herzog, Zeits. f. Physik **89**, 447 (1934).

Microwave Spectroscopy in the Region of Three to Five Millimeters*

ALEX. G. SMITH, WALTER GORDY, JAMES W. SIMMONS, AND WILLIAM V. SMITH
Department of Physics, Duke University, Durham, North Carolina

(Received October 4, 1948)

Exploratory investigations in the region of the electromagnetic spectrum between 3.3- and 5-mm wave-length have shown that useful work can be done here with available sources and detectors. Higher rotational transitions of BrCN and ICN have been observed with satisfactory signal-to-noise ratios at pressures low enough to resolve the nuclear quadrupole splittings. These measurements indicate that the minimum detectable absorption is 10^{-5} neper per cm with the present spectroscope. The B_0 value of HCN has been determined as 1.4789 cm^{-1}, in agreement with infra-red results. The quadrupole coupling factor for the nitrogen nucleus in this molecule has been found to be 4.7 mc.

I. INTRODUCTION

THE application of microwave harmonic generators to the study of gas absorptions was first described by R. Beringer, who used the technique in the study of oxygen-nitrogen mixtures at relatively high pressures in the wave-length region from 4.8 mm to 6.1 mm.[1] A silicon-tungsten crystal driven by a one-centimeter signal generator was used as an energy source, the harmonics arising in the crystal being isolated from energy of the fundamental wave-length by means of a wave-guide filter. Although harmonics higher than the second are also present in a signal thus derived, they are considerably less intense, and need occasion no confusion in working with the second harmonic. In this laboratory we have employed the second harmonic of the shorter wave-length klystron sources now available to make spectroscopic studies at wave-lengths as short as 3.3 mm.

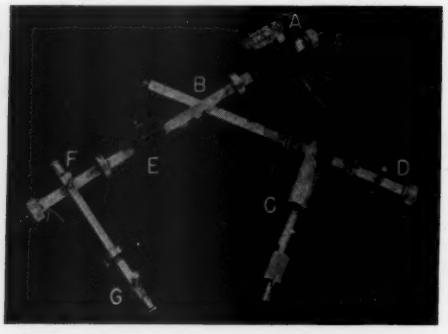

FIG. 1. Microwave components. *A* is the reflex klystron, *B* a directional coupler, *C* the *J*-band cavity wavemeter, *D* a *J*-band crystal mount, and *E* a variable attenuator. *F* is the frequency multiplier and *G* an *H*-band crystal mount. Normally, the cell is inserted between the multiplier and the *H*-band crystal mount.

* This research was supported by U. S. Air Force Contract No. W-28-099-ac-125 with the Air Materiel Command, Watson Laboratories.

[1] R. Beringer, Phys. Rev. 70, 53 (1946).

The most obvious advantages resulting from extending the high frequency coverage of microwave spectroscopy are the possibilities of studying a greater variety of molecules and of observing higher rotational transitions where centrifugal distortions may be studied. For example, the first rotational transition of carbon monoxide and the fifteenth rotational line of ICN both occur near three millimeters. Ultimately, the over-all ability to detect absorption lines should be greater in the millimeter than in the centimeter region. Even now, the considerable losses in source and detector sensitivities are largely balanced by the marked increase in gas absorption with frequency (varying as ν^3 in the case of a linear molecule). An analysis of the results for BrCN indicates that an absorption of 10^{-5} neper per cm is detectable with the present spectroscope.

II. INSTRUMENTATION

Figure 1 is a photograph of the essential microwave components, with the cell omitted. The multiplier unit is driven by Raytheon reflex klystrons operating in the region of six to ten millimeters. The magnitude of the fundamental energy is of the order of ten milliwatts. The wave guide components used in this band are made from scaled and simplified designs of standard centimeter-wave-length equipment. They have been employed extensively in this laboratory for spectroscopic work in the region below *K*-

band.[2–4] Figure 2A shows the design of the multiplier. This simple crossed wave-guide construction has proven as efficient in practice as a more complex model embodying chokes to prevent feedback of second harmonic energy into the larger wave guide. The small guide cuts off at 5.6 mm, so that it is useful as a filter for all fundamental wave-lengths longer than this. For fundamental wave-lengths between seven and ten millimeters the larger guide is made of the size indicated in the drawing; for shorter wave-lengths it is reduced to 0.180×0.086 inch. By connecting an indicator to the Sperry cable fitting, all of the components associated with the fundamental wave-length may be put in tune, including the multiplier crystal. For detection of the second harmonic energy, scaled-down versions of conventional crystal mounts are employed (Fig. 2B). Sylvania 1N26 crystals are used both for multiplication and for detection. Germanium crystals probably would be greatly superior as multipliers, but these are at present unavailable. It has been necessary to select crystals with great care, and their frequency sensitivity is such that the selection must be repeated every two or three thousand megacycles. There appears to be little correlation between the performance of a crystal as a multiplier and as a detector. Approximate measurements made at five millimeters indicate that the detected second

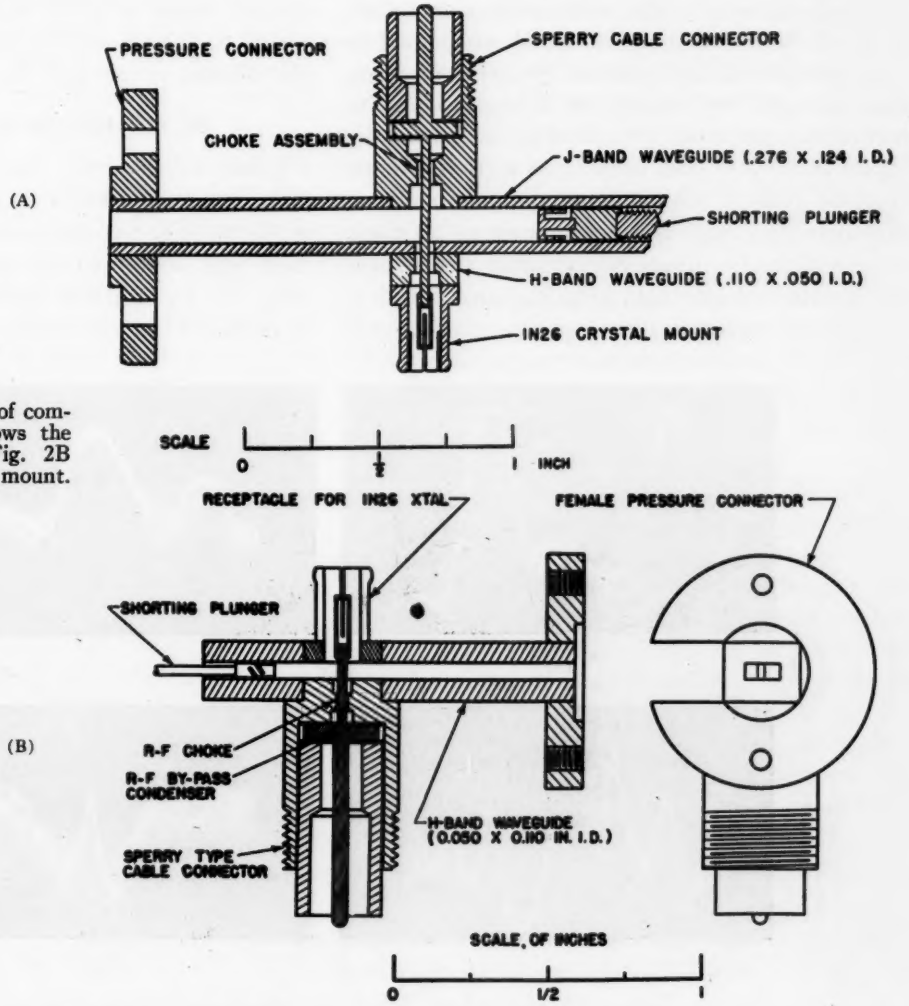

FIG. 2. Cross sections of components. Figure 2A shows the frequency multiplier; Fig. 2B shows the *H*-band crystal mount.

[2] W. Gordy, A. G. Smith, and J.W. Simmons, Phys. Rev. **71**, 917 (1947).
[3] O. R. Gilliam, H. D. Edwards, and W. Gordy, Phys. Rev. **73**, 635 (1948).
[4] A. G. Smith, H. Ring, W. V. Smith, and W. Gordy, Phys. Rev. **74**, 370 (1948).

TABLE I. Observed attenuation of 5-millimeter radiation by various wave guides.

Wave-guide dimensions	Band designation	Wave-guide material	Attenuation, db/ft.
2.92 ×1.42 in.	*S*	Brass	0.10
0.95 ×0.45	*X*	Brass	0.25
0.420×0.170	*K*	Silver	0.43
0.276×0.124	*J*	Silver	0.64
0.110×0.050	*H*	Silver	1.25*

* Calculated.

harmonic signal is of the order of thirty decibels below the level of the detected fundamental signal.

For spectroscopy, a 15-foot cell is inserted between the multiplier unit and the detector. The cell is 2.92×1.42 inches in cross section, tapering eighteen inches at either end to the dimensions of the *H*-band components, which are joined to it by means of choke-to-flange connections. Thin mica windows are sealed on at these points to permit evacuation of the cell. The reason for the choice of a cell of such large cross section is made clear by Table I, which shows the results of empirical studies made at five millimeters. At these wave-lengths the losses occurring in wave guide of "normal" proportions would be prohibitive in view of the small amount of energy that is available. No difficulty has been experienced with modes or resonances in the oversize wave guide.

The method of presentation is that originally described by Gordy and Kessler.[5] The klystron is frequency-modulated by means of a saw-tooth voltage of about 15 cycles per second applied to the reflector electrode. The resulting mode envelope (Fig. 3D) is rejected by a preamplifier with a narrow pass-band extending from 150 c.p.s. to 500 c.p.s., whereas absorption lines are sufficiently sharp at the gas pressures ordinarily used to be passed and presented on an oscilloscope. The filtering action of the amplifier also eliminates the baseline "roll" caused by r-f reflections in the wave-guide system. Frequency measurements are made at the fundamental frequency, using a cavity wavemeter whose pip is added to the signal from the cell in a push-pull transformer preceeding the amplifier.

III. MOLECULAR ABSORPTIONS

Table II lists the rotational transitions of ICN, BrCN, and HCN which have been observed in the three-to-five-millimeter region. Each transition was found to be split into several lines (Fig. 3) by nuclear quadrupole interactions. Wavemeter measurements are not sufficiently

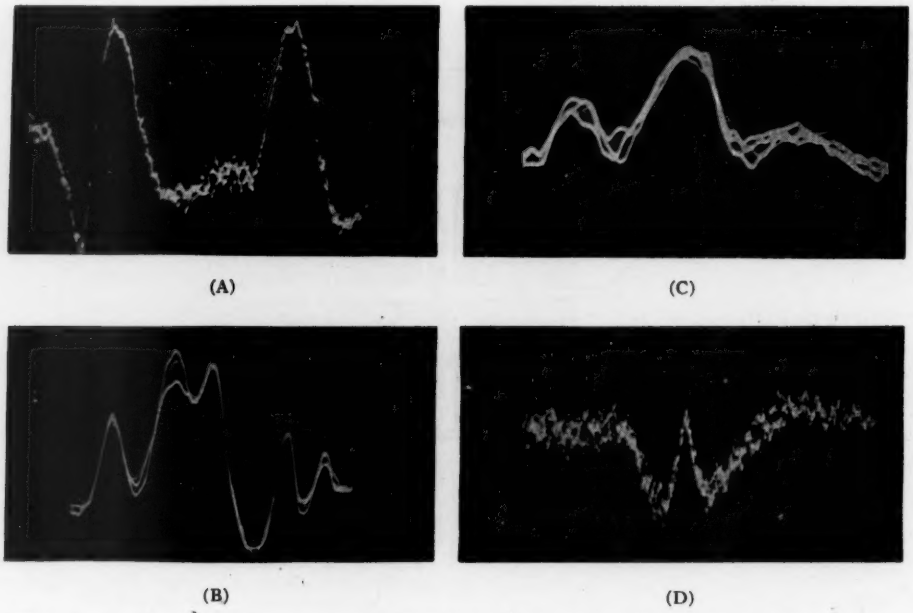

FIG. 3. Oscilloscope photographs of molecular rotational transitions in the three to five millimeter region: 3A, $Br^{81}C^{13}N^{14}$ at 73,742 mc; 3B, $IC^{13}N^{14}$ at 83,864 mc; 3C, $H^{1}C^{13}N^{14}$ at 88,671 mc, all at gas pressures of 5×10^{-3} mm of Hg. Figure 3D shows HCN at a pressure of 1 mm, the entire klystron mode envelope being presented here.

accurate to permit evaluation of the centrifugal distortions of the molecules, but measurements will be made later in this laboratory with a frequency standard to investigate this effect. The $J=4\rightarrow5$ transition of ICN and the $J=3\rightarrow4$ transition of BrCN have been measured to an accuracy of 0.1 mc in this way.[5]

Figure 3C shows the spectrum of the $J=0\rightarrow1$ transition of $H^1C^{12}N^{14}$ observed at 88,671 mc (3.38 mm), with a gas pressure of 5×10^{-3} mm of mercury. The B_0 value determined from this frequency is 1.4789 ± 0.0002 cm^{-1}, which is in good agreement with the value of 1.4784 cm^{-1} derived by Herzberg[6] from infra-red data.[7,8] The splitting of the lines resulting from quadrupole interaction of the nitrogen nucleus was measured by producing frequency markers through modulation with a calibrated signal generator in the manner described by Dailey *et al.*[9] The separations measured in this way were 1.4 mc and 2.1 mc, corresponding to a quadrupole coupling factor $eQ(\partial^2V/\partial z^2)$ of 4.7 mc. This value is appreciably larger than the factors previously determined for the cyanogen halides,[4] and is essentially the same as that found by Ring, Edwards, Kessler, and Gordy for CH_3CN.[10]

In Fig. 3D is shown the unresolved transition at a pressure of one millimeter. Here no filtering has been used in the detecting circuit, so that the entire klystron mode envelope is presented. (The poor signal-to-noise ratio results from the use of an amplifier of 200-kc band width to provide high fidelity.) The peak absorption α in cm^{-1} of a linear molecule in the microwave region ($h\nu\ll kT$ and J small) may be expressed as[11]

$$\alpha=\frac{4\pi^2Nf_v h\mu^2\nu^3}{3c(kT)^2\Delta\nu},$$

TABLE II. Observed rotational transitions of ICN, BrCN, and HCN.

Molecule	Transition	Frequency in mc	Wave-length in mm
$Br^{81}C^{12}N^{14}$	$J=8\rightarrow9$ (Fig. 3A)	73,742	4.07
$Br^{79}C^{12}N^{14}$	$J=8\rightarrow9$	74,165	4.04
$IC^{12}N^{14}$	$J=11\rightarrow12$	77,413	3.88
$Br^{81}C^{12}N^{14}$	$J=9\rightarrow10$	81,936	3.66
$Br^{79}C^{12}N^{14}$	$J=9\rightarrow10$	82,405	3.64
$IC^{12}N^{14}$	$J=12\rightarrow13$ (Fig. 3B)	83,864	3.58
$H^1C^{12}N^{14}$	$J=0\rightarrow1$ (Fig. 3C)	88,671	3.38

where N = No. of molecules per cc in absorbing path, f_v = fraction of molecules in lowest vibrational state, μ = permanent dipole moment in e.s.u., $2\Delta\nu$ = line width at half-power points, and h, c, ν, k, T are standard nomenclature. For HCN, $\mu=2.65\times10^{-18}$ e.s.u.[12] Our observed line width is $2\Delta\nu=50\pm15$ megacycles at a pressure of one millimeter and temperature of 300°K. The sample contained 86 percent C^{12}, while $f_v=97$ percent. The calculated intensity is $\alpha=9\times10^{-3}$ cm^{-1} (or 4.5×10^{-3} neper per cm), almost ten times as strong as the 3,3 ammonia line at 23,870 megacycles, heretofore the strongest observed microwave absorption.

For the 15-foot cell used, the calculated absorption at the resonant frequency is 98 percent. The observed absorption was between 90 and 100 percent. This intense absorption accounts for the large probable error in the line width, since the line shape is quite distorted.

The results thus far obtained in this undeveloped region of the electromagnetic spectrum show that useful work can be done with available equipment. Considerable improvement can be achieved in sensitivity and in precision measurements. Development of the region along each of these lines is proceeding in this laboratory. As an extension of the techniques described above, quite useful quantities of third harmonic energy have been obtained from a multiplier driven by standard 2K33 K-band klystrons. The third harmonic of these oscillators (fundamental power of the order of 30 milliwatts) is comparable in intensity to the second harmonic of the less energetic millimeter tubes. Experiments with the fourth harmonic are now being undertaken.

[5] W. Gordy and M. Kessler, Phys. Rev. **71**, 540 (1947).
[6] G. Herzberg, *Infrared and Raman Spectra of Polyatomic Molecules* (D. Van Nostrand Company, Inc., New York, 1945), p. 391.
[7] P. F. Bartunek and E. F. Barker, Phys. Rev. **48**, 516 (1935).
[8] G. Herzberg and J. W. T. Spinks, Zeits. Physik **91**, 386 (1934).
[9] Dailey, Kyhl, Strandberg, Van Vleck, and Wilson, Phys. Rev. **70**, 984 (1946).
[10] H. Ring, H. Edwards, M. Kessler, and W. Gordy, Phys. Rev. **72**, 1262 (1947).
[11] J. H. Van Vleck and V. F. Weisskopf, Rev. Mod. Phys. **17**, 227 (1945), inserting value of $|\mu_{ij}|^2$ appropriate for a linear rotator.
[12] S. Werner, Zeits. f. physik. Chem. (B), 371 and 391 (1929).

Screening and Relativistic Effects on Beta-Spectra

C. LONGMIRE AND H. BROWN
Pupin Physics Laboratories, Columbia University, New York, New York

(Received October 11, 1948)

The effect of screening by atomic electrons on the form of allowed beta-ray spectra of the Fermi theory is calculated approximately, with the assumption of a screened potential based on the Thomas-Fermi model of the atom. The apparent deviation from theory caused by neglecting screening is given for the beta-emitters S^{35}, Cu^{64}, and RaE. Another smaller source of error in interpreting experimental results is the use of the non-relativistic approximation to the Coulomb correction factor. These effects cannot be neglected in an accurate analysis of data for Cu and heavier elements.

I. INTRODUCTION

RECENT measurements by Cook and Langer[1–4] of the beta-ray spectra of Cu^{64}, Cu^{61}, N^{13}, and S^{35} have been interpreted as indicating a discrepancy between the Fermi theory and experimental fact. However, the results of Albert and Wu for S^{35} [5] and Cu^{64} [6] suggest that much of the discrepancy is due to scattering in the source and the source-backing when these are of the thickness used by Cook and Langer. The fact that for Cu^{64} the positron curve of Cook and Langer deviates much more in the Kurie plot from the Fermi allowed curve than does their electron curve is consistent with this explanation, since comparable numbers of positrons and electrons scattered into the low energy region would show up as a greater discrepancy in the Kurie plot of the positrons (because there are so few positrons at low energies).

Since the actual deviations may be small, it seems worth while to consider some small refinements of the Fermi theory which, though implicit in the theory itself, have hitherto not been considered in the interpretation of experimental data. One such refinement is the modification of the Coulomb correction factor to include the effect of screening by atomic electrons; this effect is calculated approximately below. Another improvement is the use, in analyzing data, of a better approximation to the Coulomb correction factor than has been used by many investigators. (The exact expression for the Coulomb factor contains complex Γ-functions which are not readily evaluated.)

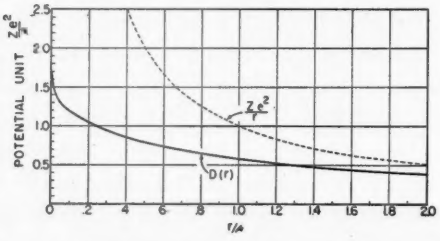

FIG. 1. Difference between Coulomb and screened Coulomb potentials.

II. THE SCREENING CORRECTION

To evaluate screening effects accurately, the screened wave functions would have to be calculated exactly. However, to make such a calculation for arbitrary atomic number Z, one would have to use an approximate screened potential, such as that provided by the Thomas-Fermi model of the atom.*

The effect of a pure Coulomb field on an allowed beta-spectrum was given by Fermi[7] in his first paper on beta-decay, and is expressed by a factor[8] $F(Z, W)$ which multiplies the spectrum

[1] C. S. Cook and L. M. Langer, Phys. Rev. **73**, 601 (1948).
[2] C. S. Cook and L. M. Langer, Phys. Rev. **74**, 227 (1948).
[3] C. S. Cook, L. M. Langer, H. C. Price, and M. B. Sampson, Phys. Rev. **74**, 502 (1948).
[4] C. S. Cook, L. M. Langer, and H. C. Price, Phys. Rev. **74**, 548 (1948).
[5] R. D. Albert and C. S. Wu, Phys. Rev. **74**, 847 (1948).
[6] Private communication. We are indebted to C. S. Wu and R. D. Albert for informing us of their results on the β-ray spectra of Cu^{64}.

* *Note added in proof:* Professor Lawrence M. Langer has kindly called our attention to an article by M. E. Rose [Phys. Rev. **49**, 727 (1936)] in which the effect of screening was estimated. Rose's results do not agree well with ours, although they are of the same order of magnitude.
[7] E. Fermi, Zeits. f. Physik **88**, 161 (1934).
[8] We use here the notation of Konopinski, Rev. Mod. Phys. **15**, 210 (1943).

obtained when the Coulomb field is ignored. Here W is the total energy of the electron. $F(Z, W)$ is unity for $Z=0$; otherwise it increases the number of low energy electrons and decreases the number of low energy positrons. $F(Z, W)$ is equal to the square of the ratio of the values of the S wave functions of the electron in the nucleus with and without the Coulomb potential (since in an allowed transition the radial wave function of the electron is replaced in the matrix element by its value at the origin). It is assumed here that both wave functions are normalized in the same way at large distances from the nucleus. In calculating the effect of screening it is necessary only to correct the value of the wave function at the origin.

The numerical values of the screening function for the Thomas-Fermi[9] model have been given by Bush and Caldwell.[10] Figure 1 shows the difference $D(r)$ between the Coulomb potential Ze^2/r and the screened potential $V(r)$, plotted as a function of the distance from the nucleus. The unit of length, $\mu=0.885a_0/Z^{\frac{1}{3}}$, and the unit of energy, Ze^2/μ, are the natural units associated with the Thomas-Fermi model. (a_0 is the Bohr radius.) For $r<\mu$ (i.e., over most of the atom), the difference between screened and unscreened potentials is remarkably constant, compared with the potentials themselves. In the region $r>\mu$, and for electron kinetic energies greater than 10 kev, the WKB method is valid for both screened and unscreened potentials. For the approximate calculation below it is specifically assumed that the difference $D(r)$ is constant (equal to D_0) up to some value of r (equal to r_0) beyond which the WKB method is valid.

How this assumption is applied can be understood by considering Fig. 2 for the case of electron emission. In Fig. 2 the solid curve represents the assumed potential, and the dashed curve represents a Coulomb potential shifted upward by a constant D_0. Let us define the following quantities relating to the electron wave function:

$B_f \equiv$ value at the origin for a free electron;
$B_a \equiv$ value at the origin for the assumed potential;
$B_s \equiv$ value at the origin for the shifted potential;
$A_f(\infty) \equiv$ amplitude at infinity for a free electron;
$A_a(\infty) \equiv$ amplitude at infinity for the assumed potential;

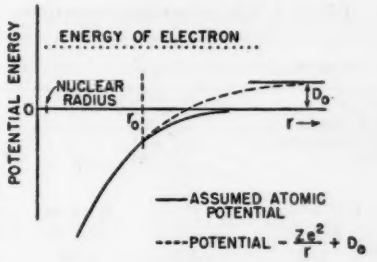

FIG. 2. Potentials used in making the approximation (for electrons).

$A_s(\infty) \equiv$ amplitude at infinity for the shifted potential;
$A_a(r_0) \equiv$ amplitude at $r=r_0$ for the assumed potential;
$A_s(r_0) \equiv$ amplitude at $r=r_0$ for the shifted potential.

Normalization in a large sphere requires

$$A_f(\infty)=A_a(\infty)=A_s(\infty). \quad (1)$$

Furthermore, since the assumed potential and the shifted potential are identical for $r<r_0$,

$$B_a/A_a(r_0)=B_s/A_s(r_0). \quad (2)$$

From these relations it follows that

$$(B_a/B_f)^2=(B_s/B_f)^2(A_s(\infty)/A_s(r_0))^2 \times(A_a(r_0)/A_a(\infty))^2. \quad (3)$$

The quantity $(B_a/B_f)^2$ is the correction factor for the screened potential; denote it by $F_c^-(Z, W)$. The term $(B_s/B_f)^2$ is the usual Coulomb correction factor for a shifted energy, $F(Z, W-D_0)$. The quantities $(A_s(\infty)/A_s(r_0))^2$ and $(A_a(r_0)/A_a(\infty))^2$ can be found, by hypothesis, from the WKB method. Therefore, Eq. (3) reduces, for electrons, to

$$F_c^-(Z, W)=F(Z, W-D_0) \times(W-mc^2/W-mc^2-D_0)^{\frac{1}{2}}. \quad (4)$$

This formula does not contain the critical radius r_0 explicitly. However, D_0 will depend (but not sharply) on r_0/μ, for D_0 is an average of the difference $D(r)$ for $r<r_0$. Strictly speaking, r_0/μ (and therefore D_0) is a function of W and of Z. But it is a reasonable approximation, for all electron kinetic energies greater than 10 kev and all Z, to set

$$D_0=Ze^2/\mu=1.13Z^{4/3}e^2/a_0, \quad (5)$$

where the value of Z is that of the residual nucleus. For the highest possible Z, it may be significantly better to use about nine-tenths of this value for D_0.

[9] E. Fermi, Zeits. f. Physik **48**, 73, **49**, 550 (1928).
[10] V. Bush and S. H. Caldwell, Phys. Rev. **38**, 1898 (1931).

TABLE I. The screening correction.

Element	Z	D_0 (kev)
S^{35}	17	1.3
Cu^{64} (electrons)	30	2.8
Cu^{64} (positrons)	28	2.7
RaE	84	11.2

(a) S^{35}

$T=W-mc$ (kev)	$\frac{F(Z,W-D_0)}{F(Z,W)}$	$\left(\frac{T}{T-D_0}\right)^{\frac{1}{2}}$	$\frac{F_c^-(Z,W)}{F(Z,W)}$	$\left(\frac{F_c^-(Z,W)}{F(Z,W)}\right)^{\frac{1}{2}}$
10	1.007	1.072	1.080	1.039
12	1.006	1.058	1.064	1.032
15	1.004	1.048	1.050	1.025
20	1.002	1.036	1.038	1.019
25	1.001	1.028	1.029	1.014
40	1.000	1.019	1.019	1.009
100	1.000	1.006	1.006	1.003

(b) Cu^{64} (electrons)

10	1.172	1.180	1.382	1.177
12	1.137	1.142	1.298	1.140
15	1.102	1.108	1.222	1.105
20	1.073	1.078	1.159	1.075
25	1.054	1.063	1.120	1.059
30	1.048	1.052	1.100	1.049
40	1.037	1.037	1.075	1.037
50	1.032	1.030	1.062	1.031
70	1.018	1.022	1.040	1.020
100	1.016	1.014	1.030	1.015
200	1.003	1.007	1.010	1.005

(c) RaE

20	1.418	1.430	2.05	1.425
50	1.112	1.135	1.255	1.120
100	1.048	1.062	1.113	1.055
150	1.025	1.042	1.067	1.033
200	1.018	1.030	1.048	1.024
500	1.006	1.012	1.018	1.009

(d) Cu^{64} (positrons)

	$\frac{F(Z,W+D_0)}{F(Z,W)}$	$\left(\frac{T}{T+D_0}\right)^{\frac{1}{2}}$	$\frac{F^+(Z,W)}{F(Z,W)}$	$\left(\frac{F^+(Z,W)}{F(Z,W)}\right)^{\frac{1}{2}}$
10	1.858	0.890	1.654	1.285
12	1.605	0.904	1.449	1.205
15	1.408	0.921	1.295	1.138
20	1.225	0.940	1.151	1.073
25	1.152	0.953	1.099	1.049
30	1.113	0.960	1.068	1.033
40	1.070	0.969	1.038	1.019
50	1.042	0.976	1.010	1.009
70	1.030	0.982	1.012	1.006
100	1.013	0.986	0.999	0.999
200	1.002	0.993	0.995	0.997

A similar analysis for the case of positron emission gives the result

$$F_c^+(Z,W)=F(Z,W+D_0)\times(W-mc^2/W-mc^2+D_0)^{\frac{1}{2}}, \quad (6)$$

where, as usual, Z in $F(Z,W)$ is negative for positrons.

The screening correction increases the numbers of both electrons and positrons, at low energies, over the values for a pure Coulomb field. The increase was to be expected for positrons, since the screening reduces the amount of barrier through which the positron must pass. Any intuitive feeling that the correction should be opposite for electrons is not borne out. Indeed, it seems that the increase of electrons can be understood physically, as follows. That a pure Coulomb field gives more low energy electrons than the free case is in contradiction to the WKB method (wave function small in regions of large kinetic energy), and is a result of the fact that the Coulomb potential dies off too rapidly with increasing r near the nucleus. But the screened Coulomb potential dies off more rapidly, and therefore the contradiction with the WKB method is accentuated.

The only non-relativistic part of the calculation was in the application of the WKB method. Since the potential is small in the region where the WKB method was applied, the non-relativistic WKB formula should be good for electron energies less than about 100 kev. Above this energy the screening correction is small, as shown by the calculations in Section IV. But before examining numerical values we consider the accuracy of various approximations to $F(Z,W)$.

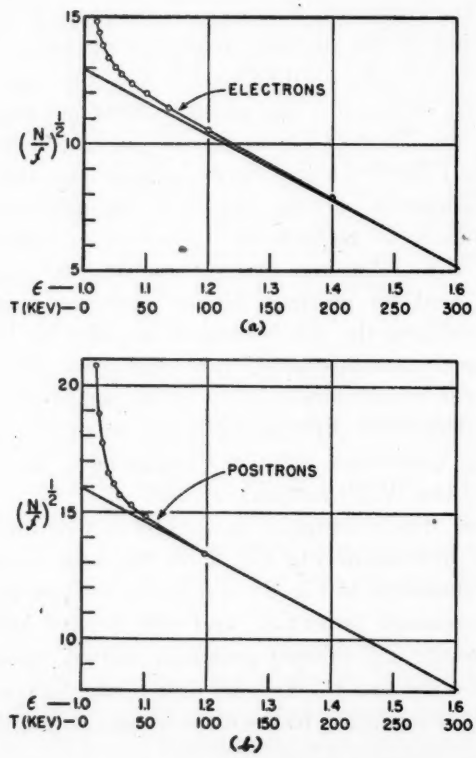

FIG. 3. The effect of screening on the electron and positron spectra of Cu^{64}. The straight lines are the results expected if the Fermi ansatz is correct; the curved lines are the results which will be obtained if the Fermi ansatz is correct but the screening is not considered. The ordinate represents, in arbitrary units, $(N/f)^{\frac{1}{2}}$, where N is the number of particles per unit momentum range and $f=\eta^2(\epsilon-\epsilon_0)^2F(Z,\epsilon)$.

TABLE II. The relativistic correction.

T (kev)	$Z=17$ $\gamma=0.110$ $s=-0.006$	29 0.212 −0.022	84 0.613 −0.209	Cu (ratio of correction at ϵ to correction at ϵ_0)
10	1.009	1.017	0.954	1.032
25	1.007	1.013	0.944	1.028
50	1.005	1.009	0.923	1.024
100	1.002	1.004	0.905	1.019
200	1.000	0.997	0.868	1.012
300	0.998	0.993	0.839	1.007
400	0.997	0.988	0.817	1.003
500	0.095	0.983	0.795	1.000
750	0.993	0.979	0.757	
1000	0.992	0.974	0.725	
1250	0.991	0.971	0.703	

TABLE III. Total effect of screening and relativistic corrections for Cu[64]

T (kev)	Correction (positron)	Correction (electron)
10	1.317	1.209
12	1.236	1.171
15	1.168	1.135
20	1.102	1.104
25	1.077	1.087
30	1.059	1.076
40	1.044	1.062
50	1.033	1.055
70	1.028	1.042
100	1.018	1.034
200	1.009	1.017
400	1.001	1.003

III. APPROXIMATIONS TO THE COULOMB CORRECTION FACTOR

There seems to be no uniform practice for the approximation to be used for the Coulomb correction factor. Fermi in his original paper deduced that the number of electrons per unit momentum range is proportional to

$$f(\epsilon)=\eta^2(\epsilon_0-\epsilon)^2F(Z,\epsilon), \tag{7}$$

where $F(Z,\epsilon)$, the Coulomb correction factor, is given exactly by

$$F(Z,\epsilon)=\eta^{2s}e^{\pi\delta}|\Gamma(1+s+i\delta)|^2. \tag{8}$$

Here ϵ is the total electron energy in units of the rest energy mc^2, η is the electron momentum in units of mc, Z is the charge of the residual nucleus, and

$$s=(1-\gamma^2)^{\frac{1}{2}}-1, \tag{9}$$

$$\delta=\gamma\epsilon/\eta, \tag{10}$$

$$\gamma=Z\alpha=Z/137. \tag{11}$$

Because these are no adequate tables of the complex Γ-function, it is necessary to approximate the expression in Eq. (8). For $Z=82.2$, Fermi gave the approximation

$$F(82.2,\eta)\approx 1/\eta+0.355. \tag{12}$$

Subsequently, Kurie, Richardson, and Paxton[11] gave the approximation

$$F(Z,\epsilon)\approx 2\pi\delta/1-\exp(-2\pi\delta)\equiv F_N(Z,\epsilon), \tag{13}$$

and remarked that it was good up to $Z=29$ (which was certainly correct for experimental accuracies attainable at the time). This formula can be derived exactly using the non-relativistic Coulomb wave functions,[12] and may therefore be called the non-relativistic approximation. Calculations carried out in Section IV show that for the recent investigations below 200 kev, with high transmission spectrometers having the accuracy claimed, the non-relativistic approximation is sufficiently accurate only for very low Z.

A better approximation, especially for large Z, was given by Bethe and Bacher.[13] In our notation it is

$$F(Z,\epsilon)\approx F_N(Z,\epsilon)\eta^{2s}(\delta^2+\tfrac{1}{4})^s = F_N(Z,\epsilon)[\epsilon^2(1+4\gamma^2)-1]^s. \tag{14}$$

The only approximation made in obtaining (14) from (8) is in setting

$$\left[\frac{1+s^2/\delta^2}{1+\dfrac{\sin^2\pi s}{\sinh^2\pi\delta}}\right]^{\frac{1}{2}}\left|\frac{\Gamma(1+s+i\delta)}{\Gamma(1-s+i\delta)}\right|=(\delta^2+\tfrac{1}{4})^s. \tag{15}$$

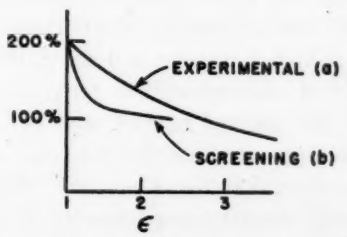

FIG. 4. The RaE spectrum, as experimentally obtained and as given by the screening correction. The curves give (a) the ratio of the number of particles found to the number predicted by Fermi theory without considering screening and (b) the ratio of the number of particles expected using screening to the number expected neglecting it.

[11] F. N. D. Kurie, J. R. Richardson, and H. C. Paxton, Phys. Rev. 49, 368 (1936).

[12] See Mott and Massey, *Theory of Atomic Collisions* (Oxford University Press, New York, 1933).

[13] H. A. Bethe and R. F. Bacher, Rev. Mod. Phys. 8, 194 (1936).

By direct calculation, this approximation seems to be accurate to about 1 percent for Z as large as 84, and to about 0.25 percent for Cu and lighter emitters. (In addition, the percentage error in this approximation depends only slowly on the energy ϵ.)

IV. THE EFFECT ON EXPERIMENTAL RESULTS

Screening Correction

Table I summarizes the calculation of the effect of screening by extranuclear electrons on the S^{35} electron, Cu^{64} positron and electron, and RaE electron spectra. The quantity $F_c^{\pm}(Z, W)/F(Z, W)$ is the ratio of the actual number of particles emitted to the number to be expected for an allowed spectrum without considering screening. The square root of this quantity, also tabulated, is the number by which the uncorrected ordinates of the Fermi[14] plot must be divided to obtain a straight line if the spectrum is of the Fermi allowed type.

For S^{35} the screening correction is extremely small even for low energies, being about 2.5 percent in the Fermi plot at 15 kev. This is in agreement with the results of Albert and Wu,[5] who found a straight line for the Fermi plot; when the screening correction is applied, their result is still a straight line within experimental error. At 10 kev the effect is approximately 4 percent and should be noticeable as a rise.

For Cu^{64} different results are obtained for positrons and electrons. Figure 3 shows what is to be expected. If the straight lines are the results expected on the Fermi model, neglecting screening, for allowed transitions, the curved lines show the effect which screening will have. Because the two parts of the correction (effective shift of energy of the emitted particle and WKB correction) are in opposite direction for positrons but in the same direction for electrons, the electron curve should depart from linearity in the Fermi plot at higher energies than the positron curve. (The energies of departure are 150 as opposed to 50 kev, if a 1 percent deviation is taken as the criterion for departure.) In fact, in the region of 200 kev the positron curve may fall below linearity by a fraction of a percent. However, the positron curve should rise much more rapidly as the energy decreases and the first part of the correction comes to predominate, until at 10 kev the electron curve should be 18 percent and the positron curve 29 percent above the expected values. This means that the actual numbers of positrons and electrons at this energy will exceed the expected numbers by 65 percent and 38 percent, respectively.

Cook and Langer[1] have reported deviations of the experimental electron and positron spectra of Cu^{64} from the shapes predicted by the Fermi theory. These deviations occur at low energies and are generally in the same direction as the screening correction. However, the screening correction is too small to account for the major part of the deviations found by Cook and Langer. Furthermore, their electron curve deviates at a lower energy than their positron curve.

RaE is the only known beta-emitter with a spectrum differing radically from the allowed shape. It is interesting to see if the difference[15] can be explained by the screening. The energy shift, rising as $Z^{4/3}$, is very much larger for RaE than for the light emitters. Hence the deviation from linearity in the Fermi plot begins at a much higher energy, being 1 percent at 500 kev and increasing with decreasing energy until at 20 kev it is 43 percent. This means that there are 2.05 times as many electrons at this energy as would be expected neglecting screening.

Comparison with experimental data[15] (Fig. 4) shows that the correction is adequate to explain the deviation from the allowed spectrum at very low energy, but falls off much too rapidly with increasing energy to explain fully the forbidden shape of the RaE spectrum.

Relativistic Correction

Using Bethe's approximation, Eq. (14), Table II gives the square root of the correction factor for various values of Z, by which the ordinates of the Kurie plot must again be divided if the non-relativistic approximation has been used, to obtain a straight line, if the Fermi theory is correct.

The final column gives the ratio of the correction factor to its value at the endpoint of the

[14] The terms "Fermi plot" and "Kurie plot" are used here interchangeably. Strictly, the first is the relativistic and the second the non-relativistic form.

[15] E. J. Konopinski, Rev. Mod. Phys. 4, 229 (1943).

Cu^{64} electron spectrum taken approximately at 500 kev. The positron endpoint is somewhat higher, which would tend to increase the numbers in the last column by about 0.1 percent for positron emission. For the electrons of this isotope $Z=30$, for the positrons $Z=28$; 29 is taken as a good approximation for both. The above tables show, as expected, that the non-relativistic approximation is best for low Z and low energy, relativistic effects being more important for electrons of higher energy in stronger Coulomb fields.

For S^{35} the relativity correction is negligible because of (a) the smallness of its magnitude everywhere, (b) the shortness of the spectrum, with $\epsilon_0 \sim 1.3$, so that the correction over the entire spectrum varies by only about 0.8 percent.

For Cu^{64} the total effect of the screening and relativity corrections is given in Table III. Again the numbers refer to the division of the ordinates in the Kurie plot—this time to correct for both screening and relativistic effects.

Figure 5 shows the results which are to be expected if both screening and relativity effects are neglected for Cu^{64} positrons and electrons. The Kurie plot for electrons should begin to deviate from linearity at about 250 kev, and for positrons at about 180 kev. In particular, the relativity correction affects the region from 50 to 250 kev. The deviations from linearity might not be noticed until lower energies are reached because of a possible tendency, in the case of a correction which extends over so much of the spectrum, to draw the straight line at a somewhat larger angle with the energy axis. With decreasing energy, the positron curve should rise more gradually at first, then more rapidly than the electron curve until at 10 kev there should be a 32 percent positron and 21 percent electron excess in the Kurie plot.

The investigators of RaE[16–18] seem to have used Fermi's approximation (Eq. (12)) of the relativistic formula, which differs by about 10 percent at 10 kev, 5 percent at 25 kev, and 1 percent at 200 kev from the approximation of Bethe. This discrepancy does not go very far toward explaining the forbidden nature of the RaE spectrum.

In calculating the effect of the screening, the non-relativistic term $\{[F_N(Z, W-D_0)/F_N(Z, W)]\}^{\frac{1}{2}}$ was actually used instead of the corresponding relativistic term $\{[F(Z, W-D_0)/F(Z, W)]\}^{\frac{1}{2}}$. Calculation shows that for the worst case (RaE) they differ at 200 kev only by 0.3 percent, which is about 10 percent of the effect of the energy shift. Furthermore, the non-relativistic WKB method was used. This leads to an error (in the opposite direction from that just mentioned) which is largest for large D_0 and largest relative to the entire screening correction for high energies. As an example, a rough calculation indicates that it amounts to about 0.7 percent in the Kurie plot for RaE at 200 kev. Since the entire method used in calculating the screening correction is probably not accurate to better

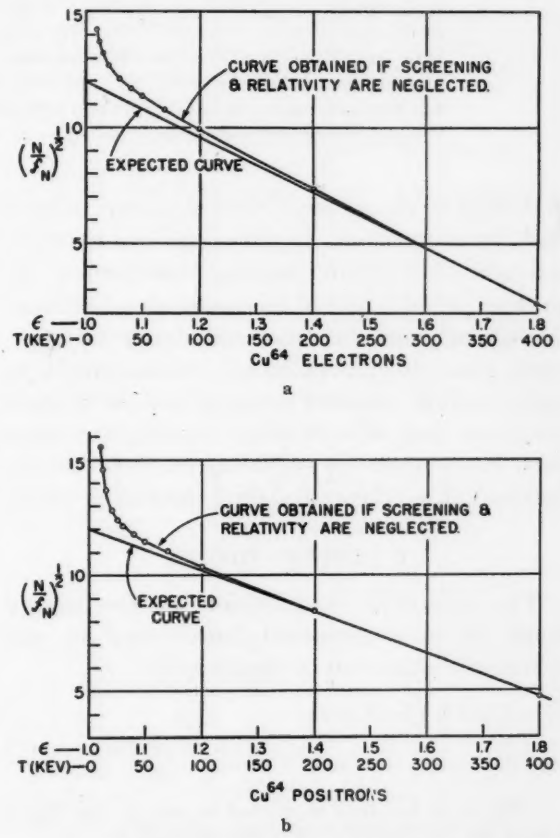

FIG. 5. The effect of neglecting screening and relativistic corrections on the positron and electron spectra of Cu^{64}. The curves are to be interpreted as those of Fig. 3, except that $f_N=\eta^2(\epsilon-\epsilon_0)^2F_N(Z, \epsilon)$.

[16] G. J. Neary, Proc Roy. Soc. **175A**, 71 (1940).
[17] A. Flammersfeld, Zeits f. Physik **112**, 727 (1939).
[18] L. M. Langer and M. D. Whitaker, Phys. Rev. **51**, 713 (1937).

than about 10 percent of the correction itself, these effects are of minor importance.

We would like to express our appreciation to Professors W. W. Havens, Jr. and L. J. Rainwater for their encouragement and for numerous helpful discussions concerning this paper.

This paper is based on work performed under Contract AT-30-1-GEN-72 for the Atomic Energy Commission, and the information covered therein will appear in the Manhattan Project Technical Series, as part of the contribution of Columbia University.

PHYSICAL REVIEW VOLUME 75, NUMBER 2 JANUARY 15, 1949

Rotational Absorption Spectrum of OCS*

M. W. P. STRANDBERG, T. WENTINK, JR.,** AND R. L. KYHL
Research Laboratory of Electronics, Massachusetts Institute of Technology, Cambridge, Massachusetts

(Received August 2, 1948)

Extended measurements in the microwave rotational spectrum of carbonyl sulfide (OCS) are presented and correlated with the data obtained by other investigators. Precision measurements of rotational transitions for $J_{1\to2}$, $J_{2\to3}$, $J_{3\to4}$, $J_{4\to5}$ allow the evaluation of precise reciprocal moments of inertia in the ground vibrational state, and the centrifugal distortion coefficient. From frequencies observed for $O^{16}C^{12}S^{32}$, $O^{16}C^{13}S^{32}$, and $O^{16}C^{12}S^{34}$, internuclear distances have been calculated. Equilibrium moments of inertia and internuclear distances cannot as yet be given, since thus far only one of the three vibrational-rotational interaction coefficients (α_2) has been reported. Theoretical considerations involving such equilibrium data are discussed. Data on l-doubling in $O^{16}C^{12}S^{32}$, $O^{16}C^{13}S^{32}$, and $O^{16}C^{14}S^{32}$ are presented. The Stark effect of carbonylsulfide has been measured in $O^{16}C^{12}S^{32}$ and $O^{16}C^{13}S^{32}$. These measurements lead to the evaluation of the dipole moment and indicate the effect of isotopic changes on the dipole moment.

CARBONYL sulfide (OCS) is known to be a linear molecule. In this paper we have attempted to correlate existing information regarding the structure of this molecule which may be deduced from the rotational absorption spectrum, and to give extended measurements in order to allow a unified presentation. We wish to point out that several other investigators have been instrumental in obtaining much of the experimental and theoretical data considered below.

I. GENERAL THEORY

The rotational contribution to the energy levels of an unperturbed linear rotor in any vibrational state can be shown to be[1]

$$W=[J(J+1)-l^2]hcB_v - [J(J+1)-l^2]^2hcD_v, \quad (1)$$

where W is in ergs, J = total orbital angular momentum quantum number, l = quantum number of angular momentum parallel to figure axis due to a degenerate bending vibration, h = Planck's constant, c = speed of light, B_v = "reciprocal moment of inertia" in cm^{-1}, and D_v = centrifugal distortion coefficient in cm^{-1}.

Thus, from the Bohr frequency condition and the selection rule $\Delta J=+1$, rotational transitions are induced in a molecule with an electric dipole moment by radiation with frequencies in cycles/sec. given by

$$\nu_{J\to J+1}=2cB_v(J+1) - 4cD_v[(J+1)^3-l^2(J+1)]. \quad (2)$$

The "reciprocal moment of inertia" of the molecule in any vibrational state is related to the moment of inertia with the atoms in the minima of the vibrational potentials through the relation[1]

$$B_v=B_e-\sum_i \alpha_i[v_i+(d_i/2)] \quad (3)$$

where $B_e=(h/8\pi^2I_ec)$ cm^{-1}, I_e = equilibrium mo-

* This work has been supported in part by the Signal Corps, the Air Materiel Command, and O.N.R.

** Now at the Brookhaven National Laboratory.

[1] G. Herzberg, *Infra-Red and Raman Spectra of Polyatomic Molecules* (D. Van Nostrand Company, Inc., New York, 1945), p. 370–371.

ment of inertia, i=index over all vibrational states, v_i=vibrational quantum number, d_i=degeneracy of vibration: 1, 2, $\cdots$, α_i=coefficient measuring vibration-rotation interaction in cm^{-1}.

It should be noted that this representation is the usual one; in view of present knowledge it would be better, perhaps, to sum over all vibrational states separately instead of grouping the degenerate ones. For example, Herzberg[2] has pointed out that there exist interaction terms in the Hamiltonian for a linear molecule which will cause the rotation levels associated with the doubly degenerate bending vibrations to split into two component levels. This splitting is referred to as l-type doubling and has been studied theoretically by Nielsen and Shaffer[3] who have shown the effect is significant, probably, only in the first excited state, i.e., where $v_1=v_3=0$, $v_2=1$, $l_2=\pm 1$. The displacements of the component levels in this case are symmetrical about the unperturbed level and are found to be

$$\Delta W_J=\pm\tfrac{1}{2}chqJ(J+1)\text{ ergs,} \qquad (4)$$

where q is in cm^{-1} and depends upon the magnitude of the interaction term.

Since the first term in (1) is essential proportional to $J(J+1)$ also, the effect of the term (4) when incorporated in the energy is effectively to give different values of α_2 to the two component states. For the transition $J\rightarrow J+1$ two absorption lines will evidently be detected at frequencies which differ by

$$\Delta\nu=2cq(J+1)\text{ cycles/sec.}$$

The term values may also be perturbed by external fields. In the presence of an electric field the energy levels of a molecule with an electric dipole moment are perturbed because of the interaction of the rotating dipole with the static electric field, i.e., the Stark effect. This perturbation energy for linear molecules in the ground vibrational state is of second order and has been shown to be[4]

$$W_{J,m}^{(2)}=\frac{4\pi^2\mu^2E^2I}{h^2}\,\frac{J(J+1)-3m^2}{J(J+1)(2J-1)(2J+3)}, \qquad (5)$$

where m=magnetic quantum number and $|m|\leq J$, μ=electric dipole moment, and E=electric field strength.

Thus, the original transition has the spatial degeneracy partly removed and the frequencies for induced transitions are now given by

$$(\nu_{\text{Stark}})_{J\rightarrow J+1}=(\nu_0)_{J\rightarrow J+1}+\Delta\nu. \qquad (6)$$

The selection rule $\Delta J=+1$, $\Delta m=0$ applies when the Stark field is parallel to the electric vector of the incident radiation, and this is the case in these experiments. This is called a π-type transition and is the only case which will be considered in this paper. When $\Delta m=0$,

$$\Delta\nu=\frac{3m^2(16J^2+32J+10)-4J(J+1)^2(J+2)}{J(J+2)(2J-1)(2J+1)(2J+3)(2J+5)}\times\left(\frac{\mu^2E^2}{h^2\nu_0}\right).$$

The perturbation of the energy levels given by Eq. (5) are indicated in Fig. 1. The absorption

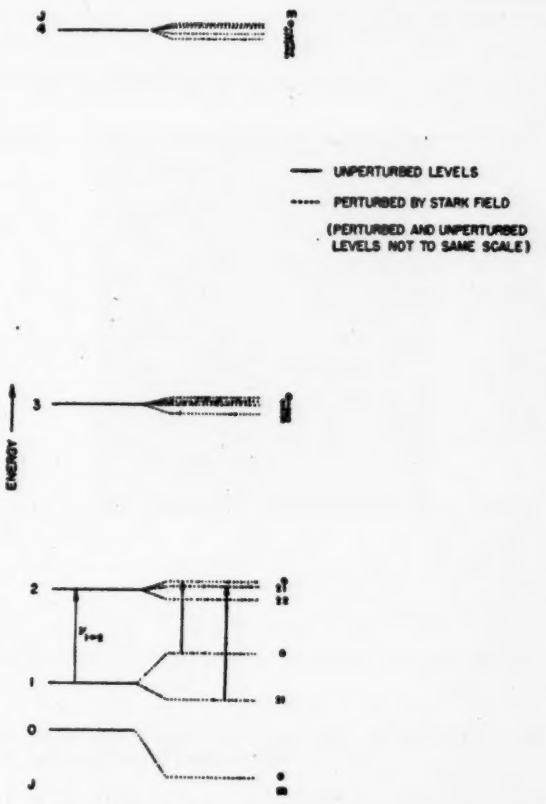

FIG. 1. Energy levels in a rigid linear rotor.

[2] Reference 1, p. 377.
[3] H. H. Nielsen and W. A. Shaffer, J. Chem. Phys. 11, 140 (1943).
[4] R. De E. Kronig, Proc. Nat. Acad. Sci. 12, 488 (1926).

spectrum for a given isotopic configuration with and without a Stark field is indicated in Fig. 2.

For the transition $J \rightarrow J+1$, $\Delta m = 0$, the square of the dipole direction cosine matrix element has a $[(J+1)^2 - m^2]$ dependence. Therefore, the intensity of each component follows a $\epsilon[(J+1)^2 - m^2]$ law; $\epsilon = 1$ when $m = 0$ and $\epsilon = 2$ for $0 < |m| \leq J$, because of the spatial degeneracy of the $+$ and $-m$ levels.

The study of the rotational absorption spectra of a molecule with various isotopic compositions with and without known electric fields can be used to deduce certain physical quantities.[5] First, if the vibrational interaction energies are ignored for zero-point vibrations, i.e., with a rigid rotor approximation, interatomic distances may be calculated if as many isotopic forms of the molecule are studied as there are structural parameters. Thus, in a linear unsymmetrical triatomic molecule with known atomic masses m_1, m_2, m_3, the moment of inertia is a function of the two interatomic distances, r_{12}, r_{23}. One may then solve the following set of equations for the interatomic distances r_{12} and r_{23}.

$$I_{(m_1 m_2 m_3 r_{12} r_{23})} = 2(J+1)h/8\pi^2\nu_0,$$

$$I_{(m_1' m_2 m_3 r_{12} r_{23})} = 2(J+1)h/8\pi^2\nu_0'.$$

The primes refer to the isotopically different molecule.

If absorptions are detected for the isotopic molecules in the ground vibrational state for two different J transitions, the centrifugal distortion energy can be evaluated (see Eq. (1)). Also if one J transition for each of the excited vibrational states is observed, the zero-point vibrational energy can be eliminated and the equilibrium moment of inertia can be evaluated. In this way the true equilibrium interatomic distances can be computed. The vibrational-rotational interaction energies must be used in the precise evaluation of the interatomic distances, since only the equilibrium distances may be assumed to be independent of nuclear mass changes.[6]

Secondly, the dipole moment of the molecule may be calculated for the molecule in any given vibrational state, and for any isotopic form, by measuring the Stark effect in that vibrational state in a known, homogeneous electric field. The dipole moment may also be inferred from the line intensities, since the absorption coefficient α_{max} in cm^{-1} can be shown to be

$$(4\pi^2 N_0 h\nu^3 \mu^2 / 3k^2 T^2 \Delta\nu c) \exp[-hcB_v J(J+1)/kT],$$

where N_0 = molecular density (molecules/unit

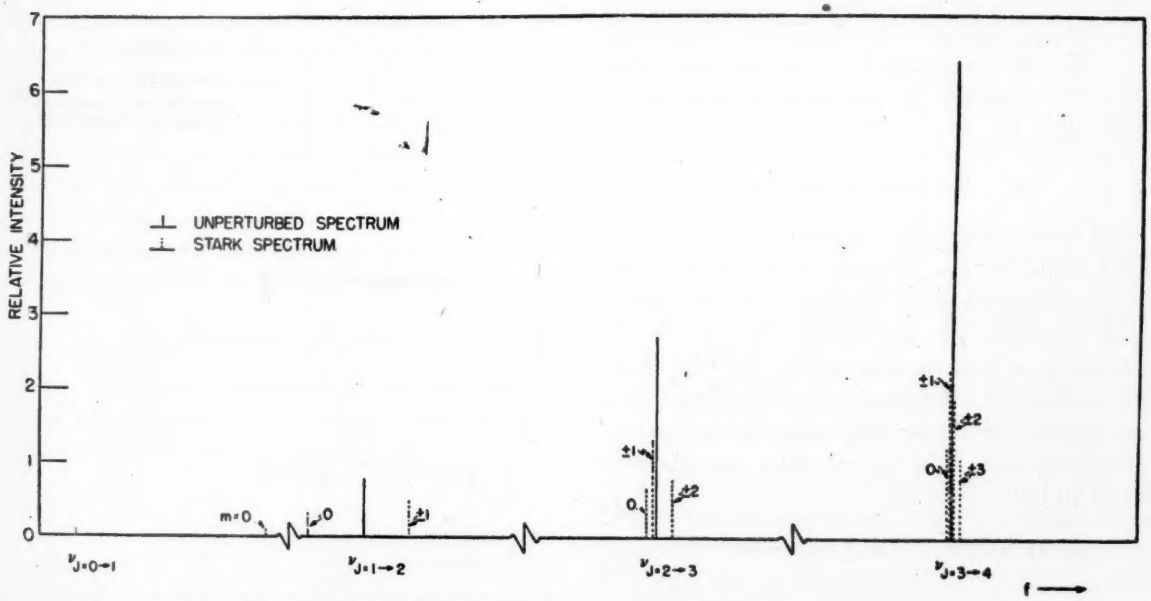

FIG. 2. Theoretical spectrum of a rigid linear rotor. Separation of unperturbed lines $= 2B_v$. Frequency scale about unperturbed lines expanded to show relative shifts in Stark effect.

[5] For an attempt to interpolate for S^{33} mass, see C. H. Townes, Phys. Rev. 72, 513 (1947).
[6] Reference 1, p. 396–397.

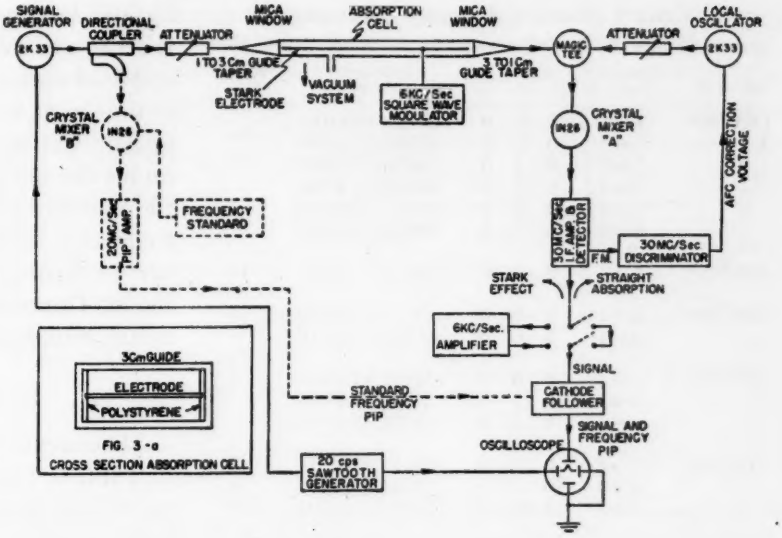

FIG. 3. Block diagram of microwave spectroscope.

volume), h = Planck's constant, ν = resonant frequency, μ = dipole moment, k = Boltzmann constant, T = gas temperature in °K, and $\Delta\nu$ = half-breadth of absorption at half-intensity. However, the dipole moment may not be evaluated by this method with facility or accuracy, since the measurement of absolute absorption depends upon so many things—e.g., the purity of the sample, the calibration of the measuring system, etc.

II. EXPERIMENTAL METHOD

Some knowledge of the structure of OCS is available from electron-diffraction data.[7] Such information is useful in calculating the reciprocal moment to an accuracy sufficient for a preliminary prediction of the spectral line frequencies to be expected in the microwave region. Alternatively, the bond distances may be calculated from the resonant bond model of Pauling.[8] A number of investigators have studied the absorption of OCS in the 24000-Mc/sec. region[9–14] and Dakin, Good, and Coles[9] have reported some preliminary Stark measurements.

The absorption lines studied by us were detected with an apparatus which has come to be known as a sweep spectroscope. The frequencies were measured with a secondary frequency standard calibrated with the National Bureau of

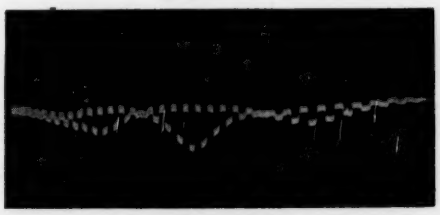

FIG. 4. Stark effect in OCS $J_{1\to2}$.

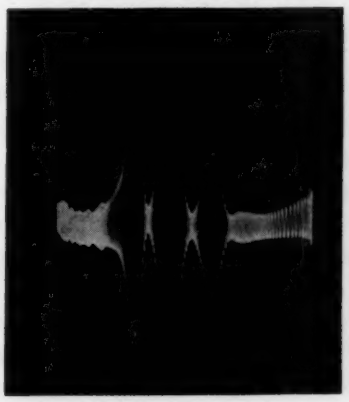

FIG. 5. Stark effect in OCS $J_{1\to2}$ (signal through narrowband 6-kc/sec. amplifier).

[7] P. C. Cross and L. O. Brockway, J. Chem. Phys. **3**, 821 (1935).
[8] L. Pauling, *Nature of the Chemical Bond* (Cornell University Press, Ithaca, 1939).
[9] T. W. Dakin, W. E. Good, and D. K. Coles, Phys. Rev. **70**, 560 (1946).
[10] W. D. Herschberger, J. App. Phys. **17**, 495 and 814 (1946).
[11] C. H. Townes, A. N. Holden, and F. R. Merritt, Phys. Rev. **71**, 64 (1947).
[12] C. H. Townes, A. N. Holden, and F. R. Merritt, Phys. Rev. **72**, 513 (1947); Phys. Rev. **74**, 1113 (1948).
[13] T. W. Dakin, W. E. Good, and D. K. Coles, Phys. Rev. **71**, 640 (1947).
[14] A. Roberts, Phys. Rev. **73**, 1405 (1948).

TABLE I. Observed absorption frequencies.

Molecule	Transition $J \rightarrow J+1$	v_1	v_2	v_3	Frequency Mc/sec.	Reference
$O^{16}C^{12}S^{32}$	1→2	0	0	0	24325.92±0.01	
	1→2	0	1	0	24380.97±0.03	
	1→2	0	1	0	24355.53±0.03	
	2→3	0	0	0	36488.82±0.03	
	3→4	0	0	0	48651.64±0.05	
	4→5	0	0	0	60814.08±0.05	
$O^{16}C^{12}S^{33}$	1→2	0	0	0	24020.3 ±0.1	12
$O^{16}C^{12}S^{34}$	1→2	0	0	0	23731.33±0.03	13
	3→4	0	0	0	47462.40±0.05	
$O^{16}C^{13}S^{32}$	1→2	0	0	0	24247.82±0.03	
	1→2	0	1	0	24300.58±0.03	
	1→2	0	1	0	24274.84±0.03	
$O^{16}C^{14}S^{32}$	1→2	0	0	0	24173.0 ±1.0	14
	1→2	0	1	0	24224.0 ±1.0	14
	1→2	0	1	0	24197.0 ±1.0	14

Standards frequency signals transmitted by WWV. We will outline only briefly both of these instruments.

The sweep spectroscope is roughly of the type in general use in the field of microwave spectroscopy.[15] Figure 3 is a block diagram of the apparatus. The absorption cell used for these measurements consists of 9.75 meters of 3-cm brass wave guide equipped with an electrode for the application of the Stark field. Figure 3a shows the electrode orientation.

Figure 4 is a picture of the $O^{16}C^{12}S^{32}$ absorption $J=1\rightarrow2$. The line is square-wave Stark-modulated at a low frequency so that the unperturbed and perturbed absorptions appear in alternate time intervals. Figure 5 shows the same absorption as it appears through a 6-kc/sec. amplifier. The sweep of Fig. 4 has been expanded considerably compared with that of Fig. 5. The $m=0$ line is on the right; $m=\pm1$ line is on the left. It is apparent that the sum of the individual absorptions equals the unperturbed absorption (center) and that their intensities obey the expected $\epsilon(2^2-m^2)$ relation.

The type of frequency standard used is described in Vol. 11 of the M.I.T. Radiation Laboratory Series[16] and is shown schematically in Fig. 6. The frequency standard "pip" is generated by the beating of the frequency-swept signal generator of the spectroscope with the frequency standard signal. If this "pip" is made to coincide in time with an absorption line, the standard frequency will be set at the line frequency plus or minus the pip amplifier i-f frequency. Therefore, the standard is set higher and lower than the line frequency, by an amount equal to the pip amplifier i-f frequency, and these two readings are made. The average of these two readings is the actual molecular absorption frequency.

III. EXPERIMENTAL DATA

Measurements of the OCS spectrum are given in Table I. The $J=1\rightarrow2$ and $J=2\rightarrow3$ transitions were measured with 2K33-type klystron generators. The $J=3\rightarrow4$ and $J=4\rightarrow5$ transitions were measured with this same type of oscillator by using the second-harmonic energy generated when the fundamental radiation is applied to a non-linear silicon crystal.

It should be noted that the error quoted is not a probable error. The standard is adjusted to WWV to at least 2 parts in 10^7. Doppler shift in

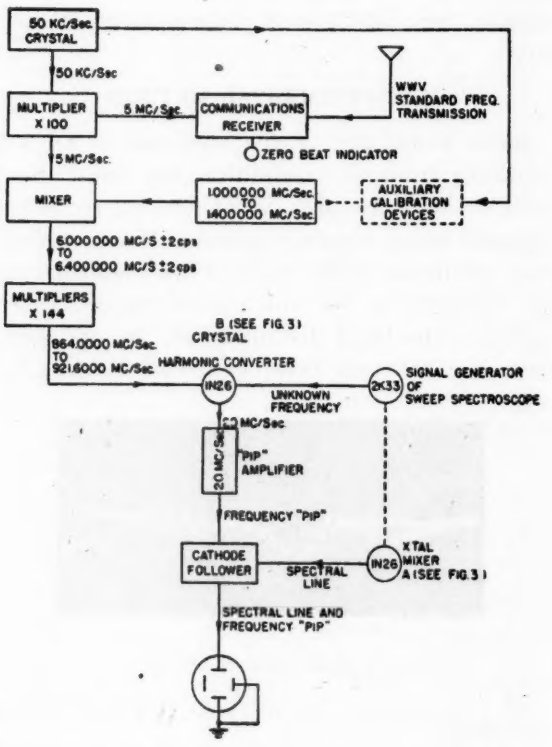

FIG. 6. Block diagram of frequency measurement scheme.

[15] R. H. Hughes and E. B. Wilson, Jr., Phys. Rev. 71, 562 (1947).

[16] M.I.T. Radiation Laboratory Series, Vol. 11, *Technique of Microwave Measurements* (McGraw-Hill Book Company, Inc., New York, 1947), p. 345–375.

TABLE II. Derived constants for OCS.

Term value parameters

Molecule	B_0 cm^{-1}	$I_{000}\times10^{-40}$ g-cm^2	cD_0 cycles/sec.	cq Mc/sec.	$c\alpha_2$ Mc/sec.	Reference
$O^{16}C^{12}S^{32}$	0.202864	138.0	1600±50	6.34±0.01	−10.61±0.01	
$O^{16}C^{12}S^{33}$	0.200319	139.7				12
$O^{16}C^{12}S^{34}$	0.197910	141.4	1400±100			
$O^{16}C^{13}S^{32}$	0.202216	138.4		6.43±0.01	−9.98±0.01	
$O^{16}C^{14}S^{32}$	0.20159	138.8		6.7 ±0.1	−9.4 ±0.3	14

Internuclear distances

	r_0(C=O)	r_s(C=O)	r_0(C=S)	r_s(C=S)	r_0(S=C=O)	Reference
Covalent radii	1.17A		1.54A		2.71A	8
OCO	1.1632	1.1615A				1
SCS			1.554			1
OCS	1.1637±0.0013*		1.5586±0.0010*		2.7223±0.0003*	
OCS	1.16 ±0.02		1.56 ±0.03		2.72 ±0.05	7

* Error determined from internal consistency of distances calculated from various isotopic forms; see text.

transmissions from WWV due to fading appears to be less than one part in 10^7 and WWV itself is claimed to be accurate to two parts in 10^8. The absorption lines are generally less than 200 kc/sec. wide when measured and readings are made to 4 parts in 10^7. The $J=1\rightarrow2$ line of $O^{16}C^{12}S^{32}$ has been measured many times over a period of 3 months giving results which are constant within ±10 kc/sec. The error quoted is thus large enough to insure reproducibility of the lines measured.

These data may be immediately reduced to yield the centrifugal stretching coefficient, the moments of inertia of the molecules in the ground vibrational state, and, to a rigid rotor approximation, the interatomic distances. These reduced data are given in Table II. We have used $h=6.6242\times10^{-27}$ erg-sec., 1 a.m.u. $=1.65990\times10^{-24}$ g, and in atomic mass units $C^{12}=12.00386$, $C^{13}=13.00754$, $S^{32}=31.98089$, and $S^{34}=33.97711$.

The $J=1\rightarrow2$ transition frequencies agree, within the experimental error, with those measured by Townes,[13] and Dakin, Good, and Coles.[13] Townes has also published values of the rotational absorption frequency of $O^{16}C^{12}S^{33}$ in the ground vibrational state and of $O^{16}C^{12}S^{32}$ in the doubly degenerate bending vibrational state.[12] We have measured the l-doubling in $O^{16}C^{13}S^{32}$ and Roberts[14] has measured the l-doubling for $O^{16}C^{14}S^{32}$. This measurement of the reciprocal moment of inertia in an excited vibrational state allows the evaluation of the α_2-coefficient in the expression for vibration-rotation interaction (Eq. (3)). Values of α_2 and q obtained are given in Table II. Since the similar coefficients for the interaction coefficients of the symmetric and antisymmetric stretching vibrations are not also known, this additional information is of no use at present in evaluating the equilibrium interatomic distances. Expressions due to Adel,[17] A. H. Nielsen,[18] and H. H. Nielsen[19] are available to calculate these unknown coefficients, but, unfortunately, the vibrational potential function of OCS is not well enough known to allow the coefficients to be computed with any accuracy. Of course, the inverse process could be performed, i.e., that of solving for the two unknown cubic force constants, by using the known α_2's determined from isotopic molecules. We have investigated this problem and feel that present precision of the necessary data, the α_2's and the centrifugal distortion coefficients, is not great enough to yield significant values for these force constants.

Dakin,[15] Townes,[12] and their collaborators have analyzed some of the factors limiting the accuracy of the determination of the dimensions of OCS. We consider the most important corrections are those due to zero-point vibrations.

Spectroscopic determination of molecular structure parameters is certainly not a new endeavor.

[17] A. Adel, Phys. Rev. **46**, 222 (1934).
[18] A. H. Nielsen, J. Chem. Phys. **11**, 160 (1943).
[19] H. H. Nielsen, Phys. Rev. **60**, 794 (1928).

Rotation and vibration-rotation spectra in the infra-red have long been used for such purposes. In fact, the dimensions of OCO, a molecule chemically and structurally similar to OCS, have been obtained from rotation-vibration spectra with corrections made for zero-point vibration. This is, of course, possible only in a linear, symmetrical, triatomic molecule, since then only one distance must be determined from the one equilibrium moment of inertia. Only unsymmetrical linear molecules possess the permanent dipole moments necessary for pure rotational absorption. However, isotopic variations are readily observed, and though corrections for vibration-rotation interaction is very difficult, useful information is still obtained by making the rigid rotor approximation.

In the case of OCS the rigid rotor approximation is not a bad one, since it is the shift in frequency of the absorption due to an isotopic substitution upon which the interatomic distances are dependent. This may be seen roughly as follows.

Since the α_i themselves are a small correction, and the change of the α_i with isotope will be a much smaller correction, we may assume α_i/B_v to be constant to a zero order of approximation. The equilibrium moments of inertia may then be written as:

$$B_e = B_v + \sum_i (\alpha_i d_i/2) = \beta^2 B_v,$$
$$B_e' = B_v' + \sum_i (\alpha_i' d_i/2) = \beta^2 B_v',$$

where

$$\beta^2 = [1 + (\sum \alpha_i d_i / 2B_v)].$$

Ignoring the vibration interaction is thus roughly equivalent to changing the interatomic distances by the factor β. In OCS the correction term $\sum_i \alpha_i d_i/2$ can be as large as 60 Mc/sec.; this will make β^2 about 1.01. Hence, the calculated interatomic distances may be high by approximately $\frac{1}{2}$ percent. The assumption that β is essentially constant is apparantly good to a rather high order, since calculations of interatomic distances from $O^{16}C^{12}S^{32}$ and $O^{16}C^{12}S^{34}$, from $O^{16}C^{13}S^{32}$ and $O^{16}C^{12}S^{32}$, and from $O^{16}C^{13}S^{32}$, $O^{16}C^{12}S^{34}$ yield identical results to about 0.1 percent, the error listed in Table II.

It might be thought that a better approximation may be made to the interatomic distances by considering three isotopic molecules and solving for the interatomic distances in terms of frequency shifts alone. The purpose here would be to use the data to yield equilibrium distances to a higher accuracy since to zero order the vibration-rotation interaction might cancel. However, this is not the case. This is easily shown by solving for the interatomic distance in terms of the equilibrium moment of inertia of the original molecule I_e^0, and the equilibrium moment of inertia with a center and end atom changed, I_e^c and I_e^e. The equilibrium distances then turn out to be:

$$r_{12} = \frac{[m_3^0/(m_1^0+m_2^0)][\delta_e - \delta_c]}{m_1^0[(m_3^0/(m_1^0+m_2^0)) - 1]},$$
$$r_{23} = (\delta_e - \delta_c)/\sum m^0,$$

where

$$\delta_e^2 = \sum m^0 \sum m^e (I_e^0 - I_e^e)/(m_3^0 - m_3^e)$$

and

$$\delta_c^2 = \sum m^0 \sum m^c (I_e^0 - I_e^c)/(m_2^0 - m_2^c).$$

By definition:

$$I_e - I_e' = \frac{h}{8\pi^2 c}\left[\frac{1}{B_v + \sum (\alpha_i d_i/2)} - \frac{1}{B_v' + \sum (\alpha_i' d_i/2)}\right]$$
$$= \frac{h}{8\pi^2 c}\left[\frac{1}{B_v} - \frac{1}{B_v'} + \frac{\sum \alpha_i' d_i}{2B_v'^2} - \frac{\sum \alpha_i d_i}{2B_v^2}\right].$$

Again to zero order the α_i's are proportional to B_e or to B_v for the reasons stated above. Thus we may write

$$(r_{12})_e = (r_{12})_v[1 - (\sum \alpha_i d_i/2B_v)]^{\frac{1}{3}},$$
$$(r_{23})_e = (r_{12})_v[1 - (\sum \alpha_i d_i/2B_v)]^{\frac{1}{3}},$$

which are the identical expressions for the distances solved with only two isotopic molecules.

It is interesting to note the similarity of the O−C and C−S distances in the related molecules OCO and SCS. This is to be expected from the simple resonant bond model of Pauling. These comparison distances are given in Table II.

IV. STARK MEASUREMENTS

Stark measurements of the permanent electric dipole moment of OCS are interesting in that

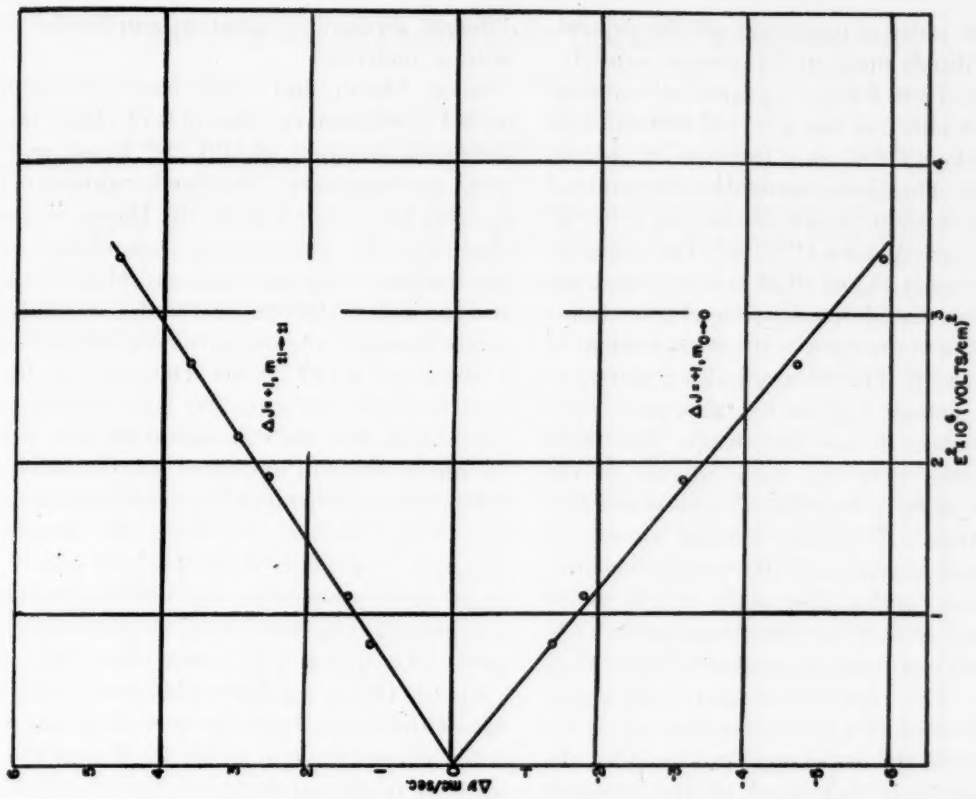

FIG 7. Stark effect in $O^{16}C^{13}S^{32}$.

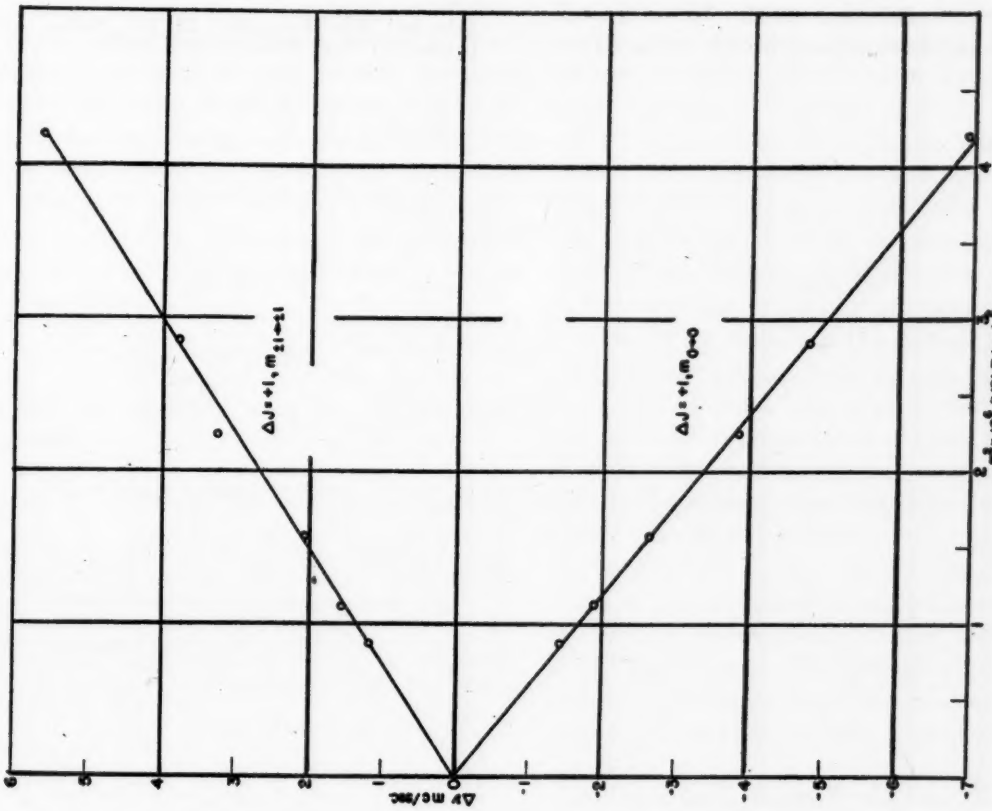

FIG. 8. Stark effect in $O^{16}C^{13}S^{32}$.

they give the order of magnitude of the dependence of the dipole moment on isotopic substitutions. Figures 7 and 8 show the experimental data for the Stark effect of the $J=1\rightarrow 2$ transition in $O^{16}C^{12}S^{32}$ and $O^{16}C^{13}S^{32}$ as a function of electric field strength. The dipole moments so determined in Debye units are 0.732 ± 1 percent for $O^{16}C^{12}S^{32}$ and 0.722 ± 1 percent for $O^{16}C^{13}S^{32}$. The probable statistical error is so low (0.25 percent) that the main error in the determination of the dipole moment is due to the error in the measurement of the field strength. This is essentially a matter of reading the voltage applied by the square-wave generator, since it can be shown that field inhomogeneities over the cross section of the wave guide slightly broaden the observed line without shifting it. The orientation of the central Stark electrode is critical in that errors in centering can cause appreciable shift of the Stark components, as well as line broadening. The septum centering in our apparatus is better than 0.5 percent. The applied voltage can be determined to better than 1 percent so that this is the limit of error of the measurement. However, the relative magnitudes are good to the probable error of fit or to 2.5 parts in 10^3. The indicated variation in dipole moment probably is due to the different zero-point vibration amplitudes in the isotopic molecules.

Good, Dakin, and Coles[9] have previously reported a preliminary value of 0.72 Debye unit for the dipole moment of $O^{16}C^{12}S^{32}$ based on Stark effect measurements. The dipole moment of OCS has also been measured by the Debye method of observing the temperature dependence of the polarization of the gas. Zahn and Miles[20] reported a value of 0.68 Debye unit and Jelatis[21] has recently repeated the measurement and arrived at a value of 0.720 ± 0.005 Debye unit for the electric dipole moment. The latter measurement checks well with our determination. The value of the dipole moment measured spectroscopically is independent of chemical impurities, as opposed to the Debye method in which the presence of impurities, especially those of a polar nature, may cause appreciable error. It should be pointed out that the spectroscopic value is determined for a given vibrational state (zero vibrational here), while the Debye method yields a statistical average of the dipole moment over all of the vibrational states of the molecule excited at the temperature of measurement.

[20] Zahn and Miles, Phys. Rev. **32**, 497 (1928).
[21] J. Jelatis, J. App. Phys. **19**, 419 (1948).

Grain Density in Photographic Tracks of Heavy Particles*

M. BLAU
Columbia University, New York, New York

(Received September 17, 1948)

The relation between grain density in photographic tracks and particle energy has been derived theoretically assuming that the probability that a grain be developed is given by $P=c(1-\exp[-b(dE/dR)^{\frac{1}{2}}])$. Using a single pair of parameters b and c we can represent with this equation all experimental curves so far published for alpha-particles, tritons, protons, π and μ mesons (University of Bristol). The agreement between experiments and theory is very satisfactory.

THE photographic emulsion as a tool in nuclear physics requires an accurate knowledge of its inherent characteristics. This topic was extensively treated in papers by Demers,[1] Cüer,[2,3] Lattes,[4,5] Webb,[6] and Perkins.[7]

There are three main problems which are of the utmost interest for photographic work in nuclear physics; the energy-range determination, the grain density in nuclear tracks, and the scattering effect in relation to the energy and the mass of nuclear particles. This paper will treat only the subject of grain density.

The grain density in photographic work plays a role similar to the ionization energy in work with cloud chambers or proportional counters. Since the formation of the latent image is based on an ionization process, it should be possible to express grain density as a function of the ionization energy or energy loss per unit of track length. An empirical relationship between grain density and range has been established by Lattes and co-workers.[4]

$$N=km^{(1-n)}R^n. \tag{1}$$

Equation (1), together with the range-energy relationship,

$$E=0.262M_0^{0.425}R^{0.575}, \tag{2}$$

is valid for all types of single charged heavy nuclear particles over a considerable range. This makes it possible to compute the necessary facts about mass and energy from the observed nuclear track provided that the variable factor n (variable with particle mass) in Eq. (1) is known or can be found experimentally. This procedure has been very successfully applied in the research on π- and μ-mesons.

Demers and Cüer,[1,3] on the other hand, tried to derive a theoretical relationship connecting the energy spent by particles passing through a photographic emulsion and the number of AgBr grains developed within the respective tracks. So far this procedure has not been satisfactory because no general equation existed which was valid for particles of different energies and masses. In other words, the photographic emulsion seems to become less sensitive the higher the specific ionization of the passing particles, and it is not possible to establish a linear relationship between grain density and energy loss.

However, considering the complexity of the photographic process, it is obvious that we cannot expect a linear law. It is necessary to take into account the phenomena of space charge and recombination which are due to the high ion density prevailing during extremely short periods within the affected grains.

The conditions here can be compared with those in highly ionized gaseous atmospheres or in "strong electrolytes." Debye and Hückel[8] solved the latter problem assuming that the mobility of ions depends on the ion concentration. Without attempting to give a detailed account

* This document is based on work performed under Subcontract S62 of Contract AT-30-2-Gen 16 for Brookhaven National Laboratory at Columbia University.

[1] P. Demers, Phys. Rev. **70**, 974 (1946).
[2] Cüer, Comptes Rendus **223**, 1121 (1946).
[3] P. Cüer, *Sci. et Ind. Photo.* **18**, 321–32, 353–59 (1947).
[4] C. M. B. Lattes, P. M. Fowler, and P. Cüer, Proc. Phys. Soc. London **59**, 883 (1947).
[5] C. M. G. Lattes, G. P. S. Occhialini, and C. F. Powell, Nature **160**, 486 (1947).
[6] J. H. Webb, Phys. Rev. **74**, 511 (1948).
[7] D. H. Perkins, Nature **159**, 126 (1947).
[8] P. Debye and E. Hückel, Physik. Zeits. **24**, 185 (1923).

of this theory, we make use of Eqs. (3)**

$$\psi = -\lim_{r=0} \frac{2e}{\epsilon r}(1-e^{-\kappa r}) = -2e\kappa/\epsilon,$$
$$\kappa = [(8\pi NZ^2e^2)/(\epsilon kT)]^{\frac{1}{2}}, \tag{3}$$

which describe the potential of an ion cloud around an isolated ion having the electric charge Ze where ϵ is the dielectric constant of the medium and n the number of ions present.

It should be noted that the magnitude of the potential is proportional not to the *number* but to the *square root of the number of* ions. Although we can not prove that an equivalent law can describe similar phenomena in the solid state we accept this idea tentatively as our working hypothesis for processes in highly ionized AgBr grains. Therefore, we describe the potential around the negatively charged specks in AgBr grains by a function $\psi \sim (n)^{\frac{1}{2}}$, where n is the number of ion pairs formed by the traversing particles. Consequently, these specks attractions only according to $(n)^{\frac{1}{2}}$ and not proportional to n.

If these considerations are correct, we can assume that the probability P for a grain to become developable within an element dR is given by an expression

$$P = dN/dR = C(1-\exp[-b(dE/dR)^{\frac{1}{2}}]), \tag{4}$$

because $(dE/dR)^{\frac{1}{2}}$ is proportional to the square root of ions produced. dN/dR is the grain density, and c and b parameters characteristic for a certain type of emulsion and processing conditions. In order to prove the validity of this equation, we compared the theoretically derived curve with experimental curves for the number of grains *versus* residual range.

The values $(dE/dR)^{\frac{1}{2}}$ were obtained from experimental—energy *vs.* range—curves in photographic emulsions using the equations[4,5]

$$dE/dR = \alpha(E/R),$$
$$(dE/dR)^{\frac{1}{2}} = (\alpha E/R)^{\frac{1}{2}}, \tag{5}$$

where E is expressed in Mev and R in microns.

Similarly, the values of dN/dR are derived from experimental $N \rightarrow R$ curves

$$dN/dR = a(N/R). \tag{6}$$

Here again the calculations are based on the experimental work performed at the University of Bristol.

Adjusting the parameters c and b in (4) in order to fit the experimental values of dN/dR for protons and alpha-particles over the range—$85 \rightarrow 2135\mu$—we can calculate the respective $N \rightarrow R$ curves using the equation

$$N = (R/a)dN/dR$$
$$= Rc/a(1-\exp[-b(dE/dR)^{\frac{1}{2}}]). \tag{7}$$

These curves are given in Fig. 1. The agreement between the calculated and experimental values (circles) is satisfactory, considering that quite a large range of energies is covered using a single pair of parameters b and c.

The numerical value of b is $b=3$; the shape of the curve is not very sensitive with respect to this parameter, and other values between 2.5 and 3 may prove more satisfactory if the low range part of the alpha-curve is investigated in more detail. The fact that b is different from unity is probably connected with the complexity of photographic emulsions; the differential stopping power and energy loss are much larger in the silver bromide grain than in the surrounding gelatine.

The parameter c represents the actual number

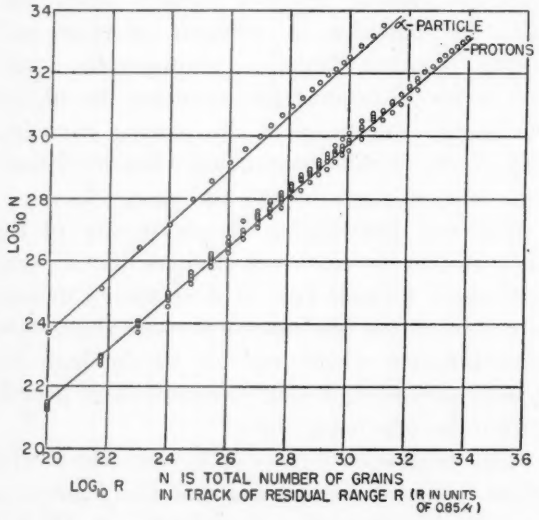

FIG. 1. Relationship between number of grains and residual range in photographic tracks of alpha-particles and protons.

** The dependence of the factor κ from the absolute temperature T will be discussed in another paper together with experiment results.

of grains present per unit length. The numerical value $c=4$ is unexpectedly high. However, it is not permitted to extrapolate the above equations without correction down to the low range of highly ionizing particles, because in this interval the stopping power of the emulsion decreases rapidly. As it is difficult by ordinary microscopic observation to resolve and count the grains at low ranges of alpha-particles, we cannot decide for the time being if the value $c=4$ is incompatible with experimental facts.

Investigating the validity of (6) and (7) for the case of mesons, we again compare with the experimental values found at the University of Bristol.

The theoretical curve for mesons can be obtained by the so-called Perkins Method, using the relation $m_p/m_m=R_p/R_m$ valid for particles of equal velocity and charge. For this purpose we plot the calculated values for $\log(dN/dR)_p$ *versus* $\log R_p$ . . . Fig. 2 and displace this curve along $\log R$ axis by distances corresponding to $-(\log m_p-\log m_m)$. In Fig. 2 such displacement is carried out for particles of twice and one-half of the proton mass. If we plot in Fig. 2 not only one or two but a family of curves, it should be relatively easy to identify the mass and charge of an unknown particle.

The grain density in tracks arising from particles of higher charge than 1 will be

$$(dN/dR)_s=C\{1-\exp[-bz(dE/dR)^{\frac{1}{2}}]\},$$

considering particles of equal velocity and provided that we are working in a region where the parameters of the range-energy equation are constant.

Another possibility is based on the use of Eq. (8)[4]

$$E=0.262m^{0.425}R^{0.575}, \tag{8}$$

whence

$$dE/dR=0.262\cdot 0.575m^{0.425}R^{-0.425},$$

which permits us to calculate the curves for particles of various mass but equal residual range.

Using Eq. (8), and substituting in Eq. (6), we obtain

$$dN/dR=C(1-\exp[-b\{(m_p/m_\mu)^{0.425}\cdot dE/dR\}^{\frac{1}{2}}]). \tag{6'}$$

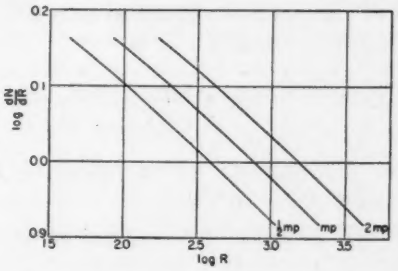

FIG. 2. Relationship between grain density and residual range of particles of different masses, corresponding to one-half the proton mass ($1/2m_p$), the proton mass (m_p), and twice the proton mass ($2m_p$).

This equation was used in order to calculate the grain density for π- and μ-mesons at 85μ-range, assuming $m\pi/m\mu=1.64$.

We find $N_\pi=115$ and $N_\mu=109$ in good agreement with the experiment.

Finally, the corresponding value for tritons at 85μ is $N_T=170$, again in complete agreement with the experiment.

In all calculations the same parameters b and c were used, and therefore we can conclude that our previous assumptions are correct, at least within the range of experiments performed up to now. Therefore, we are entitled to calculate in advance theoretical curves for particles of different charge and mass. We can then expect to identify within the limits of the photographic method the type of particles which give rise to the observed tracks.

Another advantage of the method consists in the fact that it permits us—again within the limits of the photographic method—to recognize particle tracks which do not start and end within the emulsion. That is especially important in cosmic-ray experiments or whenever the production rate of particles of different types has to be established.

Let us assume that we have observed a track —sufficient in length—which does not start or end in the emulsion but has distinctly different grain densities toward the two observed end points.

We then assign to the point of lower grain density the values R_z and $(dN/dR)_{R_z}$, and to the point with higher density R_{z-a} and $(dN/dR)_{R_{z-a}}$. Using Eq. (4), we can calculate (dE/dR) resp. $(dE/dR)_{R_{z-a}}$.

The quotient $(dE/dR)_{R_z}/(dE/dR)_{R_{z-a}}$ is inde-

pendent of the particle mass and only a function of the respective ranges.

$$(dE/dR)_{R_x}/(dE/dR)_{R_{x-a}}=R_x^{0.425}/(R_{x-a})^{0.425}$$
$$=1/[1-(a/R_x)]^{0.425}. \quad (9)$$

Equation (9) permits us to calculate R_x and consequently R_{x-a}.

However, knowing the residual range of our particle, we are in the same position as before and can assign to our track one of the family of curves in Fig. 2.

Our curves and equations have been compared only with experiments in Ilford emulsion. We can expect, however, that they will be equally valid for Eastman Kodak emulsion, changing slightly the parameters b and c.

PHYSICAL REVIEW VOLUME 75, NUMBER 2 JANUARY 15, 1949

Radioactivity of C^{10} and O^{14}

R. SHERR, H. R. MUETHER, AND M. G. WHITE
Palmer Physical Laboratory, Princeton University, Princeton, New Jersey†

(Received October 4, 1948)

A new activity, O^{14}, has been produced from N^{14} by a (p,n) reaction and is found to decay with a half-life of 76.5±2 sec. by the emission of 1.8±0.1-Mev positrons and a 2.3-Mev gamma-ray. Rough threshold measurements indicate that the gamma- and beta-rays are in cascade. C^{10}, formed by a (p,n) reaction in B^{10}, has been carefully reexamined and shown to decay with a half-life of 19.1±0.8 sec. by the emission of 2.2±0.1-Mev positrons and a gamma-ray of approximately 1 Mev. The Coulomb energy formula for this type of mirror nucleus is shown to be valid, but the same theoretical difficulties are encountered here as are already known from the long lives of Be^{10} and C^{14}.

INTRODUCTION

IT is well known that an important contribution to the mass of a nucleus is the classical Coulomb energy which arises from the positive nuclear charge. A particularly convincing demonstration of this fact is obtained[1,2] from the study of positron spectra of those "mirror" nuclei which are characterized by having one more proton than neutrons (e.g., Be^7, C^{11}, N^{13}, O^{15}, etc.). The emission of a positron merely interchanges the number of neutrons and protons, and on the assumption that specifically nuclear forces between nucleons in similar states are equal and independent of the charge, one can attribute the entire energy release of the mirror nuclei to Coulomb energy and the neutron-proton mass difference. Coulomb energy can be calculated in a classical way, assuming the nuclear charge to be uniformly distributed over a volume proportional to the number of nucleons. Taking the nuclear radius to be $r=1.44\times10^{-13}A^{\frac{1}{3}}$, where A is the mass number, one obtains $E_c=0.60Z(Z-1)A^{-\frac{1}{3}}$. E_c is the Coulomb energy in Mev and Z is the atomic number. The agreement[1] of this expression with the experimental values obtained from the positron spectra of mirror nuclei shows that the assumptions regarding equality of $p-p$, $n-n$ forces is largely justified, and, further, that the nuclear volume is approximately proportional to the number of nucleons. One important aspect of Fermi's theory of β-decay, the relation between half-life and energy, also receives confirmation from these β-transitions.

The properties of other light nuclei are not so well understood either from the point of view of nuclear structure or β-theory.[2] Thus, in nuclei of the type $A=4n+2$ it is found that two members of the series (He^6 and F^{18}) decay with half-lives which imply allowed transitions between states presumably differing in spin by 1. This experi-

† Assisted by the Joint Program of the Office of Naval Research and the Atomic Energy Commission.

[1] E. Wigner, Phys. Rev. 56, 519 (1939); M. G. White, E. C. Creutz, L. A. Delsasso, and R. R. Wilson, Phys. Rev. 59, 63 (1941); Additional references to the present and related questions are given in these papers and also in reference 2 below.

[2] E. J. Konopinski, Rev. Mod. Phys. 15, 209 (1943).

mental fact apparently requires the acceptance of Gamow-Teller selection rules. On the other hand, a more serious difficulty is that presented by other members of the series Be^{10}, C^{14}, Na^{22}, P^{30}, etc., whose (ft)†† values correspond to highly forbidden transitions, whereas allowed transitions are to be expected on the basis of GT rules. The most puzzling transitions of the $4n+2$ nuclei were $Be^{10}\rightarrow B^{10}\leftarrow C^{10}$. Be^{10} and C^{10} are similar to the mirror nuclei discussed above in that they differ only in the interchange of two protons and neutrons; the other quantum numbers of their ground states are expected to remain unchanged. The mass difference $(C^{10}-Be^{10})$ should be accounted for by the additional Coulomb energy of the former, and the transitions of both mirror nuclei to the ground state of B^{10} should be of the same character (i.e., both equally allowed or forbidden). Attempts to explain the allowed character of the $C^{10}-B^{10}$ transitions and the forbidden character of the $Be^{10}-B^{10}$ transition were unsuccessful. The theory of nuclear structure required that Be^{10} and C^{10} be simply related as described above, while the theory of β-decay required that the ground states be quite different.

The present experiment was undertaken to reexamine the radioactivity of C^{10} and to search for the radioactivity of O^{14}, which is related to C^{14} and N^{14} in the same manner as the lighter triad. While some of the measurements cannot be considered as final, sufficient information has been obtained to show that the ground states of Be^{10} and C^{10}, and of C^{14} and O^{14}, are probably of similar quantum character, as required by the theory of nuclear levels of light nuclei. The new results show that the previously reported activity of C^{10} [3] was in error. The presently observed C^{10} is a positron emitter of half-life 19.1 ± 0.8 sec. with a β-spectrum limit of 2.2 ± 0.1 Mev, accompanied by nuclear γ-radiation in the neighborhood of 1 Mev. O^{14} has been found to be a positron emitter of half-life 76.5 ± 2 sec. with a β-energy of 1.8 ± 0.1 Mev, accompanied by nuclear γ-radiation of 2.3 Mev. These results will be discussed later.

EXPERIMENTAL PROCEDURE

In order to permit rapid chemistry on the radioactivities produced by protons on various targets, a gas flow system was used similar to that employed by Sommers and Sherr.[4] The target material was placed in a small copper cell (Fig. 1) which terminated a probe of the usual cyclotron variety. A small amount of finely powdered target material was held in place at the tip of the cell by a mat of glass wool. The internal proton beam of the cyclotron entered through a 1-mil copper foil covering the cell.

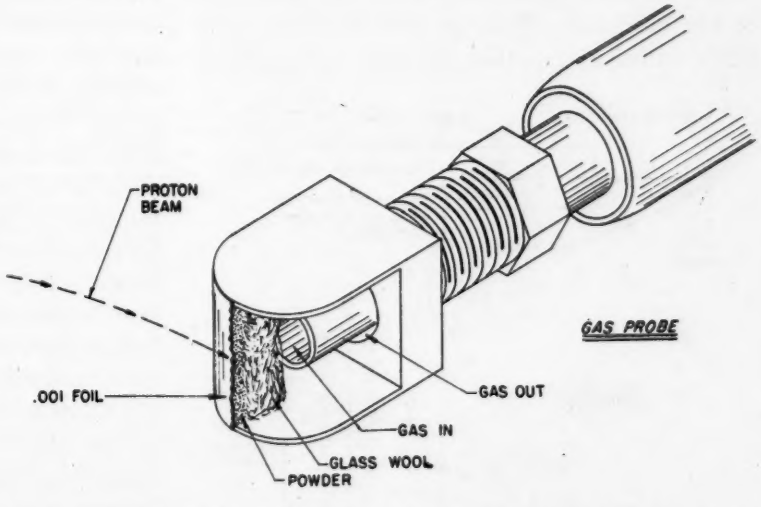

FIG. 1. Cyclotron probe for collection of radioactive gases evolved in the bombardment of powdered targets. These gases are swept to an inspection cell by a flushing gas.

†† The product (ft) should be approximately constant for a given type of transition (see references 1 and 2). In this expression, t is the half-life while f is a certain integral over the energy spectrum of the β-particles and is related to the half-life by $1/t=(1/\log 2)Gf(W_0,Z)$. G depends on the matrix elements of the nucleons. $W_0=1+(E_\beta/mc^2)$ where E_β is the upper limit of the spectrum.

[3] L. A. Delsasso, M. G. White, W. Barkas, and E. C. Creutz, Phys. Rev. 58, 586 (1940).

[4] H. S. Sommers, Jr. and R. Sherr, Phys. Rev. 69, 21 (1946).

After or during irradiation the radioactive gases formed and released by the bombardment were swept to an inspection chamber by a flushing gas by way of the concentric tubes in the probe as indicated in Fig. 1. The gas handling system is shown in Fig. 2. The essential features are the various solenoid operated "hose pinching" valves and the inspection chamber. The system was sufficiently flexible to permit varied types of operation (continuous flow, bombardment in vacuum, etc.). For purposes of chemistry or purification, tubes of absorbing materials and traps of various kinds were easily inserted in the flow line. The inspection chamber has two 2-mil copper windows, permitting the simultaneous use of two mica window Victoreen Model "VG" counters. For some of our measurements it was necessary to trap the desired radioactive gases on $CaCl_2$ or NaOH. Powders of these materials were held across the center of the inspection chamber by wire mesh screens with the gas inlet and outlet so arranged that the gas could leave only by passing through the absorbing material. The pulses from the Geiger counters were fed to scaling circuits and finally to a double channel recording oscillograph (Brush Model BL-202). For short period activities decay curves were obtained by counting pulses on the paper tape of the Brush oscillograph as a function of time. By means of an electrical control box the operations of bombardment, flushing, and recording were made automatic, so that measurement could be started within a fraction of a second after ending the bombardment. While this method of production of radioactive gas is very inefficient in terms of the total radioactivity available, sufficient activity could be obtained for most of the measurements.

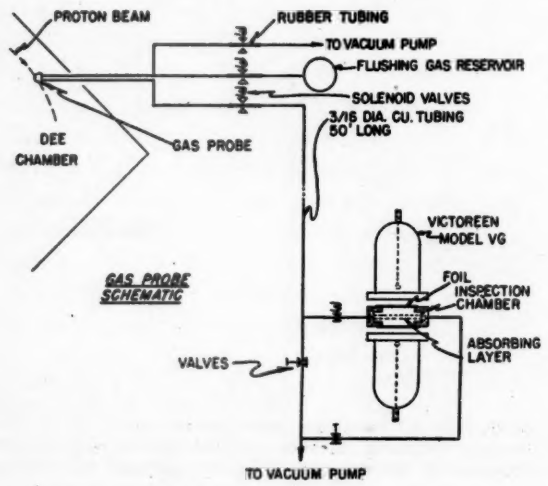

FIG. 2. Schematic drawing of the gas probe system, showing the probe, control valves, and counting arrangement.

The chemical processes by which radioactive gases were obtained from various target materials were a source of considerable puzzlement, but also of great convenience. In bombarding all boron containing substances (H_3BO_3, borax, CaF_2BF_3, and boron metal), the radioactive carbon produced by a (p, n) reaction appeared at the inspection chamber in the form of CO_2. The CO_2 was absorbed in a layer of ascarite (NaOH on asbestos) while nitrogen and neon activities were pumped off. No evidence of formation of CO was found. In the case of the oxygen radioactivities, the compound KSCN was used as target material, and the oxygen appeared in the form of H_2O. The latter was collected on a layer of $CaCl_2$, while carbon, nitrogen, and other activities were pumped off. As was to be expected, the yield of radioactive gas was higher for more finely divided target material.

C^{10}

Bombardment of boron metal or boron compounds with 0.5 μa of protons at approximately 17 Mev energy gave carbon activities decaying as shown in Fig. 3. In addition to the well-known 20.5-min. activity of C^{11} produced by a (p, n) reaction in B^{11}, a new period of 19.1 sec. was found. The decay curve of Fig. 3 was obtained from the same boron powder used by Delsasso, *et al.*[3] in the earlier work on C^{10}. No evidence was found at 17 Mev for the shorter period reported by them. Direct measurements were made on the boron powder irradiated at 7 Mev by pushing the bombardment probe to a smaller radius. This target then showed a period of 9–10 sec. However, a similar irradiation with highly purified B_4C showed only a weak 20-sec. period and the C^{11} period. It must be concluded that the 8.8-second activity previously reported resulted from an impurity in the boron powder. In Fig. 4 is shown the decay of the radioactive gases produced in enriched CaF_2, $B^{10}F_3$ containing 95 percent B^{10} instead of 18.4 percent, and trapped by ascarite. The ratio of the 19-sec. activity to

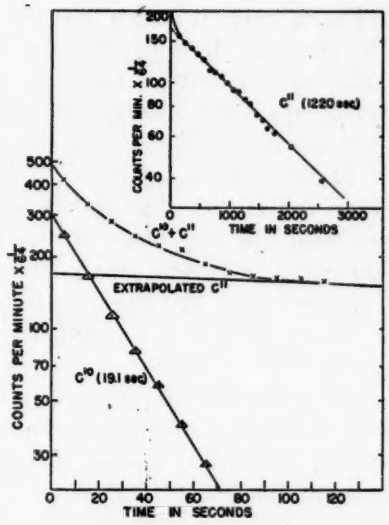

FIG. 3. Decay of radioactive gases from bombardment of boron by protons. The upper graph shows the C^{11} decay, and the lower graph shows the C^{10} decay.

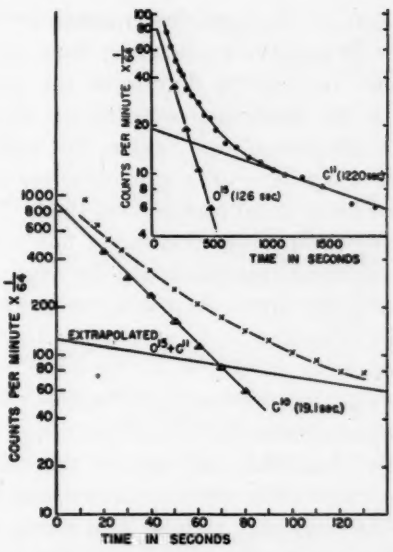

FIG. 4. Decay of radioactive gases from bombardment of CaF_2, $B^{10}F_3$ by protons. The gases have been trapped by ascarite. The upper graph shows the longer period activities, the lower graph shows the C^{10} decay.

the C^{11} activity was enhanced by a factor of the order of 50 over that for ordinary boron, indicating the correctness of the assignment of this new period to C^{10}.

It was observed that for all unenriched targets the ratio of C^{10} to C^{11} remained constant (within the limits imposed by differences in bombarding time). To make certain that the 19-sec. activity was carbon, a series of chemical tests were made by Professor John Turkevich of the Chemistry Department. The radioactive gas was dissolved in a $Ba(OH)_2$ solution. CO_2 was precipitated as $BaCO_3$. A carrier was then provided by addition of Na_2CO_3, which precipitates $BaCO_3$. The solution was filtered and the $BaCO_3$ was placed under the counter. The entire procedure was completed within 20 sec. after ending bombardment. Although recovery was not complete, the C^{10}/C^{11} ratio in the filter paper was the same as in the case where the radioactive gas was trapped on ascarite. The only other likely gaseous activity which would behave like CO_2 in this analysis is SO_2. Additional tests were made to examine this possibility. The radioactive gas was passed for one minute into a solution containing NaOBr. At this point Na_2CO_3 carrier solution was added, the mixture shaken and then treated with HCl liberating copious amounts of gas. The gas was passed over ascarite, which was then found to be radioactive with periods of approximately 19 sec. and 21 min. The purpose of this radiochemical analysis was to eliminate SO_2 as a source of activity. If there were any SO_2 in the original gas it would dissolve in the NaOBr to form sodium sulfate. The latter would not decompose into a gaseous product on treatment with HCl. However, we did detect activity in the ascarite with the original periods and relative strength. These findings are consistent with the view that CO_2 in the original gas dissolved in the NaOBr and was liberated by the HCl, and again trapped by ascarite. We, therefore, ascribe the 19.1-sec. period to C^{10} and the 21-min. period to C^{11}.

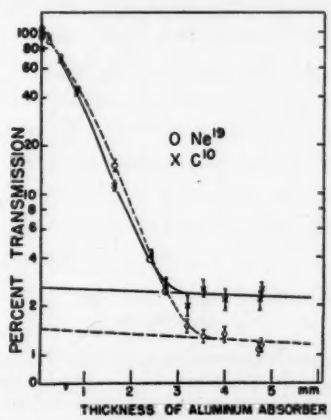

FIG. 5. Positron absorption curves for Ne^{19} and C^{10}, taken under identical geometrical conditions. The abscissae refer to added aluminum absorber.

The sign of the particles emitted by C^{10} was found to be positive by bending them in a magnetic field. In order to determine the maximum energy of the positron spectrum, an absorption curve in aluminum was taken. For calibration purposes a similar curve was obtained for Ne^{19} produced by a (p, n) reaction on PbF_2. Ne^{19} was chosen for comparison because it has a half-life of 20.3 sec.[5] and approximately the same energy. Both activities were examined as gases in the inspection chamber (i.e., no chemical absorbing materials were used), so as to have identical geometries. Measurements on a number of decay curves gave a value of 18.2 ± 0.6 sec. for the half-life of Ne^{19} and 19.1 ± 0.8 sec. for the half-life of C^{10}. The lower value obtained at present for Ne^{19} may be instrumental, although no source of error is apparent. It may be that in the previous work the period was lengthened by the presence of a small amount of impurity in the solid target used. The present decay curves were simple over a factor of 100 in counting rate, while the earlier decay curves were carried over only a factor of 10 in activity.

The absorption curves for Ne^{19} and C^{10} are shown in Fig. 5, where it is seen that the energies are nearly identical. It is to be noted that the γ-ray background activity is higher by a factor of two in the case of C^{10}, showing the presence of nuclear γ-radiation in the decay of this nucleus; the Ne^{19} background is assumed to be solely annihilation radiation.[5] Because of statistical fluctuation near the end point of the positron absorption curve, it is difficult to determine directly a precise range. We have, therefore, analyzed the absorption data of Fig. 5 by the method of Bleuler and Zünti.[6] These authors developed approximate theoretical curves for the absorption of β-spectra of different energies in aluminum and corrected the theoretical curves to agree with experimentally determined curves for various Z as well as E_β. Their results are summarized in Fig. 6 and Fig. 7 of their paper.[6] Their method of determining the energy of an unknown substance from its absorption curve is essentially as follows: the absorber thicknesses corresponding to reduction of the intensity of $\frac{1}{2}$, $\frac{1}{4}$, $\frac{1}{8}$, etc., are designated as d_1, d_2, d_3, etc. To each value of d_n there corresponds an energy, E_n, which is the maximum energy of the β-spectrum. If the spectrum is simple and allowed, the various E_n should be identical. Bleuler and Zünti found that by applying their curves to previously published absorption curves for various radioactivities, they were able to obtain energy values which agreed very well with β-spectrographic values, frequently to a higher degree of accuracy than the values given by the original authors of the absorption data. The success of their method in handling data taken under various experimental conditions and the fact that our geometry is not very different from their own, suggests that an analysis of the present data in this fashion is probably fairly accurate. In Fig. 6, the absorption data for C^{10} and Ne^{19} are replotted with the γ-ray background subtracted in each case. (The abscissa includes the counter windows and copper foil of the inspection chamber.) Comparison with the curves of Bleuler and Zünti gives the following values of E_β (corrected for Z and sign of particle) corresponding to successive d_n: for Ne^{19} 2.33, 2.34, 2.31, 2.33, 2.33, 2.32 Mev, or an average of 2.33 Mev; for C^{10} 2.28, 2.23, 2.17, 2.18, 2.18, 2.17, or

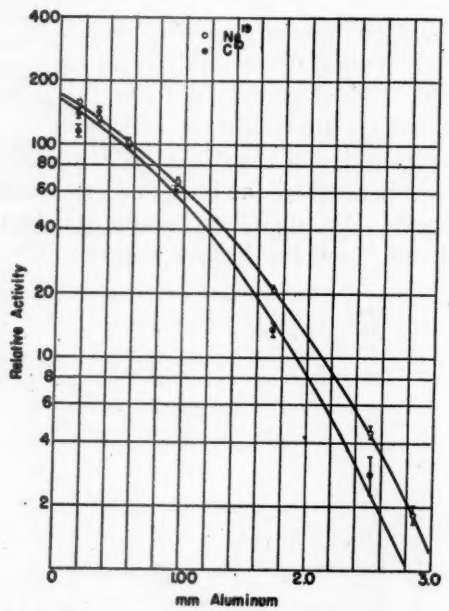

FIG. 6. Positron absorption curves for Ne^{19} and C^{10}. The data of Fig. 5 are replotted with γ-ray backgrounds subtracted. The abscissae have been corrected for the counter window and the inspection cell window.

[5] M. G. White, L. A. Delsasso, J. G. Fox, and E. C. Creutz, Phys. Rev. 56, 512 (1939).

[6] E. Bleuler and W. Zünti, Helv. Phys. Acta 19, 375 (1946).

2.20 Mev average. The value of 2.33 Mev for Ne^{19} is somewhat higher than the previously reported value[5] of 2.2 Mev as determined with a cloud chamber, but in good agreement with the value of 2.3 Mev as determined by absorption.[5] In view of the fact that the method of Bleuler and Zünti as used by them in the manner described above on the data of other workers gave values which were frequently in better agreement with spectrographic values than cloud-chamber evaluation, the presently determined values are accepted as essentially correct; i.e., for Ne^{19}, $E_\beta = 2.3 \pm 0.1$ Mev and for C^{10}, $E_\beta = 2.2 \pm 0.1$ Mev.

As noted above, the high γ-ray background of C^{10} indicates the existence of nuclear γ-radiation in addition to annihilation radiation. Many attempts were made to obtain a good lead absorption curve, but since the ratio of C^{10} to C^{11} at the highest proton energy was of the order of 1, it was impossible to obtain the desired accuracy. Attempts to filter out the C^{11} radiation by large thickness of Pb failed, indicating that the C^{10} radiation was not appreciably harder than annihilation radiation. Figure 7 shows the final results of these measurements; for comparison, an absorption curve for C^{11} annihilation radiation is included. For the latter an absorption coefficient of 1.36 cm^{-1} was obtained; this value is lower than the correct value for 510-kev radiation by 25 percent, as a result of the poor geometry used in these measurements. The average absorption coefficient for the C^{10} radiation is 0.68 ± 0.14 cm^{-1}. On the assumption that this value is low in the same ratio as for the 510-kev radiation, a corrected value of 0.85 ± 0.18 cm^{-1} is obtained, corresponding to an average gamma-ray energy of 960 ± 200 kev.

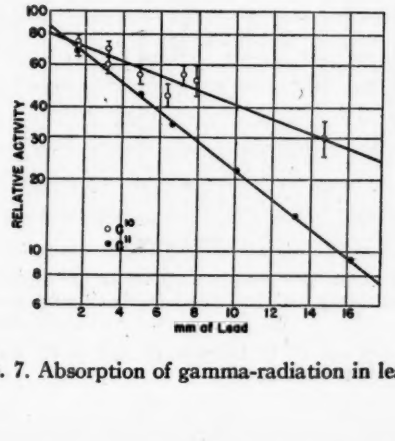

FIG. 7. Absorption of gamma-radiation in lead.

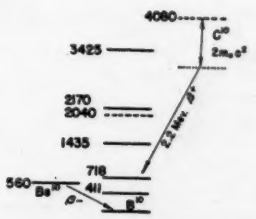

FIG. 8. Energy level diagram of Be^{10}, B^{10}, and C^{10}. The energies are given in kev. The dashed lines represent calculated values.

DISCUSSION OF RESULTS FOR C^{10}

On the basis of present measurements it is difficult to derive the decay scheme of C^{10}. However, in combination with the known levels in B^{10} and the decay energy of Be^{10}, a tentative decay scheme can be presented. The β-ray absorption curve (Fig. 5) shows that there is an appreciable amount of γ-radiation per β-particle. The C^{10} positron absorption curve (Fig. 6) appears to be simple, whereas if the 2.2-Mev β-transition corresponded to a transition to the ground state of C^{10}, one would expect the β-absorption curve to be complex. Certainly no softer component of the order of 1 Mev with intensity comparable to the 2.2-Mev spectrum can be present. It is therefore assumed that the C^{10} decays to an excited state of B^{10} with subsequent emission of gamma-radiation. In comparing isobars of type $(4k+\nu\pi)$, $(4k+\nu\nu)$, and $(4k+\pi\pi)$, where k is a low integer and ν and π represent a neutron and proton, respectively, one is permitted by the Pauli principle to have both extra nucleons in the *same* orbital state. The differences in binding energies are then to be attributed to differences in Coulomb energy and to differences in the spin interactions of the extra nucleons with each other and with the alpha-particle core. The extra proton and neutron in $(4k+\nu\pi)$ are expected to have parallel spins, as in the ground state of the deuteron, while in $(4k+\nu\nu)$ and in $(4k+\pi\pi)$ the extra particles almost certainly have antiparallel spins. However, since C^{10} differs from Be^{10} only in the interchange of the two extra neutrons and protons, one expects from the equality of $p-p$ and $n-n$ forces that the ground states of these two nuclei are of similar quantum mechanical character. As we remarked earlier, this hypothesis has been verified for simple mirror nuclei of the type where only one

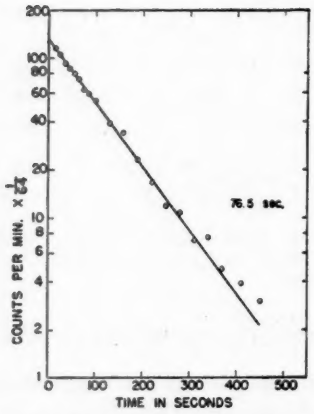

FIG. 9. Decay of radioactive gases produced by bombardment of KSCN by protons and trapped by $CaCl_2$.

nucleon is interchanged. If this assumption is correct for the interchange of two nucleons, then the difference in binding energy of C^{10} and Be^{10} is due to Coulomb forces alone and can be calculated by Eq. (1). Furthermore, by use of the experimentally known $Be^{10}-B^{10}$ mass difference and the Coulomb formula, one can obtain the $C^{10}-B^{10}$ mass difference in the following way. There should be an excited state, B^{10*}, which has exactly the same quantum-mechanical character as the ground states of Be^{10} and C^{10}. The non-Coulomb forces should be the same for these isobars,††† and consequently one can calculate the mass differences from the Coulomb formula above, not forgetting the neutron-proton mass difference. From the alpha-particle model point of view we consider the three isobars as consisting of a core of two alpha-particles *plus* either two neutrons, a neutron and a proton or two protons *all* with antiparallel spins and *all* in the same orbital state. On the above basis one obtains $B^{10*}-Be^{10}=1.48$ Mev and, since $Be^{10}-B^{10}$ is measured[7] to be 0.560, we find $B^{10*}-B^{10}=2.04$ Mev. Similarly, $C^{10}-B^{10*}=2.04$ Mev from the Coulomb formula and, therefore, $C^{10}-B^{10}=2.04+2.04=4.08$ Mev.

A detailed consideration of known B^{10} excited states and their relation to our observations is presented in Fig. 8 where levels found by Lauritsen *et al.*[8] are indicated. These levels occur at 411, 718, 1435, 2170, and 3425 kev. In addition to these levels there may be levels at 1024 and 2924 kev. It must be borne in mind that these levels were stimulated by heavy particles in the reactions $B^{10}(p, p\gamma)B^{10}$, $Be^{9}(dn)B^{10}$, and $Be^{9}(p\gamma)B^{10}$; so there is always the possibility that β-ray transitions cannot excite them. The dashed level in B^{10} at 2040 kev is the one we have calculated on the assumption that it is identical in quantum-mechanical character with the ground state of Be^{10}, and the dashed ground level in C^{10} at 4080 was obtained from Be^{10} as explained above. The agreement between the calculated level at 2040 kev and that observed by Lauritsen at 2170 kev lends support to the model we have used. On the basis of this diagram positron transitions to the various levels below 3 Mev should be possible. The corresponding values of E_β would be 0.9, 1.6, 2.3, 2.7, and 3.1 Mev (and also 2.0 Mev if there is a level at 1024 kev).

The positron energy of 2.2 ± 0.1 Mev observed by us agrees well with the assumption of a beta-transition to the 718-kev level of B^{10}. Our observation of an average gamma-ray energy of 960 ± 200 kev accompanying the C^{10} decay is

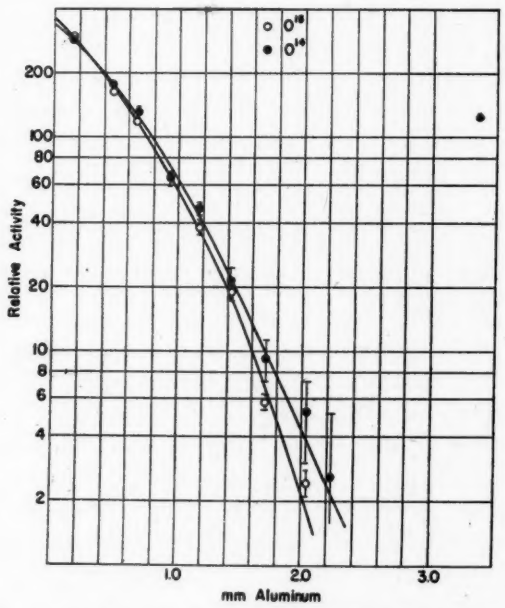

FIG. 10. Positron absorption curve for O^{14} and O^{15}. The gamma-ray backgrounds have been subtracted.

††† It is to be noted that the present assumption that the specifically nuclear $n-n$, $p-p$, and $p-n$ forces are identical is broader than that required for a discussion of the usual mirror nuclei (C^{11}, N^{13}, etc.), which require only equality of the $n-n$ and $p-p$ forces.

[7] E. M. MacMillan, Phys. Rev. **72**, 591 (1947).

[8] T. Lauritsen, C. B. Dougherty and V. K. Rasmussen, Phys. Rev. **74**, 1566 (1948).

consistent with the emission of 718-kev radiation, but may indicate the presence of more energetic γ-rays.

It is to be noted that we have assumed that the shape of the beta-absorption curve indicates a simple spectrum. However, transitions to other levels with intensity of the order of 10 or 20 percent cannot be excluded without more extensive verification of the application of the method of Bleuler and Zünti to the present data. One might expect transitions to the other available levels in B^{10}. A transition to the ground state would be inconsistent with the forbidden character of the Be^{10} decay. A transition to the 411-kev level could also occur in the Be^{10} decay if such transitions were allowed; as it has not been observed in Be^{10}, it may be assumed to be an improbable mode of decay for C^{10}. (Lauritsen *et al.*[9] have observed that the ground level and the 411-kev level must be similar in character and very different from the 718-kev level.) There remains the possibility of transitions to the 1435- and 2170-kev levels, which would give β-energies of 1.6 and 0.9 Mev. It is not possible to evaluate the probability of the former transition, but the latter transition is certainly allowed if it in reality corresponds to the level in B^{10} analogous to the ground state of Be^{10} and C^{10}. Assuming that the decay probability is proportional to W_0^5, one would expect a 0.9-Mev beta-transition to occur about 1/30 as frequently as the observed 2.2-Mev transition. This represents too small a relative intensity to be observed in the present experiment.

Feenberg and Goertzel[10] have calculated the Coulomb energy by a quantum-mechanical method which takes into account the effect of the Pauli exclusion principle on the mean separation of the protons. Above mass number eleven their results depart very little from the classical description, but at mass ten and below they predict measurable departures and can apparently account for the well-known oscillatory characteristics of the Coulomb energy of light nuclei. If one computes the Coulomb energy difference of $C^{10}-B^{10}$ by a straightforward application of their theory, one gets $C^{10}-B^{10}=3.7$ Mev instead of 4.08 as previously calculated. Also, $B^{10*}-B^{10}=1.70$ Mev. For two reasons we find these energy differences subject to doubt. First, their $C^{10}-B^{10}$ energy difference, taken with our β-energy of 2.2 Mev, would leave only 0.5 Mev for a γ-ray, assuming cascade. This quantum energy is not consistent with our measured γ-ray energy. Second, the $B^{10*}-B^{10}$ energy difference implies a level in B^{10} at 1.7 Mev which to date has not been found.

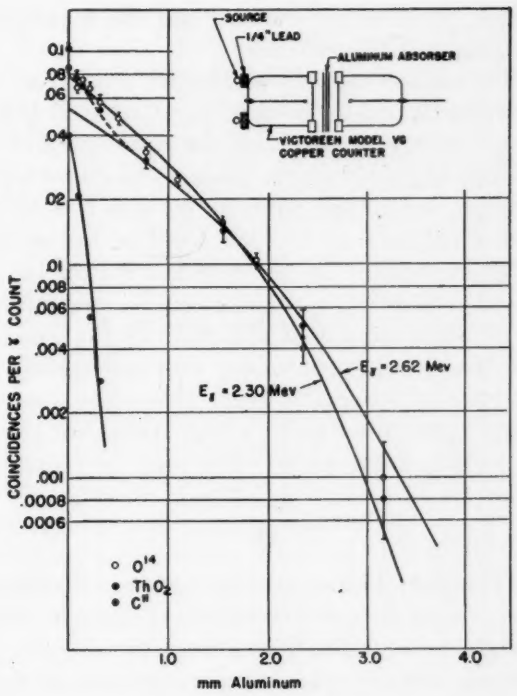

FIG. 11. Coincidence absorption measurements of gamma-radiations of O^{14}. The insert shows the counting arrangement.

If one employs the minimum values allowed by Feenberg and Goertzel's theory, there is no disagreement either with classical Coulomb calculations or with experiment. The flexibility in the theory arises from allowing the nuclear radius of the lightly bound $4k+1$ nuclei to depart slightly from the assumed smooth $A^{\frac{1}{3}}$ dependence. A slight expansion in radius of this nuclear series reduces the amount of symmetry effect which has to be introduced to make the Coulomb energy agree with experiment. When the theory is then applied to the more tightly bound $4k+2$ nuclei there is little difference, for mass ten and

[9] T. Lauritsen, W. A. Fowler, C. C. Lauritsen, and V. K. Rasmussen, Phys. Rev. **73**, 636 (1948).
[10] E. Feenberg and G. Goertzel, Phys. Rev. **70**, 597 (1946).

above, between the classical and the quantum-mechanical Coulomb energy.

The ratio of the cross section for production of C^{10} from B^{10} and C^{11} from B^{11} is ~ 0.03 at 17 Mev. At an energy of ~ 7 Mev, the ratio is 5×10^{-4}. Threshold for C^{10} on the basis of the above level diagram is 5.4 Mev, while for C^{11} it is 2.98 Mev. The small ratio at 17 Mev could be due either to an abnormally low cross section for the (p, n) reaction in B^{10} or to more effective competition by other possible reactions than in the case of the B^{11}. The present energy and half-life of C^{10} lead to an (ft) value of 2020. This value is somewhat higher than that for He^6 (1160) but lower than the usual values observed for allowed transitions.[2]

O^{14}

O^{14} has not hitherto been reported in the literature. Using the gas flow technique developed for C^{10} we have discovered a 76.5-sec. activity in several nitrogen containing compounds as well as in nitrogen gas. The most intense activity was obtained by trapping the gases from KSCN on $CaCl_2$. Apparently the activity from the KSCN is carried away in the form of water. Nitrides of titanium, zirconium, magnesium, and calcium were tried with only moderate success. A proton beam current of 0.5 microampere at 17 Mev was used in most of the bombardments.

Using the KSCN powder as target material and $CaCl_2$ as absorbing agent for the radioactive gas decay, curves of the type shown in Fig. 9 have been obtained. The decay curves were simple over a factor of 50 or more. Averaging over a large number of runs gave a half-life of 76.5 ± 2 sec. Magnetic analysis identified the particles as positively charged.

There remained the possibility that a slight amount of 126-sec. O^{15} produced from N^{15} was present. However, the half-life remained unchanged when measured through a thickness of lead which reduced the relative intensity of annihilation radiation by a factor of 50. Since the abundance $N^{14}/N^{15}=262$, one would expect at most only a few percent of O^{15}. Curves of various mixtures of 76-sec. and 126-sec. activities were drawn and compared with the decay curves. From this comparison it was concluded that there was certainly less than 10 percent O^{15} present in the decay curves at 17 Mev. From this figure it is estimated that $\sigma_{15}/\sigma_{14}<25$, a somewhat more favorable ratio for the production of O^{14} than that for production of C^{10}, for which $\sigma_{11}/\sigma_{10}=30$.

The chemical behavior of the 76.5-sec. period was studied in the following way. A mixture of 70 percent nitrogen gas and 30 percent hydrogen gas, bombarded in a carefully cleaned probe tip, was continuously swept through a filter of ascarite, then through a tube of platinized asbestos and finally through a layer of $CaCl_2$ in the inspection chamber. The purpose of the ascarite was to remove $C^{11}O_2$ (C^{11} from $N^{14}(p\alpha)C^{11}$) and H_2O^{14}, but allowing O_2, NO, etc., to pass through. With the catalyst at room temperature an equilibrium counting rate of 200 (arbitrary)/min. was obtained, but with H_2 turned off the rate dropped to 8/min. Also, H_2 alone, and H_2+N_2 without the catalyst gave no activity. These tests are consistent with the view that the 76.5-sec, activity is oxygen, and that the oxygen and hydrogen in the presence of the catalyst unite to form H_2O which is trapped on the $CaCl_2$. It was found that at elevated temperatures (100° or more) it was unnecessary to add H_2 to obtain the activity in the $CaCl_2$. Presumably, there was sufficient adsorbed hydrogen in the system to carry through the conversion under the more efficient operation of the catalyst at higher temperatures.

For purposes of comparison of absorption curves, O^{15} was produced by proton bombardment of PbF_2. The Ne^{19} activity was pumped off while the O^{15}, produced presumably by a $F^{19}(p, \alpha n)O^{15}$ reaction, was trapped as water in $CaCl_2$. The average half-life obtained for O^{15} was 126 ± 2 sec., in excellent agreement with the accepted value of 126 sec.[11] Absorption curves for O^{15} and O^{14} were obtained which were very similar to those for Ne^{19} and C^{10} (Fig. 5). In the present case, the γ-ray background for O^{14} was 6 percent of the zero absorber yield, while for O^{15} it was 2.0 percent, indicating the presence of nuclear γ-radiation in the O^{14} decay. From the ratio of these figures, 3.0, and assuming linear energy response of the counters to γ-radiation, one may expect a single γ-ray of the order of 2 Mev or several softer rays to be associated with the decay of O^{14}.

[11] G. T. Seaborg, Rev. Mod. Phys. 16, 1 (1944).

The β-ray absorption curves of O^{14} and O^{15} with background subtracted are shown in Fig. 10. It is seen that the O^{14} is slightly more energetic than O^{15}. Application of the technique of Bleuler and Zünti as described above gave for O^{15} the values 1.66, 1.68, 1.68, 1.68, 1.69, 1.68, 1.68 Mev for successive values of E_n. The average value of 1.68 Mev is in excellent agreement with the accepted value[11] 1.7 Mev. For O^{14} the successive values of E_n are 1.81, 1.80, 1.77, 1.76, 1.78, 1.80, 1.84 Mev, giving an average value of 1.78 Mev. Considering the slight scatter of the measured points, the positron energy of O^{14} is taken to be 1.8 ± 0.1 Mev. The O^{14} β-spectrum appears to be simple, and if a harder component, of the order of 3–4 Mev, is present, its intensity must be less than 5 percent of the 1.8-Mev spectrum.

An absorption curve of the γ-radiation of O^{14} in lead showed that the radiation detected was predominantly hard, the absorption coefficient corresponding to the minimum in lead. To determine the energy more precisely, the absorption of the Compton secondaries was measured using counters in coincidence in the usual fashion.[6,12] The results and a sketch of the arrangement are shown in Fig. 11. Because of the difficulty in determining the range of the secondaries, the curve was analyzed with the aid of the curves given by Bleuler and Zünti[6] for this type of measurement. For calibration purposes there was available a quantity of ThO_2 of unknown history. The ThO_2 was used under the same geometrical conditions as the O^{14}; the results are given in Fig. 11. The ThO_2 curve is obviously complex; the solid curve corresponds to a 2.62-Mev gamma-ray as given by Bleuler and Zünti and has been fitted to the last four points. The agreement is very good. With this reassurance, the best fit to the O^{14} data was found to be the curve drawn through the O^{14} points and represents an energy of 2.30 Mev. As is evident from the absorption curve for annihilation radiation (C^{11}) in Fig. 11, the contribution of secondaries due to the annihilation radiation in the O^{14} curve is negligible except for the smallest absorbers. On the basis of range comparison, disregarding the complexity of the ThO_2 curve, it would appear that the O^{14} radiation was as hard as the 2.62-Mev ThC″ gamma-ray. As a lower limit, the range of the secondaries is greater than 0.86 g/cm², corresponding to an $h\nu$ of 2.1 Mev. In view of the uncertainty of the calibration source (a single line source would be preferable) the gamma-ray energy of O^{14} is taken to be $2.3^{+0.3}_{-0.1}$ Mev. If the curves of Bleuler and Zünti[6] can be applied to the present data, one can conclude that the γ-spectrum is essentially simple. Assuming that the sensitivity of the counters is a linear function of the gamma-ray energy, one can estimate the ratio of the backgrounds of O^{14} and O^{15} as obtained in the β-absorption curves to be 3.3, in reasonable agreement with the observed ratio of 3.0.

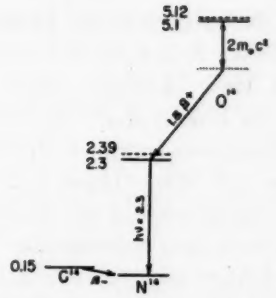

FIG. 12. Energy level diagram of O^{14}, N^{14}, and C^{14}. The energies are given in Mev. The dashed lines represent calculated values.

DISCUSSION OF RESULTS FOR O^{14}

The radiation of O^{14} appears to be a simple positron spectrum of maximum energy 1.8 Mev, followed by a γ-ray of 2.3 Mev. The β-energy in combination with the 76.5-sec. half-life give an (ft) value of 3350. If there are any transitions to the ground state of N^{14}, our absorption curves suggest that they occur with a probability less than five percent of that for the 1.8-Mev transitions.

Hornyak and Lauritsen[13] have summarized the experimental evidence for the excited states of N^{14}. The lowest of these levels is at 4.0 Mev according to their analysis. Of particular interest here is the designation of a level at 5.4 Mev on the basis of the observation of neutrons and gamma-rays from the $C^{13}(d, n)N^{14}$ reaction. This level was taken to be confirmed by the measurements of the energies of gamma-radiation from

[12] W. A. Fowler, C. C. Lauritsen, and T. Lauritsen, Rev. Mod. Phys. 20, 236 (1948).

[13] W. F. Hornyak and T. Lauritsen, Rev. Mod. Phys. 20, 214 (1948).

the $C^{13}(p, \gamma)N^{14}$ reaction by Lauritsen *et al.*[14] The gamma-rays found by the latter were 8.1, 5.4, and 2.8 Mev. However, these values have been revised by Fowler *et al.*[12] on the basis of new field coil calibrations for their cloud chamber to 8.1, 5.8, and 2.3 Mev. These new values may indicate the existence of a level at 2.3 Mev, the 5.8-Mev gamma-ray representing a transition from the 8.1-Mev level to the 2.3-Mev levels. Our presently observed gamma-ray of 2.3 Mev supports this interpretation.

It is, of course, possible that the 2.3-Mev radiation of O^{14} represents a transition between levels above 4 Mev in N^{14}. The subsequent harder radiation could hardly be overlooked in the γ-ray measurements. Additional evidence for the assumption that the 2.3-Mev gamma-ray found by us follows the 1.8-Mev β-transition is found in a rough determination of the threshold for the (p, n) reaction. The gas probe was progressively inserted to shorter radii in the cyclotron and bombardments carried out as previously. The threshold was found to be $6.0\ ^{+0.5}_{-?}$ Mev, the lower limit being indeterminate as it was difficult to determine the loss of energy in passing through the copper foil of the gas cell. This threshold value is definitely too low to allow the 2.3-Mev radiation to come from high lying levels in N^{14} and is in reasonable agreement with the calculated threshold of 6.3 ± 0.3 Mev for the suggested sequence of a 1.8-Mev β-transition followed by a 2.3-Mev γ-transition.

Calculations of the energy N^{14*} and O^{14}, assuming that their wave functions are the same as for C^{14} and using Eq. (1) (cf., discussion of C^{10} above), give the following results: $N^{14*}-N^{14}=2.39$ Mev and $O^{14}-N^{14}=5.12$ Mev.†††† A positron transition to the N^{14*} level gives a positron energy of 1.71 Mev, while the subsequent γ-ray $N^{14*}\rightarrow N^{14}$ would have an energy of 2.39 Mev. The agreement of these values with the observed values of $E_\beta=1.8\pm0.1$ Mev and $E_\gamma=2.3\pm0.2$ Mev is excellent. These results are summarized graphically in Fig. 12.

[14] T. Lauritsen, C. C. Lauritsen, and W. A. Fowler, Phys. Rev. **59**, 241 (1941).

†††† Calculations on the basis of the method of Feenberg and Goertzel (reference 10) give essentially the same results for the present case.

CONCLUSION

On the basis of these preliminary results on the radiation from C^{10} and O^{14}, it appears safe to conclude that beta-transitions from the ground states of these nuclei to the ground states of B^{10} and N^{14} have a forbidden character. As the corresponding transitions $Be^{10}\rightarrow B^{10}$ and $C^{14}\rightarrow N^{14}$ are also forbidden, the present results agree with the prediction of nuclear theory that the isobaric pairs C^{10} and Be^{10}, and O^{14} and C^{14} should have similar configurations. Theoretical expectations that the mass differences of these isobaric pairs can be attributed to the excess Coulomb energies of the isobars of higher atomic number are confirmed by our measurements. Moreover, the calculated position of the excited level in B^{10} and in N^{14} which corresponds to the ground state configuration of $Be^{10}-C^{10}$ and of $C^{14}-O^{14}$ seems to be checked by experiment. In contrast to these successful predictions of nuclear theory,[15] there remain the theoretical difficulties in explaining the forbidden character of the beta-transitions to the ground states.‡

The authors are pleased to acknowledge valuable discussions with Professor E. Wigner on the theoretical implications of these experiments. We are indebted to Professor J. Turkevich of the Department of Chemistry for his advice and assistance in establishing the chemical identity of the radioactive isotopes. We also wish to thank the members of the cyclotron group and the electronic shop for their cooperation and assistance.

[15] The arguments concerning the similarity of Be^{10}, B^{10*}, and C^{10} and of C^{14}, N^{14*}, and O^{14} given in this paper used a specific nuclear model (i.e., α-particle substructure). However, Wigner has shown (Phys. Rev. **51**, 106 (1937)) that this similarity arises quite generally from the essential equality of the forces between nucleons.

‡ *Note added in proof:* These theoretical difficulties may have been resolved in the case of $Be^{10}-B^{10}$ by the recent measurements of the spin of B^{10} by W. Gordy, H. Ring, and A. B. Burg [Phys. Rev. **74**, 1191 (1948)]. These authors find a spin of 3, rather than the previously assumed value of 1. With the assumption that Be^{10} has spin 0, the ΔJ for the β-transition is 3. (See also M. Goldhaber, Phys. Rev. **74**, 1194 (1948).) On the other hand, the C^{14} and N^{14} spins are known to be 0 and 1 respectively.

Electronic Interaction in Electrical Discharges in Gases*

JULIUS H. CAHN**
*Sloane Physics Laboratory, Yale University,*** *New Haven, Connecticut*

(Received October 8, 1948)

The Boltzmann transfer equation has been solved for the case of high current densities and low field strengths where electrostatic interactions may not be neglected. The solution has been examined for two different electron-molecule cross sections for momentum transfer. In one, the cross section varies inversely with electron velocity, and the distribution is found to be Maxwellian at all electron densities. In the other, the cross section is assumed independent of the electron energy. On the latter assumption, the solution varies from the Davydov distribution at low electron densities to the Maxwellian distribution at high densities. Curves have been drawn showing the transition of the distribution as the density increases. The corresponding values of average energy, drift velocity, and average velocity have been tabulated.

I. INTRODUCTION

THIS paper deals with the effects of electrostatic interaction in low voltage discharges in gases. The field strengths are limited in order to rule out inelastic collision phenomena.

The present theory of electrical discharges, which neglects inelastic collisions and electron interaction but includes the motion of the molecules, was first developed by Davydov[1] in 1936. Davydov's electron velocity distribution function reduces to that obtained originally by Druyvesteyn[2] in 1930, and later by Morse, Allis, and Lamar,[3] in which molecular motion is neglected.

The theory which has been developed here is an extension of Davydov's work, in that it considers only elastic collisions, with the addition of electron-electron encounters. We find that below electron densities of 10^6/cc our distribution function reduces to that of Davydov, while at very high densities, the limiting form of the distribution function is Maxwellian. These results are to be expected, and therefore the chief interest lies in our treatment of the problem. This is particularly true in view of a paper in 1939 by Haseltine[4] in which the same problem was considered but in which the analytical difficulties proved excessive.

Our good fortune in reducing this problem is largely due to a paper by Landau[5] in 1936, in which he developed an approximation to the coulomb interaction term in the Boltzmann transfer equation.[6] Because of the long range of the force, a majority of the Coulomb collisions involve a small momentum exchange, and, accordingly, Landau expands in powers of the momentum exchange.

We also justify and make use of an assumption which Haseltine found useful. When considering the momentum balance equation, there proves to be a certain range of electron and molecule densities, in which the electron-molecule collisions are the more important. Here the electrostatic interactions may be neglected insofar as momentum conservation, but not energy conservation, is concerned.

II. ANALYTICAL FORMULATION OF THE PROBLEM

A central part of the theory of gas discharges concerns the determination of the electron velocity distribution function $f(\mathbf{r}, \mathbf{v})$, the solution of the Boltzmann transfer equation.[6] Our distribution f is normalized to the electron density n. We consider an infinite gas with a constant impressed field E. The field strength for the re-

* Part of a dissertation presented to the Faculty of the Graduate School of Yale University, in partial fulfillment of the requirements for the degree of Doctor of Philosophy.

** Now at the University of Nebraska, Lincoln, Nebraska.

*** This work was assisted by the Office of Naval Research, United States Navy, under Contract N6ori-44.

[1] B. Davydov, Physik. Zeits. Sowjetunion 8, 59 (1935), 9, 433 (1936).

[2] M. J. Druyvesteyn, Physica 10, 69 (1930).

[3] P. M. Morse, W. P. Allis, and E. S. Lamar, Phys. Rev. 48, 412 (1935).

[4] W. R. Haseltine, J. Math. and Phys. 18, 174 (1939).

[5] E. Landau, Physik. Zeits. Sowjetunion 10, 154 (1936).

[6] L. Boltzmann, *Vorlesungen uber Gastheorie* (Leipzig, 1896), 1, Ch. II and III.

mainder of the paper will be represented by $\gamma = eE/m$, where e, m are the charge and mass of the electron. We assume equal ion and electron densities. In such an environment, the steady state electron distribution is the solution of

$$\gamma \cdot \Delta f = (\partial_e f/\partial t)_1 + (\partial_e f/\partial t)_M, \tag{1}$$

in which $(\partial_e f/\partial t)_1$ is the time rate of change of f with respect to electron-electron collisions, $(\partial_e f/\partial t)_M$ the time rate of change of f with respect to all other collisions, and Δ the velocity gradient operator.

The second term on the right of (1) includes both ions and molecules. We assume both to be in equilibrium at the absolute temperature T. Before evaluating $(\partial_e f/\partial t)_M$ we introduce the quantity $\lambda(v)$, defined as the mean free path for momentum transfer in terms of the differential scattering cross section, $\sigma(\theta, v)d\omega$ by the relation

$$1/\lambda(v) = N \int \sigma(\theta, v)(1-\cos\theta)d\omega, \tag{2}$$

in which N is the density of scattering centers, θ is the angle, and $d\omega$ the solid angle into which the electron is scattered. The composite mean free path λ for collisions with molecules and ions is given by

$$1/\lambda = 1/\lambda_m + 1/\lambda_i, \tag{3}$$

in which λ_m is the mean free path for molecules and λ_i is that for ions. The approximate calculation of λ_i is generally made using the Debye-Huckel[7] shielding radius ρ as the upper limit of the collision parameter.[8] The approximate value of λ_i is then

$$1/\lambda_i = (n\pi e^4/\bar{\epsilon}_r^2)\ln(\rho\bar{\epsilon}_r/e^2), \tag{4}$$

where $\rho = (\bar{\epsilon}_r/12\pi ne^2)^{\frac{1}{2}}$, $\bar{\epsilon}_r$ is the average relative electron-ion energy, and n is the electron or ion density. If we assume the electron-molecule cross section to be of the order of 10^{-15} cm^2, the ratio λ_i/λ_m for one-volt electrons is

$$\lambda_i/\lambda_m = N/n(10)^{-3}, \tag{5}$$

where N is the molecular density. Relation (5) gives us an accurate estimate of the role played by the ions in the discharge.

The form of $(\partial_e f/\partial t)_M$ is derived by Chapman and Cowling.[9] If we expand $f(\mathbf{v})$ in the form

$$f(\mathbf{v}) = f_0(v) + v_z f_1(v), \tag{6}$$

with the field in the z direction, and write s for v^2, their expression is

$$\left(\frac{\partial_e f_0}{\partial t}\right)_M = \frac{\delta}{\beta s^{\frac{1}{2}}}\frac{d}{ds}\frac{s^2}{\lambda(s)}\left(\frac{df_0}{ds} + \beta f_0\right),$$
$$\left(\frac{\partial_e v_z f_1}{\partial t}\right)_M = -v_z\frac{s^{\frac{1}{2}}f_1}{\lambda(s)}, \tag{7}$$

where $\delta = 2m/M$ is twice the ratio of electronic to molecular mass and $\beta = m/2kT$, k being Boltzmann's constant.

The calculation of $(\partial_e f/\partial t)_1$, as stated in the introduction, was indicated by Landau.[5] He expanded this term in powers of the momentum exchanged on collision, retaining terms of the second order, as the zeroth and first-order terms vanish. The result was that $(\partial_e f/\partial t)_1$ could be expressed as the velocity divergence of a vector $\mathbf{J}$,

$$(\partial_e f/\partial t)_1 = \nabla \cdot \mathbf{J}. \tag{8}$$

The vector $\mathbf{J}$ is most conveniently written using the summation convention over repeated indices. Letting $i = x, y, z$,

$$J_i(\mathbf{v}) = \mathfrak{L} \int_{v' \text{ space}} \left[f'(\mathbf{v}')\frac{\partial f(\mathbf{v})}{\partial v_j} - f(\mathbf{v})\frac{\partial f'(\mathbf{v}')}{\partial v_j'}\right] \times (u^2\delta_{ij} - u_i u_j)/(u^3)d\mathbf{v}', \tag{9}$$

where δ_{ij} is the Kronecker delta and $\mathfrak{L} = 2\pi e^4/m^2 \ln\bar{\epsilon}\rho/e^2$. The vector u is the relative velocity $\mathbf{v}' - \mathbf{v}$ of the scattering (primed) eleetron relative to the incident (unprimed) electron; $\bar{\epsilon}$ is the relative electron energy $\frac{1}{2}mu^2$.

In order to carry out the integration in (9) after substituting (6), we found suitable the coordinate system devised by Hylleraas[10] for the helium ion in which v serves as polar axis for v'.

The manner of performing the angular integration is shown in Appendix I. As a result,

[7] P. Debye and E. Huckel, Physik. Zeits. **24**, 185 (1923).
[8] B. Davydov, Physik. Zeits. Sowjetunion **12**, 269 (1937).
[9] S. Chapman and T. G. Cowling, *The Mathematical Theory of Non-Uniform Gases* (Cambridge University Press, New York, 1939), pp. 348 *et seq.*
[10] E. A. Hylleraas, Zeits. f. Physik **54**, 347 (1929).

$\mathbf{J}$ may be written in the form

$$\mathbf{J}(\mathbf{v})=\mathfrak{L}'\mathbf{v}\int_0^\infty (5U^{00}+5v_zU^{01}+2v_zU^{10}+2v^2U^{11}+f_1f_1')v'dv'+\mathbf{k}\mathfrak{L}'\int_0^\infty [v^2U^{10}+v^2v_zU^{11}+5(f_0'f_1-f_0f_1')-3v_zf_1'f_1]v'dv', \quad (10)$$

where $\mathbf{k}$ is a unit vector in the z direction, $\mathfrak{L}'=(8\pi)/(15)\mathfrak{L}$, and

$$U^{kl}=f_k'\frac{\partial f_l}{v\partial v}-f_l\frac{\partial f_k'}{v'\partial v'}.$$

The calculation of the velocity divergence of $\mathbf{J}(\mathbf{v})$ is most easily carried out if $\mathbf{J}$ is expressed as a vector in spherical coordinates. The isotropic and anisotropic terms of $(\partial_e f/\partial t)_1$ are separated in the form

$$(\partial_e f/\partial t)_1=\nabla\cdot\mathbf{J}=(\partial_e f_0/\partial t)_1+(\partial_e v_z f_1/\partial t)_1. \quad (11)$$

The results of the differentiation as performed in Appendix II are

$$\left(\frac{\partial_e f_0}{\partial t}\right)_1=\frac{10}{s^{\frac{1}{2}}}\frac{d}{ds}s^{\frac{1}{2}}(Af_0'+Bf_0)+\frac{2}{s^{\frac{1}{2}}}\frac{d}{ds}s^{5/2}(Cf_1'+Df_1),$$

$$\left(\frac{\partial_e v_z f_1}{\partial t}\right)_1=v_z\left\{\frac{10}{s^{\frac{1}{2}}}\frac{d}{ds}s^{5/2}(Af_1'+Bf_1)+\frac{6}{s^{\frac{1}{2}}}\frac{d}{ds}s^{5/2}(Cf_0'+Df_0)-5(2Cf_0'+Df_0+Bf_1)\right\}, \quad (12)$$

where the primes now refer to differentiation with respect to $s\equiv v^2$. We define the four coefficients A, B, C, and D in the following way:

$$A=\mathfrak{L}'\int_0^\infty f_0ds, \quad B=\mathfrak{L}'f_0(0),$$

$$C=\mathfrak{L}'\int_0^\infty f_1ds, \quad D=\mathfrak{L}'f_1(0).$$

We now have analytic expressions for (1) and so can assemble the Boltzmann equation. It will immediately be observed in (7) and (12) that both terms on the right of (1) can be expressed as sums of isotropic and anisotropic terms. These represent the first two terms of an expansion in Legendre polynomials following the form of the expansion of $f(\mathbf{v})$ in (6). The left-hand side of (1) separates in similar fashion, giving rise to the following pair of simultaneous integro-differential equations:

$$\left(\frac{\partial_e f_0}{\partial t}\right)\equiv\frac{10}{s^{\frac{1}{2}}}\frac{d}{ds}s^{\frac{1}{2}}(Af_0'+Bf_0)+\frac{2}{s^{\frac{1}{2}}}\frac{d}{ds}s^{5/2}(Cf_1'+Df_1)+\frac{\delta}{\beta s^{\frac{1}{2}}}\frac{d}{ds}\frac{s^2}{\lambda(s)}(f_0'+\beta f_0)=\frac{2}{3}\frac{\gamma}{s^{\frac{1}{2}}}\frac{d}{ds}s^{\frac{1}{2}}f_1, \quad (13a)$$

$$\left(\frac{\partial_e f_1}{\partial t}\right)\equiv\frac{10}{s^{\frac{1}{2}}}\frac{d}{ds}s^{5/2}(Af_1'+Bf_1)+\frac{6}{s^{\frac{1}{2}}}\frac{d}{ds}s^{5/2}(Cf_0'+Df_0)-5[2Cf_0'+Df_0+(B+s^{\frac{1}{2}}/5\lambda(s))f_1]=2\gamma f_0'. \quad (13b)$$

Equation (13a) is seen to be exact. This is necessary for the conservation of particle density, since the transport of mass, written as

$$n\Delta m=\int_{v\text{ space}} m(\partial_e f/\partial t)d\mathbf{v},$$

must vanish.[11] The integrated Eq. (13a) is the energy balance equation. This is shown by computing the energy transport

$$n\Delta\epsilon=\int_{v\text{ space}}\epsilon\left(\frac{\partial_e f}{\partial t}\right)d\mathbf{v},$$

making use of both sides of (1). Because of symmetry only the isotropic parts of (1) survive the integration, so we need only consider (13a). From

[11] See reference 9, pp. 47 *et seq.*

TABLE I. Mean values calculated from (23) at different electron densities n.

n	$\bar{v}$ (cm/sec.)	$\bar{\epsilon}$ (electron volts)	$\bar{v}_z$ (cm/sec.)
10^8	$3.1(10)^7$	0.32	$2.5(10)^5$
10^{10}	$2.7(10)^7$	0.22	$3.4(10)^5$
10^{12}	$1.1(10)^7$	0.072	$7.5(10)^5$

the left hand side of (13a) we find on performing a partial integration that

$$n\Delta\epsilon=-\int_0^\infty(\tfrac{1}{2}ms)\Big[10(Af_0'+Bf_0)+2s(Cf_1'+Df_1)+\frac{\delta s^{\frac{1}{2}}}{\beta\lambda(s)}(f_0'+\beta f_0)\Big](2\pi s^{\frac{1}{2}}ds),$$

while from the right hand side of (13a),

$$n\Delta\epsilon=-\int_0^\infty(\tfrac{1}{2}ms)\left(\frac{2\gamma f_1}{3}\right)(2\pi s^{\frac{1}{2}}ds),$$

where of course $\epsilon=\frac{1}{2}ms$. Assuming detailed balancing, the integrands of both expressions must be equal, which leads to the equation

$$10(Af_0'+Bf_0)+2s(Cf_1'+Df_1)+\frac{\delta s^{\frac{1}{2}}}{\beta\lambda(s)}(f_0'+\beta f_0)=\tfrac{2}{3}\gamma f_1. \quad (14)$$

Equation (14) will be seen to be the first integral of (13a) with the constant of integration set equal to zero to suppress singular solutions of f.

Momentum balance is assured by (13b). The rates at which momentum and energy are added to the electron gas by the applied field are easily computed from the left hand sides of (13b) and (13a) to be eEn and $eE\bar{v}_z n$, respectively.

III. SOLUTION OF THE TRANSFER EQUATION

Equations (13b) and (14) in the variable v take the form

$$(10A+\delta v/\beta\lambda(v))f_0'+2v(10B+\delta v/\lambda(v))f_0+2v^2(Cf_1'+2vDf_1)=(4/3)\gamma v f_1, \quad (15)$$

$$\tfrac{3}{2}Cf_0''+[3Dv+(C-\gamma)/v]f_0'+10Df_0+5/2Af_1''+(5Bv+10A/v)f_1'+(20B-v/\lambda(v))f_1=0. \quad (16)$$

The simplifications we have found necessary, but which will yield results of interest, are twofold. Haseltine[4] assumed that in the momentum balance Eq. (16) the electron-electron impacts could be neglected relative to the electron-molecule collisions. In the energy balance Eq. (15) the situation differs materially in that the electron loses a large fraction of its energy when colliding with another electron, while in a collision with a molecule the electron loses a fraction $\delta=2m/M$ of its energy. If we compare the coefficient of f_0 in (15) with that of f_1 in (16), the term in B will be seen to have a very much greater importance in (15) than in (16), verifying Haseltine's assumption. It will be noted, however, that at sufficiently high electron densities the electron-electron interaction terms in (16) must be retained. Consequently, we neglect the interaction terms in (16), obtaining with Haseltine[4] and Morse, Allis, and Lamar,[3]

$$\gamma f_0'+[v^2/\lambda(v)]f_1=0. \quad (17)$$

The second simplification comes in neglecting terms in f_1^2 relative to f_0^2 in (15), which then reads

$$(10A+\delta v/\beta\lambda(v))f_0'+2v(10B+\delta v/\lambda(v))f_0=4/3\gamma v f_1. \quad (18)$$

The elimination of f_1 in (18) by (17) leads to a simple first-order equation in f_0 whose solution is

$$f_0=N_0\exp\left\{-\int_0^v\frac{(10B\lambda/\delta)\beta v+\beta v^2}{(4/3)((\beta\gamma\lambda)^2/\delta)+(10\beta A\lambda/\delta)\beta v+\beta v^2}(2\beta v dv)\right\}, \quad (19)$$

where N_0 is the normalization constant.

Our solution (19) is quite general in that the dependence of λ on v has not been specified. For precise investigations of particular gas discharges it is often desirable to use the empirical electron-gas cross sections, which (19) permits. Equation (19) has a drawback in that it is a non-linear integral equation, because of the presence of the normalization constant in B and the integral form of A.

We have investigated (19) for two assumed cross sections. In case (a) the cross section is inversely proportional to v, and in (b) the cross section is independent of electron energy.

In case (a) the time $\tau=\lambda/v$ between collisions is a constant. Then (19) reduces to

$$f_0=N_0\exp\left\{-\frac{(10B\tau/\delta)+1}{(4/3)(\beta(\gamma\tau)^2/\delta)+(10\beta A\tau/\delta)+1}\beta v^2\right\}. \tag{20}$$

Computing A and B from their definitions, we find that

$$\beta A=B[1+(4/3)(\beta(\gamma\tau)^2)/\delta],$$
$$B=N_0\mathfrak{L}',$$

so that

$$f_0=N_0\exp(-mv^2/2k(T+T')), \tag{21}$$

where $\frac{3}{2}kT'=\frac{1}{2}M(\gamma\tau)^2$ is the excess of electron energy above the thermal energy $\frac{3}{2}kT$ of the gas molecule. The normalization constant N_0 is then

$$N_0=n[m/2\pi k(T+T')]^{\frac{3}{2}}.$$

The drift velocity $\bar{v}_z$ of the electrons is calculated from f_1 as given by (17), and is

$$\begin{aligned}\bar{v}_z&=\frac{1}{n}\int_{v\text{ space}} v_z^2 f_1 d\mathbf{v},\\ &=\frac{4\pi}{3n}\int f_1 v^4 dv,\\ &=\gamma\tau.\end{aligned} \tag{22}$$

This result shows that the energy by which the electron exceeds the molecule is just that which the molecule would have if streaming with the electron drift velocity.

It would appear that the electron temperature $T+T'$ were independent of the electron density. This is not the case, because in our formulation of the problem we have assumed equal ion and electron densities. Referring to (5), it is apparent that when $n>10^{-3}N$, the ions determine the magnitude of λ in (3). Hence τ will decrease when n increases above $10^{-3}N$, causing T' to drop off with n^2. At sufficiently high electron densities, then, the electrons approach thermal equilibrium with the gas. It would not be proper to speak of the dependence of the drift velocity on n, since the dependence of τ on n above is only qualitative. The actual electron-ion cross section goes not with $1/v$ but $1/v^4$, so that at very high densities the proper electron-ion cross section must be included in (19).

We next consider the case where λ is constant. While it is possible to carry out the integration in (19), the resulting expression is too complicated for manipulation and will not be written down. It is preferable to investigate (19) numerically. In the variable $x=mv^2/2kT$,

$$f_0=N_0\exp\left\{-\int_0^x\frac{(10B\lambda/\delta)\beta^{\frac{1}{2}}x^{\frac{1}{2}}+x}{\alpha+(10(\beta A\lambda)/\delta)\beta^{\frac{1}{2}}x^{\frac{1}{2}}+x}dx\right\}. \tag{23}$$

The constant α replaces $4/3(\gamma\beta\lambda)^2/\delta$. Assuming a field strength of 1 volt/cm, a mean free path λ of 10^{-2} cm, and a gas temperature of 300°K, α takes the value 100. In Fig. 1 are shown the normalized energy distribution curves for three illustrative electron densities. The function closely resembles the Davydov distribution for densities up to $n=10^9$/cc. Above $n=10^9$, the function makes a rapid change-over, as shown by the curve at $n=10^{10}$/cc. At $n=10^{11}$/cc the curve is very similar to $n=10^{12}$/cc, where the distribution has become Maxwellian at the temperature T.

The mean velocity $\bar{v}$, energy $\bar{\epsilon}$, and the drift velocity $\bar{v}_z$ have been computed and are shown in Table I. The mean energy and velocity are seen to decrease while the drift velocity increases, with increasing n. The act of increasing the density evidently lowers the entropy of the discharge in reducing the isotropic part of the distribution function while the drift velocity increases.

It is of interest to note that for electron densities of the order of 10^{12}/cc the electrons in a gas having a $1/v$ cross section are T' degrees hotter than the electrons in a gas having a constant cross section. This is because a $1/v$ cross section implies a reduced efficiency for momentum transfer at higher energies. Consequently, such a gas favors the population of higher electron energy

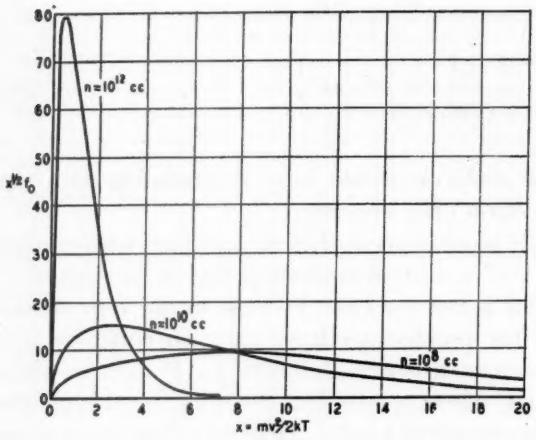

FIG. 1. Normalized energy distribution curves for three illustrative electron densities. $E=1$ volt/cm; $\lambda=10^{-2}$ cm; $\alpha=100$.

states over the gas in which the cross section is independent of energy.

CONCLUSION

The functional behavior of (19) amply justifies the interaction terms (12). We are now in a position to use (12) in the further investigation of inelastic processes in d.c. discharges and in extending work of Margenau and Hartman[12] on high frequency discharges to high current densities.

ACKNOWLEDGMENTS

The writer wishes to thank Professor Henry Margenau for his encouragement and guidance throughout the course of this work, and also to thank Professor Lars Onsager for a number of illuminating discussions and ideas.

APPENDIX I

Angular Integration of J

It was found necessary to employ the coordinate system devised by Hylleraas,[10] as shown in Fig. 2. The velocity $\mathbf{v}$ of the incident electron is referred to xyz coordinates, while the velocity $\mathbf{v}'$ of the scattering electron is referred to a coordinate system having $\mathbf{v}$ as polar axis. The azimuth of $\mathbf{v}'$ is measured by the angle χ. The purpose of this choice of coordinate systems is to permit integration over all $\mathbf{v}'$ for arbitrary $\mathbf{v}$, thereby preserving the functional dependence of $\mathbf{J}$ on $\mathbf{v}$. The volume element for the $\mathbf{v}'$ integration is $d\mathbf{v}'=v'dv'udud\chi/v$. Because of the appearance of the rectangular components v_x', v_y', and v_z' of $\mathbf{v}'$, Table II is used to transform to the system having $\mathbf{v}$ as polar axis, in which the rectangular components of $\mathbf{v}'$ are

$$v_1'=v'\sin\psi\cos\chi,$$
$$v_2'=v'\sin\psi\sin\chi, \text{ and}$$
$$v_3'=v'\cos\psi.$$

We note that

$$\nu_1=v_x/v, \quad \nu_2=v_y/v, \quad \nu_3=v_z/v,$$

and

$$\cos\psi=v^2+v'^2-u^2/2vv'.$$

The limits of integration for the respective variables are:

Variable	Lower limit	Upper limit
v'	0	∞
u	$v'-v$	$v'+v$
χ	0	2π.

It was found convenient to define the following quantities:

$$U^{kl}\equiv f_k'/v(\partial f_l)/(\partial v)-f_l/v'(\partial f_k')/(\partial v'),$$
$$V_i^{kl}\equiv f_k'(\partial f_l)/(\partial v_i)-f_l(\partial f_k')/(\partial v_i'),$$

and

$$V_i\equiv f'(\partial f)/(\partial v_i)-f(\partial f')/(\partial v_i'),$$

where i, j, $=x$, y, and z, and k, l, $=0$ and 1. With these abbreviations, we may write (9) as

$$\mathbf{J}=\mathfrak{L}\int V_j(u^2\delta_{ij}-u_iu_j)/(u^3)dv'. \qquad (I.1)$$

Assuming the explicit form of $f(\mathbf{v})$ as given by (6),

$$\mathbf{V}=\mathbf{V}^{00}+v_x'\mathbf{V}^{10}+v_z\mathbf{V}^{01}+v_xv_z'\mathbf{V}^{11}$$
$$+\mathbf{k}(f'f_1-ff_1'), \quad (I.2)$$

where $\mathbf{k}$ is the unit vector in the z direction. When (I.2) is substituted in (I.1), the resulting

TABLE II. Transformation scheme to relative coordinate system in which $\mathbf{v}$ serves as polar axis.

	v_x'	v_y'	v_z'
v_1'	λ_1	λ_2	λ_3
v_2'	μ_1	μ_2	μ_3
v_3'	ν_1	ν_2	ν_3

[12] H. Margenau and L. M. Hartman, Phys. Rev. **73**, 309 (1948).

expression may be represented by

$$\mathbf{J}=\mathbf{J}^{00}+\mathbf{J}^{01}+\mathbf{J}^{10}+\mathbf{J}^{11}$$
$$+\mathfrak{L}\int(f'f_1-ff_1')\frac{\mathbf{k}u^2-u_z\mathbf{u}}{u^3}d\mathbf{v}'. \quad \text{(I.3)}$$

The computation of individual terms J_i^{kl} is facilitated by the identity

$$V_j^{kl}(u^2\delta_{ij}-u_iu_j)/(u^3)$$
$$\equiv f_k'/v(\partial f_l)/(\partial v)(v_i/u-(\mathbf{v}\cdot\mathbf{v}'-v^2)/u^3)$$
$$-f_l/v'(\partial f_k')/(\partial v')(v_i'/u-(\mathbf{v}\cdot\mathbf{v}'-v'^2)/u^3).$$

After substituting the angular expressions for v_x', v_y', and v_z' and integrating over the angles χ and ψ, we obtain for J_i^{00} the result

$$J_i^{00}=\mathfrak{L}\int V_j^{00}(u^2\delta_{ij}-u_iu_j)/(u^3)d\mathbf{v}'$$
$$=8\pi v_i\mathfrak{L}/3\int_0^\infty U^{00}v'dv'.$$

In computing J_i^{10} we discover that cylindrical symmetry causes J_x^{10} and J_y^{10} to be alike except for subscript, and different from J_z^{10}. We obtain

$$J_x^{10}=\mathfrak{L}\int v_x'V_j^{10}(u^2\delta_{xj}-u_xu_j)/(u^3)d\mathbf{v}'$$
$$=16\pi v_xv_z\mathfrak{L}/15\int_0^\infty U^{10}v'dv',$$
$$J_y^{10}=16\pi v_yv_z\mathfrak{L}/15\int_0^\infty U^{10}v'dv',$$

and

$$J_z^{10}=16\pi/15(v_z^2+\tfrac{1}{2}v^2)\mathfrak{L}\int_0^\infty U^{10}v'dv'.$$

In addition to these integrations, the following must be computed:

$$\mathfrak{L}\int(f'f_1-ff_1')(\mathbf{k}u^2-u_z\mathbf{u})/(u^3)$$
$$=8\pi\mathfrak{L}/15\mathbf{v}\int_0^\infty f_1'f_1v'dv'$$
$$+8\pi\mathfrak{L}/15\mathbf{k}\int_0^\infty[5(f_0'f_1-f_0f_1')-3v_zf_1'f_1]v'dv'.$$

It is not necessary to compute more of the J_i^{kl},

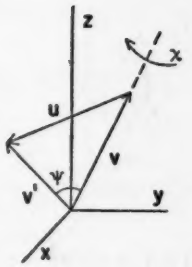

FIG. 2. Coordinates for J integrations.

as they may be obtained by changes of indices. Combining the results of the computation into the single vector $\mathbf{J}$, we have

$$\mathbf{J}(\mathbf{v})=\mathfrak{L}'\mathbf{v}\int_0^\infty(5U^{00}+5v_zU^{01}$$
$$+2v_zU^{10}+2v_z^2U^{11}+f_1f_1')v'dv'$$
$$+\mathbf{k}\mathfrak{L}'\int_0^\infty[v^2U^{10}+v^2v_zU^{11}$$
$$+5(f_0'f_1-f_0f_1')-3v_zf_1'f_1]v'dv',$$

which is Eq. (10). The constant $\mathfrak{L}'$ replaces $8\pi/15\mathfrak{L}$.

APPENDIX II

Calculation of $\nabla\cdot\mathbf{J}$

The expression of $\mathbf{J}$ as a vector having components in spherical coordinates was found useful in carrying out the divergence operation. In terms of its rectangular components, the spherical components of $\mathbf{J}$ are

$$J_v=J_x\sin\theta\cos\varphi+J_y\sin\theta\sin\varphi+J_z\cos\theta,$$
$$J_\theta=J_x\cos\theta\cos\varphi+J_y\cos\theta\sin\varphi-J_z\sin\theta, \quad \text{(II.1)}$$
$$J_\varphi=-J_x\sin\varphi+J_y\cos\varphi.$$

The polar axis is taken in the z direction so that we can take advantage of the symmetry of the problem. This causes J_φ to vanish, as can be readily verified. Substitution of the rectangular components of $\mathbf{J}$ in (II.1) immediately gives

$$J_v=\mathfrak{L}'\int_0^\infty[5vU^{00}+5v^2U^{01}\cos\theta+3v^2U^{10}\cos\theta$$
$$+3v^2U^{11}\cos^2\theta+5(f_0'f_1-f_0f_1')\cos\theta$$
$$+vf_1'f_1(1-3\cos^2\theta)]v'dv',$$

and

$$J_\theta = \mathfrak{L}\int_0^\infty \{[v^2U^{10}+5(f_0'f_1-f_0f_1')]\sin\theta + \tfrac{1}{2}[v^3U^{11}-3vf_1'f_1]\sin 2\theta\}v'dv'.$$

The divergence can then be calculated to be

$$\nabla\cdot\mathbf{J} = 1/v\sin^2\theta\left(\frac{\partial}{\partial v}v^2\sin\theta J_v + \frac{\partial}{\partial\theta}v\sin\theta J_\theta\right)$$
$$= \mathfrak{L}'\int_0^\infty \{15U^{00}+5v(\partial U^{00})/(\partial v)+5v^2U^{11} + v^3(\partial U^{11})/(\partial v)+[20vU^{01}+5v^2(\partial U^{01})/(\partial v) + 12vU^{10}+3v^2(\partial U^{10})/(\partial v) + 5(f_0'(\partial f_1)/(\partial v)-f_1'(\partial f_0)/(\partial v)) - 2vU^{10}]\cos\theta\}v'dv'. \quad \text{(II.2)}$$

In the process of calculation, wherever a non-linear trigonometric expression appeared, it was expanded in Legendre Polynomials, the constant and linear terms alone being retained. It was found convenient to work with the variable $s=v^2$, in terms of which (II.2) becomes

$$\nabla\cdot\mathbf{J} = \mathfrak{L}'\int_0^\infty \{15U^{00}+10s(\lambda U^{00})/(\partial s)+5sU^{11} + 2s^2(\partial U^{11})/(\partial s)+[20U^{01}+10s(\partial U^{01})/(\partial s) + 10U^{10}+6s(\partial U^{10})/(\partial s) + 5(f_0'(\partial f_1)/(\partial s)-f_1'(\partial f_0)/(\partial s))]v_z\}ds', \quad \text{(II.3)}$$

where now

$$U^{kl} = f_k'(\partial f_l)/(\partial s)-f_l'(\partial f_k')/(\partial s').$$

We are forced to define the following functional constants:

$$A = \mathfrak{L}'\int_0^\infty f_0 ds, \quad C = \mathfrak{L}'\int_0^\infty f_1 ds,$$
$$B = \mathfrak{L}'f_0(0), \qquad D = \mathfrak{L}'f_1(0).$$

These appear in the final solution, so that in solving the differential aspect of the Boltzmann equation we still are faced with the solution of a non-linear integral equation.

If we separate the isotropic and anisotropic terms of $\nabla\cdot\mathbf{J}$ in the form

$$\nabla\cdot\mathbf{J} = (\partial_e f_0/\partial t)_1+(\partial_e v_z f_1/\partial t)_1,$$

we obtain

$$\left(\frac{\partial_e f_0}{\partial t}\right)_1 = (10)/(s^{\frac{1}{2}})\frac{d}{ds}s^{\frac{1}{2}}(Af_0'+Bf_0) + (2)/(s^{\frac{1}{2}})\frac{d}{ds}s^{5/2}(Cf_1'+Df_1)$$

and (II.4)

$$\left(\frac{\partial_e v_z f_1}{\partial t}\right)_1 = v_z\{10/s^{\frac{1}{2}}\frac{d}{ds}s^{5/2}(Af_1'+Bf_1) + 6/s^{\frac{1}{2}}\frac{d}{ds}s^{5/2}(Cf_0'+Df_0) - 5(2Cf_0'+Df_0+Bf_1)\},$$

the primes in (II.4) indicating differentiation with respect to s.

Remarks on the Determination of a Central Field of Force from the Elastic Scattering Phase Shifts

V. BARGMANN
Palmer Physical Laboratory, Princeton University, Princeton, New Jersey
(Received October 4, 1948)

It is shown by an explicit example that a central field of force is not uniquely determined by the phase shifts for an S-wave. Hylleraas' recent paper is discussed, and an error in his argument is pointed out.

INTRODUCTION

IT is interesting to know to what extent a central field of force is determined by the phase shifts which are used in computing the elastic scattering cross sections according to quantum mechanics. Recently two methods[1,2] have been suggested which would even allow determination of the field of force from the phase shifts for one single value of the angular momentum (for example, $l=0$). Clearly, these methods can be generally valid only if no two different potentials give rise to the same phase shifts.

In this note we shall exhibit, however, two potentials, V_1 and V_2 ($V_1 \neq V_2$), which yield the same phase shifts for S-waves (cf. (13a) and (13b)).

Let $\psi(r)$ be the wave function (for angular momentum 0) of a particle moving in a central field $V(r)$, and set $\phi=r\cdot\psi$. In the non-relativistic case, ϕ satisfies the differential equation

$$d^2\phi/dr^2+k^2\phi=V(r)\cdot\phi, \qquad (1)$$

k being the wave number. (The units are so chosen that the energy of the particle equals k^2. If ordinary units are used both E and V must be multiplied by $\hbar^2/2m$, where m is the mass of the particle.) We assume that the integral $\int_0^\infty |V(r)|\,dr$ converges, so that the usual scattering theory may be applied.

Following R. Jost's paper on the S-matrix,[3] we introduce two independent solutions of (1), *viz.*, $f(k,r)$ and $f(-k,r)$, which for large r are asymptotically equal to e^{-ikr} and to e^{ikr}, respectively, and we set

$$f(k)=f(k,0); \quad f(-k)=f(-k,0). \qquad (2)$$

For real values of k the functions $f(k,r)$ and $f(-k,r)$ are complex conjugate, and $f(k)\neq 0$. Since $\phi=r\cdot\psi$, an admissible solution of (1) must vanish for $r=0$. Hence,

$$\phi(r)=(1/2i|f(k)|)\times\{f(k)f(-k,r)-f(-k)f(k,r)\}. \qquad (3)$$

Asymptotically, $\phi(r)\sim\sin(kr+\eta)$, where the phase shift η is determined by

$$e^{i\eta}=f(k)/|f(k)| \quad \text{or} \quad S(k)=e^{2i\eta}=f(k)/f(-k). \qquad (4)$$

(The $S(k)$ are the proper values of the S-matrix associated with Eq. (1).) As has been shown by Jost,[3] the function $f(k,r)$ may also be used (and is analytic in k) for complex k with negative imaginary parts, in particular for $k=-i\kappa$, where $\kappa>0$. A bound stationary state is obtained if the exponentially decreasing solution $f(-i\kappa,r)$ vanishes at $r=0$, i.e., if $f(-i\kappa)=0$. Its energy is then given by

$$E=k^2=-\kappa^2 \qquad [f(-i\kappa)=0, \quad \kappa>0]. \qquad (5)$$

It follows from (4) and (5) that two potentials with the same function $f(k)$ yield the same phase shifts and the same stationary energy values.

CONSTRUCTION OF THE EXAMPLE

The potentials considered are Eckart potentials[4] of the form

$$V(r)=K[\sigma,\beta,\lambda]\equiv-\sigma\lambda^2\beta e^{-\lambda r}/(1+\beta e^{-\lambda r})^2, \qquad (6)$$

where $\lambda>0$, and $\beta>-1$. We shall restrict ourselves to the values $\sigma=2$ and $\sigma=6$. (With respect to this choice cf. the Appendix.)

[1] Carl-Erik Fröberg, Phys. Rev. **72**, 519 (1947).
[2] E. A. Hylleraas, Phys. Rev. **74**, 48 (1948).
[3] R. Jost, Helv. Phys. Acta **22**, 256 (1947).
[4] C. Eckart, Phys. Rev. **35**, 1303 (1930).

(a) $\sigma=2$

(This potential is also discussed by Jost (reference 3, p. 260).) Here

$$f(k,r)=e^{-ikr}(2k+i\mu(r))/(2k-i\lambda), \quad (7)$$

with

$$\mu(r)=\lambda(\beta e^{-\lambda r}-1)/(\beta e^{-\lambda r}+1). \quad (7a)$$

Clearly,

$$\mu(0)=\nu\equiv\lambda(\beta-1)/(\beta+1); \quad \mu(\infty)=-\lambda. \quad (8)$$

It is easily verified that (7) is a solution of the Schrödinger equation (1), since $d\mu/dr=\frac{1}{2}(\mu^2-\lambda^2)$ $=-2\lambda^2\beta e^{-\lambda r}/(1+\beta e^{-\lambda r})^2$, and $d^2\mu/dr^2=\mu\cdot(d\mu/dr)$. Moreover, for large r, $f(k,r)\sim e^{-ikr}$, since $\mu(\infty)=-\lambda$. From (7) we obtain (cf. (8))

$$f(k)\equiv f(k,0)=(2k+i\nu)/(2k-i\lambda). \quad (9)$$

The function $f(-i\kappa)$ vanishes for $\kappa=\frac{1}{2}\nu$, so that there exists a bound stationary state, with energy $E=-\frac{1}{4}\nu^2$, if $\nu>0$, i.e., if $\beta>1$.

(b) $\sigma=6$

As may again be directly verified, here

$$f(k,r)=e^{-ikr}\frac{4k^2+6ik\mu(r)+\lambda^2-3\mu(r)^2}{(2k-i\lambda)(2k-2i\lambda)}, \quad (10)$$

$$f(k)=\frac{4k^2+6ik\nu+\lambda^2-3\nu^2}{(2k-i\lambda)(2k-2i\lambda)}, \quad (11)$$

where $\mu(r)$ and ν are defined by (7a) and (8), respectively. The bound stationary states are obtained from the equation $f(-i\kappa)=0$, $(\kappa>0)$. There exists one stationary state if $2-\sqrt{3}<\beta$ $\leqq 2+\sqrt{3}$, and there exist two if $\beta>2+\sqrt{3}$. ($2\pm\sqrt{3}$ are the two roots of the equation $\lambda^2-3\nu^2=0$.)

Consider now $V_1(r)=K[6,1,\lambda]$ (λ arbitrary). Then $\nu=0$ (cf. (8)), and, by (11),

$$f_1(k)=(2k+i\lambda)/(2k-2i\lambda). \quad (12)$$

Set, further, $V_2(r)=K[2,\beta',\lambda']$ (β' and λ' to be determined). By (9), $f_2(k)=(2k+i\nu')/(2k-i\lambda')$. Hence $f_1(k)=f_2(k)$ if $2\lambda=\lambda'$, and $\lambda=\nu'=\lambda'(\beta'-1)/(\beta'+1)$, i.e., $\beta'=3$. Consequently, the two potentials

$$V_1(r)=-6\lambda^2e^{-\lambda r}/(1+e^{-\lambda r})^2, \quad (13a)$$

and

$$V_2(r)=-24\lambda^2e^{-2\lambda r}/(1+3e^{-\lambda r})^2, \quad (13b)$$

lead to the same function $f(k)$, and therefore to the same phase shift η (cf. (4)).

$V_1(r)$ and $V_2(r)$ have the common value $-3\lambda^2/2$ at $r=0$, their integrals (extended over all r) are both equal to -3λ, and they give rise to stationary states with the same energy, *viz.*, $E=-\frac{1}{4}\lambda^2$.

If V_1 and V_2 are expressed as

$$V_1(r)=-3\lambda^2/2\cosh^2(\tfrac{1}{2}\lambda r),$$
$$V_2(r)=-2\lambda^2/\cosh^2(\lambda(r-a)); \quad a=(\ln 3)/2\lambda,$$

it is seen that $V_1(r)$ has its minimum at $r=0$, and defines an attractive force for all r, while $V_2(r)$ reaches its minimum at $r=a$, defining a repulsive force for $r<a$, and an attractive force for $r>a$. Moreover, the two potentials differ in their asymptotic behavior. The expression

$$D=\left\{\int_0^\infty (V_1(r)-V_2(r))^2dr \Big/ \int_0^\infty (V_1(r)+V_2(r))^2dr\right\}^{\frac{1}{2}},$$

may serve as a measure for the deviation of $V_1(r)$ from $V_2(r)$. One finds $D=0.162$.

Evidently our result only proves that the phase shifts for the angular momentum zero do not determine the potential $V(r)$, but we cannot yet assert that the knowledge of all phase shifts (for arbitrary values of the angular momentum) is insufficient for the unique determination of $V(r)$. C. Møller[5] has proved that one can construct infinitely many different Hamiltonians which yield the same phase shifts, i.e., the same S-matrix. It is not obvious, however, that one can find among them a Hamiltonian which corresponds to an ordinary central field of force.

REMARKS ON HYLLERAAS' PAPER

We again restrict ourselves to the case $l=0$. For a given $V(r)$, Hylleraas[2] introduces two solutions of the Schrödinger equation,[6] *viz.*, $v_1(r)$, which is given by Eq. (3) above, and $v_2(r)$, which may be expressed as

$$v_2(r)=(1/2|f(k)|)\times\{f(k)f(-k,r)+f(-k)f(k,r)\}, \quad (14)$$

[5] C. Møller, Kgl. Danske Vid. Sels. Math.—Fys. Medd 24, No. 19 (1946). Cf. p. 33.

[6] For the details the reader is referred to Hylleraas' paper. (H 13), for example, is a reference to Eq. (13) of his paper.

and which asymptotically equals $\cos(kr+\eta)$. Let $V(r)$ and $U(r)$ be two potentials, η and ξ the corresponding phase shifts, and v_1, v_2 and u_1, u_2 the associated wave functions. Set $Y_k(r)=u_1v_1$, and $Z_k(r)=u_1v_2+u_2v_1$. Hylleraas asserts the general validity of the equation

$$V(r)-U(r) = (4/\pi)(d/dr)\int_0^\infty \sin(\eta-\xi)Z_k(r)dk. \quad (15)$$

[The foregoing equation differs from Hylleraas' (cf. (H 13)) in two minor points. (a) In order to avoid the appearance of divergent integrals we have interchanged differentiation with respect to r and integration with respect to k. (b) The signs of V and U are inverted, because Hylleraas' V corresponds to our $-V$ in the Schrödinger equation (cf. his Eq. (3)).] One would infer from (15) that $\eta=\xi$ implies $V(r)=U(r)$, whereas we have seen above that $V(r)$ is not uniquely determined by η.

Hylleraas bases his proof on the assumption that his equations (H 14) and (H 15) are equivalent, and that it is therefore sufficient to establish (H 14). In reality, these two equations are independent, since (H 14) corresponds to an orthogonality relation, and (H 15) to a completeness relation. The latter appears particularly doubtful if either one of the potentials V, U gives rise to a bound state, because then the solutions of the Schrödinger equation which belong to the continuous spectrum do not form a complete system of functions.

The writer has checked Eq. (H 15) for $V=K[2,\beta,\lambda]$, $U=K[2,\beta',\lambda']$. Then the functions Y_k and Z_k may be computed from (7), (3), and (14), and the integral in (H 15) evaluated explicitly. The following result was obtained: (H 15) holds if and only if the Schrödinger equations for both V and U have no discrete spectra, i.e., if $\beta\leqq 1$ and $\beta'\leqq 1$. This seems to indicate that Hylleraas' formula (cf. Eq. (15) above) may be generally valid if neither V nor U give rise to bound states. (Note that this holds for the example which Hylleraas discusses at the end of his paper.) The writer has not attempted a proof of this conjecture.

APPENDIX

For arbitrary values of σ, the function $f(k,r)$ associated with the potential $V(r)=K[\sigma,\beta,\lambda]$ (cf. (6)) is found to be

$$f(k,r)=e^{-ikr}(1+\beta e^{-\lambda r})^{\tau}F(\tau+(2ik/\lambda),\tau, 1+(2ik/\lambda),-\beta e^{-\lambda r}), \quad (16)$$

where $\tau=\frac{1}{2}(1-(1+4\sigma)^{\frac{1}{2}})$, and F is the hypergeometric function. If $\sigma=n(n+1)$ $[n=1,2,\cdots]$, then $\tau=-n$, and F is a polynomial of n-th degree. One obtains the expressions (7) and (10) by setting $n=1$ and 2, respectively, and inserting $(\lambda+\mu(r))/(\lambda-\mu(r))$ for $\beta e^{-\lambda r}$.

Note added in proof: In the meantime the writer has worked out a number of additional examples. In particular, it is possible to construct potentials which (for S-waves) give equal phase shifts, but bound states of different energy values. This fact is of interest with respect to the theory of the S-matrix. It is also possible to find a non-vanishing potential which does not give any S-scattering. A detailed account will be published later.

PHYSICAL REVIEW VOLUME 75, NUMBER 2 JANUARY 15, 1949

Condensation of Pure He^3 and Its Vapor Pressures between 1.2° and Its Critical Point

S. G. Sydoriak, E. R. Grilly, and E. F. Hammel
Los Alamos Scientific Laboratory, Los Alamos, New Mexico

November 29, 1948

ON October 13, 1948 the authors succeeded in condensing[1] pure He^3 prepared by E. S. Robinson and R. M. Potter of the laboratory. The isotope was "grown" from pure tritium solutions by β-decay of the tritium. The latter

[1] Although the evidence is not conclusive, indications are that we have observed a transition to a liquid rather than a solid state. This is suggested by the similarity of Fig. 1 to what one would expect for a gas-liquid transition and by the approximate agreement between observed densities and those calculated from the critical constants by use of van der Waal's and Dieterici's equations of state.

was initially separated from traces of He^4 by passage through a palladium valve. The He^3 was purified by absorption of H_2 and T_2 in uranium, followed by repeated passages successively over (1) hot CuO followed by a liquid air trap and (2) hot Ca, thus removing all other impurities except the rare gases.

These results seem especially interesting since so much doubt has existed over the properties of He^3. London and Rice[2] suggested that this isotope would not liquefy at all, at least not under any "normal" conditions. Their argument was based on the large zero-point energy calculated for He^3 which they found to be sufficient to compensate entirely the potential energy of the van der Waal's cohesive energy. Tisza[3] also doubted that He^3 would liquefy unless "entirely unheard of properties" of viscosity were exhibited by the liquid. Fairbank, Reynolds, and Lane[4] measured the vapor pressure difference between He^4 and solutions enriched to 0.16 percent He^3 in the temperature range from 1.3° to 4.2°K. Using ideal solution concepts, they calculated vapor pressures of pure He^3. An extrapolation of $\log P$ *vs.* $1/T$ led to a normal boiling point of 2.9°K.

In these experiments 20 cc S.T.P. of He^3 was used. The He^3 was permitted to condense into the bottom of a 1.2-mm I.D. stainless steel capillary immersed in a bath of liquid well helium at depths of, usually, 5 or 10 mm. The immersion depth was held constant by gradually raising the Dewar as the bath evaporated, the capillary being fixed with respect to its vacuum system. A double Wilson seal surrounding the capillary made this immersion adjustment possible even when pumping on the bath. In order to minimize the effect of the dead volume of the capillary in the temperature region between bath and room temperature, the upper part of the capillary was surrounded by two shells of heavier tubing in thermal contact with the capillary at the top (room temperature) end and at a point 4 cm from the bottom. Being far better heat conductors than the capillary, these shells had the effect of raising the temperature of the capillary at all points on the capillary not immersed in the liquid, thus greatly reducing the dead space.

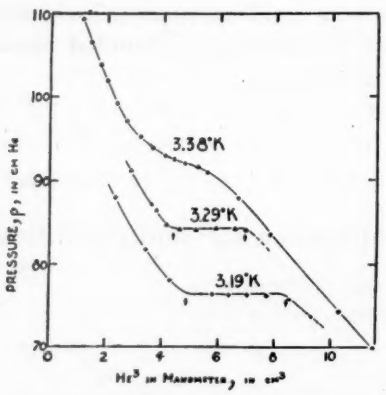

FIG. 1. "Isotherms" in the vicinity of the critical point.

The room temperature end of the capillary was connected to a combined mercury manometer and simple Toepler pump such that by raising the mercury levels in the manometer, He^3 could be transferred into the capillary and its pressure there measured. Condensation was assumed to be taking place if the equilibrium pressure in the capillary was independent of the volume of helium remaining in the manometer.

Figure 1 shows the data for three different temperatures. Flats on the two lower curves indicate the vapor pressures of He^3 corresponding to 3.19°K and 3.29°K. The upper curve corresponds to a temperature of 3.38°K which is believed to be above the critical temperature T_c, since at T_c a horizontal inflection would be observed. From these data and other runs at intermediate temperatures we have chosen $T_c = 3.3_4$°K corrected as explained below.

As a check on the equilibrium temperature inside the capillary, He^4 was condensed there. Its vapor pressure was found to be greater than the bath pressure by an amount corresponding to a temperature difference of 0.01_2°K. The same temperature excess inside the capillary was observed at bath temperatures of 4.0, 3.3, and 1.4°K. We are tentatively assuming that the same temperature excess existed when He^3 was being condensed and have adjusted our temperatures accordingly.

It has been previously observed that open and closed bulb vapor pressure thermometers may

[2] F. London and O. K. Rice, Phys. Rev. **73**, 1188 (1948).
[3] Laszlo Tisza, Physics Today **1**, 26 (1948).
[4] Fairbank, Reynolds, Lane, McInteer, Aldrich, and Nier, Phys. Rev. **74**, 345 (1948).

indicate different bath temperatures, but no satisfactory explanation for this has been advanced.[5] Our observations lead us to suggest that a heat flow down to the bulb may give rise to an appreciable temperature gradient through the walls of the immersed portion of the bulb. This thermal flow appears to be due to both conduction in the capillary wall and convection of the gas within it. Since an open-bottomed tube communicates directly with the liquid, the vapor pressure measured with such a device should correspond more closely to the bath pressure.

The possibility of a pressure difference due to the surface tension of the liquid should also be considered.

The vapor pressure measurements are summarized in Table I and in Fig. 2, which also shows vapor pressures for He^4 determined at Leiden in 1937. It is interesting to note that at 1.2°K the vapor pressure of He^3 is 35 times as great as that of He^4, suggesting the potential usefulness of He^3 for thermometry at low temperatures. At 1°K He^4 vapor pressures are near the limit of accurate measurement. Indications are that He^3 could be used down to 0.5°K or perhaps even lower. The pressure at 0.5°K is 0.12 mm Hg if our data are extrapolated on the assumption of constant latent heat below 1.4°K.

TABLE I. Vapor pressures of He^3 from 1.2° to 3.3°K.

T, °K	P, mm Hg
1.21_1	23
1.33_4	32
1.52_4	54
1.63_5	70
1.79_6	99
1.97_7	141
2.04_7	159
2.15_2	195
2.32_7	255
2.58_0	366
2.81_7	495
3.03_2	634
3.20_1	764
3.29_7	842
3.33_5	872
(3.3_4)	(875) critical point
(3.2_0)	(760) boiling point

[5] W. H. Keesom, *Helium* (Elsevier Publishing Company, Inc., New York, 1942), p. 193.

A curve through the experimental points shows the normal boiling point to be 3.2₀°K. Extrapolation to the critical temperature gives for the critical pressure $p_c = 875$ mm Hg. Putting these values of p_c and T_c in van der Waal's equation, we find the critical density to be $\rho_c = 0.036$ g/cm³. By Dieterici's equation we find $\rho_c = 0.046$. Since for He^4 the accepted value of ρ_c lies midway between the values calculated from these two equations, we have chosen $\rho_c = 0.041$ g/cc.

It is possible to determine the density of the liquid from these data provided one knows to what level the liquid rises in the immersed

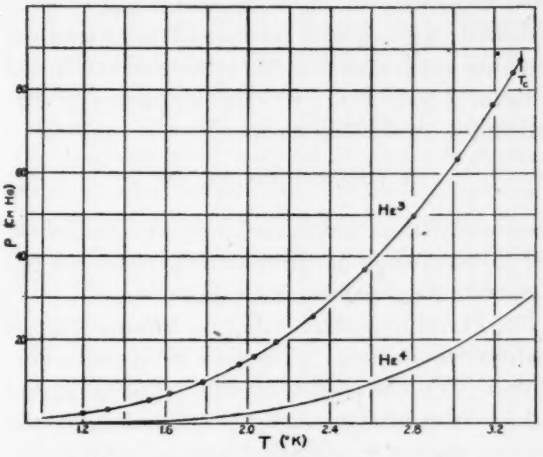

FIG. 2. Vapor pressures of He^3 and He^4.

capillary before a significant rise in its vapor pressure occurs. This gives the volume corresponding to the mass of gas admitted at constant vapor pressure (plus a correction for the dense gas displaced in the process). With our capillary the level inside is found to rise some millimeters above the bath when He^4 is being condensed, and it is therefore necessary to get data for two or more immersion depths in order to make a reasonable estimate of the liquid density. The evidence so far is that near T_c the densities calculated above are approximately correct and that with decreasing temperature a very rapid rise in density occurs. At 2.8° it may be as much as a factor of two higher. We are now prepared to risk using a glass capillary in order to check these density estimates.

On the Experimental Value of the Fine Structure Constant

H. A. BETHE* AND C. LONGMIRE
Columbia University, New York, New York

December 6, 1948

TAUB and Kusch[1] have recently measured the ratio of the magnetic moments of electron and proton, with accuracy hitherto unattained, by measuring the ratio of the "flop-frequencies" of the electron and proton spins in a strong magnetic field. The result is

$$\mu_P/\mu_e=(1.51927\pm0.00010)\times10^{-3}. \quad (1)$$

On the other hand, Nafe and Nelson[2] have measured with great precision the hyperfine structure separation of the ground state of the H-atom. Their result for the frequency ν corresponding to the separation is

$$\nu=1420.410\pm0.006 \text{ Mc}. \quad (2)$$

Taub and Kusch have combined the results (1) and (2) to give an accurate determination of the fine-structure constant, $\alpha=e^2/hc$.

The Fermi hyperfine-structure formula,[3] when modified to include (*a*) Breit's relativistic correction,[4] (*b*) the effect of the reduced mass,[5] and (*c*) the electromagnetic correction to the electron magnetic moment,[6] may be written, for hydrogen,

$$\nu=\alpha^2\left[\frac{16}{3}\left(\frac{\mu_P}{\mu_e}\right)cR_\infty(1+\tfrac{3}{2}\alpha^2)\times\left(1+\frac{m}{M}\right)^{-3}\left(1+\frac{\alpha^2}{2\pi}\right)\right]. \quad (3)$$

Here the last three terms in the square bracket are, in the order of their appearance, the corrections (*a*), (*b*), and (*c*) above. R_∞ is the Rudberg constant, and c is the velocity of light. Equation (3) is regarded as an equation for the unknown.

Experimentally, the least accurately known quantity in (3) is the ratio of moments. However, there are also theoretical uncertainties in the derivation of (3), *viz.*:

(1) It has been assumed that the proton has a point magnetic dipole, whereas meson theory would indicate a current distribution over the range of the nuclear forces. If this is taken as $\hbar/\mu c$(μ=meson mass=285 m), and if only the extra moment $\mu_P-\mu_D$ (Dirac moment) is so distributed, the right-hand side of (3) should be corrected by an amount of the relative order of magnitude

$$-\frac{\mu_P-\mu_D}{\mu_P}\frac{m}{\mu}\alpha\approx-1.6\times10^{-5}. \quad (4)$$

(2) The electron has also been assumed to have a point magnetic dipole, in disagreement with Schwinger's result that the electromagnetic correction represents a "smeared" dipole distributed over a region of the order of the Compton wave-length. This may give a correction to Eq. (3) of the relative order

$$-\frac{\alpha^2}{2\pi}\approx-0.8\times10^{-5}. \quad (5)$$

(3) The ratio of the electron moment to the Bohr magneton has been assumed to have the theoretical value, $1+\alpha/2\pi=1.00116$. The average of the experimental values is slightly higher (1.00119); if it were taken, the theoretical value of ν would be increased by a relative amount $+6\times10^{-5}$.

The result for $1/\alpha$ would, in each case, be changed by one-half of these fractions.

Equations (1), (2), and (3) give the result

$$1/\alpha=137.041\pm0.005. \quad (6)$$

This value is in disagreement with the value given by Dumond and Cohen,[7] namely,

$$1/\alpha=137.021\pm0.007 \quad (7)$$

* On leave from Cornell University.

[1] We are indebted to Drs. Taub and Kusch for information concerning their results before publication.

[2] John E. Nafe and Edward B. Nelson, Phys. Rev. **73**, 718 (1948).

[3] E. Fermi, Zeits. f. Physik **60**, 320 (1930).

[4] G. Breit, Phys. Rev. **35**, 1447 (1930).

[5] G. Breit and E. R. Meyerott, Phys. Rev. **72**, 1023 (1947).

[6] P. Kusch and H. M. Foley, Phys. Rev. **72**, 1256 (1947); J. Schwinger, Phys. Rev. **73**, 416 (1948).

[7] J. W. M. Dumond and E. R. Cohen, Rev. Mod. Phys. **20**, 82 (1948).

(but it does not disagree with the earlier value 137.030 ± 0.015 of Birge).[8]

In order to check whether the discrepancy with the value of Dumond and Cohen is real, we have carried out least-square calculations similar to those of Dumond and Cohen, but with some differences in input data. Referring to Table VII of Dumond and Cohen, we have made the following changes:

(1) The value of e^2/m, from the refractive index for x-rays (item 4 of their table) must be corrected for scattering by the atomic nuclei. The electrons give a contribution proportional to Ze^2/m, and the nucleus adds $(Ze)^2/MA$ to this (A = atomic weight, M = proton mass), so that the effect of the electrons is multiplied by $1+mZ/MA$. This correction changes the input value of e^2/m by a relative amount of -2.7×10^{-4}.

(2) We have omitted the direct determination of hc/e^2 from the x-ray fine structure (item 7) since this input datum should, according to recent theory, be corrected upwards by an (absolute) amount $1/2\pi$, because of the extra magnetic moment of the electron. (If it is so corrected, it becomes higher than our result for hc/e^2, *viz.*, 137.11, so that its inclusion among the input data would further increase our result for $1/\alpha$.)

(3) We have omitted items 8, 9, and 10 entirely because their probable errors are large. This was done merely to simplify the numerical work. This omission of a small part of the input data *ought* not to influence the result by an amount comparable to or greater than the probable error.

(4) The remaining items 1, 2, 3, 5, and 6 were used without change.

The least-squares method of combining these data (using the Faraday, Avogadro's number, and Planck's constant as unknowns) gives

$$1/\alpha=137.033\pm0.007. \qquad (8)$$

The error was determined, as in the article of Dumond and Cohen, by projecting the error ellipsoid on the α-direction.

[8] Raymond T. Birge, Rev. Mod. Phys. 13, 233 (1941).

The large difference between the values (7) and (8) compared to the errors quoted is not entirely due to the correction of item 4. About one-half (0.006) of the change is the result of neglecting items 7, 8, 9, and 10, and shows an inconsistency between these items and the first six. There are other inconsistencies in the input data; one is the long-recognized smallness of the experimental value of h/e (item 6, as determined from the Duane-Hunt limit). We find further that neglecting item 4 in addition to items 7, 8, 9, and 10 leads to the value $1/\alpha=137.040$; hence item 4 is inconsistent with the others. Fluctuations in the result due to neglect of a *small* part of the input data are, of course, to be expected, but the probable error assigned to the result ought to cover these fluctuations. The errors assigned in (7) and (8) are seen to be too small. The error-ellipsoid method of computing errors, which is based on the multiplication of the Gaussian distributions of individual experiments to obtain a resultant Gaussian, does not adequately take into account inconsistencies in the input data.

We conclude that there is no definite discrepancy between the new value (6) of $1/\alpha$ and the value computed from other experiments. The new value is probably the more reliable.

The largest inconsistency in the input data seems to exist (still) for the Duane-Hunt limit (item 6). The least-squares solution leading to (8) also leads to a value of h/e which is larger that the experimental value by a relative amount of 4.7×10^{-4}, a discrepancy of 1.6 times the experimental error given. However, this discrepancy happens to have practically no effect on the value of hc/e^2 (although it has larger effects on e and h separately). If item 6 is neglected entirely (this is equivalent to making item 6 agree with the other data), $1/\alpha$ is changed by an absolute amount of only -0.001. Therefore, if there were any essential disagreement between the new value (6) of $1/\alpha$ and the value from other experiments, it would not be because of the Duane-Hunt limit.

Letters to the Editor

PUBLICATION of brief reports of important discoveries in physics may be secured by addressing them to this department. The closing date for this department is five weeks prior to the date of issue. No proof will be sent to the authors. The Board of Editors does not hold itself responsible for the opinions expressed by the correspondents. Communications should not exceed 600 words in length.

On the Mesic Charge

TAISUKE OKAYAMA
Osaka Dental College, Osaka, Japan
October 20, 1948

WHEN we adopt Dirac's hole theory, it is necessary that the electron in the negative state satisfy the same wave equation satisfied by the positron in the positive state. As a matter of fact, this is fulfilled in the case of the electromagnetic field, which is described by a vector field. In this case, the wave equation of an electron is

$$\left(\frac{i\hbar}{c}\frac{\partial}{\partial t}+\frac{e}{c}A_0+i\hbar\rho_1\boldsymbol{\sigma}\,\mathrm{grad}-\frac{e}{c}\mathbf{A}\rho_1\boldsymbol{\sigma}-\rho_3 mc\right)\psi=0. \quad \text{(I)}$$

On the other hand, in the case of a pseudovector field, the wave equation is*

$$\left(\frac{i\hbar}{c}\frac{\partial}{\partial t}+\frac{e}{c}A_0\rho_1+i\hbar\rho_1\boldsymbol{\sigma}\,\mathrm{grad}-\frac{e}{c}\mathbf{A}\boldsymbol{\sigma}-\rho_3 mc\right)\psi=0. \quad \text{(II)}$$

Let ψ be a solution of Eq. (II) in a positive energy state, then $\bar{\psi}$, the complex conjugate of ψ, must satisfy

$$\left(\frac{i\hbar}{c}\frac{\partial}{\partial t}-\frac{e}{c}A_0\bar{\rho}_1+i\hbar\bar{\rho}_1\bar{\boldsymbol{\sigma}}\,\mathrm{grad}+\frac{e}{c}\mathbf{A}\bar{\boldsymbol{\sigma}}+s\bar{\rho}mc\right)\bar{\psi}=0.$$

Now, putting $\psi^*=\rho_2\sigma_y\bar{\psi}$, the equation satisfied by ψ^* becomes

$$\left(\frac{i\hbar}{c}\frac{\partial}{\partial t}+\frac{e}{c}A_0\rho_1+i\hbar\rho_1\boldsymbol{\sigma}\,\mathrm{grad}-\frac{e}{c}\mathbf{A}\boldsymbol{\sigma}-\rho_3 mc\right)\psi^*=0$$

which is the *same* equation as (II) itself.

As the time factor $e^{i\omega t/\hbar}$ is contained in the ψ^*, ψ^* is considered as the wave function of $-\omega$, the negative energy state. Since the solution in the positive energy state corresponds exactly to the solution in the negative one, a hole in the negative state must be considered as an electron in the positive state. The hole theory proper, however, cannot be applied in this case because there is no charge conservation. Thus the possibility of the application of Dirac's hole theory depends critically upon the form of the interaction.

This idea can be applied immediately to the meson field. Considering only the nuclear field between nucleons, we wish to investigate under what conditions a hole in the negative energy state of the nucleon can be considered as a nucleon with the inverse mesic charge in the positive energy state. As we shall discuss in the following, the various forms of the interaction behave differently in this respect. In doing the calculations we must, in the complex wave functions, distinguish the imaginary number for the electric charge from that for the mesic charge, denoting them, for instance, by i and j respectively. ($i^2=-1$, $j^2=-1$.)

Case 1. *Scalar Mesic Field.* The solution of the equation of a nucleon with mesic charge (f_1, f_2) in the negative energy state corresponds to the solution of a nucleon with mesic charge $(f_1, -f_2)$ in the positive energy state, where f_1, f_2 are the two interaction constants defined in Table I.

If we take account of conservation of mesic charge, the hole theory cannot be held but a case $f_1=0$.

Case 2. *Pseudoscalar Mesic Field.* The solution of the wave equation of a nucleon in the negative energy state corresponds to the solution of a nucleon with unchanged mesic charge in the positive energy state. Therefore, the hole theory cannot hold because there is no conservation of mesic charge.

Case 3. *Vector Mesic Field.* A hole in the negative energy state of a nucleon with mesic charge (g_1, g_2) can be regarded as a nucleon with inverse mesic charge $(-g_1, -g_2)$ in the positive energy state, so that there is conservation of mesic charges. Thus the hole theory may be used for both interactions.

Case 4. *Pseudovector Mesic Field.* The solution of the wave equation for a nucleon with mesic charge (g_1, g_2) in the negative state corresponds to the solution for a nucleon with mesic charge $(g_1, -g_2)$ in the positive energy state. Requiring conservation of mesic charge, the hole theory can only hold if we put $g_1=0$.

Only future experiments may decide whether there are really mesic charges, positive and negative. For this purpose, we must investigate phenomena proportional to the first power of the mesic charge; for instance the mesic-magnetic force. Since it is unlikely that a negative proton exists, it is rather probable that a hole in the negative state of a nucleon corresponds to a nucleon with *inverse* mesic charge in the positive state. If there are really mesic charges with a charge conservation theorem, then many types of interaction between nucleons and mesic field can be excluded. Further, one may expect the existence of cascade showers of the hard component of the cosmic rays in the very high energy region. Further research on these will be reported elsewhere.

TABLE I. Definition of interaction constants.*

Type	Interaction terms
Scalar	$-(\tau^+/K)f_1\rho_3 U-4\pi c f_2\tau^+U^+-(1/K^2)f_2\tau^+\rho_1\boldsymbol{\sigma}\,\mathrm{grad}U$ +Hermit conj.
Vector	$-(\tau^+/K)g_1\rho_1\boldsymbol{\sigma}\mathbf{U}-4\pi c g_2\tau^+\rho_2\boldsymbol{\sigma}\mathbf{U}^+$ $+(4\pi c g_1/K)\tau^+\,\mathrm{div}\mathbf{U}+(\tau^+/K^2)g_2\rho_3\boldsymbol{\sigma}\,\mathrm{rot}\mathbf{U}$ +Hermit conj.
Pseudoscalar	$-(\tau^+/K)f_1\rho_3 U-4\pi f_2 c\tau^+\rho_1 U^+-(f_2/K^2)\tau^+\boldsymbol{\sigma}\,\mathrm{grad}U$ +Hermit conj.
Pseudovector	$-(\tau^+/K)g_1\boldsymbol{\sigma}\mathbf{U}+4\pi c g_2\tau^+\rho_2\boldsymbol{\sigma}\mathbf{U}^++(\tau^+/K)4\pi c g_1\rho_1\,\mathrm{div}\mathbf{U}^+$ $+(\tau^+/K^2)g_2\rho_3\boldsymbol{\sigma}\,\mathrm{rot}\mathbf{U}$ +Hermit conj.

* U; field variable; U^+: canonical conj. of U.

* We assume the pseudovector type interaction.

Note on Dirac's Theory of Magnetic Poles

H. A. WILSON
Rice Institute, Houston, Texas
October 28, 1948

DIRAC'S result that $e_0g_0=hc/4\pi$ [1] where e_0 is the elementary electric point charge and g_0 the elementary point magnetic pole may be obtained very simply from classical electrodynamics and quantum mechanics.

The electromagnetic momentum per unit volume in a vacuum due to an electric field F and a magnetic field H is equal to the vector product of F and H divided by $4\pi c$. With $F=e/r^2$ and $H=g/r^2$ this gives for the angular momentum in the field around a charge e and pole g the value eg/c. This result was obtained by J. J. Thomson about the year 1900.[2]

According to quantum-mechanical theory any angular momentum must be an integral or half-odd integral multiple of $h/2\pi$ so that $eg=nhc/2\pi$ or $(n+\frac{1}{2})hc/2\pi$ where $n=0, 1, 2, 3\cdots$.

If we take the half-odd value, then $hc/4\pi$ is the smallest possible value of eg and so $e_0g_0=hc/4\pi$.

[1] P. A. M. Dirac, Phys. Rev. **74**, 817 (1948).
[2] J. J. Thomson, *Elements of the Mathematical Theory of Electricity and Magnetism* (1900).

The Magnetic Moments of the Neutron and Proton

J. M. LUTTINGER*
Swiss Federal Institute of Technology, Zurich, Switzerland
October 13, 1948

THE method of calculating the correction to the magnetic moment of the electron given recently by the author[1] has been applied to the calculation of the magnetic moments of the neutron and proton in the pseudoscalar meson theory. The calculations are carried out for the charged and uncharged theories, using the theory of holes to describe the behavior of the heavy particles. A consistantly relativistic treatment has been used throughout, the only approximation being in the use of second-order perturbation theory. Finite results are obtained for all the quantities calculated.

One may write for the interaction energy of the nucleon and meson fields in the presence of a static magnetic field:[2]

Neutral mesons

$$\mathcal{H}_{\rm int}=(4\pi)^{\frac{1}{2}}f[\psi_P^*(\sigma\cdot\nabla\phi-\gamma_S\pi)\psi_P+\psi_N^*(\sigma\cdot\nabla\phi-\gamma_S\pi)\psi_N]+2\pi f^2[(\psi_P^*\gamma_S\psi_P)(\psi_P^*\gamma_S\psi_P)+(\psi_N^*\gamma_S\psi_N)(\psi_N^*\gamma_S\psi_N)].$$

Charged mesons

$$\mathcal{H}_{\rm int}=(8\pi)^{\frac{1}{2}}f[\psi_P^*(\sigma\cdot D\phi-\gamma_S\pi^*)\psi_N+\psi_N^*(\sigma\cdot D^*\phi^*-\gamma_S\pi)\psi_P]+4\pi f^2[(\psi_P^*\gamma_S\psi_N)(\psi_N^*\gamma_S\psi_P)+(\psi_N^*\gamma_S\psi_P)(\psi_P^*\gamma_S\psi_N)].$$

Here f is the coupling constant; ψ_P, ψ_N the (quantized) wave functions of the proton and neutron, respectively; ϕ, π the (quantized) meson field and its conjugate momentum; $D\equiv\nabla-ieA_0$, A_0 is the vector potential of the static magnetic field, and finally $\gamma_S=i\alpha_1\alpha_2\alpha_3$. It may be mentioned that the terms quadratic in the coupling constant are not unique;[2] however, both possible versions of the Hamiltonian lead to the same magnetic moments.

Using now the exact solutions of the Dirac equation for the nucleons and of the Klein-Gordon equation for the mesons (both with an external homogeneous magnetic field present), we calculate the contribution of $\mathcal{H}_{\rm int}$ to the x energy, for the special state in which the nucleon has simply the energy M, and no mesons are present.[1] This choice of the state was essential in avoiding the divergencies in the calculation of the magnetic moment of the electron, and is also essential here for the proton. However, for the case of the neutron any state would do, and we choose this special state only for simplicity of calculation. Since the mean value of $\mathcal{H}_{\rm int}$ is zero, we must resort to second-order perturbation theory. The calculation is straightforward, proceeding in a very similar fashion to that for electrons. We quote only the results:

Neutral theory

$$\mu_N=0,$$

$$\mu_P=-\frac{4}{\pi}(f\mu)^2\frac{1}{\delta^3}\left(\frac{1}{4}+\frac{\delta^2}{2}-\frac{\delta^3}{2(4-\delta^2)^{\frac{1}{2}}}\cos^{-1}\frac{\delta}{2}-\frac{\delta^2(1-\delta^2)}{2}\log\frac{1}{\delta}\right).$$

Charged theory

$$\mu_N=\frac{-4}{\pi}(f\mu)^2\frac{1}{\delta^3}\left(1-\frac{\delta(2-\delta^2)}{(4-\delta^2)^{\frac{1}{2}}}\cos^{-1}\frac{\delta}{2}-\delta^2\log\frac{1}{\delta}\right),$$

$$\mu_P=\frac{4}{\pi}(f\mu)^2\frac{1}{\delta^3}\left(\frac{1}{2}-\delta^2-\frac{\delta}{(4-\delta^2)^{\frac{1}{2}}}(2-4\delta^2+\delta^4)\cos^{-1}\frac{\delta}{2}+\delta^2(2-\delta^2)\log\frac{1}{\delta}\right).$$

Here μ_N, μ_P are the additions (resulting from the mesons) to the magnetic moments of the neutron and proton, respectively, in units of the nuclear magneton, δ the ratio of meson to proton (or neutron) mass, and μ is the meson mass. By simply adding the results of the neutral and charged theories one may obtain the results for the "charge symmetrical" theory.

The numerical calculation for reasonable values[3] of the meson mass and coupling constant give results which are in disagreement with experiment, both in the charged and in the symmetrical theory. Whether the difficulty here lies in the model (pseudoscalar mesons with a pseudovector type of coupling) or in the use of perturbation theory can only be decided by an exact calculation with this model. Table I shows the results which should be compared with

TABLE I. Values of μ_N and μ_P.

Meson mass	Neutral theory	Charged theory	Symmetrical theory
325, electron masses	$\mu_N=0$ $\mu_P=-2.8$	$\mu_N=-8.0$ $\mu_P=2.5$	$\mu_N=-8.0$ $\mu_P=-0.3$
200, electron masses	$\mu_N=0$ $\mu_P=-2.8$	$\mu_N=-9.3$ $\mu_P=3.6$	$\mu_N=-9.3$ $\mu_P=0.8$

the experimental values $\mu_N = -1.91$, $\mu_P = 1.79$. It is obvious that the ratio μ_N/μ_P is also wrong in all theories.

Similar calculations have been carried out by the author for pseudoscalar mesons with pseudoscalar coupling $(\psi\beta\gamma_\nu\phi\psi)$, and by F. Villars[4] for vector mesons. The former case yields results identical to those above, while the latter yields divergent ones.

The details of the calculation and a complete discussion of the results will be published soon.

I should like to thank Dr. F. Villars for suggesting this problem and for much help in its solution, and also Professor W. Pauli and Dr. Res Jost for many stimulating conversations.

* National Research Fellow.
[1] J. M. Luttinger, Phys. Rev. **74**, 893 (1948).
[2] N. Kemmer, Proc. Roy. Soc. **166**, 127 (1938). We use units with $\hbar = c = 1$.
[3] F. Villars, Helv. Phys. Acta **XX**, 476 (1947).
[4] F. Villars, private communication.

Interpretation of Dependence of Resistivity of Germanium on Electric Field

E. J. Ryder and W. Shockley
Bell Telephone Laboratories, Murray Hill, New Jersey
December 1, 1948

IT has been observed by Bray[1] that there is a pronounced decrease in the resistance of samples of high back voltage germanium under high field strength pulse conditions. This has been interpreted as a bulk effect arising in the interior of this sample. The experiment described in this letter shows that in the sample studied there was no appreciable bulk effect even at fields much higher than usually reported, but that pronounced lowering of resistance can result from transistor action[2] i.e., the injection of holes into the *N*-type material from a metal contact.

The experimental arrangement was that shown in Fig. 1. The sample consists of a wedge-shaped block about 0.05 cm thick, 0.7 cm long, 0.35 and 0.05 cm wide at the base and apex, respectively. Rhodium-plated electrodes with soldered wire connections were made at the ends. The resistivity and resistance were 1 ohm-cm and 120 ohms. Voltage pulses with amplitudes up to 540 volts in both polarities were applied to this sample. This gave rise to field strengths of at least 6000 volts per centimeter at the narrow end. These field strengths are at least 10 times larger than those required to produce a lowering of resistance by 50 percent in the Bray effect in ordinary samples. However, as is indicated in the diagram, when the narrow end was negative there was no appreciable increase in current during the pulse and the resistance remained substantially constant, the value being the same as that measured under d.c. conditions at low voltages where the unit was substantially non-rectifying. Thus this experiment shows that a high field alone in the germanium is not sufficient to result in a modulation of its resistance. However, when terminal number 1 was made positive, an increase in conductance of about 40 percent was found. The interpretation of these experiments is as follows: In the case where electrode 1 is made positive, holes enter the germanium where the field strength is high, and are thus drawn through it before they recombine, and in this way produce an appreciable modulation of its resistivity in the narrow region where the important part of the resistance of the specimen arises. When terminal 1 is negative, no holes enter from it and holes injected from terminal 2 are spread over a wide area where their concentration is so small as to produce an inappreciable lowering of resistance.

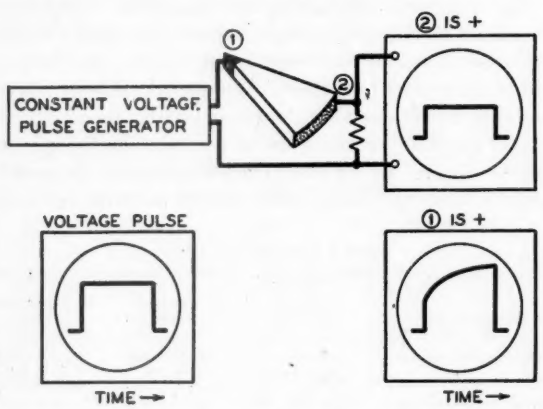

FIG. 1. Schematic diagram of experimental arrangement and wave shape of voltage and current pulses.

We are indebted to J. R. Haynes for a stimulating suggestion which led to this form of the experiment.

[1] Ralph Bray, K. Lark-Horowitz, and R. N. Smith, Phys. Rev. **72**, 530 (1947); Ralph Bray, Phys. Rev. **74**, 1218 (1948).
[2] J. Bardeen and W. H. Brattain, Phys. Rev. **74**, 230, 231 (1948).

Influence of Order on the Saturation Magnetic Moment

J. E. Goldman
Westinghouse Research Laboratories, East Pittsburgh, Pennsylvania
and
R. Smoluchowski
Carnegie Institute of Technology, Pittsburgh, Pennsylvania
December 7, 1948

IN a previous paper[1] the authors reported the influence of ordering on magnestostriction of Fe-Co alloys. From the theory which explained satisfactorily these results it followed that the saturation moment of the ordered alloy should be about 4 percent higher than in the random alloy. This was based upon the assumption that the local magnetic moments are determined by the average electron density of a pair of neighbors, and the resulting magnetic moment is that obtained from the so-called Pauling curve. This theoretical result now has been confirmed experimentally.

Measurements of the saturation moment of pure, cold-worked, quenched, and annealed Fe-Co alloys at the 50:50 atomic composition were made to a high degree of accuracy. Two identical coils of 500 turns each were connected in

series opposition and placed in the uniform field of the Westinghouse electromagnet. These were connected to a ballistic galvanometer which was calibrated against a standard mutual induction. Saturation flux density was measured by placing the sample in one of the coils and noting the deflection of the galvanometer when the field was reversed. Measurements were made at fields up to 12,500 oersteds to assure that the samples were saturated. The results are shown below:

	Saturation moments in Bohr magnetons per atom	
	Theoretical	Observed
Disordered	2.27	2.25
Ordered	2.37	2.35

The authors wish to thank Mr. R. W. Ure, Jr., for assistance in the measurements.

[1] J. E. Goldman and R. Smoluchowski, Phys. Rev. **75**, 140 (1949).

Multiple Scattering with Energy Loss

LESLIE L. FOLDY*
University of Rochester, Rochester, New York
December 6, 1948

RECENTLY, the scattering of particle tracks in photographic emulsions has been applied to the determination of the mass of π- and μ-mesons.[1] For heavier particles the scattering is so small that measurements must be made over ranges where the energy loss of the particle due to ionization cannot be ignored. It is therefore useful to have formulas for the mean-square projected scattering angle and the mean-square projected transverse displacement for a particle which has traversed a thickness t of material with due account taken of the energy loss by ionization over this thickness. A calculation of these quantities was made by the author and was to be submitted for publication, but the same results obtained by L. Eyges by the same method recently appeared in a Letter to the Editor.[2] We would, however, like to append to the above results a reformulation of the equations which is better suited to their application to particle mass determinations, together with some numerical calculations for Ilford C_2 emulsions.

For the purpose of determining the mass of a particle from the curvature of its track it is convenient to use as coordinate along the track, the residual range of the particle rather than the thickness of material traversed, since the energy of the particle at any point along the track is determined by its charge, mass, and residual range.

For the determination of the scattering from a residual range R_0 to a residual range R, we therefore write $t=R_0-R$. The mean-square projected scattering angle per unit length, g ($=2/W^2$ in Eyges' notation), will now be a function only of the residual range, the mass and charge of the particle, and the composition of the material through which the particle is passing. For a given material the energy of a particle of mass m and charge + or − Ze at the residual range R may be written

$$E(R)=(m/M)\mathcal{E}[(Z^2M/n)R],$$

where M is some unit of mass (which we take for convenience to be the proton mass), and $\mathcal{E}$ is a function which depends only on the composition of the material through which the particle passes. To a sufficiently good approximation for our purposes, the mean-square scattering angle for a given material may be taken to vary as the square of the charges, and indirectly, as the square of the energy of the particle. Hence we may write

$$g(R)=(Z^2M^2/m^2)G[(Z^2M/m)R],$$

where G again is a function whose form depends only on the material traversed. Let

$$M_n(t)=\int_0^t \frac{2t^n}{W^2(t)}dt=\int_0^t g(t)t^n dt=\int_{R_0}^R g(R)(R_0-R)^n dR$$
$$=\int_{R_0}^R \frac{Z^2M^2}{m^2}G\left(\frac{Z^2M}{m}R\right)(R_0-R)^n dR$$
$$=Z^{-2n}\left(\frac{M}{m}\right)^{1-n}\int_{\rho_0}^{\rho} G(\rho)(\rho_0-\rho)^n d\rho,$$

where $\rho_0=(Z^2M/m)R_0$ and $\rho=(Z^2M/m)R$, and let

$$N_n(\rho)=\int G(\rho)\rho^n d\rho.$$

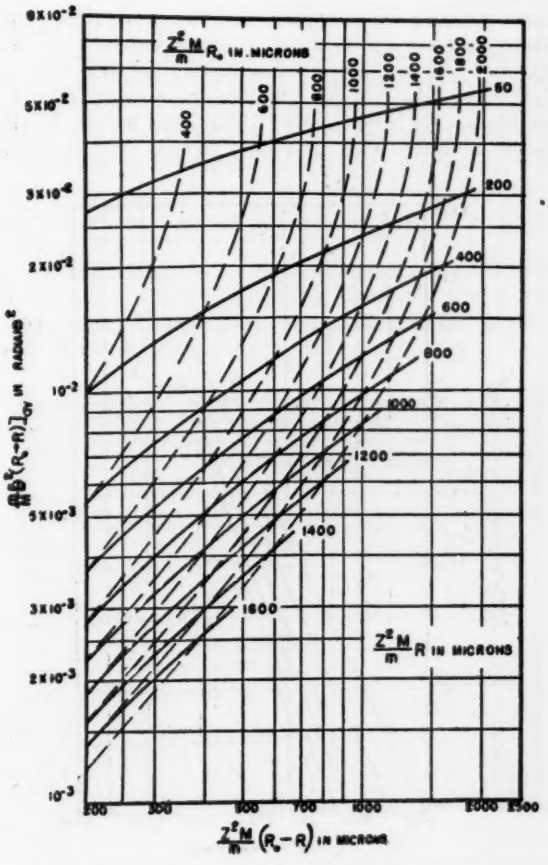

FIG. 1. Mean-square projected angle of scattering, $\langle\theta^2(R_0\to R)\rangle_{Av}$, for a particle of charge + or −Ze and mass m in traveling from a residual range R_0 to a residual range R in Ilford C_2 emulsion (M = proton mass).

The functions $N_n(\rho)$ then depend only on the properties of the material traversed and not on the properties of the particle traversing the material. The functions $A_0(t)$, $A_1(t)$, $A_2(t)$, introduced by Eyges are related to our M_0, M_1, M_2 by

$$A_0(t)=2M_0(t),$$
$$A_1(t)=2[tM_0(t)-M_1(t)],$$
$$A_2(t)=2[t^2M_0(t)-2tM_1(t)+M_2(t)].$$

The mean-square projected scattering angle from R_0 to R is given by

$$\langle\vartheta^2(R_0\rightarrow R)\rangle_{Av}=\tfrac{1}{2}A_0(t)=(M/m)[N_0(\rho)-N_0(\rho_0)],$$

and the mean-square transverse displacement from R_0 to R is given by

$$\langle y^2(R_0\rightarrow R)\rangle_{Av}=\tfrac{1}{2}A_2(t)=t^2M_0(t)-2tM_1(t)+M_2(t)$$
$$=(m/Z^4M)[\rho^2\{N_0(\rho)-N_0(\rho_0)\}-2p\{N_1(\rho)-N_1(\rho_0)\}+\{N_2(\rho)-N_2(\rho_0)\}].$$

Consequently,

$$(m/M)\langle\vartheta^2(R_0\rightarrow R)\rangle_{Av}\quad\text{and}\quad(Z^4M/m)\langle y^2(R_0\rightarrow R)\rangle_{Av}$$

are functions only of $\rho_0=(Z^2M/m)R_0$ and $\rho=(Z^2M/m)R$ for a given material within the limits of the approximation made above.

In many cases $G(\rho)$ can be represented fairly well for a given material by an equation of the form $G(\rho)=A\rho^n$ where A and n are constants of the materials. Then N_0, N_1, and N_2 are given, respectively, by $A\rho^{n+1}/n+1$, $A\rho^{n+2}/n+2$, $A\rho^{n+3}/n+3$. Thus, in the case of Ilford C_2 emulsions, $G(\rho)$ is represented within a few percent by the above formula with $A=2.93\times10^{-2}n=-1.128$, with M=proton mass and length measured in microns.[3] In Figs. 1 and 2 are plotted $(m/M)\langle\vartheta^2(R_0\rightarrow R)\rangle_{Av}$ and $(Z^4M/m)\langle y^2(R_0\rightarrow R)\rangle_{Av}$ as functions of $\rho_0-\rho=(Z^2M/m)\times(R_0-R)$ for various values of ρ_0 and ρ. These curves should be useful in determining the mass of a particle from the curvature of tracks in an Ilford C_2 emulsion.

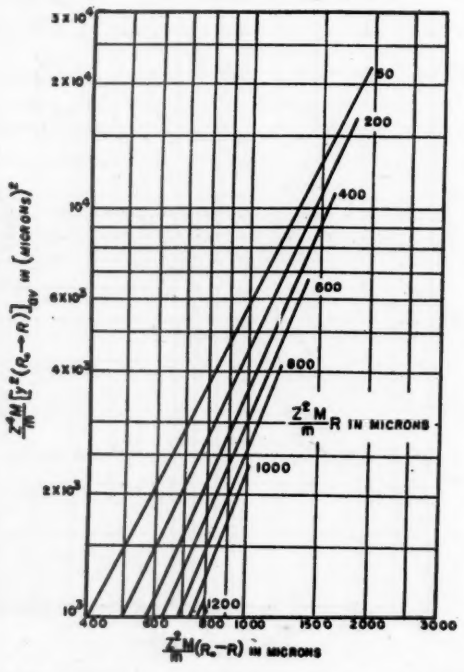

FIG. 2. Mean-square projected transverse displacement, $\langle y^2(R_0\rightarrow R)\rangle_{Av}$, for a particle of charge $+$ or $-Ze$ and mass m in traveling from a residual range R_0 to a residual range R in Ilford C_2 emulsion. (M=proton mass).

The aid of Mr. Albert Simon with the numerical calculations is gratefully acknowledged. This work was assisted by the Joint Program of the Office of Naval Research and the Atomic Energy Commission.

* On leave from Case Institute of Technology during the summer of 1948.

[1] S. Lattimore, Nature **161**, 518 (1948); V. Goldschmidt-Clermond, D. T. King, H. Muirhead, and D. M. Ritson, Proc. Phys. Soc. (London) **61**, 183 (1948).

[2] L. Eyges, Phys. Rev. **74**, 1534 (1948).

[3] These values were obtained by using the range-energy relation for Ilford C_2 emulsions and the formula

$$g(E)=(a/E^2)\ln(bEM)^{\frac{1}{2}}$$

with $a=2.48\times10^{-4}$ (Mev)^2/micron, $\ln b=16.58$ with b in (proton mass $\times$Mev)$^{-1}$, given by S. A. Gousmit and W. T. Scott (Phys. Rev. **74**, 1537 (1948)). The formula is applicable over the range from 200 to 2000 microns for protons.

On the Definition of the "Effective Range" of Nuclear Forces

F. C. BARKER AND R. E. PEIERLS
The University, Birmingham, England
December 6, 1948

IN his discussion of the neutron-proton force, Blatt[1] uses the effective range r_e defined by the equation

$$k\cot\delta=-a^{-1}+\tfrac{1}{2}r_ek^2 \tag{1}$$

where k is the wave vector, δ the phase for s-scattering, and a the "scattering radius." Terms proportional to k^4 are neglected.

It is the purpose of this note to point out that the effective range can be expressed by elementary means in terms of the wave function for zero energy.

We start from the well-known relation:[2]

$$\frac{d}{dk^2}\left(\frac{u'}{u_R}\right)=-\frac{1}{u(R)^2}\int_0^R u^2dr \tag{2}$$

where u and u' are the wave function and its derivative, and R is any radius. For sufficiently large distance

$$u=A\sin(kr+\delta) \tag{3}$$

and (2) becomes

$$\cot(kR+\delta)-k\csc^2(kR+\delta)[R+(d\delta/dk)]=-2kA^{-2}\csc^2(kR+\delta)\int_0^R u^2dr. \tag{4}$$

Choosing a value of R such that

$$kR+\delta=(n+\tfrac{1}{2})\pi \tag{5}$$

with integer n,

$$\frac{d\delta}{dk}=2A^{-2}\int_0^R u^2dr-R. \tag{6}$$

Using the identity

$$\int_0^R\sin^2(kr+\delta)dr=\tfrac{1}{2}R+(1/4k)\sin2\delta \tag{7}$$

which holds by virtue of (5), we have

$$\frac{d\delta}{dk}=2\int_0^R [A^{-2}u^2-\sin^2(kr+\delta)]dr+(1/2k)\sin 2\delta. \quad (8)$$

By making R tend to infinity, and some simple substitutions

$$2\frac{d}{dk^2}(k\cot\delta)=-2\csc^2\delta\int_0^\infty [A^{-2}u^2-\sin^2(kr+\delta)]dr. \quad (9)$$

According to (1) r_e is equal to (9) taken for $k=0$. For small k

$$\sin(kr+\delta)\sim\sin\delta(1+kr\cot\delta)=\sin\delta[1-(r/a)].$$

Choosing

$$A=\csc\delta, \quad (10)$$

we have finally

$$r_e=-2\int_0^\infty \{u^2(r)-[1-(r/a)]^2\}dr. \quad (11)$$

Here $u(r)$ is the zero-energy wave function, normalized according to (3) and (10) in such a way that the integrand of (11) vanishes at large distances.

[1] J. M. Blatt, Phys. Rev. **74**, 92 (1948), Eq. (1).
[2] H. A. Bethe and R. Peierls, Proc. Roy. Soc. **A149**, 176 (1935), Eq. (7).

Mass Spectrographic Assignment of Rubidium Isotopes*

FREDERICK L. REYNOLDS, D. G. KARRAKER, AND D. H. TEMPLETON
Radiation Laboratory and Department of Chemistry, University of California, Berkeley, California
December 2, 1948

WE have used a mass spectrograph to investigate rubidium isotopes produced by bombardment of bromine (ammonium bromide) with helium ions in the Berkeley 60-inch and 184-inch cyclotrons. The 60° deflection spectrograph is similar to that of Lewis and Hayden[1] but with larger dimensions and all-metal construction.[2]

In each bombardment with 20- to 100-Mev helium ions there was a good yield of rubidium activity with half-life about 6 hours. The rubidium activities were separated from the target material using 20–30 micrograms of inactive rubidium carrier and divided into two portions. One part was further purified and used for decay and absorption measurements. The other major portion was placed on the tungsten filament of the mass spectrograph as the nitrate or chloride. The Rb^+ ions produced by heating this filament were analyzed by the instrument and caught on a photographic plate. The mass scale was fixed by the lines of natural Rb^{85} and Rb^{87}. Lines at masses 81 and 82 were shown to be radioactive both by the photographic transfer technique (Fig. 1), and by counting with a Geiger counter provided with a narrow slit. The radioactivity of natural Rb^{87} is far too weak to interfere with these experiments. With 80-Mev helium ions, 5.0-hour Rb^{81} predominated in the mixture, and with 20-Mev helium ions almost pure 6.3-hour Rb^{82} was obtained. Otherwise, the similar half-lives would have made characterization of the radiations, which are listed in Table I, very difficult. The signs of the particles were determined with a crude 180° deflection beta-spectrograph. The energies listed in Table I were obtained with this instrument or from absorption measurements with aluminum, beryllium, or lead, as indicated.

TABLE I. Radiations from rubidium isotopes.

Isotope	Half-life	Radiations	Produced by
Rb^{81}	5.0 hours	β^+ 0.9 Mev (abs. Al) e^- 0.2 Mev (spect.) γ 0.8 Mev (abs. Pb) K x-rays (abs. Al, Be)	Br-α-2n Br-α-4n
Rb^{82}	6.3 hours	β^+ 0.9 Mev (abs. Al) γ 1.0 Mev (abs. Pb) K x-rays (abs. Al, Be)	Br-α-n Br-α-3n

There are approximately equal numbers of positrons and conversion electrons from Rb^{81}. There are several x-rays and gamma-rays per positron, so that the decay is 60 to 80 percent by electron capture. The possibility of a short-lived krypton daughter complicates the interpretation of these radiations. For Rb^{82} the positron to conversion electron ratio is probably greater than five. Again, there are more x-rays and gamma-rays than positrons, corresponding to 80 to 90 percent electron capture.

The previously reported[3] 6.5-hour rubidium activity assigned to Rb^{84} was presumably Rb^{82}, or a mixture of Rb^{82} and Rb^{81}. No description of the radiations was reported.

Attempts to observe a krypton daughter of Rb^{81} have shown no positive results. This fact is consistent with the recent assignment of the 34-hour krypton (Kr^{79} or Kr^{81})[4] activity to Kr^{79} by Woodward, McCown, and Pool.[5] Our experiments were not very sensitive for radiations as weak as those reported for the 13-second and 55-second krypton activities,[4] and we can make no statement concerning them as daughters of Rb^{81}.

Experiments are under way to characterize some longer-lived activity due to Rb^{83} and Rb^{84} produced in these same bombardments. Barber[6] has reported a 40-day positron emitter which he attributed to Rb^{84}.

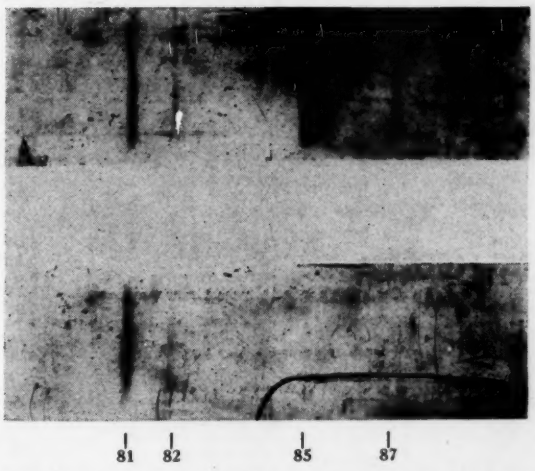

FIG. 1. The original plate shows natural Rb^{85} and Rb^{87} and radioactive Rb^{81} and Rb^{82}. The "transfer" plate is placed emulsion-to-emulsion with the original for several hours before either is developed, to locate radioactive material.

The cooperation of Mr. J. T. Vale, Mr. B. Rossi, and the crews of the 184-inch and 60-inch cyclotrons is gratefully acknowledged.

* This paper is based on work performed under the auspices of the Atomic Energy Commission.

[1] L. G. Lewis and R. J. Hayden, U. S. Atomic Energy Commission Report MDDC 1556, *A Mass Spectrograph for Radioactive Isotopes* (1947); R. J. Hayden, Phys. Rev. **74**, 650 (1948).

[2] We are greatly indebted to Dr. A. J. Dempster, Dr. M. G. Inghram, and Dr. R. J. Hayden for information and advice concerning their techniques and the design of this instrument.

[3] J. O. Hancock and J. C. Butler, Phys. Rev. **57**, 1088 (1940).

[4] G. T. Seaborg, Rev. Mod. Phys. **16**, 1 (1944).

[5] L. L. Woodward, D. A. McCown, and M. L. Pool, Phys. Rev. **74**, 761 (1948).

[6] W. C. Barber, Phys. Rev. **72**, 1156 (1947).

Three Additional Collateral Alpha-Decay Chains

W. W. MEINKE, A. GHIORSO, AND G. T. SEABORG
Department of Chemistry and Radiation Laboratory, University of California, Berkeley, California

December 2, 1948

CONTINUATION of investigations of the type which led to the observation of artificial radioactive chains collateral to the natural thorium and actinium families[1] have led to the identification of an additional collateral chain and partial identification of two others. In each case, after irradiation of thorium in the Berkeley 184-inch cyclotron the target was dissolved, and the first element in the series was isolated in an essentially weightless fraction. As before,[1] the decay and energy of the alpha-particles were measured with standard alpha-particle counting devices and an alpha-particle pulse analyzer[2] equipped with a fast sample-changing mechanism and identification of members of one of the series (the first to be mentioned) was aided by successive recoil collections.

TABLE I. Measured half-lives and energies.

Isotope	Type of radiation	Half-life	Energy of radiation (Mev)
$_{92}U^{229}$	α	58±3 min.	6.42
$_{90}Th^{225}$	α	7.8±0.3 min.	6.57
$_{88}Ra^{221}$	α	31±1.5 sec.	6.71
$_{86}Em^{217}$	α	$\sim 10^{-3}$ sec.	7.74
$_{84}Po^{213}$	α	4.2×10^{-6} sec.	8.34
$_{82}Pb^{209}$	β^-	3.32 hr.	0.70
$_{83}Bi^{209}$	Stable		
$_{92}U^{228}$	α	9.3±0.5 min.	6.72
$_{90}Th^{224}$	α	(~1 sec., predicted)	7.20
$_{88}Ra^{220}$	α	($\sim 10^{-2}$ sec., predicted)	7.49
$_{86}Em^{216}$	α	($\sim 10^{-6}$ sec., predicted)	8.07
$_{84}Po^{212}$(ThC′)	α	3×10^{-7} sec.	8.78
$_{82}Pb^{208}$	Stable		
$_{91}Pa^{226}$	α	1.70±0.15 min.	6.81
$_{89}Ac^{222}$	α	(~10 sec., predicted)	6.96
$_{87}Fr^{218}$	α	($\sim 10^{-2}$ sec., predicted)	7.85
$_{85}At^{214}$	α	($\sim 10^{-6}$ sec., predicted)	8.78
$_{83}Bi^{210}$(RaE)	β^-	5.0 days	1.17
$_{84}Po^{210}$	α	140 days	5.30
$_{82}Pb^{206}$	Stable		
$_{91}Pa^{225}$	α	22±1 hr.	6.09
$_{89}Ac^{224}$	α	2.9±0.2 hr.	6.17
$_{87}Fr^{220}$	α	27.5±1.5 sec.	6.69
$_{85}At^{216}$	α	$\sim 3\times10^{-4}$ sec.	7.79
$_{83}Bi^{212}$(ThC)	α(34%)	60.5 min.	6.05
	β^-(66%)		2.20
$_{81}Tl^{208}$(ThC″)	β^-	3.1 min.	1.82
$_{84}Po^{212}$(ThC′)	α	3×10^{-7} sec.	8.78
$_{82}Pb^{208}$	Stable		
$_{91}Pa^{227}$	α	38±1 min.	6.46
$_{89}Ac^{223}$	α	2.2±0.1 min.	6.64
$_{87}Fr^{219}$	α	~0.02 sec.	7.30
$_{85}At^{215}$	α	$\sim 10^{-4}$ sec.	8.00
$_{83}Bi^{211}$(AcC)	α(99.7%)	2.16 min.	6.62
	β^-(0.3%)		
$_{81}Tl^{207}$(AcC″)	β^-	4.76 min.	1.47
$_{82}Pb^{207}$	Stable		

The irradiation of thorium with 100-Mev helium ions resulted in the observation of the following collateral branch of the artificial $4n+1$, neptunium, radioactive family[3-5] shown with Po^{213} and its decay products:

$$_{92}U^{229}\xrightarrow{\alpha}{}_{90}Th^{225}\xrightarrow{\alpha}{}_{88}Ra^{221}\xrightarrow{\alpha}{}_{86}Em^{217}\xrightarrow{\alpha}{}_{84}Po^{213}\xrightarrow{\alpha}{}_{82}Pb^{209}\xrightarrow{\beta^-}{}_{83}Bi^{209}\text{ (stable).}$$

The mass type was identified by observation of the characteristic energy of the Po^{213} alpha-particles as well as the growth of 1.5-day Pa^{229} as the electron-capture branching decay product of U^{229} (ratio $K/\alpha=\sim5$) and the growth of 10.0-day Ac^{225} as the electron-capture decay product of Th^{225} (ratio $K/\alpha=\sim0.1$). The measured half-lives and energies for the members of this series are summarized in Table I.

Immediately after 120-Mev helium ion bombardment of thorium the uranium fraction contains another series of five alpha-emitters, which is apparently a collateral branch of the $4n$ family:

$$_{92}U^{228}\xrightarrow{\alpha}{}_{90}Th^{224}\xrightarrow{\alpha}{}_{88}Ra^{220}\xrightarrow{\alpha}{}_{86}Em^{216}\xrightarrow{\alpha}{}_{84}Po^{212}(\text{ThC}')\xrightarrow{\alpha}{}_{82}Pb^{208}\text{ (stable).}$$

The 9.3-minute half-life of U^{228} controls the decay rate of the series, with the half-lives of all the other members too short for them to be isolated and separately studied in our experiments. The mass type was identified by observation of the characteristic energy of the Po^{212}(ThC′) alpha-particles and the growth of 22-hour Pa^{228} as an electron-capture branching decay product of U^{228} (ratio $K/\alpha=\sim0.25$).

Similarly the protactinium fraction of 150-Mev deuteron-bombarded thorium shows a series of alpha-particle emitters whose rate of decay is controlled by the 1.7-minute half-life of the parent with the subsequent members all too short-lived to be isolated and separately studied. Although the mass type has not yet been identified through known daughters as above, general considerations with regard to the method of formation and half-life of the parent substance, and the energies of all the members of the series suggest a collateral branch of the $4n+2$ family:

$$_{91}Pa^{226}\xrightarrow{\alpha}{}_{89}Ac^{222}\xrightarrow{\alpha}{}_{87}Fr^{218}\xrightarrow{\alpha}{}_{85}At^{214}\xrightarrow{\alpha}{}_{83}Bi^{210}(\text{RaE}).$$

The measured alpha-particle energies of the individual members of the U^{228} and Pa^{226} series, assigned according to alpha-decay systematics in this region,[6] are shown in Table I. Also included for those members where the half-lives have not been measured are values predicted according to recent correlations between alpha-particle energies and corresponding half-lives.[7] Table I also contains

our latest half-lives and energies for the members of the previously reported[1] Pa^{227} and Pa^{228} collateral chains. The radioactive properties of ThC, RaE, AcC, Po^{213}, and daughters are the accepted values taken from the literature.[8]

The cooperation of Professor R. L. Thornton, Mr. J. T. Vale, and the 184-inch cyclotron group is gratefully acknowledged. This paper is based on work performed under the auspices of the Atomic Energy Commission.

[1] A. Ghiorso, W. W. Meinke, and G. T. Seaborg, Phys. Rev. **74**, 695 (1948).
[2] See Ghiorso, Jaffey, Fobinson, and Weissbourd, "An alpha pulse analyzer apparatus," Plutonium Project Record **14B**, 17.3 (1948), to be issued.
[3] English, Cranshaw, Demers, Harvey, Hincks, Jelley, and May, Phys. Rev. **72**, 253 (1947).
[4] Hagemann, Katzin, Studier, Ghiorso, and Seaborg, Phys. Rev. **72**, 252 (1947).
[5] G. T. Seaborg, Chem. Eng. News **26**, 1902 (1948).
[6] I. Perlman, A. Ghiorso, and G. T. Seaborg, Phys. Rev. **74**, 1730 (1948).
[7] I. Perlman, A. Ghiorso, and G. T. Seaborg, unpublished work.
[8] G. T. Seaborg and I. Perlman, Rev. Mod. Phys. **20**, 585 (1948).

Correction and Addendum: Scattering of Particles by the Gas in a Synchrotron*

[Phys. Rev. **74**, 140 (1948)]

NELSON M. BLACHMAN AND ERNEST D. COURANT
Brookhaven National Laboratory, Upton, Long Island, New York

CORRECTION: The formula for P in the title of Fig. 1 should read like the right side of Eq. (18).

For the word "half" in the title of Table I, read "10 percent of."

For b in the second-last line of page 143, read B.

For $-A$ in Eq. (18) read 0.

For $\frac{1}{2}\pi$ at the end of the fourth-last paragraph of the article, read $1/2\pi$.

More accurate calculations show that for a 10 percent loss of particles, $\eta=0.0855$ rather than 0.089.

Addendum: This note considers the effect of an initial betatron oscillation on the probability of surviving scattering of a particle being accelerated in a synchrotron or betatron. Let β be the amplitude of this initial oscillation. With appropriate choice of $t=0$, this oscillation contributes to both sine and cosine oscillations the amplitude $\beta/2^{\frac{1}{2}}$. Thus, $(1/2)\beta^2$ should be added to the right sides of Eqs. (7) and (8), and $(1/2)\beta^2(T_i/T_f)^{\frac{1}{2}}$ to the right side of (10). The maximum value of $\eta=\langle b^2\rangle/2A^2$ now occurs when

$$T/T_1=4/(1+\beta^2/2A^2\eta_0)^2,$$

in which η_0 is the maximum value η would have if $\beta=0$; it is

$$\eta=(\eta_0+\beta^2/16A^2)^2/\eta_0 \approx\eta_0+\beta^2/8A^2$$

for small β/A.

For example, for 10 percent loss, $\eta_0=0.086$. If $\beta=2.5$ cm and $A=8$ cm, then $\eta=0.0982$. The higher loss can be read from Fig. 1—14.5 percent—or compensated for by a reduction in pressure of $\beta^2/8A^2\eta_0=14$ percent.

This calculation underestimates the loss by tacitly assuming not that the initial amplitude is β, but that the initial amplitudes obey a Rayleigh distribution with β the r.m.s. initial amplitude. It overstimates the loss by including that (small) loss which would have occurred while the amplitude of betatron oscillation was building up to initial value.

Another approach eliminates both of these errors but is unable to take account of the damping of the initial oscillation, thus overestimating the loss. This is to use the solution of (17) satisfying the boundary condition

$$p(0, B)=\delta(B-\beta) \text{ for } 0\leq B\leq A$$

rather than $\delta(B)$. This solution is

$$p=(2B/A^2)\sum_{s=1}^{\infty} J_0(\lambda_s\beta/A)[J_1(\lambda_s)]^{-2} \times J_0(\lambda_s B/A)\exp(-\lambda_s^2\xi/A^2),$$

whence

$$P(\xi)=\int_0^A p\,dB=2\sum_{s=1}^{\infty} J_0(\lambda_s\beta/A)\exp(-\lambda_s^2\xi/A^2)/\lambda_s J_1(\lambda_s),$$

with $\xi=(1/2)\langle b^2\rangle$.

For $\eta=\xi/A^2=0.086$, $\beta/A=0.3125$, as before, this gives $P=18.9$ percent. For $\eta_0\geq 0.3$, only one term of this series is significant, and it is seen that the number of protons surviving with $\beta=\beta$ is $J_0(\lambda_1\beta/A)$ times the number with $\beta=0$ ($\lambda_1=2.4048$, the first root of J_0); for $B/A=0.3125$ this ratio is 86.4 percent.

* Work done under the auspices of the Atomic Energy Commission.

The Beta-Ray Spectra of Cu^{64}

C. S. WU AND R. D. ALBERT
Columbia University, New York, New York
December 6, 1948

RADIOACTIVE Cu decays either by positron- or negatron-emission to Ni or Zn with a half-life of 12.8 hours. In 1945 Backus[1] reported disagreement between the observed ratio of the number of positrons to the number of

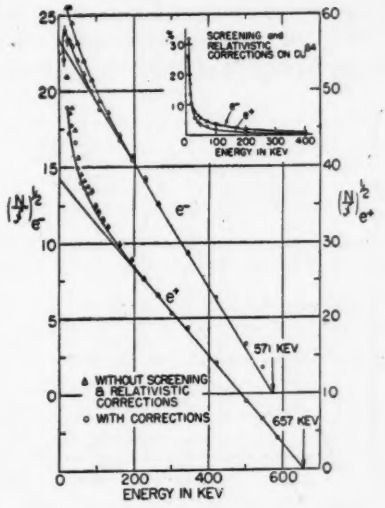

FIG. 1. Fermi plots of Cu^{64} negatron and positron spectra.

electrons in the region below 50 kev as compared to that predicted by the Fermi theory of beta-disintegration. Recently, Cook and Langer[2] investigated both the positron and negatron spectra from Cu^{64} over the entire energy region and found that both negatrons and positrons at low energies are too numerous to be accounted for by theory. Since the technical difficulties involved in the study of the beta-ray spectrum at very low energy are considerable, it is desirable to know how far the remaining discrepancies between experiment and theory at low energy can be reduced by improving experimental technique and employing a more rigorous Coulomb correction factor in interpreting the data.

The Columbia University solenoid β-ray spectrometer[3,4] was used in this investigation. In order to distinguish between electrons and positrons, a simple modified baffle system has been used and is found to transmit particles of one sign only, introducing no detectable scattering. The axis of the spectrometer is at least six feet away from any walls and is orientated along the earth's magnetic meridian. The vertical component of the earth's magnetic field is compensated by means of a pair of Thomson coils.

The radioactive Cu^{64} was prepared by intense deuteron bombardment of copper in the Columbia cyclotron. In carrying out the chemical purification and preparation, precautions for yielding high specific activity were particularly stressed. In the first few preliminary runs, the source was prepared by direct deposition of a drop of $CuSO_4$ solution on a collodion film. The deposit tends to crystallize at the edge of the drop and, therefore, forms a non-uniform source.

A more uniform source can be obtained by adding a trace of detergent to the $CuSO_4$ solution or from a colloidal suspension of $Cu(OH)_2$. The source backings used throughout this investigation were thin collodion film of about $4\mu g/cm^2$. The counter window consisted of 5 or 6 layers of collodion film of 3–$4\mu g/cm^2$ each. Auxiliary experiments showed that this counter window should have negligible effects on the electron distribution above 20 kev.

Several runs with sources varying from 0.3 mg/cm² to ~0.1 mg/cm² showed a gradual but consistent reduction of deviation *versus* the source thickness at low energy region. Therefore, the importance of preparing extremely thin and uniform sources can never be over emphasized. With the thinnest source (~0.1 mg/cm²) prepared with the present facilities, the deviation was found to be much less than previously reported.

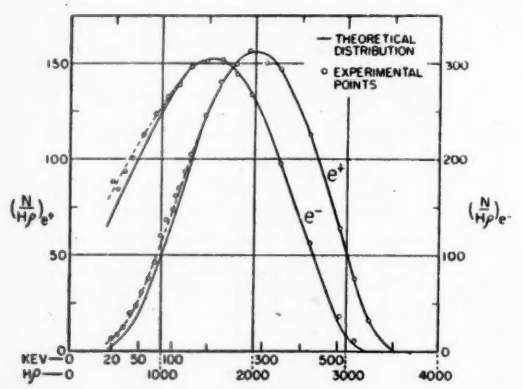

FIG. 2. Momentum spectra of Cu^{64} negatrons and positrons.

In comparing the experimental data with the Fermi theory, the Coulomb correction factor has been reexamined and modified. Longmire and Brown[5] recently calculated the screening effect due to atomic electrons and the relativistic effect (which has often been neglected for $Z<29$) for Cu^{64} electrons and positrons. These corrections are considerable for electrons of energies below 200 kev and for positrons of energies below 100 kev (Fig. 1). Applying these corrections, the observed electron distribution (Fig. 1) agrees with the theory from upper energy limit down to ~70 kev. At least part of the remaining discrepancy could very well be due to the finite thickness of the source. The deviation in the case of positron appears to start at a much higher energy ~200 kev (Fig. 1). If these deviations are due to the scattering of electrons or positrons into the low energy region, the effect would be much more pronounced in the case of positrons because there are so few positrons at low energies. This can better be illustrated by comparing the area under the momentum distribution curves (Fig. 2) where the difference between the experimental and theoretical distribution for both positrons and electrons is about 1-2 percent of the total emission, while the previous work[2] reported an excess of 9 percent for positrons and 6 percent for electrons.

In view of the large decrease in the deviation resulting from the use of thinner and more uniform sources and the use of a more rigorous Coulomb correction factor, it seems probable that the remaining small observed deviation is instrumental and the Cu^{64} spectra are actually of the allowed type.

We wish to thank Professors W. W. Havens, Jr., L. J. Rainwater, and J. R. Dunning for their constant interest and valuable discussions. This document is based on work performed under Contract AT-30-1-Gen 72 with the Atomic Energy Commission and Columbia University.

[1] J. Backus, Phys. Rev. **68**, 59 (1945).
[2] C. S. Cook and L. M. Langer, Phys. Rev. **73**, 601 (1948).
[3] C. M. Witcher, Phys. Rev. **60**, 32 (1941).
[4] C. S. Wu, W. W. Havens, Jr., R. Albert, and G. Grimm, Phys. Rev. **73**, 1259(A) (1948).
[5] C. Longmire and H. Brown, in press.

Additional Ferromagnetic Resonance Absorption Measuremets on Supermalloy

W. A. YAGER
Bell Telephone Laboratories, Murray Hill, New Jersey
November 24, 1948

THE results of a ferromagnetic resonance absorption experiment at 24,050 megacycles on a specimen of annealed Supermalloy were compared with theory[1] in a previous letter.[2] The λ in the relaxation term, $-\lambda[\mathbf{M}-\chi_0\mathbf{H}]$, was assumed constant in this analysis. It is now found that better agreement between theory and experiment is obtained by setting $\lambda \alpha H_s$. Furthermore,

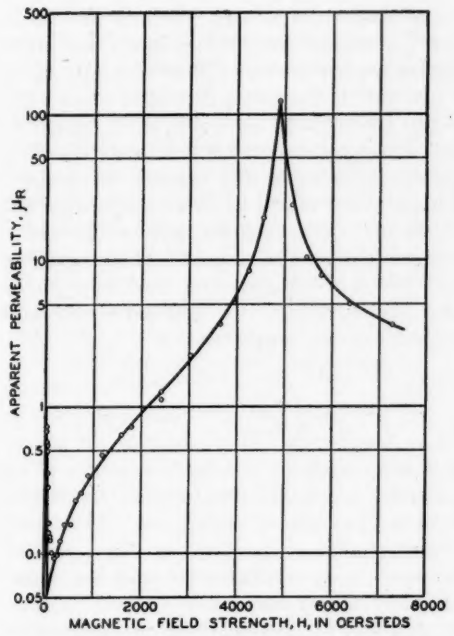

FIG. 1. Ferromagnetic resonance absorption in annealed Supermalloy at 23,900 Mc.

recent and more accurate measurements on Supermalloy[3] disclose a minimum in the μ_R *vs.* H curve at low field strengths, and also confirm the value of $g=2.17$, previously reported.

The test procedure differed but little from that previously described except that the resonant cavity was redesigned to improve the accuracy of the measurements. The test specimen formed the end wall instead of the narrow side walls of the cavity, and was clamped in place to avoid the undesirable soldering operation. Further improvement in accuracy was obtained by adjusting the opening of the symmetrical coupling window. A miniature motor-generator set indicated the static magnetic field strength; the reference magnet for calibrating this device was checked by the Bureau of Standards.

The results of the new measurements are compared with theory in Fig. 1, in which the points represent the experimental data, and the curve shows the theoretical variation with $\lambda/H=2.28\times10^5$ rad./sec.-oersteds. The plotted field values have been corrected for the demagnetizing field of 60 oersteds. The agreement between theory and experiment is very good over the entire range investigated except that the experimental data tend to round off the sharp minimum. The g factor is again found to be 2.17, in agreement with the value previously reported.

These measurements establish the existence of a minimum as well as a maximum in the μ_R *vs.* H curve; this behavior is consistent with theory. The energy dissipation in the ferromagnetic material is proportional to:

$$\mu_R{}^{\frac{1}{2}}=[(\mu_1{}^2+\mu_2{}^2)^{\frac{1}{2}}+\mu_2]^{\frac{1}{2}}.$$

μ_1 and μ_2 are the real and imaginary parts of the r-f permeability. For small damping, $\mu_2\ll1$ at low field strengths. Consequently, $\mu_R<1$ in the approximate range $\mu_1=1$ to $\mu_1=-1$ and will be a minimum when $\mu_1\to0$. In annealed Supermalloy (Fig. 1), $\mu_R<1$ at fields below 2000 oersteds, is a minimum in the neighborhood of 200 oersteds, and then increases rapidly toward one as $H\to0$. The resonance equations[1] show that μ_1 has two zero points—one at $\omega\cong\gamma B$ which corresponds to minimum absorption, the other at $\omega\cong\gamma(BH)^{\frac{1}{2}}$ which corresponds to maximum absorption. In principle, one can solve the two zero-point equations simultaneously for γ and $4\pi M_s$. This procedure is not very accurate for the case of Supermalloy since the minimum occurs undesirably close to the demagnetizing field. For the case of nickel, however, the minimum occurs at 1700 oersteds, and the value of $4\pi M_s$ calculated in this way is in good agreement with the accepted value.

In the region where $\mu_R<1$, the material is effectively diamagnetic with respect to the r-f magnetic field and the effective resistivity, $\rho\mu_R$, is less than the d.c. resistivity, ρ. It is, therefore, possible to reduce the effective resistivity of a ferromagnetic metal by the proper application of a relatively weak magnetic field. For the ideal case of no damping, the effective resistivity, the flux density, and the microwave attenuation all decrease to zero, and the skin depth becomes infinite at the minimum.

The effect of cold working a specimen of annealed Supermalloy is shown in Fig. 2; the resonance curve is

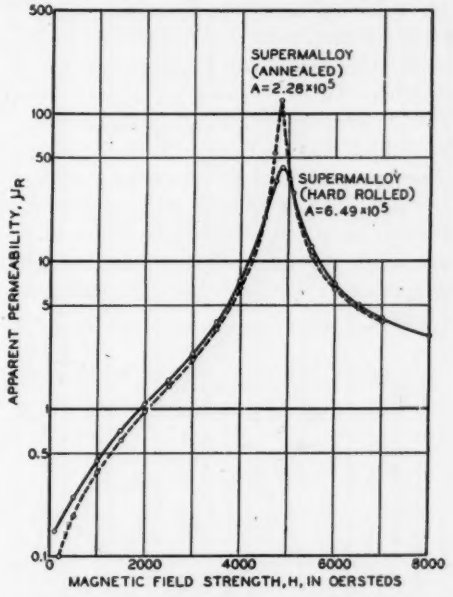

FIG. 2. The effect of hard rolling upon the ferromagnetic resonance absorption in Supermalloy at 23,900 Mc.

broadened ($\lambda/H=6.49\times10^5$ rad./sec.-oersteds) without noticeably altering the g factor when account is taken of the effect of magnetic crystalline anisotropy upon the resonance condition.

I am indebted to Dr. R. M. Bozorth of these Laboratories for his interest and helpful suggestions in connection with this investigation.

[1] C. Kittel, Phys. Rev. **71**, 270 (1947); **73**, 155 (1948).
[2] W. A. Yager and R. M. Bozorth, Phys. Rev. **72**, 80 (1947).
[3] W. A. Yager, Phys. Rev. **73**, 1247 (1948).

Ferromagnetic Resonance Absorption in Heusler Alloy

W. A. YAGER AND F. R. MERRITT
Bell Telephone Laboratories, Murray Hill, New Jersey
November 24, 1948

THE g factors calculated from ferromagnetic resonance absorption measurements at microwave frequencies on nickel,[1,2] iron,[1,2] cobalt,[1] Supermalloy,[3,4,8] and zinc-manganese ferrite,[5] using the expressions derived by Kittel,[6] are all significantly greater than the free spin value of 2.00, whereas the apparent g factor deduced from Barnett's[7] gyromagnetic ratio experiments are all significantly less than 2.00 with one exception, Heusler alloy (Mn−Cu−Al), for which the free spin value was obtained. The reality of this difference in g factor as determined by the two methods now seems well established on the basis of the normal field experiment on Supermalloy[8] and Hewitt's[5] measurements on a ferrite sphere. Both experiments demonstrate the correctness of Kittel's resonance formulas for the various test conditions and also the reality of the high g factors obtained in the microwave measurements.

The g factors deduced from a measurement of the Zeeman splitting, as in a microwave resonance experiment, is expected theoretically to be equal to the apparent g factor deduced from a gyromagnetic ratio experiment only if the spin-orbit system is acted on by central fields. In the presence of inhomogeneous crystalline electric fields, the equality no longer holds. This has been shown in the case of paramagnetic salts by Gorter and Kahn.[9] No detailed treatment of ferromagnetic substances has been given, although Polder[10] has made some pertinent observations.

It seemed probable that in a material such as Heusler alloy for which the apparent g factor from the gyromagnetic measurements is equal to 2.00, the g factor from microwave resonance absorption may also be equal to 2.00. This equality appears to be indicated by the measurements described below.

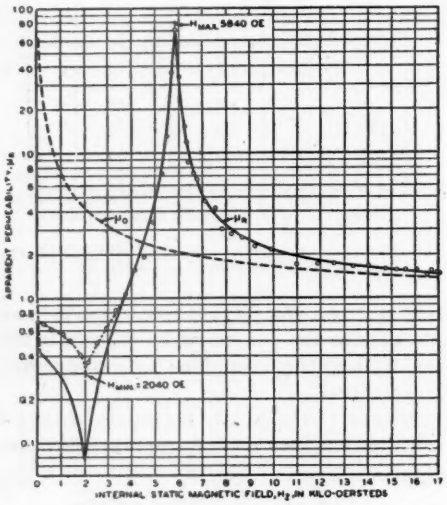

FIG. 1. Ferromagnetic resonance absorption in Heusler alloy at 23,900 Mc.

Test specimens 0.75 inch in diameter and of various thicknesses were machined from a cast ingot of Heusler alloy having the composition: 26 percent Mn, 61 percent Cu, 13 percent Al. They were then heat treated at 750°C in hydrogen for one hour, air cooled, and aged at 200°C for 48 hours. The resonant cavity[4] previously described was used in this experiment, the resonant frequency being 23,880 megacycles. Figure 1 shows the results obtained on a 0.040-inch thick specimen oriented parallel to the static magnetic field. The plotted field strength has been corrected for the demagnetizing field of $NB_s/4\pi=260$ oersteds. The equations[4] for maximum and minimum energy absorption are, respectively,[5]

$$\omega=\gamma[(H_{\max}+B_s)H_{\max}]^{\frac{1}{2}},$$
$$\omega=\gamma(H_{\min}+B_s),$$
$$\gamma=ge/2mc.$$

$B_s=4\pi M_s$ is the saturation induction and the H's are the internal static magnetic fields (applied $H-NB_s/4\pi$) for maximum and minimum absorption. The experimental values are: applied $H_{\max}=6100$ oersteds, applied $H_{\min}=2300$ oersteds, $\omega=15.006\times10^{10}$ rad./sec. and $N/2\pi=0.0405$. Solving the equations for g and B_s, we obtain: $g=2.01$, and $B_s=6425$. Similar measurements on a 0.020-inch specimen gave the following results: applied $H_{\max}=6050$ oersteds, applied $H_{\min}=2370$ oersteds, $\omega=15.01\times10^{10}$ rad./sec., $N/4\pi=0.0208$, $B_s=6250$, and $g=2.01$. Thus it is seen that the g factor of Heusler alloy has essentially the free spin value as determined by both the microwave resonance absorption and Barnett's experiments.

The points in Fig. 1 represent the experimental data, and the solid curve represents the theoretical variation with $\lambda/H=2.53\times10^5$ rad./sec.-oersteds. The agreement between theory and experiment is good except that the experimental data tend to round off the theoretical minimum. This same behavior has been observed in unpublished data for annealed nickel and to a much lesser extent in annealed Supermalloy.[4] The resonance in Heusler alloy is much sharper than that observed in nickel and iron and is comparable to that found in annealed Supermalloy.

We are indebted to Dr. C. Kittel and Dr. R. M. Bozorth of these Laboratories for their interest and helpful suggestions in connection with this investigation.

[1] J. H. E. Griffiths, Nature **158**, 670 (1946).
[2] W. A. Yager, paper in preparation.
[3] W. A. Yager and R. M. Bozorth, Phys. Rev. **72**, 80 (1947).
[4] W. A. Yager, Phys. Rev. **75**, 316 (1949).
[5] W. H. Hewitt, Jr., Phys. Rev. **73**, 1118 (1948).
[6] C. Kittel, Phys. Rev. **71**, 270 (1947); **73**, 155 (1948).
[7] S. J. Barnett, Proc. Am. Acad. Arts and Sci. **75**, 109 (1944); Phys. Rev. **66**, 224 (1944).
[8] C. Kittel, W. A. Yager, and F. R. Merrit, Amsterdam Conference on the Physics of Metals, 1948 (to appear in Physica).
[9] C. J. Gorter and B. Kahn, Physica **7**, 753 (1940).
[10] D. Polder, Phys. Rev. **73**, 1116 (1948).

Disintegration of Hg^{203}

HILDING SLÄTIS AND KAI SIEGBAHN
Nobel Institute for Physics, Stockholm, Sweden
November 30, 1948.

IN a recent letter D. Saxon[1] has given a report on some measurements on 43-days $Hg^{203,205}$. We have also

investigated this activity lately and though many of our final results agree with Saxon's, we believe that some of these ought to be discussed. First the mass assignment has now been definitely proved (in accordance with Inghram *et al.*[2]) to be 203 by magnetic isotope separation in this laboratory of the irradiated sample (from Oak Ridge). The activity was then actually depositing on the mass number 203 (paper in course of publication by our separation group in Arkiv. f. Mat., Astr. o. Fys.).

To get the upper limit for the continuous β-spectrum, which in this case is very soft and badly masked by strong internal conversion lines right at the upper limit, one has to base the Fermi analysis mainly on the softer part of the spectrum where on the other hand absorption is most pronounced.

This absorption does not only occur in the counter window but of course also in the source itself. In the case of Hg^{203} where the specific activity was not too good, this latter correction is hard to estimate. To get rid of this difficulty, we have determined the upper limit in another way so that the strong β-line is practically eliminated. Since the whole β-spectrum is followed by the γ-line one would expect the (β, γ) coincidence spectrum taken in the coincidence spectrometer[3] to give a distribution corresponding to the simple continuous β-spectrum *without* the β-line. One can then base the Fermi analysis on points which are nearer to the end point, where the absorption ought to be small. One could, however, also expect to get a very small coincidence effect due to the simultaneous

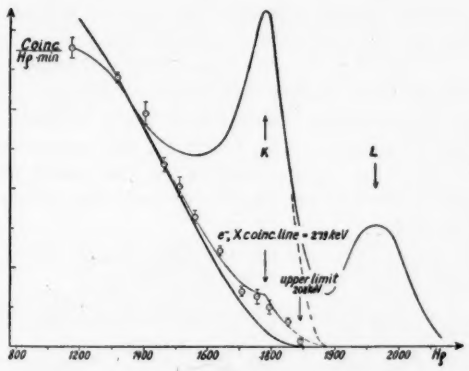

FIG. 1. β-spectrum of Hg^{203}. The thin curve through the measured points belong to the β-γ-coincidence spectrum. The strong curve represents the continuous β-spectrum, when the e^-, X coincidence line is eliminated by the method of least squares.

emission of internal conversion electrons focused in the spectrometer and x-rays emitted when the atomic shell is refilled. The efficiency of the γ-counter for this radiation ($EK_\alpha = 70$ kev) is fortunately very low in our arrangement, so that the e^-, X coincidence line would be small in intensity. The coincidence spectrum is shown in Fig. 1. As can be seen, the strong β-lines (K and L) have been replaced by the last part of the continuous spectrum on which a very small e^-, X coincidence line is superimposed. This effect can further easily be corrected for, using the method of least squares. Making the Fermi plot one arrives at a value of 208 kev for the upper limit of the β-spectrum, which is very nearly the same as that given by Saxon.

The γ-energy was also determined by a newly built large double focusing β-spectrometer with $\rho = 50$ cm (in course of publication). Figure 2 shows the internal con-

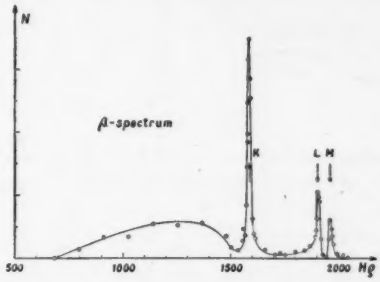

FIG. 2. β-spectrum of Hg^{203} obtained with the double focusing spectrometer with high resolving power.

version spectrum. The window was not very thin, which makes an analysis of the continuous spectrum difficult. To get the required resolution the sample furthermore had to be evaporated in a thin layer which limited the statistical accuracy of individual points. However, we were then able to resolve the L- and M-conversion electron lines completely. The intensity ratio between the K- and L-lines is in good agreement with Saxon's value, namely, equal to ~ 3. The ratio between the L- and M-lines, not resolved by Saxon but estimated to be ≥ 12, is however considerably smaller. The photoelectron spectrum was also investigated using a lead foil 3μ thick (Fig. 3). K-, L- and M-photo lines can be observed. The spectrograph was calibrated with the annihilation radiation and also with the ThB F-line (1383.8 H_ρ). The energy of the γ-line can be determined from both the three internal conversion lines and the three lead photo-lines. Since the evaporated sample could not be considered as infinitely thin, the correct calibration factor to be used in the case of the internal conversion measurement should be somewhere between the annihilation radiation factor and the ThB F-line factor.

The former factor gives too high values and the latter too low. The photoelectron spectrum should give correct results, provided one can extrapolate the factor obtained from the annihilation radiation at 511 kev with the 3-μ thick lead foil down to these lower energies. Table I shows the results. As can be seen, the agreement between the different values is quite close. As a mean value of the

TABLE I.

Line	Energy of γ-line in kev with ThB calibration	with annh. calibration
K-β-line	278	280
L-β-line	277	279
M-β-line	279	281
K-photo-line		279
L-photo-line		279
M-photo-line		278

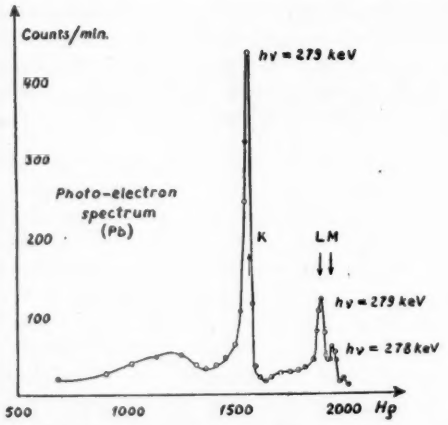

FIG. 3. Photoelectron spectrum from 3-μ Pb converter, released by the 279-kev Hg^{203} γ-ray.

γ-energy we can use $E_\gamma = 279 \pm 2$ kev. The corresponding value of Saxon is 286 ± 5 kev.

Another point of interest is that the 279-kev excited level in Ta^{203} can also be obtained in a different way. A. Lutz, M. Pool, and J. Kurbatov[4] when examining the β-radiation from 52-hour Pb (ascribed by them to Pb^{205}) found internal conversion lines corresponding to γ-rays of 270 and (possibly) 470 kev (explained as Compton electrons). Since the 270-kev radiation is very probably the same γ-line as our 279 kev, it is then almost certain that the 52-hour Pb has the mass 203 and decays by K-capture to Ta^{203} with emission of a γ-ray of 279 kev. A fuller description will appear in Arkiv. f. Mat., Astr. o. Fys.

[1] D. Saxon, Phys. Rev. **74**, 849 (1948).
[2] M. G. Inghram, D. C. Hess, Jr., and R. J. Hayden, Phys. Rev. **71**, 561 (1947).
[3] K. Siegbahn and A. Johansson, Arkiv. f. Mat., Astr. o. Fys. **34A**, No. 10 (1946).
[4] A. L. Lutz, M. L. Pool, and J. D. Kurbatov, Phys. Rev. **65**, 61 (1944).

Single Crystal Growth of Scheelite

S. ZERFOSS, L. R. JOHNSON, AND O. IMBER
Naval Research Laboratory, Washington, D. C.
November 29, 1948

SCHEELITE, $CaWO_4$, has been shown to be one of the most efficient crystals for gamma-ray counter applications.[1] For this purpose clear, transparent, single crystal material of reasonable size ($\sim$0.5 cc) is required. Since natural scheelite of sufficient purity and size is quite rare, it is necessary to resort to some laboratory growth technique.

Our experiments show that scheelite of sufficient purity and size can be grown by either of two techniques: (a) by flame fusion, the Vernueil process, and (b) from the melt by the gradient technique.

The flame fusion process, such as is used for production of synthetic sapphires, has been described elsewhere.[2] In this process the feed material is carried, as a fine powder, into one of the lines of an oxygen-hydrogen burner and caused to melt in the flame. The molten material is collected on a refractory support and is caused to grow into a single crystal by suitable manipulation of the flame, feed, etc. The conditions necessary to cause satisfactory growth unfortunately cannot be precisely stated and contain a large personal factor. Our burner was of standard design and consisted of two concentric cylindrical tubes, 25 mm and 2.5 mm I.D., respectively. The central tube extended to within 25 mm of the outer tube face. It was through this central tube, connected to an overhead hopper, that the powder (-200 mesh) was introduced into the flame. $CaWO_4$ of fluorescent grade, made either by sintering or precipitation, was first used as a feed material and yielded cloudy polycrystalline boules. We attribute this result to the WO_3 deficiency of the powder or to volatilization of WO_3 or to both of these factors. Clear boules were first obtained after 4–10 percent by weight of WO_3 (-200 mesh) was mechanically incorporated into the feed, thus reducing the loss of WO_3 during growth. Any excess was apparently volatilized although best results were obtained with 4 percent WO_3 addition. Considerable trouble was experienced with cracking of the boules during cooling. This cracking was reduced by the use of a smaller radiation space around the boule. Material of the size $4 \times 4 \times 4$ mm was obtained by this method.

Much larger and more satisfactory material was grown from the melt by the gradient technique. In this process a melt of the material in a cone-shaped crucible was slowly lowered through a temperature gradient.[3] Platinum crucibles, 18 or 31 mm in diameter with 60-degree cone tips, have been used in our work. The crucible, filled with the melt, was held in a platinum resistance furnace at 1625°C* and slowly lowered through the furnace gradient (an average of 59 degrees/cm for an elevator lowering of 125 cm) at a speed of 3.2 hours/cm. The raw material was fluorescent grade $CaWO_4$ without any addition.

We have obtained satisfactory single crystal boules yielding fragments $5 \times 5 \times 5$ mm by this process but as described above serious cracking of the boules was experienced unless it was allowed to cool quite slowly after solidification.

The fluorescent and counter behavior of scheelite by either technique was entirely satisfactory.

* The melting point of scheelite has not been reported in the literature. As determined by us it is 1576° ±5°C.
[1] Robert J. Moon, Phys. Rev. **73**, 1210 (1948).
[2] FIAT Final Report No. 655, 12/28/45, Bull. Acad. Sci. U.S.S.R. Physics Series No. 5–6, p. 505–8 (1946).
[3] Rev. Sci. Inst. **7**, 133 (1936); Phys. Rev. **36**, 1663 (1930); O. F. Tuttle and P. H. Egli, J. Chem. Phys. **14**, 571 (1946).

Nuclear Shell Structure and Isomerism*

EUGENE FEENBERG
Department of Physics, Washington University, St. Louis, Missouri
October 15, 1948

THE shell structures[1–4]

$(1s)^2$
$(1s)^2\,(2p)^6$
$(1s)^2\,(2p)^6\,(2s)^2$
$(1s)^2\,(2p)^6\,(2s)^2\,(3d)^{10}$
$(1s)^2\,(2p)^6\,(3d)^{10}\,(4f)^{14}\,(5g)^{18}$

are suggested by the fact that proton or neutron numbers 2, 8, 10, 20, and 50 are associated with particularly stable and abundant nuclear species. The $2s$ and $3p$ levels must be omitted to form the shell at 50, although the rectangular well potential would place both lower than $5g$.

The apparent upward drift of the $2s$ and $3p$ levels with increasing N and Z may be accepted as a working hypothesis and utilized in the interpretation of the spins, magnetic moments, quadrupole moments, radioactive transitions, and isomerism of nuclei containing one particle outside of closed shells or with one particle missing from a closed shell.[5]

A closed shell of 40 particles having the structure

$$(1s)^2\ (2p)^6\ (3d)^{10}\ (4f)^{14}\ (3p)^6\ (2s)^2$$

is suggested by the properties of odd nuclei, containing 37, 39, and 41 neutrons or protons. Accordingly, one infers that the $3p$ and $2s$ levels rise above $5g$ shortly after the closing of the "40" shell. If the spacing of $3p$, $2s$, and $5g$ levels is small at N or $Z=40$, the closed shell should not be marked by exceptional stability and, hence, should not be revealed by studies of stability and abundance. The evidence from isomerism for the proposed shell structure is summarized in Table I.

TABLE I. Correlation of isomerism with spin values predicted by the shell model.*

N or Z	Nucleus	Shell structure	Isomerism**	Spin: Shell model	Spin: Experimental**
37	$_{28}Ni^{65}$	$\langle 3p\rangle^{-1}$	no	$\langle 1/2, 3/2\rangle$	——
37	$_{30}Zn^{67}$	$\langle 3p\rangle^{-1}$	no	$\langle 1/2, 3/2\rangle$	5/2
37	$_{37}Rb^{85}$	$\langle 3p\rangle^{-1}$	no	$\langle 1/2, 3/2\rangle$	5/2
37, 50	$_{37}Rb^{87}$	$(3p)^{-1}$	no	1/2, 3/2	3/2
37	$_{37}Rb^{89,91,97}$	$\langle 3p\rangle^{-1}$	no	$\langle 1/2, 3/2\rangle$	——
39	$_{30}Zn^{69}$	$(2s)^{-1}$	yes	1/2	——
39	$_{32}Ge^{71}$	$(2s)^{-1}$	yes	1/2	——
39	$_{39}Y^{87}(B)$	$(2s)^{-1}$	yes	1/2	——
39, 50	$_{39}Y^{89}$	$(2s)^{-1}$	no	1/2	(1/2)
39	$_{39}Y^{91}(B)$	$(2s)^{-1}$	yes	1/2	——
39	$_{39}Y^{95,97}$	$(2s)^{-1}$	no	1/2	——
41	$_{32}Ge^{73}$	$(5g)'$	no	7/2, 9/2	——
41	$_{34}Se^{75}$	$(5g)'$	no	7/2, 9/2	——
41, 50	$_{41}Cb^{91}(B)$	$(5g)'$	no	7/2, 9/2	——
41	$_{41}Cb^{93}$	$(5g)'$	no	7/2, 9/2	9/2
41	$_{41}Cb^{95}(B)$	$(5g)'$	yes	7/2, 9/2	——
41	$_{41}Cb^{97}(B)$	$(5g)'$	no	7/2, 9/2	——
49	$_{34}Se^{83}$	$(5g)^{-1}$	yes	7/2, 9/2	——
49	$_{36}Kr^{85}$	$(5g)^{-1}$	yes	7/2, 9/2	——
49, 38	$_{38}Sr^{87}$	$(5g)^{-1}$	yes	7/2, 9/2	9/2
49, 40	$_{40}Zr^{89}$	$(5g)^{-1}$	yes	7/2, 9/2	——
49	$_{49}In^{111,117}$	$(5g)^{-1}$	no	7/2, 9/2	——
49	$_{49}In^{113}$	$(5g)^{-1}$	yes	7/2, 9/2	9/2
49	$_{49}In^{115}$	$(5g)^{-1}$	yes	7/2, 9/2	9/2
51	$_{36}Kr^{87}$	$(4d)'$	no	3/2, 5/2	——
51, 38	$_{38}Sr^{89}$	$(4d)'$	no	3/2, 5/2	——
51, 40	$_{40}Zr^{91}$	$(4d)'$	no	3/2, 5/2	——
51	$_{42}Mo^{93}(C)$	$(4d)'$	yes	3/2, 5/2	——
51	$_{51}Sb^{121}$	$(4d)'$	no	3/2, 5/2	5/2
51	$_{51}Sb^{123}$	$(4d)'$	no	3/2, 5/2	7/2
51	$_{51}Sb^{125}(B)$	$(4d)'$	no	3/2, 5/2	——
51	$_{51}Sb^{127,129}$	$(4d)'$	no	3/2, 5/2	——
51, 82	$_{51}Sb^{133}$	$(4d)'$	no	3/2, 5/2	——

* $\langle\ \rangle$—shell model unreliable; (1/2)—experimental determination uncertain; (B)—Z certain, N probable; (C)—Z certain, N limited to a few possibilities.

** Experimental information from charts by E. H. Segrè (revised April 1948) and G. Friedlander and M. L. Perlman (revised to April 1948).

TABLE II. Correlation of isomerism with odd N and Z in even-odd and odd-even nuclei.*

N or Z	Number of known stable and radioactive odd nuclei	Number of cases of isomerism
29	7–8	1(A), 1(B)
31, 33, 35, 37	22–26	0(?)
39	6	2(A), 2(B)
41	4–6	1(A)
43	3–5	3(A), 1(B)
45	3	2(A)
47	5	4(A)
49	9	6(A)
51, 53, 55, 57, 59, 61	37–47	0(?)
63	5–6	1(A)

* (A)—Z and N certain; (B)—Z certain; N probable.

The spin values listed in the table are based on the assumption that all the angular momentum is supplied by the odd particle or hole. Considering the evidence from isotopes and isotones differing by two mass units, one expects the assumption to hold in 4 out of 5 cases; in particular, it should hold when only one particle is missing from closed shells or when only one particle is present outside of closed shells. When the assumption fails, the computed spin is not likely to be off by more than one unit.

The numbers 37, 39, 41, 49, and 51 appearing in column 1 represent values of N or Z at the beginning and end of closed shells for which predictions of spin are possible. Known stable and radioactive nuclei are listed in column 2. The incomplete structure symbols in column 3 denote the level occupied by the odd particle or hole. "Yes" in the 4th column means that the nucleus in question possesses an isomeric state. The computed spin appears in the 5th column.

The shell model may fail at N or $Z=37$ because of the large number of low configurations having even parity ($2s$, $5g$, and $4d$ orbits all even) while there is only one configuration, $(3p)^{-1}$, of odd parity. It, therefore, is likely that configuration interaction produces a ground state of even parity and unpredictable spin (in this connection note that $_{37}Rb^{85}$ and $_{30}Zn^{67}$ have spin 5/2). In one case, $_{37}Rb^{87}$, the association of the very stable closed shell at $N=50$ with $Z=37$ greatly reduces the number of low even configurations, thus, perhaps, accounting for the success of the shell model in predicting the spin and magnetic moment of $_{37}Rb^{87}$ (spin 3/2, moment 2.75, a predominantly $^2P_{3/2}$ state).

The occurrence of many examples of isomerism when the predicted spin values are 1/2, and 7/2, 9/2 provides strong support for the proposed shell structure. Equally important is the fact that isomerism is rare (one doubtful example) when the predicted spin is 3/2 or 5/2. Table II exhibits the distribution of isomerism against the odd number of the pair N, Z. From the large number of isomeric nuclei at N or $Z=39$ one may infer that the two closely spaced configurations

$$(1s)^2\ (2p)^6\ (3d)^{10}\ (4f)^{14}\ (2p)^6\ (2s)^1$$
$$(1s)^2\ (2p)^6\ (3d)^{10}\ (4f)^{14}\ (2p)^6\ (5g)^1,$$

assisted by configuration interaction, determine the ground

state and the first excited state of such systems. An occasional inversion of the two levels (spin 7/2 or 9/2 in the ground state) is not unlikely and would not prejudice the occurrence of isomerism.

* This research was supported in part by U. S. Navy Contract N6ORI 117.

[1] W. Elsasser, J. de phys. et rad. **5**, 625 (1934).
[2] E. P. Wigner, Phys. Rev. **51**, 947 (1937).
[3] W. H. Barkas, Phys. Rev. **55**, 691 (1939).
[4] M. G. Mayer, Phys. Rev. **74**, 235 (1948).
[5] E. Feenberg and K. C. Hammack, Bull. Am. Phys. Soc. **23**, No. 7, 10 (1948).

Comparison of Atmospheric Methane Content above Flagstaff, Arizona, and Columbus, Ohio

ARTHUR ADEL
Arizona State College, Flagstaff, Arizona
November 29, 1948

A CONTINUOUS, high resolution map of the infra-red solar spectrum, 2 microns to 14 microns, was obtained by the author in 1940, at the Lowell Observatory. The experiment was performed with a 2400-line-per-inch grating in a Pfund type, automatically recording spectrometer of aperture *f*:5 and focal length of 30 inches. That portion of the map between 7 microns and 14 microns has been published, with a reference to the unpublished segment between 2 microns and 7 microns.[1]

Early in 1948, M. Migeotte[2] identified absorption lines of the methane fundamentals ν_3 (3.3 microns) in solar spectra recorded at Columbus, Ohio, and ν_4 (7.7 microns) in the solar spectrum map recorded at Flagstaff.

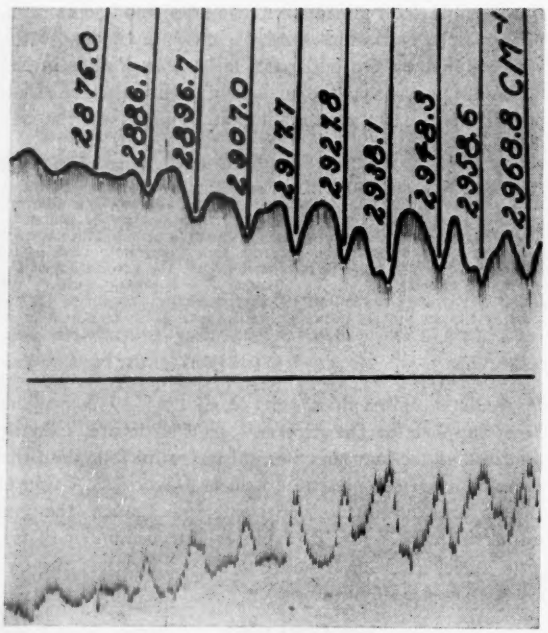

FIG. 1. The grating solar spectrum near 3.4 microns, observed at Flagstaff, Arizona, on the morning of October 28, 1940. It shows ten lines in the *P*-branch of ν_3 of methane (CH_4). Reproduction of the original record of galvanometer deflection *versus* grating position.

The fundamental ν_3 (3.3 microns) is clearly resolved in the unpublished portion of the Flagstaff map and it serves importantly in drawing a comparison between the amounts of methane above Flagstaff and Columbus. ν_3 is far superior to ν_4 for the purposes of such a comparison, because of the much heavier absorption by water vapor at 7.7 microns and the far greater water vapor content of the atmosphere over Columbus relative to Flagstaff.

Figure 1 shows ten lines in the *P*-branch of ν_3 of methane as observed in the solar spectrum at Flagstaff on the morning of October 28, 1940. The detailed agreement between this curve and the one obtained by Migeotte[2] is remarkable. The central intensities of the latter do not exceed those of the former by as much as one might have expected in view of the fact that the work at Columbus was done with a 7200-line-per-inch grating. It is significant that the fractional energy absorption is closely the same for the two spectra, thus indicating a widespread and uniform distribution of methane above the earth.

[1] Arthur Adel, Astrophys. J. **94**, 451 (1941).
[2] Marcel Migeotte, Phys. Rev. **73**, 519 (1948); Astrophys. J. **107**, 400 (1948); Phys. Rev. **74**, 112 (1948).

The Isotopic Constitution of Ytterbium

RICHARD J. HAYDEN, DAVID C. HESS, JR., AND MARK G. INGHRAM
Argonne National Laboratory, Chicago, Illinois
December 8, 1948

THE isotopic constitution of ytterbium was first investigated by Aston.[1] Using anode rays from ytterbium bromide, he observed isotopes at masses 171, 172, 173, 174, and 176 and estimated their abundances photometrically. Later Dempster[2] using his Tesla spark ion source found isotopes at masses 168 and 170. He gave estimates for the abundances of these two isotopes but not for the abundances of the other isotopes. Dempster's figures for 168 and 170 and Aston's values for the other isotopes, corrected for the presence of the lighter isotopes, are given in the first row of Table I. In 1941 Wahl[3] investigated ytterbium using careful photometric mass spectrographic methods. His results are given in the second row of Table I. He did not observe the 168 isotope and so he assumed Dempster's value in his calculation of percentages. He did not quote limits of error but he did give his mean mass, uncorrected for packing fraction, as 173.068±0.006. This would indicate that he believed his abundance ratios good to 1 percent.

Because of the historical unreliability of photometrically measured isotopic abundances, an electrometric determination seemed desirable. The ion source used was a tungsten surface ionization filament similar to that pre-

TABLE I. Isotopic abundances (percent) of the ytterbium isotopes.

Investigator	168	170	171	172	173	174	176
Aston and Dempster	0.06	2	9	23	17	37	12
Wahl		4.21	14.26	21.49	17.02	29.58	13.38
Authors	0.140 ±0.002	3.034 ±0.030	14.34 ±0.14	21.88 ±0.22	16.18 ±0.16	31.77 ±0.32	12.65 ±0.13

viously used for the mass determination of active isotopes.[4] The instrument and techniques employed in this mass analysis were the same as those used in the measurement of the isotopic constitution of lanthanum and cerium.[5] Two different samples of Yb_2O_3 were analyzed. The first was secured from Adam Hilger, Ltd. (laboratory number 1071), while the second was an exchange column purified sample obtained from Dr. D. H. Harris of the Clinton Laboratories. There was no detectable difference in the isotopic constitution of the two samples. The values quoted in the third row of Table I are the averages of thirty separate determinations on each sample. The mean deviation of each percentage was about 1 percent of that percentage. Because of the large number of readings the precision should be better than this by a factor of one over the square root of the number of determinations. However, since we have not as yet been able to rule out systematic mass discriminations because of selective emission from the surface ionization source, or because of non-linearity of the 10^{10}-ohm resistor over the wide current range used, to better than 1 percent we do not wish to quote any limits closer than this.

The following upper limits for the natural occurrence of other isotopes of ytterbium were set: $Yb^{166}<0.002$ percent, $Yb^{167}<0.002$ percent, $Yb^{169}<0.01$ percent, $Yb^{175}<0.02$ percent, $Yb^{177}<0.01$ percent, $Yb^{178}<0.002$ percent.

With the assumption of zero packing fraction for the ytterbium isotopes the chemical atomic weight of ytterbium calculated from the new abundances is 173.046 ±0.006. The international value, chemically determined, is 173.04.

[1] F. W. Aston, Nature **133**, 327 (1934); Proc. Roy. Soc. **A146**, 46 (1934).
[2] A. J. Dempster, Phys. Rev. **53**, 727 (1938).
[3] W. Wahl, Naturwiss. **29**, 536 (1941).
[4] R. J. Hayden, Phys. Rev. **74**, 650 (1948).
[5] M. G. Inghram, R. J. Hayden, and D. C. Hess, Jr., Phys. Rev. **72**, 967 (1947).

A Measurement of the Half-Life of Double Beta-Decay from $_{50}Sn^{124}$ *

E. L. Fireman
Department of Physics, Princeton University, Princeton, New Jersey
November 29, 1948

If two isobars differ by two units in atomic number, the heavier may decay into the lighter by double beta-decay.[1,2] This is the simultaneous emission of two negatrons if the heavier has lower atomic number or the simultaneous emission of two positons, 1 positon+1K capture, or 2K captures if the heavier has higher atomic number. The half-life depends markedly upon whether or not two neutrinos are emitted in the process. If no neutrinos are emitted, the half-life is of the order of 10^{10} times shorter than if two neutrinos are emitted (see Table I). The reason for this large difference in half-life arises from the number of cells in phase space available for the transition.

Table I. Theoretical half-life for allowed double negaton emission.

Atomic mass difference	0	0.52 Mev	1.04 Mev	1.56 Mev	2.08 Mev	2.60 Mev
2 neutrinos	∞	$2.6\cdot10^{27}$ yr.	$2.4\cdot10^{25}$ yr.	$1.3\cdot10^{24}$ yr.	$2.1\cdot10^{23}$ yr.	$4.3\cdot10^{22}$ yr.
No neutrinos	∞	$2.1\cdot10^{16}$ yr.	$2.7\cdot10^{15}$ yr.	$6.5\cdot10^{14}$ yr.	$2.2\cdot10^{14}$ yr.	$8.3\cdot10^{13}$ yr.

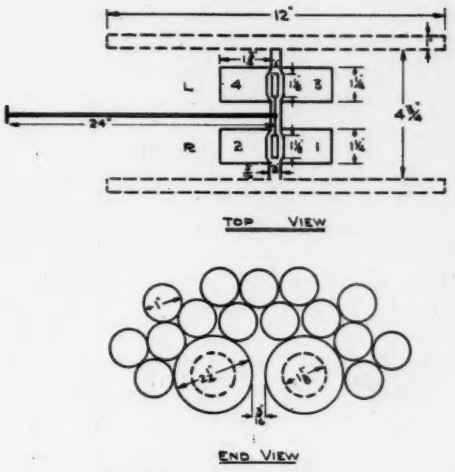

Fig. 1. Experimental arrangement.

In the present work an experimental investigation of $_{50}Sn^{124}$ which belongs to isobaric triplet $_{50}Sn^{124}-_{52}Te^{124}-_{54}Xe^{124}$ has been carried out. The experimental arrangement consists of four thin window counters (3 mg/cm² mica) connected in pairs to coincidence circuits L and R. These counters are shielded by anticoincidence counters and by an Fe and Pb box. Two specimens** of Sn (25 g) identical in all respects except for isotopic constitution are placed between the thin window counters. These specimens are called A and B. Specimen A contains 54 percent of Sn^{124}; specimen B contains 0.4 percent of Sn^{124}. The position of the specimens between the counters is interchanged by rotating the specimen holder through 180° (see Fig. 1).

Coincidences and single counts from both specimens are recorded simultaneously. The specimen holder is rotated through 180° every other hour and the positions of the specimens in the holder are interchanged every 20 hours. These data are summarized in Table II.

In all situations specimen A gives 2 coincidence counts/hr. more than specimen B. By repeating this type of measurement with Al absorbers over one side of each specimen an absorption curve is obtained. This absorption curve is similar to that of electrons from a spectrum with an energy end point between 1.0 Mev and 1.5 Mev. The single counts from specimens A and B both give 6.5±0.3 counts/min. If one interprets this effect as double beta-decay from Sn^{124}, one obtains a half-life between $0.4\cdot10^{16}$ yr. and $0.9\cdot10^{16}$ yr. Other alternative explanations for these observations have been considered but none have been found to be plausible. This result would indicate that double beta-decay is unaccompanied by neutrinos. A further consequence of these results pointed out to the author by Professor J. R. Oppenheimer is that the neutron-proton charge difference is exactly equal to the electron charge.

TABLE II. $L(A)$ gives the coincidences from specimen A between counters L, and $R(B)$ gives the coincidences from B between counters R. Holder 0° and 180° are the two holder positions. Positions 1 and 2 are positions for the specimens in the holder.

Pos. 1	Holder 0° Coin. counts/hr.	$L(A)$ 16.4±0.3	$R(B)$ 14.3±0.3
	Holder 180° Coin. counts/hr.	$L(B)$ 14.4±0.3	$R(A)$ 15.9±0.3
Pos. 2	Holder 0° Coin. counts/hr.	$L(B)$ 14.6±0.3	$R(A)$ 16.4±0.3
	Holder 180° Coin. counts/hr.	$L(A)$ 16.4±0.3	$R(B)$ 13.9±0.3

A detailed report of this work is being prepared for publication in the Physical Review.

The author is grateful to Professor R. Sherr for accepting the supervision of this research and to Professor E. P. Wigner for many profitable discussions.

* This work is assisted by the Office of Naval Research.
** These isotopes were obtained from Oak Ridge.
[1] Maria Goeppert-Mayer, Phys. Rev. **48**, 512 (1935).
[2] W. H. Furry, Phys. Rev. **56**, 1184 (1939).

Internal Conversion Electrons from Metastable Te^{125}

R. D. HILL AND G. SCHARFF-GOLDHABER
Department of Physics, University of Illinois, Urbana, Illinois*
AND
G. FRIEDLANDER
*Brookhaven National Laboratory,** Upton, New York*
December 6, 1948

RECENTLY, it has been found[1] that an isomer of the stable isotope Te^{125} with a half-life of two months grows out of Sb^{125} (2.7 yr.). Absorption measurements of its radiations showed that it decays through a highly converted isomeric transition of approximately 120-kev energy.

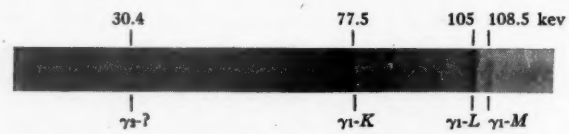

FIG. 1. Internal conversion spectrum of Te^{125*}, $\gamma_1 = 109.3$ kev.

The decay of Te^{125} has now been followed for a longer period and the half-life was found to be 58±4 days. For a more accurate measurement of the energy of the isomeric transition, a source of a few microcuries of Te^{125} was separated from Sn irradiated with slow neutrons at Oak Ridge. It was subjected to an analysis in a 180° magnetic beta-ray spectrograph previously described.[2] Three lines corresponding to the K, L, and M conversion electrons of a 109.3-kev gamma-ray were obtained after a 36-hr. exposure. A longer exposure of about one week yielded, in addition, a weak line produced by conversion electrons of 30.4 kev, for which we cannot state the gamma-ray energy since we do not know in which shell the conversion took place. Figure 1 shows the spectrum of the conversion lines. A part of a microphotometer trace of the film is reproduced in Fig. 2. Using the density-intensity calibration recently described,[3] we obtained the relative intensities of the lines from a number of microphotometer traces. The average relative intensities are given in Table I. It follows that the K/L intensity ratio is ~1.5, the L/M ratio ~3.5. From the half-life and energy, and from the lower limit of 0.99 for the total internal conversion coefficient, it was previously concluded[1] that the effective $\Delta l = 5$ for this transition. According to Drell's[4] recent calculations, the K/L ratio obtained by us is compatible with an effective $\Delta l = 5$, if one assumes that this transition is "parity forbidden," and that 95 percent is 2^4-pole magnetic while the rest is 2^5-pole electric. The spin change between the metastable state and ground state would then be 4. The role of the very weak transition is at present in doubt. Further experiments are needed to decide whether it has to be ascribed to Te^{125*}.

TABLE I. Average relative intensities in lines.

$B\rho$ gauss-cm	Line energy kev	Assignment	Gamma-ray energy kev	Relative intensity
975.2	77.5	$\gamma_1 - K$	77.5 + 31.8 = 109.3	100
1147	105.1	$\gamma_1 - L$	105.1 + 4.35 = 109.45	67
1169	108.6	$\gamma_1 - M$	108.6 + 0.58 = 109.18	19
598.6	30.4	$\gamma_2 - ?$		6

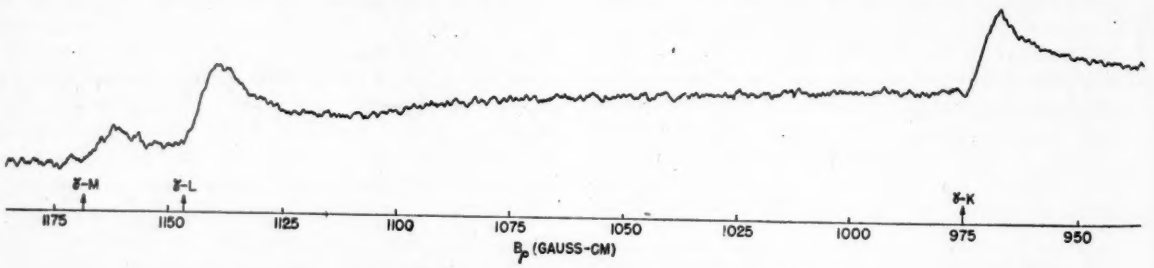

FIG. 2. Microphotometer trace of the internal conversion electron lines from the 109.3-kev gamma-ray of Te^{125*}.

* Assisted by the joint program of the Office of Naval Research and the Atomic Energy Commission.
** Research work carried out under the auspices of the Atomic Energy Commission.
[1] G. Friedlander, M. Goldhaber, and G. Scharff-Goldhaber, Phys. Rev. **74**, 981 (1948).
[2] R. D. Hill, Phys. Rev. **74**, 78 (1948).
[3] R. D. Hill and J. W. Mihelich, Phys. Rev. **74**, 1874 (1948).
[4] S. D. Drell, Phys. Rev. in press.

Proceedings of the American Physical Society

Minutes of the Meeting at Chicago, November 26–27, 1948

THE 287th meeting of the American Physical Society, reverting to the tradition of prewar years, was held at the University of Chicago on the Friday and Saturday after Thanksgiving, being the 26th and 27th of November, 1948. With its registration of 455, this was the third largest meeting ever held at Chicago, being exceeded only slightly by the Christmas meeting of 1947 and considerably by the June meeting of 1946 which was the scene of the presentation of so many papers lately declassified. Adequate halls were available, and the meeting ran very smoothly, owing to the preparations of Professor W. H. Zachariasen who was the local committee chairman. There had to be two or three or four simultaneous sessions throughout, except on part of Friday afternoon, and some of the Saturday afternoon sessions were quite protracted. In time to come we shall have to choose between compressing three days' work into two, or quitting the Thanksgiving week end.

There were ten invited papers on a great variety of subjects; most were bespoken from the universities in Illinois and in adjacent states, but M. von Laue gave a graphic account of the present state of our science in Germany, and D. E. Gray introduced the study of the abstracting problem currently being conducted by the American Institute of Physics. There were also three invited papers composing a Symposium arranged by our Division of Solid-State Physics. Contributed ten-minute papers numbered one hundred and four. Post-deadline papers were given by E. R. Grilly of Los Alamos (introduced by John Marley) and M. Forró of Barat College.

The dinner of the Society was held on Friday evening at International House, 252 being present and Vice President Loomis presiding in the unavoidable absence of the President. Enrico Fermi gave the only after-dinner speech.

The Council met on Friday morning and elected one candidate to Fellowship and the unprecedented number of six hundred and twenty-one candidates to Membership, bringing the membership of the Society to a total exceeding seven thousand eight hundred. The names of these new members are appended. The Council voted to donate, to the ten Japanese and fifteen German institutions of learning to which Physical Review and Reviews of Modern Physics had been donated for the period from mid-1941 to mid-1948, additional copies of these journals extending to the end of 1949. J. R. Oppenheimer was nominated to the Governing Board of the American Institute of Physics for a term commencing in February 1949. Two amendments to the Constitution of the Society were proposed by the Council, and will shortly be distributed to the members.

Reports reaching the office of the Society indicate that we have lost the following members through death: William Brauner (Alden, Pa.); E. F. Burton (F, Toronto); C. W. Chamberlain (F, Michigan State); H. D. Fagan (Xavier); C. E. Haller (RCA); C. T. Keniston (Urbana); L. W. Taylor (Oberlin); R. C. Tolman (F, California Institute of Technology).

Elected to Fellowship: D. K. Coles.

Elected to Membership: Carl A. Accardo, Edward N. Adams, II, M. K. Al-Ghita, Gordon A. Allen, Donald M. Allison, Jr., Adolph B. Amster, Leonard Aronowitz, Hack Arroe, Peter Astbury, Douglas Atack, Robert Avery, Frederick Ayer, II, René Ballini, Samuel J. Bame, Jr., J. M. Barnóthy, George R. Barse, Eugene I. Barth, Robert E. Bass, Harold F. Batho, Simon H. Bauer, Carleton A. Bayless, J. G. Bayly, Charles P. Bean, F. Bedewi, E. R. Bell, William E. Bell, Raymond S. Berkowitz, Alan Berman, Joseph B. Bernstein, Aaron Besner, John B. Birks, Willard B. Birtley, Russel F. Bjorklund, Charles L. Blair, André Blanchard, Duncan C. Blanchard, Edmund J. Blau, Arnold L. Bloom, David R. Blosser, Clarence A. Boddie, Emily E. Boggs, Dan I. Bolef, Rollon O. Bondelid, Fernand Bonenfant, Eli Botkin, G. M. Barthold Bouricius, J. Kent Bowker, W. S. Boyle, C. E. Bradford, Edward L. Brady, Sydney W. Breckon, Frances M. Breit, D. Allan Bromley, Robert M. Broudy, Alward E. Brown, Calvin F. Brown, Gerald E. Brown, William C. Brown, William W. Brown, Joseph A. Bruner, Frederick J. Bueche, M. Loren Bullock, Mary P. Burgan, Robert Buschert, Matt G. Bushner, Howard E. Bussey, Thomas D. Cabot, Jr., William A. Calder, Alastair Cameron, Israel

Cantor, W. J. Carr, Jr., John L. Carter, Jr., Judith M. Cassidy, John G. Castle, Jr., Ray N. Cauble, Vincent dePaul Cavanaugh, Charles C. Chadwick, Robert E. Chaffee, Raymond Chastel, Jack E. Chatelain, Wolfgang J. Choyke, Vito M. Cifichiello, Robert G. Cochran, James R. Coe, Leslie Cohen, René Cohen, Thomas E. Cole, Clifford B. Collins, J. Frank Coneybear, Anna M. Conforto, William S. Corak, Louis Costrell, Robert E. Coulehan, George Cowper, Bernd Crasemann, Cyril D. Curtis, Charles F. Curtiss, Joseph A. Cyphers, John E. Dacey, Paul B. Daitch, Thomas I. Davenport, Jack P. Davidson, Jr., Harry F. Davis, II, R. E. Davis, Roland W. Davis, Irving E. Dayton, Ralph W. DeBlois, Herbert W. Deem, Joseph DeFelice, A. J. Dekker, Victor Delano, Stanley Deser, J. F. Dibrell, Jr., Paden F. Dismore, William J. Dittrich, Thomas W. Donaven, Winthrop T. Doolittle, Jr., Donald L. Drukey, John M. Dudley, George F. D. Duff, Nelson M. Duller, Jr., Frits K. du Pre, Arthur Eckstein, Ellsworth A. Edling, Charles Edwards, Joachim B. Ehrman, Robert J. Eichelberger, Harvey Einbinder, Melvin Eisner, Robert B. Elliott, Robert S. Elliott, Jason A. Ellis, Jan M. Engel, Leo F. Epstein, Stephen Eros, John R. Eshbach, Tilden C. Euster, John S. Evans, Jr., Arno W. Ewald, Thomas E. Eyles, Hsu Yun Fan, Pao-hsien Fang, Monroe Farber, Frank E. Faris, George W. Farwell, Lewis G. Fauble, Arnold M. Feingold, Charles Feldman, Olaf H. Fernald, Richard A. Ferrell, William H. Fiden, Donald E. Findley, John C. Fisher, Philip C. Fisher, Hugh M. Fitzpatrick, James W. Fitzwilliam, Carson C. Flammer, Anna Foner, Scott E. Forbush, M. Forró, Peter E. Fossum, Clarence M. Fowler, Jamshed K. Fozdar, Henry E. Frachtman, Norman C. Francis, Peter Franken, Elizabeth J. Frazier, Burton E. Freeman, Theodore K. Freeman, Phyllis S. Freier, Claude Fremont, Seymour Friedman, Albert D. Frost, Jr., Eugene Frowe, Glenn M. Frye, Jr., John L. Gammel, Murray Gell-Mann, Sydney Geltman, Claude Geoffrion, Dal C. Gerneth, Albert Ghiorso, Harold F. Gibson, Hugh A. Glassford, Paul H. Gleichauf, Lawrence E. Glendenin, Nicholas Glyptis, Walter B. Goad, Jr., Nat Hartwell Godbold, Murray C. Goddard, Bernard Gold, Eugene Goldberg, Joshua N. Goldberg, Lionel J. B. Goldfarb, Oscar D. Gonzalez, William B. Good, Philip Goodman, William H. Gordon, Jr., Joseph G. Gorman, C. J. Gorter, Tibor Graf, Frederick H. Grannis, Dwight E. Gray, Sidney Gray, Julius Green, John Greenaway, David Greene, George W. Greenlees, Martin Greenspan, Reynold Greenstone, Wayland C. Griffith, Edward J. Groth, Jr., Eric R. B. Gross, George R. Grove, Richard H. Gundelfinger, Torsten Gustafson, H. S. Gutowsky, Walter Haelg, W. E. Haisley, Charles A. Halijak, Georges Hall, Richard E. Halsted, Harold J. Hamilton, Robert S. Hansen, Gerard G. Harris, Paul W. Harrison, Jr., Sol E. Harrison, Robert D. Hatcher, Ruth A. Hellar, Robert L. Hellens, Allan F. Henry, Lloyd O. Herwig, Joseph W. Hickman, George W. Hinman, Joseph G. Hirschberg, Jr., Martin A. Hirshfeld, A. L. Hodson, Ragnar Holm, Keith O. Househam, Ning Hu, Charles M. Huddleston, Dorothy Huffman, Thos. E. Hull, D. M. Hunten, Frankin C. Hurlbut, Dwight A. Hutchison, Virgil M. Hutchison, Harvey I. Israel, Donald Glenn Ivey, Hugh D. Ivey, John David Jackson, Wilbur Nelson Jarmie, Willibald K. Jentschke, Hans S. Joachim, Arthur L. Johnson, Charles Yothers Johnson, Cleland H. Johnson, Mary Johnson, Robert A. Johnson, Virgil R. Johnson, Robert Bruce Johnston, Ernest A. Jones, Harrison Milas Jones, Seymor Kant, Jerome Karle, Ira L. Karp, Clarence J. Karzmark, Walter E. Kaskan, Walter Yoneo Kato, Isadore Katz, John William Kauffman, Walter Kauzmann, Georges Kayas, Paul R. Keeler, Jr., Robert E. Kell, E. W. Keller, Russell B. Keller, Jr., George G. Kelley, F. M. Kelly, Joseph M. Kelly, Henry A. Kent, Larkin Kerwin, Henry Charles Kessler, Jr., John David Keys, William L. Kincaid, Frederick Shelly Kirn, Albert J. Kirschbaum, Joseph M. Kirshner, S. S. Kistler, Oskar Klein, Ernest Koenigsberg, George T. Kokotailo, Carol Kousnetz, James S. Kouvelites, Alan Z. Kranz, Samuel Krimm, Robert Louis Kyhl, Walter Barber LaBerge, John L. Lackler, John S. Lagarias, Edmund V. Laitone, Richard W. Lamphere, Robert A. Langevin, Harry H. Landon, Jr., Arthur Alfred Lavine, David Hughes Lawrence, Thomas E. Lawrence, Joel Smith Lawson, Jr., Christopher P. Leavitt, William L. Lehmann, James E. Leiss, Robert E. LeLevier, John Mark Anthony Lenihan, Charles Sebastian Lerch, Jr., Irving Lessin, Isadore H. Levine, John Levinson, Cyrus Levinthal, Alfred D. Levitas, Gething M. Lewis, LaVerne F. Lewis, Fa-Si Li, Manfred Lindner, Howard H. Loar, Howard C. Long, Dr. Conrad L. Longmire, Norman Lord, John R. Low, Jr., William Hunter Lucke, Harry Montgomery Luhrs, Rufus Lumry, Ernest A. Lynton, Alexander Daniel MacDonald, William J. MacIntyre, Richard Madey, Robert Malm, Edward R. Manring, Donald E. Marlowe, Harvey Marron, Ernest A. Martinelli, Julien J. Mason, Donald F. Mastick, Keith Benson Mather, Robert Laurance Mather, Genevieve Mathison, W. Wallace Mathison, Sumner Mayburg, Frank L. McCrackin, Paul N. McCreery, Edward L. McDevitt, S.J., William S. McEwan, Carl L. McGinnis, John S. McIntosh, Alexander S. McKay, William O. McMinn, Gilbert Eric McMurtrie, William L. Mead, Jenn Kueh Mei, William Wayne Meinke, Theodore C. Merkle, Jr., Klaus Peter Meyer, Daniel R. Miller, Donald Henry Miller, Jack Culbertson Miller, Robert A. Miller, Robert Vance Miller, Stanley Custer Miller, Jr., F. Stanley Minshall, Edward Eugene Mitchell, Jack Pitts Mize, Dr. C. Møller, Paul Molmud, John Hastings Montague, Lawrence J. Monville, S.J., Milton Lewis Moon, Ernest Julius Moore, Allan Henry Morrish, Thomas E. Morrisson, Harold W. Morrow, Jr., Joseph W. Motz, William Gates Moulton, James H. Mulligan, Jr., Elmore H. Mundell, Jr., Earle E. Muschlitz, Jr., Maurice G. Mylroi, Eugene L. Naegele, Yoshinao Nakada, Casimir Z. Nawrocki, John R. Neighbours, Ivan R. Neilsen, Lauro Xavier Nepomuceno, Peter W. Neurath, Gordon Frank Newell, Nathan M. Newmark, Elmer Nielsen, Rosalie Noble, Robert Novick, Ralph E. Nuelle, Warren E. Nyer, Carl Raymond Oberman, W. Opechowski, S. Robert Orr, William C. Overton, Jr., Michael John Ozeroff, Martin E. Packard, Daphne Grace Padfield, Roger W. Paine, Jr.,

Felix S. Palubinskas, Lee W. Parker, Geoffrey Parry, Dr. Imre F. Patai, Arthur S. Pavlovic, Bayard P. Peakes, Marshall C. Pease, III, Virgil G. Peck, Stanford S. Penner, John P. Perry, Jr., William F. Pesold, R. H. Peterson, Aihud Pevsner, Alroy B. Phillips, William Eugene Plaisted, Sister M. Gonzaga Plantenberg, O.S.B., Martin Plotkin, Lawrence M. Politzer, Ilia G. Poppoff, Karl G. Porges, Donald H. Porter, Leroy R. Posey, Jr., A. J. Pressesky, Glenn W. Preston, Edward Warren Price, William J. Price, Morton Prince, Robert H. Pullen, Ira Pullman, Thomas M. Putnam, Jr., Claude Leonard Pyle, Benton Seymour Rabinovitch, Eugene Rabinowitch, Julia Ann Randall, Volney K. Rasmussen, Jr., E. R. Rathbun, Jr., William Shelton Rawls, Edward B. Rawson, Joseph L. Raymond, Bernard Reich, Melvin Reier, Alfred Reifman, Charles Austin Reilly, Robert A. Reitz, Gerard-Andre Renard, André Reno, Irving Resnick, John H. Reynolds, Leon M. Reynolds, Cecil R. Rhorer, Robert J. Rickett, Brandon G. Rightmire, John E. Roberts, Albert L. Robinson, James E. Robinson, Plinio S. Rocha, George D. Rochester, William C. Roesch, Hartley Rogers, Jr., George L. Rogosa, David Rose, David John Rose, Jack W. Rose, John C. Rose, Norman Rostoker, Paul Allen Roys, John Ruze, Eugene J. Saletan, Edwin E. Salpeter, George Samos, Edmund W. Samuel, Allen R. Sandage, Theodore M. Sanders, Jr., Lydia G. Savedoff, Oliver A. Schaeffer, Erich Scharf, Larry Schecter, Daniel Schiff, Moe I. Schneebaum, Sol Schneider, Louis J. Schoen, A. A. Schulke, Clarence W. Schultz, Floyd V. Schultz, Charles M. Schwartz, Nathan Schwartz, John D. Seagrave, Benjamin Segall, Emanuel J. Seldin, Donald W. Sencenbaugh, Edward A. Sevian, Robert G. S. Sewell, Mathew M. Shapiro, Norman M. Shapiro, Rita Sharcoff, W. M. Sharpless, Jack Sherman, Robert G. Shields, Edward S. Shire, Robert G. Shreffler, Lowell M. Shuck, Harrison Shull, Michell J. Sienko, Werner Sigrist, Sam Silverman, Kenneth M. Simpson, Marshall H. Sirvetz, Erwin A. Sittig, Bernard Smith, C. Scudder Smith, Donald Smith, James E. Smith, Ralph L. Smith, Jr., Conway W. Snyder, Stuart Snyder, John C. Soderstrum, Allan L. Sorem, Allan Louis Sorem, Frank Spayth, Edward G. Spencer, Nathan Spielberg, Sidney Spital, Kenneth G. Standing, Alfred G. Stebler, Marvin N. Stein, David W. Steinhaus, Jack S. Steller, Evelyn Stephens, Walter Steuber, Donald Stevenson, Paul M. Stier, Thomas G. Stinchcomb, Robert J. Stirton, William R. Stratton, Karl Strauch, Ellis Strick, Minnie Strick, Richard N. Stuart, K. W. Taconis, Charles J. Taylor, Jr., Jack E. Taylor, John R. Terrall, Henry C. Thacher, Jr., Ernest R. Thackeray, Stanley G. Thompson, William B. Thompson, Robert N. Thurston, John H. Tinlot, Jay Tittman, Eugene Tochilin, Frank S. Tomkins, Edward C. Toops, Bert Jack Toppel, George T. Trammell, Harry I. Treiber, Edmund B. Tucker, A. H. Turnbull, David Turnbull, Errett S. Turner, Thomas J. Turner, Frank G. Ullman, Roland W. Ure, Jr., Giorgio Valle, Gerard J. van der Maas, Brother Godfrey Vassallo, Andrew Vazsonyi, Putcha Venkateswarlu, Victor V. Verbinski, Leopold Vigneron, Raymond E. Vinson, G. H. Visser, Arthur D. Voorhis, Robert O. Wales, William H. Walker, Virginia F. Walters, Hugh A. Watson, Harvey E. Wegner, Charles E. Weir, Erwin K. E. Weise, Tunis Wentink, Jr., James P. Wesley, Edward James West, Mack J. West, Willem F. Westendorp, John W. Weymouth, Stanley L. Whitcher, Louise G. White, Oliver M. White, John M. Wilcox, Wayne G. Wild, Wentworth Wilder, Jr., Richard A. Williams, Paul E. Wilkinson, Wesley W. Winter, Ross C. Winterbottom, Matthius J. Wolf, Lincoln Wolfenstein, S. A. Wouthuysen, William E. Wright, Oleg I. Yadoff, William A. Yager, Jack S. Yampolsky, Florian B. Yanoski, Henry L. Yeagley, Jan L. Yntema, Felix H. Young, James A. Young, Jr., Byron L. Youtz, Carroll W. Zabel, Igor N. Zavarine, Herbert Zeiger, Robert J. Zentner, Clayton M. Zieman, Bernd Zondek, William J. Zwart, Leo Zwell.

KARL K. DARROW, *Secretary*
American Physical Society
Columbia University
New York 27, N. Y.

Invited Papers on the General Programme

Excited States of Nuclei. M. GOLDHABER, *University of Illinois.*

The Problem of Abstracting the Periodical Literature of Physics. D. E. GRAY, *American Institute of Physics.*

Phenomenological Quantum Electrodynamics. J. M. JAUCH, *State University of Iowa.*

The Present State of Physics in Germany. M. VON LAUE, *Goettingen, Germany.*

Nuclear Resonance Line Widths as Functions of Temperature. G. E. PAKE, *Washington University.*

An Infra-Red Recording Spectrograph of High Resolution, Yielding Precise Wave-Length Measurements. E. R. PECK, *Northwestern University.*

Neutrons Correlated with Charged Cosmic-Ray Particles. R. D. SARD, *Washington University.*

Recoils from Neutrino Emission. C. W. SHERWIN, *University of Illinois.*

Excitation of Nuclei by X-Rays and Electrons. BERNARD WALDMAN, *University of Notre Dame.*

Study of New Elements by X-Ray Diffraction Methods. W. H. ZACHARIASEN, *University of Chicago.*

Invited Papers of the Division of Solid-State Physics

Physical Principles Involved in the Transistor, a Semiconductor Triode. JOHN BARDEEN, *Bell Telephone Laboratories.*

Calculations of the Changes in the Conductivity of Metals Produced by Cold Work. J. S. KOEHLER, *Carnegie Institute of Technology.*

Fundamental Aspects of Diffusion in Solids. FREDERICK SEITZ, *Carnegie Institute of Technology.*

Beta-Radioactive Substances

A1. Absolute Determination of the Emission Rate of Beta-Rays.* R. K. CLARK AND G. FAILLA, *Columbia University.*—The active material is mounted on a thin aluminum foil suspended in the center of a large stainless steel tank which is evacuated. With ionization thus eliminated, the observed current leaving the source structure is a measure of the number of electrons emitted per unit time. The current is measured by a compensation method using a Lindemann electrometer as a null instrument. The effects of the surroundings are studied by means of supplementary "screens" and "cans" which are placed in turn around the source structure, with potentials up to 2900 volts applied. This also gives some information about the low energy end of the spectrum of those particles which leave the source structure. The results for P^{32} and S^{35} are compared with values determined by other methods.

* This abstract is based on work performed for the Atomic Energy Commission.

A2. Shape of the Beta-Spectrum of RaE.* LAWRENCE M. LANGER, *Indiana University.*—Many beta-disintegrations which involve periods and energies corresponding to *forbidden* transitions apparently yield momentum distributions which have *allowed* shapes. It seemed worth while, therefore, to remeasure the beta-spectrum of the forbidden transition in RaE to determine whether this distribution is really different from the allowed shape. The measurements were made in the 40-cm radius of curvature, 180° focusing shaped field spectrometer[1] under very ideal conditions. The source, electrolytically separated from RaD from which the polonium had previously been extracted, was deposited on a backing of Zapon 0.02 mg/cm² thick. The source thickness was much less than 0.1 mg/cm². The counters were filled with 9 cm of argon plus 1 cm of alcohol. For the measurements at the low energy end of the spectrum, a counter with a Zapon window which transmits electrons down to 2.0 kev was used. The Fermi plot of the data is definitely not the straight line which is characteristic of an allowed transition. The present data are in remarkably excellent agreement with the results of Neary[2] down to 70 kev. The experimental conditions for the present measurements were essentially the same as those under which marked deviations from the Fermi theory were found for the allowed transitions in Cu^{64}, Cu^{61}, and N^{13}.

* This work is supported by a grant from the Frederick Gardner Cottrell fund of the Research Corporation and by the joint program of the Office of Naval Research and Atomic Energy Commission.
[1] Lawrence M. Langer and C. Sharp Cook, Rev. Sci. Inst. 19, 257 (1948).
[2] G. J. Neary, Proc. A175, 71 (1940).

A3. Screening and Relativistic Effects on Beta-Spectra. C. LONGMIRE AND H. BROWN, *Columbia University.*—In interpreting data on beta-ray spectra, apparent deviations from the Fermi allowed form may be caused by neglect of the effect of screening by atomic electrons and by use of the non-relativistic approximation to the Coulomb factor. The effect of the screening on the Coulomb factor has been calculated approximately for arbitrary Z, using a method based on the Thomas-Fermi screened potential. The effect of screening is found to be an increase in the number of both positrons and electrons at low energies. Numerical results are given for S^{35}, Cu^{64}, and RaE. By use of a better approximation to the relativistic Coulomb correction factor, the error incurred by using the non-relativistic form is estimated for various emitters. It is found that for sufficiently thin sources of Cu^{64} (for example) the neglect of the screening and relativistic effects contributes a considerable fraction of the apparent deviation from the Fermi theory.

A4. A New Radioactive Isotope of Oxygen.* R. SHERR, H. R. MUETHER, AND M. G. WHITE, *Princeton University.*—The radioactive gases produced by high energy proton bombardment[1] of nitrogen compounds have been examined. In addition to the well known C^{11} activity, produced by the reaction $N^{14}(p,\alpha)C^{11}$, a new positron activity of 76.5±2 sec. half-life was found. Chemical tests have shown that the latter is caused by an isotope of oxygen. Absorption measurements yielded a maximum energy of 1.8±0.1 Mev for the positrons and an energy of 2.3 Mev for γ-radiation. The absorption curves for both radiations appear to be simple, suggesting a decay scheme in which the γ-ray is in cascade with the positron. A rough threshold measurement supports the assignment of this new activity to O^{14}. The absence of a positron transition to the ground state of N^{14} indicates that this transition is forbidden, as is the similar transition from C^{14} to N^{14}. Simple Coulomb calculations show that O^{14} may make an allowed positron transition of 1.7 Mev to an excited state of N^{14} at 2.4 Mev, in excellent agreement with our observed values.

* Assisted by the Joint Program of the Office of Naval Research and the Atomic Energy Commission.
[1] Sherr, Muether, and White, Bull. Am. Phys. Soc. 23, No. 5, Abstract T7, 1948.

A5. The Radioactive Decay of K^{40}. J. J. FLOYD, C. D. CORYELL, AND L. B. BORST, *Brookhaven National Laboratory.*—A sample of potassium chloride fourteenfold enriched in K^{40} was obtained from the Stable Isotope Division of the U. S. Atomic Energy Commission. The partial disintegration constant for beta-ray emission was found to be $(3.9\pm.4)\times10^{-10}$ yr^{-1}. An absorption curve through aluminum was found to have a shape identical to that of RaE but having a maximum energy of 1.9±.2 Mv. Considerations of stability of Ca^{40} as compared to A^{40} lead to the assignment of the known gamma-ray of energy 1.5 Mv to the calcium transition. Recent determinations of argon concentrations in potassium bearing minerals by H. E. Suess, G. H. Cady, and us lead to a partial disintegration constant for argon formation of $0.3\text{–}0.8\times10^{-10}$ yr^{-1}. The disappearance of K^{40} is therefore thought to be characterized by $T_{\frac{1}{2}}=(1.3\pm.3)\times10^{9}$ yr.

A6. Disintegration of Mn^{54} into the Isobar Fe^{54}. J. D. KURBATOV AND DONALD GIDEON,* *The Ohio State University.*—In addition to the already known disintegration

of Mn^{54} into the isobar Cr^{54} by orbital electron capture, a search has been made for disintegration into a second isobar Fe^{54} by electron emission. Mn^{54} was removed with high specific activity from iron activated by deuterons, was aged and carefully purified. The study of a thin film of Mn^{54} was made predominantly by cloud chamber. In 2000 pictures no positron tracks were found. Electrons were observed in large number. The energy of the electrons was measured using 1800 tracks, and the upper limit evaluated as about 1.0±Mev. The ratio of the number of disintegrations by means of electron capture to electron emission was estimated as exceeding one thousand.

* Present address: University of Notre Dame.

A7. An Investigation of Bremsstrahlung by Means of the Nuclear Isomerism of Indium. WALTER C. MILLER AND BERNARD WALDMAN, *University of Notre Dame.*—The metastable state of In^{115} has been used as a detector of a narrow energy band in the continuous x-ray spectrum produced by a monoenergetic electron beam on gold targets. The thin target x-ray isochromat ($h\nu = 1.04$ Mev) has been investigated in the neighborhood of the short wave-length limit. This isochromat is finite at the threshold and constant for at least 400 kev. This is in agreement with Guth's theory and verifies the assumption that the excitation of In^{115*} is a line absorption. Both the thin target and thick target x-ray excitation curves for In^{115} have been obtained in the region from 1.0 to 2.6 Mev. The thin target curve exhibits a step-like character from 1.0 to 1.9 Mev. The thick target curve below 2.0 Mev exhibits straight-line segments as expected from the thin target curve, but above 2.0 Mev there are no straight line segments, in good agreement with the thin target data and theory. The over-all cross section (per electron incident on a 34 mg/cm² gold target) is 10^{-34} cm² in the region of the threshold. Evidence is presented for the existence of a lower activation level between 0.8 and 0.9 Mev with an over-all cross section (for a similar target) of the order of 10^{-36} cm².

A8. Nuclear Isomerism of Selenium Produced by X-Rays. D. N. GIDEON, W. C. MILLER, AND B. WALDMAN, *University of Notre Dame.*—The metastable state of selenium assigned[1] to Se^{77*} has been produced in metallic selenium by x-rays from the Notre Dame pressure electrostatic generator. The sample was irradiated for two minutes by x-rays from a thick gold target bombarded with an electron beam of approximately 100 microamperes. The activity of the Se^{77*} decayed with a half-life of 17.5 ±1.0 seconds.[2] An excitation curve and an absorption curve for the conversion electrons in aluminum were obtained. The excitation curve, which extends over the range 0.76 Mev to 2.2 Mev, indicates that measurable activity is produced with an electron energy of 0.76 Mev. The curve has an abrupt change of slope at the energy 1.45±.05 Mev; this is interpreted as an energy level in selenium at 1.45 Mev. From the absorption curve the energy of the conversion electrons appears to be 135±15 kev, in agreement with the measured[2] gamma-ray energy of ~150 kev.

[1] M. Goldhaber and C. O. Muehlhouse, Bull. Am. Phys. Soc. 23, 56 (1948).
[2] J. R. Arnold and N. Sugerman, J. Chem. Phys. 15, 703 (1947).

A9. Radiations from Cd^{115} and $^{*}In^{115}$.† C. E. MANDEVILLE, M. V. SCHERB,†† AND W. B. KEIGHTON, *Bartol Research Foundation.*—Metallic cadmium was irradiated by slow neutrons for one hour in the Oak Ridge pile. After chemical purification, the cadmium fraction was found to emit the characteristic 1.03-Mev beta-rays and 0.6-Mev gamma-rays of the 2.5-day Cd^{115}. The beta-gamma coincidence rate was observed to decrease from an extrapolated value of 0.093×10^{-3} coincidence per beta-ray at zero absorber thickness to zero at 0.14 g/cm² in aluminum, indicating an inner beta-ray group at 0.46 Mev and that the high energy spectrum is non-coincident with any gamma radiation. A small gamma-gamma coincidence rate was noted in the cadmium fraction. Coincidence measurements showed that the 4-hour isomer of indium (115) decays with the emission of a single partially converted gamma-ray. These coincidence data confirm the level diagram presented by Lawson and Cork.[1]

† Assisted by the joint program of ONR and the AEC.
†† Now at Princeton University.
[1] Lawson and Cork, Phys. Rev. 57, 982 (1940).

A10. The Beta- and Gamma-Radiation of Ta^{182}.* LOUIS A. BEACH, CHARLES L. PEACOCK, AND ROGER G. WILKINSON, *Indiana University.*—A survey of the radiations of Ta^{182} has been made down to energies of the order of 3 kev with a small 180° spectrometer. The beta-ray spectrum is complicated by the presence of at least 20 conversion lines. A Fermi plot of the beta-rays is a straight line down to about 0.25 Mev and yields an end point at 0.525 Mev. To facilitate the assignment of the gamma-ray energies, the photo-electrons ejected from a thin lead radiator were studied. Fourteen peaks occur below 0.25 Mev as well as 5 lines above 1 Mev. The high energy lines are caused by three gamma-rays of energies 1.13, 1.22, and 1.24 Mev. The assignment of the low energy gamma-rays by an analysis of the conversion lines and photo-electron peaks is attempted, with fair agreement with Cork's[1] results. However, even with the added information obtained from the photo-electron lines and the relative intensities it is difficult to make a unique determination in some cases. No attempt is made to suggest a decay scheme for the numerous gamma-rays so obtained.

* Assisted by the joint program of the Office of Naval Research and Atomic Energy Commission.
[1] M. Cork, Phys. Rev. 72, 581 (1947).

A11. The Radiations of W^{187} and Au^{199} in the Low Energy Region.* CHARLES L. PEACOCK AND ROGER G. WILKINSON, *Indiana University.*—The use of a very thin window G-M tube detector in a small 180° spectrometer has made it possible to extend our study of W^{187} to energies

down to 3 kev. We find conversion lines corresponding to two gamma-rays having energies of 0.078 and 0.138 Mev. This agrees with the results of Valley,[1] obtained with photographic plate detection, with the exception of a gamma-ray at 0.101 Mev which we could not find. Furthermore, the photo-electron line previously assigned[2] as a K photo-line corresponding to a gamma-ray of 0.21 Mev now appears to be the L line caused by the gamma-ray at 0.138 Mev. This correction tends to corroborate the tentative decay scheme previously given. Au^{199} resulting from the decay of Pt^{199}, produced by the n-γ reaction on Pt^{198} in the Oak Ridge pile, has also been studied. All of the radiations lie below 0.32 Mev. Superimposed upon the continuous beta-ray spectrum are 9 conversion lines that may be attributed to 4 gamma-rays having energies of 0.025, 0.052, 0.164, and 0.214 Mev. The Fermi plot of the beta-rays is non-linear and has an end point at 0.32 Mev.

* Assisted by the joint program of the Office of Naval Research and Atomic Energy Commission.

[1] G. E. Valley, Phys. Rev. 59, 686 (1941).
[2] C. L. Peacock and R. G. Wilkinson, Phys. Rev. 74, 297 (1948).

A12. The Gamma-Rays Following Au^{198} β-Decay. D. Saxon and R. Heller, *Argonne National Laboratory.*—The internal conversion spectrum following Au^{198} β-decay has been carefully covered partically at low energies. We find no trace of the 0.157 and 0.208 Mev γ-rays reported by Levy and Greuling,[1] and Dumond, Lind, and Watson,[2] as present in 15 percent ratio to the 0.411-Mev γ-ray. From our statistical errors, and assuming electric multipole radiation, the lower limit for detection of the γ's is 1 to 4 percent. This checks the recent work of Peacock and Wilkinson,[3] who suggest Hg^{197} as the impurity giving the low energy γ-rays. The K and L lines given the energy of the single γ-ray as 415 ± 5 kev. The conversion coefficients are:

$E(\gamma)$	K	$L+M$	$K+L+M$	$\frac{K}{L+M}$
415 kev	3.56 percent	1.32 percent	4.88 percent	2.69

From the K to L ratio and the curves of Hebb and Nelson,[4] the spin charge of the γ-ray is found to be 3.

[1] V. W. Levy and E. Greuling, Phys. Rev. 73, 83 (1948).
[2] J. W. M. DuMond, D. A. Lind, and B. B. Watson, Phys. Rev. 73, 1392 (1948).
[3] C. L. Peacock and R. G. Wilkinson, Phys. Rev. 74, 297 (1948).
[4] M. H. Hebb and E. Nelson, Phys. Rev. 58, 486 (1940).

Nuclear Apparatus, Nuclear Masses, Nuclear Theory

B1. Survey of Nuclear Energy Possibilities. Cecil B. Ellis, *Office of Naval Research.*—In devising a new nuclear power source the fundamental problem would be to obtain a sufficient number of suitable projectiles cheaply. At least 10^{15} per sec. are needed and probably many more. These projectiles must be either electrically or thermally accelerated by external equipment, or generated by the nuclear reaction (or a combination of the two). The solutions to be sought fall into three groups: (a) charged-particle bombardment systems of high yield, (b) new nucleon-rearrangement chain reactions, and (c) new fundamental-particle transformations yielding potent projectiles. Avenues of approach in each of these categories will be discussed.

B2. Nuclear Reactor at Brookhaven National Laboratory. Lyle B. Borst.—Construction of the Brookhaven reactor is progressing well and initial operation is expected early in 1949. The reactor is an air-cooled unit constructed of graphite and unenriched uranium. The maximum thermal neutron flux is expected to be 5×10^{12} neutrons per square centimeter per second. The experimental facilities include one twelve-inch square hole penetrating the reactor structure and a number of four-inch square holes extending through the reactor and both shields. Equipment may be inserted in these holes or they may be used as sources of collimated neutron beams. The top shield consists of removable four-foot square blocks to accommodate thermal columns and large equipment to utilize the thermal leakage neutron flux in excess of 10^{11} neutrons per square centimeter per second. The ancillary facilities include a specially designed laboratory building for research in physics, chemistry, biology and medicine and a hot laboratory capable of handling up to fifty curies of two Mev gamma-emitters.

B3. Betatron Model. D. W. Kerst, G. D. Adams, H. W. Koch, C. S. Robinson, *University of Illinois.*—A 70-Mev model for the 300-Mev betatron is operating. It was constructed to test field shape, flux-biasing,[1] unidirectional excitation, and flux forcing. The field exponent, n, is 1 at the injection radius, 0.25 at the wall 3.6 cm within, and 0.5 at the orbit. Vertical space is 2.0 cm. Increasing n at injection by coils on the poles does not alter the yield appreciably. Field inhomogenities at injection time are generally less than 0.1 gauss. This is accomplished by separating the biased flux yoke from the field magnets, and by carrying all iron in the field magnets through the same magnetic cycle. Electrons can be injected as early as 8 microseconds after the unidirectional pulse starts. The field at the 26 cm orbit radius reaches 9200 gauss and is forced to be closely proportional to the central flux by parallel connection of field and flux coils. X-ray yield is about $10^{-3}R$ per pulse at 1 meter. A section of the flux yoke is reserved for radiation compensation. Much of the component work has been done by other members of the betatron staff.

[1] D. W. Kerst, Phys. Rev. 68, 233 (1945).

B4. Low Energy Radiations in Proportional Counters. G. C. Hanna, B. Pontecorvo, and D. H. W. Kirkwood, *Chalk River Laboratories.*—The proportional counter technique for the investigation of low energy radiations has been developed.[1] Argon-methane and xenon-methane gas mixtures have been used in a variety of counters. The pulse energy spectrum is recorded on a thirty-channel pulse analyzer. Reference will be made to the problems of:

(1) the energy resolution achievable (statistical and instrumental limitations); (2) the useful range of gas multiplication; (3) amplifier design (noise level and paralysis when investigating the low energy component of an extended spectrum). *L*-orbital electron capture has been observed: argon[37] was introduced into the counter and energy peaks corresponding to the capture of K and L_I electrons have been observed. A preliminary investigation of the tritium spectrum is in accord with the work just published by Curran *et al.*[2] In this field two complementary methods of calibration are available, characteristic x-rays fired into the counter from outside and the introduction of argon[37] into the counter itself. Other uses of this technique include the investigation of soft nuclear gamma-radiations, isomeric transitions, and various x-ray problems.

[1] Kirkwood, Pontecorvo, and Hanna, Phys. Rev. **74**, 497 (1948).
[2] Curran, Angus, and Cockcroft, Nature **162**, 302 (1948).

B5. Temperature Dependence of Efficiency of a Naphthalene Scintillation Counter. R. S. CLAASSEN AND R. W. BOOM, *University of Minnesota* (Introduced by John H. Williams).*—In investigating the efficiency of a naphthalene crystal as a gamma-ray detector,[1] a strong dependence of efficiency (total counts above noise level) upon temperature of the crystal has been found. The naphthalene crystal, which had been prepared by slow cooling, was held at several temperatures while the 931A photo-multiplier tube was held at dry ice temperature to reduce dark current background. The pulses from the tube were amplified by a linear amplifier and counted by a 10-channel discriminator. Using a radium source the ratio of the efficiency (total counts) for the crystal at −70°C to the efficiency at 0°C was 1.4. The ratio of efficiencies between −180°C and 0°C was 2.2. The shape of the pulse height distribution curve was the same for the various temperatures within experimental error. This would indicate that these ratios could be obtained using a simple discriminator at a single setting. An arrangement in which the tube and crystal were cooled together and a single discriminator was used to count the pulses gave the above ratios within experimental error.

* This work was supported in part by the Office of Naval Research
[1] H. Kallmann, Natur. and Technik (July, 1947).

B6. A New Proton Spectrometer. E. M. HAFNER, W. F. DONOGHUE, AND H. SNYDER, *Brookhaven National Laboratory.**—For the purpose of obtaining accurately focused lines from particle groups produced in nuclear reaction, a new type of focusing geometry has been studied. It consists of a uniform magnetic field covering a half-plane with target and photographic emulsion detector located in the field-free region. A monokinetic group of particles comes to second-order focus at some point on a line depending on incident energy and the *Q* of the reaction, after a deflection of about 110°. A group of particles which, as a result of finite recoil of the target nucleus is not homogeneous in energy over the aperture, comes to second-order focus at some point on a different line, depending upon the masses of the particles involved and the angle of observation. In the case of reactions involving nuclei of mass less than 20, the shift of the focal line with one unit change in mass can easily be observed as a change in the characteristic shape of the focused line. It is, therefore, possible to assign data to a particular isotope and, in addition, to work with chemically impure targets without ambiguity. Such an instrument should lead to further developments in the technique of nuclear spectrometry, and a design which will handle a maximum proton energy of 10 Mev is under way for use with the Brookhaven Van de Graaff.

* Research carried out under the auspices of the Atomic Energy Commission at Brookhaven National Laboratory.

B7. On Making Thin Nylon Films. J. RICHARDS, J. BROWN, F. FELBER, D. SAXON, *Argonne National Laboratory.*—We wish to report our method for making thin Nylon films by dropping an appropriate solution onto water in the manner used commonly for Collodion, Zapon, and Formvar. Nylon will dissolve in isobutyl alcohol with sufficient concentration if heated to boiling water temperature. Care in heating will help to eliminate troublesome air bubbles. The water used should be distilled and kept in a dust-free environment. The *p*H of the water should be checked and if found as much as 1 unit acid or basic, neutralized. This is necessary to allow complete and uniform expansion of the film on the water surface. A single drop on water will give a film ~0.01 mg/cm². Multiple layers can be easily made to eliminate microscopic pinholes. Such films have been successfully used on a β-spectrometer counter.

B8. Packing Fractions of the Nickel Isotopes. A. E. SHAW, *Argonne National Laboratory.*—The packing fractions of the nickel isotopes have been measured using a double-focusing mass spectrograph equipped with the new ion source previously described.[1] A hydrocarbon comparison line was provided for each of the nickel isotope lines by introducing benzene vapor directly into the ionization chamber. Thus both the nickel vapor and the benzene vapor were ionized simultaneously by the same 600-volt electrons. Second-order spectra were photographed to obtain a comparison line for ^{58}Ni since no line corresponding to $m/e=58$ has been observed with benzene. First-order spectra contained the four doublets which were used for the measurements of ^{60}Ni, ^{61}Ni, ^{62}Ni and ^{64}Ni. Each value of doublet separation was the result of five separate measurements that were reproducible to ±0.002

TABLE I.

Doublet	Number of doublets	F_2-F_1	F_1
$^{58}Ni^{+2}$—$^{12}C_2H_3$	7	24.96	−8.29±0.07
^{60}Ni—$^{12}C_5$	10	11.90	−8.69±0.08
^{61}Ni—$^{13}C_5H$	9	13.24	−8.75±0.08
^{62}Ni—$^{13}C_5H_2$	10	14.74	−9.01±0.05
^{64}Ni—$^{13}C_4{}^{13}CH_3$	7	16.02	−8.62±0.08

mm. Table I gives a summary of the packing fractions ($\times 10^4$). The results of Okuda[2] will be discussed.

[1] A. E. Shaw, Phys. Rev. 73, 1222 (1948).
[2] T. Okuda *et al.*, Phys. Rev. 59, 104 (1941).

B9. On the Origin of the Elements. R. A. ALPHER AND R. C. HERMAN, *Johns Hopkins University,** AND G. A. GAMOW, *George Washington University.*—Continuing preliminary work on the neutron-capture theory of the relative abundance of the elements,[1] we have investigated in greater detail the following cases: (1) the building-up of the elements taking into account neutron decay but not the universal expansion[2] gives a better fit to the abundance data than previously reported,[1] and requires an initial neutron density of 5×10^{-9} gm/cm^3; (2) the building-up of deuterium only, with both neutron decay and universal expansion included[3] yields a matter density $\rho=7.2\times10^{-3}t^{-1}$ gm/cm^3 if the parameters are adjusted to give a relative concentration 0.5 for hydrogen. We have also interpreted the extremely low relative abundances of some of the light elements on the basis of thermonuclear reactions following the main building-up process in an expanding universe.[4] Finally, impressed with the large relative abundances of the elements in the vicinity of iron, we are led to suggest that they may have been caused by the thermal evaporation of particles from the various nuclear species, the relative rates depending on the binding energy per particle.

* A portion of this work was supported by the U. S. Navy, Bureau of Ordnance.
[1] Alpher, Bethe, and Gamow, Phys. Rev. 73, 803 (1948); and R. A. Alpher, Phys. Rev. (in press).
[2] R. A. Alpher and R. C. Herman, Phys. Rev. (in press).
[3] G. A. Gamow, Nature (in press).
[4] Alpher, Herman, and Gamow, Phys. Rev. (in press).

B10. Principle of Regularity and Continuity of Nuclear Series. WILLIAM D. HARKINS AND MARTIN POPELKA, JR., *University of Chicago and Universal Oil Products Company.*—In papers between 1915 and 1923 (e.g., W. D. Harkins, Phil. Mag. 42, 305 (1931)) it was shown that a plot of the stable atomic species revealed that the general pattern is the same as that exhibited by the radioactive series. In that year this principle was used in a chart (J. Frank. Inst.) which predicted the nuclear species of all of the elements. For the even He-Th series of mass $4w$, 27 species were known and 51 were predicted, and for the U, $4w+2$ series, 16 were known and 51 predicted, between atomic numbers 2 and 80. Of these predicted species almost every one is now known. Members of these even series have even isotopic numbers, and every species exhibits an even atomic number. There are now known 83 members of the He-Th series; and 77 of the U series of a higher isotopic number than zero, 160 species in all. Although between these 160 species there are 131 vacancies ($I=0$; protons, odd; neutrons, odd) not a single one of these is known.

B11. An Interpretation of Nuclear Shell Structure.* EUGENE FEENBERG AND KENYON C. HAMMACK, *Washington University.*—Certain numbers of neutrons and of protons are associated with particularly stable and abundant nuclear systems.[1-4] These numbers correlate in an interesting fashion with the degeneracy of energy levels in the model of free particles in a potential well having a central depression for light nuclei (N or $Z\leqq20$) and a central elevation (wine bottle shape) for heavy nuclei.[1] The Coulomb force between protons, acting in opposition to the uniformizing action of the specifically nuclear forces causes the particle density in heavy nuclei to vary from a minimum value at the center to a maximum near the boundary.[5,6] This effect provides a qualitative explanation of the central elevation, since the low interior particle density is correlated with a small contribution from that region to the expectation value of the specifically nuclear interaction energy. The spins, magnetic moment, quadripole moments and radioactive transitions of nuclei with a small number of particles outside of closed shells or missing from closed shells provide valuable corroborative evidence on the angular momentum and parity of the single particle levels.[5,7]

* Research supported in part by U. S. Navy Contract N6ori117
[1] W. Elsasser, J. de phys. et rad. 5, 625 (1934).
[2] E. Wigner, Phys. Rev. 51, 947 (1937).
[3] W. H. Barkas, Phys. Rev. 55, 691 (1939).
[4] M. G. Mayer, Phys. Rev. 74, 235 (1948).
[5] E. Feenberg, Phys. Rev. 59, 593 (1941).
[6] E. Wigner, Bicentennial Symposium, University of Pennsylvania (1940).
[7] D. R. Inglis, Phys. Rev. 53, 470 (1938).

B12. Consequences of Generalized Meson Field Theories. ALEX E. S. GREEN, *University of Cincinnati.*—If a meson field theory is generalized to admit in the field Lagrangian all the derivatives of the field coordinates up to the σth in the manner previously noted,[1] then we may expect that in the final expression for the interaction energy of nucleons the usual meson potential will be replaced by a sum of σ meson potentials, where the meson masses and the relative couplings are given uniquely by algebraic relationships involving the constants appearing in the field Lagrangian. We find in several important cases that the relative couplings are such that not only are the inadmissible R^{-3} and R^{-2} singularities removed but also, in three or four meson theory, the objectionable R^{-1} singularity. Examples are cited. A closely related result is the fact that generalization justifies the cutting off of short wave-lengths in the evaluation of the interaction, and self-energy integrals.

[1] A. Green, Phys. Rev. 73, 519 (1948).

B13. Fluctuations in Energy Loss of Fast Charged Particles Passing through Matter. K. R. SYMON, *Wayne University.**—Given the probability $\chi(E',E)dE'dt$ that a particle of energy E suffers a loss of energy between E' and $E'+dE'$ in going a distance dt, we ask for the probability $P(E,E^0,t)dE$ that a particle of initial energy E^0 has an energy between E and $E+dE$ after traveling a distance t. Differential equations are obtained for the average energy $\langle E\rangle_{Av}$, and the central moments $\langle(\Delta E)^n\rangle_{Av}$, in terms of the moments $\chi_n(E)=\langle(E')^n\rangle_{Av}$ of the function $\chi(E',E)$. An approximation is made which is valid for heavy particles

for thicknesses t up to 85 percent of their range. The equations can then be solved. The resulting integrals have been evaluated numerically, and curves constructed from which $\langle E\rangle_{Av}$, $\langle(\Delta E)^2\rangle_{Av}$, and $\langle(\Delta E)^3\rangle_{Av}$ can be determined for thicknesses up to 85 percent of the range, for mesons or protons with kinetic energies from 0.01 to 10 times their rest energies. Curves for mean range $\langle R\rangle_{Av}$ and for $\langle(\Delta R)^2\rangle_{Av}$ and $\langle(\Delta R)^3\rangle_{Av}$ *vs.* E^0 have also been computed. The probability distribution function $P(E,E^0,t)$ can be fairly well represented for this range of energies and thicknesses by a one-parameter family of curves. The range-energy curve agrees, where it overlaps, with those given by Livingston and Bethel, and by Wheeler and Ladenburg.[2]

* This work was done at Harvard University under a National Research Council Predoctoral Fellowship.
[1] Rev. Mod. Phys. 9, 245 (1937).
[2] Phys. Rev. 60, 756 (1941).

Optical Physics

C1. Vibrational Spectra of Some Tribromomethanes. SHIRLEY E. ROSSER* AND FORREST F. CLEVELAND, *Illinois Institute of Technology.*—As part of an investigation of molecules of the type CBr_3X (where X is hydrogen, deuterium, or one of the halogens), Raman frequencies, semi-quantitative relative intensities, and quantitative depolarization factors have been obtained for CBr_3H, CBr_3Cl, and CBr_4. For CBr_3H, the sample was in the liquid state; for CBr_4, the sample was in solution in carbon tetrachloride and in benzene; and for CBr_3Cl, the spectra were also obtained for carbon tetrachloride and benzene solutions, but in this case it was necessary to add 5 percent of amylene to prevent the solution from turning brown. In the determination of the depolarization factors, both components were obtained simultaneously by means of a split-field Polaroid disk. A series of eight calibration marks was placed on each plate and separate calibration curves were prepared for each line. The intensities were obtained by use of a microdensitometer and corrections were made for the polarization at the prism of the spectrograph and for convergence errors. Infra-red absorption spectra were obtained also for the same samples used in the Raman spectra work, using an automatic, self-recording spectrometer with a rock-salt prism. The region covered in the infra-red measurements was from 700 to 4000 cm^{-1}.

* Now at Lynchburg College, Lynchburg, Virginia.

C2. Force Constants for the CBr_3H, CBr_3D, and CBr_4 Molecules. ARNOLD G. MEISTER, *Illinois Institute of Technology.*—Using the Wilson FG matrix method it was found that of the fifteen force constants required for the potential energy function of CBr_3H and CBr_3D one had to be made zero, while for two others only a value of a linear combination of the two could be obtained. The vibrational frequencies were calculated for both molecules using the same set of force constants and the agreement with the observed values was within 2 percent. However, in order to improve the agreement, six force constants had to be modified so that all the force constants for both molecules are no longer the same. In order to obtain exact agreement between the calculated and observed values of the fundamental frequencies for CBr_4, it was found that of the seven force constants required only two could be transferred from the other molecules. In almost all cases the force constants are in good agreement with the values given by Decius[1] except where he assumed the force constant concerned was equal to zero.

[1] J. C. Decius, J. Chem. Phys. 16, 214 (1948).

C3. The Vibrational Spectra of Some Trichloromethanes. JAMES P. ZIETLOW, FORREST F. CLEVELAND, AND ARNOLD G. MEISTER, *Illinois Institute of Technology.*—As part of an investigation of molecules of the type CCl_3X (where X is hydrogen, deuterium, or one of the halogens), Raman frequencies, semi-quantitative relative intensities, and quantitative depolarization factors have been obtained for CCl_3H and CCl_3Br in the liquid state. In the determination of the depolarization factors, both components were obtained simultaneously by means of a split-field Polaroid disk. A series of eight calibration marks were placed on each plate, and the measurements were made by use of a Gaertner microdensitometer. A more detailed description of the method has been given elsewhere.[1] The depolarization factor measured for the 718 cm^{-1} in CCl_3Br is rather high for an A_1 vibration and may be due to a superposition of this fundamental with the combination band (295+420) cm^{-1}. Also a large difference exists for CCl_3Br between the value given by Delwaulle and Francois and the present value for the depolarization factor of the 247 cm^{-1} line. A potential energy function containing only terms of the second degree and requiring fourteen force constants was used to calculate the frequencies for CCl_3H and CCl_3D. The calculated and observed values agree to within two percent.

[1] Forrest F. Cleveland, J. Chem. Phys. 13, 101 (1945).

C4. Vibrational Spectrum of Hexachloroethane. ROSE A. CARNEY* AND FORREST F. CLEVELAND, *Illinois Institute of Technology.*—Raman frequencies, relative intensities, and depolarization factors have been obtained (in saturated solutions in carbon tetrachloride and ethyl alcohol) for hexachloroethane, using Hg 4358A for excitation. Although much previous data have been obtained for this molecule, there was uncertainty in regard to some of the frequencies, the intensities were mostly visual estimates, the depolarization data were not obtained by a very reliable method, and no infra-red data were were recorded in the literature. The

TABLE I.

Frequency			Relative intensity		Depolarization factor	
Others	Hamilton	Carney	Hamilton	Carney	Hamilton	Carney
144	162	164	vw	1	P	**
220	223	225	45	42	0.80	0.86
340	340	339	37	56	0.86	0.87
432	431	434	100	100	0.15	0.01
858	859	858	22	16	0.81	0.83
978	975	977	3	3	0.35	**

results of this investigation to date are compared with those of previous workers in the Table I. The symbols vw and P mean *very weak* and *polarized*, respectively. A hundred-hour exposure is being made to obtain reliable depolarization factors for the weak lines indicated by the symbol**.

* Now at St. Procopius College, Lisle, Illinois.

C5. Infra-Red Absorption Spectrum of Dimethyldiacetylene. FORREST F. CLEVELAND, *Illinois Institute of Technology*, AND K. W. GREENLEE AND E. E. BELL, *Ohio State University*.—The infra-red absorption spectrum of freshly prepared dimethyldiacetylene has been obtained for the vapor existing above the solid or liquid at temperatures of 25°, 40°, 60°, 80°, 85°, and 110°; for the gas at 130°C; and for CCl_4 and cyclohexane solutions. A Beckman IR-2 spectrophotometer with rock-salt optics was used. With the gas or vapor, two strong, seven medium, four weak, and two very weak bands were observed; and with the CCl_4 solution, two strong, six medium, three weak, and one very weak bands were obtained. The nondegenerate frequencies for this molecule had been calculated previously by Meister and Cleveland[1] using the Wilson FG matrix method, and the results for the A_1 frequencies were compared with the Raman frequencies observed by them. At that time, however, no observed infra-red frequencies were available for comparison with the calculated $\bar{A}_2$ frequencies. The calculated values of the $\bar{A}_2$ frequencies were 903, 1368, 2131, and 2946 cm^{-1}; the corresponding observed values for the CCl_4 solution were 940, 1369, 2157, and 2920 cm^{-1}; and for the gaseous state the observed values were 941, 1379, 2163, and 2947 cm^{-1}.

[1] Arnold G. Meister and Forrest F. Cleveland, J. Chem. Phys. 15, 349 (1947).

C6. Thermodynamic Properties of Diiodoacetylene and Some Symmetrical-Top Acetylenes. JOSEPH S. ZIOMEK* AND FORREST F. CLEVELAND, *Illinois Institute of Technology*.—The heat content, free energy, entropy, and heat capacity of diiodoacetylene, methylchloroacetylene, methylbromoacetylene, methyliodoacetylene, and methyldeuteroacetylene have been calculated, to a rigid rotator, harmonic oscillator approximation, for the ideal gaseous state at 1 atmos. pressure, from their respective boiling points to 1000°K. The functions were calculated using Meister's frequency assignments,[1] which were based upon the Raman spectra for the liquid state or in solution, for all of the substances except methyldeuteroacetylene, for which the fundamental frequencies were those calculated by Meister using the Wilson FG matrix method, with force constants transferred from methylacetylene. Nuclear spin and isotope mixing were neglected in the calculations. The internuclear distances and the bond angles needed for calculation of the moments of inertia, used in getting the rotational and translational contributions, were those given in Meister's paper.

* Now at De Paul University, Chicago, Illinois.
[1] Arnold G. Meister, J. Chem. Phys., October 1938.

C7. Vibrational Spectra of Trans-Dichloroethylene. E. KREUSCH AND J. S. ZIOMEK, *De Paul University*, AND FORREST F. CLEVELAND, *Illinois Institute of Technology*.—Using previously described methods,[1] Raman displacements, relative intensities, and depolarization factors for *trans*-dichloroethylene (ClHC=CHCl) in the liquid state were found to be: 350 (100) 0.61; 711 (3) 0.47; 763 (23) 0.86; 846 (42) 0.40; 1274 (77) 0.52; 1578 (55) 0.33; 1634 (5) 0.72; 1693 (6) 0.48; 3073 (37) 0.43; and 3141 (4) 0.61, where the first figure is the Raman displacement in cm^{-1}, the figure in the parenthesis is the relative intensity measured with a microdensitometer, and the third figure is the depolarization factor. Trumpy and Paulsen have suggested that the 3141 cm^{-1} line is depolarized, but the present results show that the 763 cm^{-1} line is the only depolarized line. In addition, the following frequencies have been observed in the infra-red absorption spectrum of the liquid: 691 (s), 767 (vw), 838 (vvs), 894 (vvs), 1070 (vw), 1200 (vvs), 1303 (vw), 1386 (vvw), 2100 (vvw), 2642 (vvw), 2642 (vvw), 3064 (s), and 4255 (vvw), where the symbols vvs, s, vw, and vvw are intensity estimates meaning very, very strong; strong; very weak; and very, very weak, respectively. Emschwiller and Lecomte[2] have reported frequencies for the liquid at 754, 812, 965, 1054, and 1164 cm^{-1}. The agreement between the two sets of infra-red data is not very satisfactory.

[1] Forrest F. Cleveland, J. Chem. Phys. 11, 1 (1943); 13, 101 (1945).
[2] G. Emschwiller and J. Lecomte, J. de phys. et rad., 8, 130 (1937).

C8. Near Ultraviolet Absorption Spectrum of Hydroquinone Catechol and Resorcinol Vapor. CARL A. BECK, *Catholic University of America*.—Frequencies of the main bands: about 75 in each case, of these compounds have been measured, with a rough ordering of intensities. The 0,0 band is indicated in each case. Some main frequencies to both sides of the 0,0 are found, making it possible to date, to assign some frequency separations in the lower and upper electronic states, referred to the 0,0 chosen. These exposures were taken with excess material in the side arm, but to further confirm the 0,0 selections, experiments with a constant number of molecules to show the temperature effect alone, are now in progress.

C9. Excitation of Mercury Vapor by Positive Alkali Ions. HAROLD E. CLARK, *Washington University*.*—For investigation of the efficiency of excitation of the Hg 2537 line by positive ion bombardment, filamentary sources of lithium and potassium ions were made of the "ion-glasses."[1] Currents as high as 100 microamperes were obtained from an ion gun of semicylindrical design. Mercury vapor was bombarded by ions of 100 to 1000 ev; the excitation radiation was photographed according to the precautions necessary for quantitative spectrophotography. The Hg 2537 line was excited most efficiently by 450 ev lithium ions and 700 ev sodium ions. The energy *vs.* efficiency curve for the former agrees fairly well with similar data of Jones.[2] The efficiency curves appear to be more velocity dependent than energy dependent. The extrapolated thresh-

old energy for excitation of the mercury line by sodium ions is 90 ev; the onset of ionization for the same collision has been determined as 88±4 volts.[3]

* Now at Union College, Schenectady, New York.
[1] J. P. Blewett and E. J. Jones, Phys. Rev. **50**, 464 (1936).
[2] E. J. Jones, Phys. Rev. **44**, 707 (1933).
[3] R. N. Varney and W. C. Cole, Phys. Rev. **50**, 261 (1936).

C10. The Intrinsic Efficiency of Fluorescence Excited by Electron Bombardment. R. L. LONGINI, *Westinghouse Research Laboratories.*—The cathodoluminescence process comprises a number of individual steps, each consisting of a small energy loss by the primary electron and the associated excitation of a lattice electron, the latter giving rise to a light quantum when it falls to its normal state. Though over-all values for the efficiency of luminescence are of engineering interest, the physicist is more likely to be concerned with the intrinsic efficiency of the elementary process. The efficiency of these processes was evaluated from experiment by taking the derivative of the light generated with respect to the electron energy absorbed by the phosphor crystal. These were large enough so that there was negligible electron penetration and thus light was generated in the same crystals at all voltages. By calculating the relevant structure of the phosphor layer, corrections were made for electrons passing between crystals. The various corrections needed because of the aluminum backing were made and light losses were calculated. The efficiency is found to be up to 28 percent for zinc-cadmium sulfide when the electrons have 15 kev energy, a value several times as high as the previously reported "mean" efficiencies.

C11. Field Measurement of Average Optical Transmission. EDWARD E. MILLER, *University of Wisconsin.*—One of the physical problems arising in agricultural research is the measurement of the sunlight transmitted to the ground through various standing crops. Because of local patches of light and shade, some method of averaging is required. This problem has been solved by electronic integration of the current passing a vacuum photocell as it is being moved over the ground. A monitoring photo-cell simultaneously integrates the light received above the crop. After a run lasting about 20 seconds, these two integrals are held in the form of voltages so that their ratio (which measures average percent transmission) can be simply obtained with a potentiometer and null-meter. Performing a complete run and clearing the integrators occupies about one minute. Features of interest are: (1) Simplicity and stability of the portable computing circuit. (2) Design of the photocell housing to simulate the angular and spectral response of a low-growing crop.

Reactions of Transmutation

J1. Angular Yield of Neutrons from the D-D Reaction.* G. T. HUNTER AND H. T. RICHARDS, *University of Wisconsin.*—The Wisconsin electrostatic generator was used to furnish deuterons whose average energy in the target was varied from 0.5 Mev to 3.7 Mev. A "thin" deuterium gas target was used, the deuterons being admitted through a 0.00005-inch nickel foil. The neutrons were detected by an energy insensitive long counter[1] placed 1 meter from the target. The neutron yield was measured at angles from 0° to 165° in the laboratory system and then corrected to the center of mass system. The yield in the center of mass system was found to be of the form $N(\theta)=K(1+A\cos^2\theta+B\cos^4\theta+C\cos^6\theta)$, the total yield being essentially constant above 1 Mev. The coefficient A was found to be negative above 1.4 Mev. An appreciable amount of $\cos^4\theta$ was needed at all energies. At energies above 2.5 Mev, best fit of data required also the inclusion of a small amount of the $\cos^6\theta$ term. Disintegration protons at 90° were observed by a proportional counter as a monitor of the reaction.

* This work was supported in part by the Atomic Energy Commission and in part by the Wisconsin Alumni Research Foundation.
[1] Hanson and McKibben, Phys. Rev. **72**, 673 (1947).

J2. *P-N* Threshold for Deuterium.* R. V. SMITH AND H. T. RICHARDS, *University of Wisconsin.*—A thin deuterium gas target has been used with the Wisconsin electrostatic generator for a preliminary study of this threshold. Momentum considerations at threshold require that the proton energy be ⅔ the deuteron binding energy (or about 3.3 Mev) and that the emerging neutrons, whose energy is 370 kv, be bunched in the forward direction. To exploit the collimation and high energy of the neutrons at threshold, a hydrogen recoil counter was used as detector. A neutron threshold consistent with the expected value was observed, but precise data will not be available until further measurements are made with the high resolution electrostatic analyzer to measure the proton energy and with a target arrangement which eliminates the energy uncertainty inherent in the passage of the proton beam through the aluminum foil separating the gas target from the vacuum system. The cross section for the reaction was estimated to be 10^{-30} cm² at 70 kv above threshold.

* This work was supported in part by the Atomic Energy Commission and in part by the Wisconsin Alumni Research Foundation.

J3. Angle Dependence of the Reaction $Li^6(d,p)Li^7$. R. W. KRONE,* S. S. HANNA, AND D. R. INGLIS, *Johns Hopkins University.*—The nature of the excited state of Li^7 at about 450 kev is of special interest as a test of nuclear spin-orbit coupling. Some clue to its nature is expected from a comparison of the angular distributions of the short-range and long-range protons from $Li^6(d,p)Li^7$. These are measured simultaneously by use of a proportional counter long enough to give observable pulses of different sizes from the two ranges of protons at one setting, and the pulses of the two ranges are distinguished by use of a ten-channel discriminator. Measurements at about 400, 600, and 800 kev bombarding energy show a remarkable similarity between the short-range and long-range angular distributions, both with considerably greater intensity forward. This may constitute evidence that the two low states of Li^7 are a ^2P, but the analysis is as yet lacking. Further work is planned at higher energies. The method was checked by observation of the previously observed reaction $Li^7(p,\alpha)\alpha$ at one energy. This work was done with a new statitron constructed in the Physics Department to

take the place of the old one which was partly dismantled during the war. The energy scale was established by observation of thick-target and thin-target resonances in Li and F, with the help of I. Resnick and J. A. Neuendorffer.

* Now at University of Kansas.

J4. Absolute Measurement of the $Li^7(p,n)$ Threshold Voltage.* W. E. SHOUPP, B. JENNINGS, W. JONES, AND M. GARBUNY, *Westinghouse Research Laboratories.*—The $Li^7(p,n)$ threshold voltage has been measured with the radio frequency ion velocity gauge,[1] an instrument which establishes a number of discrete calibration points on the absolute voltage scale. Calculation of the voltage of any one of these calibration points involves only two easily measurable physical quantities, the length of the drift space in the cavity and the beam modulation frequency. These measurements can be made to an accuracy of about 0.05 percent. The voltage of the Westinghouse Van de Graaff generator, with which this work was done, was stabilized to about 0.1 percent using the biased corona point method with a compensating generating voltmeter as a source of error signal. The generating voltmeter was also used to make the small interpolation between the velocity gauge calibration point at 1.8915 mv and the lithium threshold at 1.8812 mv. The results of several preliminary measurements place the threshold at 1.8812 mv ±0.0019 mv. Work is continuing to increase the accuracy of this measurement.

* Assisted by the Joint Program of the Office of Naval Research and the Atomic Energy Commission.
[1] W. Alter, M. Garbuny, and J. W. Coltman, Phys. Rev. 72, 528A (1947).

J5. Total Cross Section of Be, N, O, Na, and Ca for Fast Neutrons. C. K. BOCKELMAN, R. K. ADAIR, H. H. BARSCHALL, AND O. SALA,* *University of Wisconsin.*—Studies of the total cross section of nuclei as a function of neutron energy have been continued. Ranges between 30 and 1000 kev were investigated, using a resolving power of 20 kev.[1] In Be only one resonance, at 625 kev, was observed, at the peak of which the cross section reaches 7*b*, indicating that it should be attributed to *p*-neutrons. In *N* small maxima were found at 440 kev and 665 kev but not at the positions of the previously observed absorption resonances. The cross section of *O* reaches 14*b* at 440 kev. This resonance has an experimental width of 45 kev and is probably due to *p*-neutrons forming a compound nucleus of spin $\frac{3}{2}$. In Na and Ca numerous peaks were found. The cross section of Ca has values below 1.5*b* over a considerable range of energies.

* Rockefeller Fellow of the University of São Paulo, Brazil.
[1] Barschall, Bockelman, and Seagondollar, Phys. Rev. 73, 659 (1948).

J6. The Gamma-Ray Spectrum from $F^{19}+H^1$ Using Photographic Emulsions Containing D_2O.* GERSON GOLDHABER, *University of Wisconsin.*—The photo-disintegration of deuterium in photographic emulsions was used for the measurement of gamma-ray energies. By soaking Ilford (C2—200μ, stripped) nuclear emulsions in D_2O, approximately 50 percent D_2O by weight was introduced into the emulsions. These emulsions, together with control emulsions containing a similar quantity of H_2O, were exposed while wet to gamma-rays from a thick CaF_2 target bombarded with 2.6 Mev protons from the Wisconsin electrostatic generator. For exposures exceeding 0.2μ ampere hours the background fog prevented track measurements. A provisional range energy relation in the wet emulsions was obtained by a rough calibration with *d-d* neutrons. The range in the wet emulsions was found to be longer by about 7 percent. A distribution curve of the photo-proton tracks in the emulsion shows two peaks corresponding to about 6 and 7 Mev gamma-rays. This agrees with the recent results of Walker and McDaniel.[1] The relative intensity of the two peaks is ~1.

* This work was supported in part by the Wisconsin Alumni Research Foundation and in part by the Atomic Energy Commission.
[1] R. L. Walker and B. D. McDaniel, Phys. Rev. 74, 315 (1948).

J7. *P-N* Reactions for Argon and Neon.* H. T. RICHARDS AND R. V. SMITH, *University of Wisconsin.*—From tabulated[1] masses one predicts the $A^{40}(pn)K^{40}$ threshold to be at 1.1 Mev proton energy and the $Ne^{22}(pn)Na^{22}$ threshold to be at 2.1 Mev. Using a BF_3 counter surrounded by paraffin for a detector, we observed a sharp and intense rise in the neutron yield from argon at a proton energy of 2.4 Mev. The cross section changed from about 10^{-29} cm² below 2.4 Mev to about 10^{-25} cm² by 2.55 Mev. The sharp rise at 2.4 Mev may correspond to the formation of K^{40} in an excited state with spin 1 or 0, and the small cross section below 2.4 Mev may correspond to the formation of K^{40} in the ground state ($I=4$) where the large spin difference between $A^{40}-K^{40}$ makes the reaction very highly forbidden. In the case of neon no neutron yield above background was observed up to 3.35 Mev proton energy. This negative result is in disagreement with Bethe's mass values[1] but is consistent with the observation[2] that a 1.3 Mev gamma-ray is in cascade with the beta-decay of Na^{22}.

* This work was supported in part by the Atomic Energy Commission and in part by the Wisconsin Alumni Research Foundation.
[1] H. A. Bethe, *Elementary Nuclear Theory* (J. Wiley & Sons, Inc., New York, 1947).
[2] Good, Peaslee, and Deutsch, Phys. Rev. 69, 313 (1946).

J8. $(p,n):(p,\gamma)$ and $(d,n):(d,2n)$ Reaction Cross Sections by Using Enriched Mo. D. N. KUNDU AND M. L. POOL, *Ohio State University.*—Molybdenum of natural isotopic composition and molybdenum enriched* in isotope 94 were subjected to bombardments with 5-Mev protons and 10-Mev deuterons. The strength of the beam in the different bombardments was carefully monitored. The nature of decay of the radioactive substances produced was determined by measuring the charged particles, x-rays and γ-rays separately. From the saturation intensities of the particles emitted during the primary disintegration process, equations were set up with the various reaction cross sections as unknowns. These equations were solved simultaneously to obtain the relative values of the cross sections. For the proton bombardments, $Mo^{94}(p,\gamma):Mo^{95}(p,n):Mo^{95}(p,\gamma):Mo^{96}(p,n)=1:260:40:400$. For the deuteron bombardments, $Mo^{94}(d,n):Mo^{95}(d,2n):Mo^{95}(d,n):Mo^{96}(d,2n)=1:13:17:2.5$. The method is applicable to a wide range of elements, and is expected to be of use in the assignment of mass numbers to newly produced radio-

active isotopes where the usual methods of mass assignments through cross-reactions is not available for lack of suitable target isotopes.

* Supplied by the Y-12 plant, Carbide and Carbon Chemicals Corporation, through the Isotopes Division, U.S.A.E.C., Oak Ridge, Tennessee.

J9. Relative Cross-Section Measurements for the Identification of Tc^{92} and Tc^{93}. M. L. POOL AND D. N. KUNDU, *Ohio State University.*—Natural Mo and Mo isotopes electromagnetically enriched* in isotopes Mo^{92} and Mo^{94} were bombarded with 5-Mev protons and 10-Mev deuterons. A rotating target was used, whenever necessary, so that two target isotopes could be bombarded under the same beam. Thus the activities produced could be satisfactorily ascribed to the appropriate target isotope. Activities of half-lives 2.7 hours, 47 minutes, and 4.5 minutes were found to be produced from Mo^{92}. The relative cross sections for the production of these activities were 44:224:1.76, respectively. On comparing these figures with those for the $(p,n):(p,\gamma)$ reactions from Mo^{95}, the 47-minute activity is assigned to Tc^{92}, the 2.7-hour and the 4.5-minute activities to Tc^{93}. Tc^{92} decays by K-capture only attended with 1.5-Mev γ-rays. For the 2.7-hour Tc^{93}, the decay is 93 percent by K-capture and 7 percent by emission of positrons of maximum energy 0.83 Mev. There are also γ-rays of energy 2.0 Mev associated with this activity.

* Supplied by the Y-12 plant, Carbide and Carbon Chemicals Corporation, through the Isotopes Division, U.S.A.E.C., Oak Ridge, Tennessee.

J10. Light-Charged Particle Emitted in Fission. K. W. ALLEN AND J. T. DEWAN, *Chalk River Laboratories.*—A study has been made of the range distribution of energetic light charged particles emitted in the fission of U^{235}, Pu^{239} and U^{233} by slow neutrons. After passing through Al absorbers, the particles in coincidence with fission fragments were detected in a proportional counter. Their specific ionization, determined by calibrating the counter with α-particles of known energy, showed that the majority, if not all, were α-particles. The observed range distribution of the particles extended to a maximum of about 50 cm of air with a peak at about 20 cm. Small differences in the maximum range and position of the peak were observed for the three elements studied. The abundance of the long range particles, which is now being investigated more precisely, is of the order of 1 in 400 fissions.

J11. The Distribution of Nuclear Charge in Fission. C. D. CORYELL, L. E. GLENDENIN, AND R. R. EDWARDS, *Oak Ridge National Laboratory.*—Little attention has previously been given to the distribution of nuclear charge in fission. Assuming that for any given mass split there is a most probable charge Z_P and a distribution around this, independent of A, various postulates for establishing Z_P are tested for consistency and for plausibility of the distribution curve. Examination of the independent fission yields of the nuclides Br^{82}, Rb^{86}, Xe^{135}, and Cs^{136} in U^{235} fission, and Cs^{136} in Pu^{239} fission, is used to eliminate the postulates that nuclear charge distributes as nuclear mass and that nuclear charge distributes to minimize radioactive potential energy at the instant of fission. The only satisfactory postulate we have found is that the most probable effective chain length (defined as $Z_A - Z_P$ where Z_A is the charge at the minimum in the Bohr-Wheeler parabola) is the same for the light and heavy fission fragments. This postulate or rule, presented publicly now in detail for the first time, has been used by Way and Wigner and has been given theoretical support by Present. The postulate has been of service in interpreting fission product gas-sweeping data (A. Turkevich and coworkers), and in detecting irregularities in fission yields (Arnold and Sugarman).

J12. Nuclear Closed Shell Effects in Fission.* L. E. GLENDENIN, *Massachusetts Institute of Technology.*—The stabilization effect of closed shells of 50 and 82 neutrons (recently discussed by Mayer[1]) in conjunction with independent yields predicted by an empirical rule for charge distribution in fission[2] can be used to explain certain anomalies observed in fission product studies. It is postulated that a primary fission product (which has already emitted the usual number of prompt neutrons) containing one neutron in excess of a closed shell will boil off this extra neutron rather than emit a β- or γ-ray as in the ordinary case. This process can explain the unexpectedly low fission yield of 86s I^{136} (83 neutrons) reported by Katcoff[3] and the anomolously high fission yield of Xe^{134} observed by Thode and Graham[4] in mass spectrometric studies. The further deductions afforded are that the 4.5-second delayed-neutron emitter identified by Sugarman[5] as an isotope of Br has a mass of 87 (isomeric with 56s Br^{87}), and that probably all of the delayed neutron emitters occurring in appreciable yield decay to a closed shell configuration.

* Supported in part by the Office of Naval Research.
[1] M. G. Mayer, Phys. Rev. **74**, 235 (1948).
[2] Glendenin, Coryell, and Edwards, the previous paper presented a this meeting.
[3] Katcoff, J. Chem. Phys., in press.
[4] Thode and Graham, Can. J. Research **25A**, 1 (1947).
[5] Sugarman, J. Chem. Phys. **15**, 544 (1947).

General Theoretical Physics

K1. Quantum-Electrodynamics. FREDERIK J. BELINFANTE, *Purdue University.*—Schwinger's generalized quantum-electrodynamics overlooks the fact that in quantized Maxwell theory "scalar photons" exist with negative energy and that Lorentz' condition excludes states without photons. Schwinger's assumption $A_\mu{}^+\Psi_0=0$ would mean that Ψ_0 is a state with a maximum number of scalar photons present, in contradiction to E.B.-statistics; furthermore it is incompatible with $\partial_\mu A^\mu\cdot\Psi_0=0$. One may avoid this difficulty by taking $\partial_\mu A^\mu\cdot\Psi_0=\mathfrak{A}_\mu{}^+\Psi_0=0$, where $\mathfrak{A}_\mu$ is Schwinger's transverse field four-vector; or one may replace the Maxwell field by a Proca field, taking the photon mass extremely small. In Maxwell's case by any of three methods one can find Møller's as well as Breit's interaction between point charges, depending on whether one calcu-

lates "relativistically" or whether the longitudinal interaction is first treated by non-relativistic "Fermi transformation." In Proca's case, "relativistic" calculation leads to different results including terms diverging for vanishing photon mass. Moreover the probability for longitudinal photon-emission diverges similarly. By non-relativistic Fermi transformation one obtains for vanishing photon mass Breit's interaction and a vanishing probability for emission of longitudinal photons, which seems preferable. A relativistic generalization of Fermi's transformation, including separation of transverse proper field and free photons, is now being investigated.

K2. Radiative Correction to the Klein-Nishina Formula. DAVID FELDMAN AND JULIAN SCHWINGER, *Harvard University.*—The divergences that mar the present form of quantum electrodynamics are encountered in two elementary phenomena, the polarization of the vacuum and the self-energy of the electron; effects that arise from the coupling of the matter and electromagnetic fields with the vacuum fluctuations of the other field. However, the divergent aspects of these two situations are concealed in unobservable charge and mass renormalization factors. The question is naturally raised whether a similar isolation of infinities can be performed in more complicated problems. It is known that this can indeed be done for the behavior of an electron in an external field, the finite radiative corrections thus obtained[1] comparing favorably with experimental evidence. We have examined the similar, but more involved problem of Compton scattering, and find that, here too, all divergences in the radiative correction of order $e^2/\hbar c$ are contained in the renormalization factors for the charge and mass of the electron. A low frequency divergence encountered in the correction to the Klein-Nishina formula is removed on including the concomitant emission of soft quanta, quite in analogy with the treatment of electron scattering.

[1] J. Schwinger, Phys. Rev. **73**, 415 (1948).

K3. On the Electromagnetic Shift of Energy Levels. J. B. FRENCH AND V. F. WEISSKOPF, *Massachusetts Institute of Technology.*—The shift of atomic energy levels caused by the coupling with the electromagnetic field is calculated by subtracting from the divergent expression for the electromagnetic self energy the expectation value of an equally divergent "mass operator" M. The latter represents the contribution of the electromagnetic mass of the electron. Certain ambiguities in the definition of M were removed by choosing the operator in a form which, according to Feynman,[1] gives for the self-energy of the free electron an expression with correct transformation properties after application of his relativistic cut-off method. All divergent terms cancel out and the level shift becomes:

$$\Delta E=\frac{e^2}{3\pi\hbar c}\left(\frac{\hbar}{mc}\right)^2\left[(\nabla^2V)_{\text{Av}}\left(\ln\frac{mc^2}{2\epsilon}+\frac{19}{30}\right)-\frac{3}{4}(\nabla V\cdot\sigma\times p/\hbar)_{\text{Av}}\right],$$

where V is the potential energy and ϵ is Bethe's[2] lower limit of integration. The other symbols are conventional. This gives 1051 megacycles for the split between the $2S_{\frac{1}{2}}$ and $2P_{\frac{1}{2}}$ levels in hydrogen.

[1] R. Feynman, Phys. Rev., in press.
[2] H. Bethe, Phys. Rev. **72**, 339 (1947).

K4. The Magnetic Internal Conversion Coefficient. S. D. DRELL, *University of Illinois.*—Conversion of magnetic multipole radiation by K-electrons is a relativistic effect depending on the spin of the electrons. Dancoff and Morrison[1] first pointed this out, giving a relativistic calculation of the magnetic internal conversion coefficient in Born approximation. A discrepancy exists between their formula for the conversion coefficient and the one obtained[2] using the Pauli two-component theory of the spinning electron. We resolve this discrepancy by introducing the four-component Dirac current for the electron into the electron-nucleus interaction matrix. We show that the calculation based on the Pauli theory fails due to the extremely singular character of the magnetic multipole potential. The formula derived indicates that magnetic conversion contributes significantly to the total conversion coefficient, particularly for medium and large Z and for soft gammas, since it approaches a large finite value whereas electric K-conversion vanishes at threshold. Large magnetic conversion will influence the experimentally observed K to L-shell conversion ratio. Its contribution to the total conversion coefficient will manifest itself in the lifetimes of isomeric levels which decay to ground via a parity forbidden transition; i.e., one in which the lowest permitted multipoles are magnetic 2^l and electric 2^{l+1}.

[1] S. M. Dancoff and P. Morrison, Phys. Rev. **55**, 128 (1939).
[2] Goertzel and Lowen, Phys. Rev. **67**, 203 (1945); Berestetzky, J. de Phys. U.S.S.R. **10**, 137 (1946).

K5. The Equation of State as an Eigenvalue Problem. JOSEPH W. WEINBERG, *University of Minnesota.*—The method used by Kramers and Wannier[1] for the two-dimensional ferromagnet is extended to one-dimensional systems of particles interacting under arbitrary forces with n nearest neighbors on each side, however near or far they may be. When a long chain of molecules is lengthened by an infinitesimal interval with or without a molecule, the grand partition function with the last n molecules held fixed, changes according to a characteristic equation, The eigenfunctions are related to the grand partition function, the kernel to the intermolecular potential function, and the eigenvalue to the Gibbs free energy. The internal energy and the volume per molecule are found explicitly from the slope of the maximum eigenvalue as a function of the parameters $1/kT$ and p/kT respectively. Unlike previous treatments, this has comparable validity at low and high densities, and hence is capable of disclosing a phase transition as a line of intersection of the surfaces of largest and next largest eigenvalues. A general proof is given that no phase transitions can occur in one-dimensional systems even in the case that many neighbors interact. Explicit equations of state have been studied with simplified models of the intermolecular potential.

[1] H. A. Kramers and G. H. Wannier, Phys. Rev. **60**, 252, (1941).

K6. Charged Bose-Einstein Particles in a Magnetic Field. M. F. M. OSBORNE, *Naval Research Laboratory.*—The problem of N charged Bose-Einstein particles in volume V has been considered. Electrostatic interactions are neglected. If T_0 is the condensation temperature in the absence of H, for $T>T_0$ the polarization $P=(I+1)\eta^2\mu^2HN/3IkTV-N\mu^2H/3VkT$ where I is the spin, $\mu=eh/4\pi mc$ and η is the intrinsic magnetic moment in units of μ. For $T<T_0$, $P=(N\mu/V)(\eta-1)(1-(T/T_0)^{\frac{3}{2}})$. These calculations imply that for a coil containing such a material as a core, at $T=T_0$, the self-inductance obtains a small change varying as $1/H$. Such an effect would be expected for a material containing free, mobile electron pairs. The calculations also indicate that the Bose-Einstein condensation of electron pairs cannot provide a theory of superconductivity, since for N/V small enough to make T_0 of the order of a superconducting temperature, the polarization $P\sim N\mu/V$ is too small to make $B=H+4\pi P$ become 0 for appreciable H, as perfect diamagnetism would require. The calculations also suggest that a condensation phenomenon may be sought in a study of metals (Pd, Gd, Ce, Tl) which absorb large amounts of deuterium, and that a comparative study of the low temperature behavior of metallic hydrides and deuterides would illuminate the effect of different statistics on the thermodynamics of gas-metal solutions.

K7. Transport Phenomena in an Ideal Bose-Einstein Gas. WILLIAM BAND, *University of Chicago.*—Because of the close resemblance of some of the equilibrium properties of liquid helium with those of a Bose-Einstein gas, it is of interest also to compare the transport phenomena in such a gas with those in liquid helium. First order perturbation theory leads to a normal heat conductivity except for a sudden increase by a factor of 2 or 3 at T_λ, the Bose-Einstein lambda-transition; its value falls again towards zero as $T\to 0$ below T_λ. In liquid helium the factor is about 10^8. Consider two enclosures filled with Bose-Einstein gas at slightly different pressures connected by a small hole. The net mass flow and isothermal heat transfer are calculated: their ratio has the classical value $2kT$ at high temperatures, as first found by Knudsen,* but below T_λ the mass flow carries only on average the zero energy of the lowest state. The hole does not prevent the transfer of particles with higher energy, which can pass freely in both directions, but the *net* flow induced by the pressure difference is effectively composed only of particles in the lowest energy state. The similarity with the flow of liquid helium through fine slits is remarkable.

* Martin Knudsen, Ann. d. Physik **34**, 603, 1911; Sophus Weber, Zeits. f. Physik **24**, 267, 1924.

K8. Use of Pressure in Thermodynamics. BORIS LEAF, *Kansas State College.*—The assumption in Gibbs' thermodynamics that one value of the pressure suffices to describe a phase in absence of external forces is inadequate. A pressure function must be defined whose gradient at any interior point balances at equilibrium the resultant of external forces and average forces of molecular interaction. We consider as thermodynamic system a differential element with pressure a function of coordinates, as in hydrodynamics. The equilibrium conditions become: constant temperature; pressure which is a continuous function of coordinates, but not necessarily constant; constant values for each species of the sum of its chemical potential and the potential of all forces, external or average intermolecular, acting on it. Quantum statistical mechanics gives results in agreement with the above, if, in conformity with the virial theorem, partial pressure P_i, satisfies, in the usual notation,

$$P_i dV = kT\Sigma_i[\partial \ln X_i(\text{max.})/\partial g_{iu}]dg_{iu}.$$

Each chemical species in a multicomponent system satisfies the usual equations for a one-component system; its intrinsic thermodynamic functions depend on its temperature and density alone.

Cosmic Rays

M1. Pretreatment of Nuclear Emulsions for Cosmic-Ray Exposures. HERMAN YAGODA AND NATHAN KAPLAN, *National Institutes of Health.*—The variable background accumulated since manufacture is eradicated by means of hydrogen peroxide vapor.[1] Additional light nuclei are incorporated by loading from a 10 percent lithium borate solution containing 5 percent glycerine. Plates are dried under reduced pressure to remove free water and are assembled in pairs with emulsion layers in contact. Several points on one member are infected with RaF, U, or Sm during the last stages of drying. The assembled pairs are wrapped in black paraffined paper to reduce subsequent access of moisture. On development the upper plate carries an autoradiograph of the infection points which permits microscopic alignment of the processed gelatin layers. The grain density of the developed alpha-tracks also serves as an indicator for latent image fading. Tracks initiated in one emulsion can be followed into the adjoining plate, thereby doubling the effective thickness of the emulsion. Preliminary exposures indicate a nuclear evaporation rate (stars per ml per day) dependent on geomagnetic latitude as well as altitude:

Altitude	Geomagnetic latitude		Ratio 50°N/1°S
	1°S	50°N	
Sea level	0.1	0.6	6
4,530 meters	3.0	20	7
27,000 meters	—	1470	—

Examples of complex nuclear evaporations recorded at sea level will be described.

[1] H. Yagoda and N. Kaplan, Phys. Rev. **73**, 634 (1948).

M2. Absorption of the Hard Component of the Cosmic Radiation in the Stratosphere.* MARCEL SCHEIN, VICTOR H. YNGVE, AND THEODORE BOWEN, *University of Chicago.*—The cosmic-ray absorption curve at 5.7 cm Hg was measured using lead thicknesses of 0, 2, 4, 8, 12, 18, and 30 cm. A large number of multiples under two centimeters of lead were found. They show little change in number between 10 cm Hg and 5.7 cm Hg and closely follow the soft com-

ponent as measured with the same apparatus. They are interpreted as being electronic showers. Multiples under 18 cm lead were also measured and show an increase of about 40 percent between 10 cm Hg and 5.7 cm Hg. This corresponds to a cross section for the production of the multiples approximately equal to the geometrical cross section of an air nucleus.

* This work and that reported under M5 and M8 was assisted by the Joint Program of the Office of Naval Research and the Atomic Energy Commission.

M3. Observations on Heavy Nuclei in Cosmic Radiation. E. P. NEY, P. FREIER, E. J. LOFGREN, AND F. OPPENHEIMER, *University of Minnesota.*—Evidence was previously presented for the existence of heavy nucleii as a component of primary cosmic radiation.[1] Approximately 300 particles have now been observed in three high altitude flights. Cloud chambers and photographic plates have been used for detection of the particles. The spectrum of atomic numbers has been investigated in a preliminary way and better approximations to the atomic numbers of the particles have been obtained by counting "δ-rays" along the tracks. The "δ-ray" count on the heavy particle tracks has been compared with the corresponding count on α-particles tracks.[2] The mean free path for nuclear collisions will be discussed. An approximate value of 4 for the ratio of the number of protons to helium nucleii has been obtained. Estimates of the energy and flux of the heavy component will be presented. Examples of heavy particle tracks, including one which stops in a photographic emulsion, will be shown.

[1] Freier, Lofgren, Ney, Oppenheimer, Bradt, and Peters, Phys. Rev. **74**, 213 (1948).
[2] The α-particle plates were kindly furnished by Eugene Gardner, Radiation Laboratory.

M4. Star Production at High Altitudes.* P. S. FREIER, E. J. LOFGREN, E. P. NEY, AND F. OPPENHEIMER, *University of Minnesota.*—Nuclear disintegrations in Ilford C2 emulsions have been observed at altitudes from 84,000 feet (24 g/cm^2 of residual atmosphere) to 95,000 feet (14 g/cm^2) on flights with General Mills balloons. One balloon went to 70,000 feet, broke, and descended. This made it possible to correct roughly for the stars produced during the ascent and descent on the other flights which stayed aloft. For stars of more than four prongs there appears to be a decrease with increasing altitude in the rate of production above 84,000 feet. This is evidence for a maximum in the number of stars produced as a function of altitude. The rate of production of stars with more than four prongs at these altitudes is approximately 1000 stars per cc per day compared to 10.5 stars per cc per day at 9200 feet.[1]

* Assisted by the joint program of the Office of Naval Research and the Atomic Energy Commission.
[1] Lattes, Occhialini, and Powell, Nature **160**, 489 (1947).

M5. The Origin of Large Cosmic-Ray Bursts at an Altitude of 3500 Meters. E. F. FAHY AND MARCEL SCHEIN, *University of Chicago.*—Experiments on large bursts have been continued at Climax, Colorado with a Carnegie Model C meter surrounded by large thicknesses of lead. The measured burst frequency is decreased by a factor of 1.52 on increasing the spherical lead shield from 10.7 cm to 26.7 cm in thickness. This means that the burst-producing radiation has a mean range of 410 g/cm^2. A discussion of the zenith angle dependence, of the intensity per unit solid angle of the burst-producing radiation, will be given by comparing the absorption in a flat absorber of finite area with the absorption in a spherical absorber. The fact that the burst-producing radiation is more absorbable in the atmosphere than in lead can be explained by postulating that this radiation is made up of π mesons with a mean life of less than 4×10^{-8} second.

M6. Note on the Light-Particle Hypotheses of Penetrating Particles in Extensive Cosmic-Ray Showers. K. SITTE, *Syracuse University.*—The momentum spectrum of penetrating particles in extensive showers has recently been measured in air (Mitra) and under about 10 cm lead (Rochester and Butler), and has been found similar to that of single mesons, with average momenta of $\gtrsim10^9$ ev/c. This result, together with earlier observations on frequency and secondary-production of penetrating particles in large air showers, is shown to rule out the suggestions put forward by Auger and by Jánossy that the penetrating component of extensive showers consists of a new type of fundamental particles with a mass between 3 and 10 electron masses. It is more likely that these particles are protons and/or other particles of strong nuclear interaction, with a mean path between two collisions of about 100 g/cm^2, which are not "catastrophically" absorbed in a single collision, but eject what might be called "knock-on protons."

M7. Production of Neutrons by the Capture of Cosmic-Ray Mesons.* GORDON W. MCCLURE AND GERHART GROETZINGER, *University of Chicago.*—We have reported the production of neutrons by the capture of negative mesons in lead at sea level.** Because of the use of a magnetic deflection system in the meson telescope the number of recorded events was small so that the estimate of two neutrons per captured meson is afflicted with a considerable error. In continuing the experiment on the summit of Mt. Evans we recorded 16 events in which the stoppage of a negative meson was followed within 80μsec. by a discharge of one of the BF_3 counters in the neighborhood of the stopping plate, and only one such event for a comparable number of positive mesons. From a determination of the efficiency of these counters one obtains an average of 4 to 7 neutrons per captured meson under the assumption that the neutrons are ejected with an energy of several Mev.

* This research was supported in part by the Office of Naval Research.
** Gerhart Groetzinger and Gordon W. McClure, Phys. Rev. **74**, 341 (1948).

M8. Nuclear Disintegrations and Mesons in the Stratosphere. JERE J. LORD AND MARCEL SCHEIN, *University of Chicago.*—A series of experiments is in progress to study the events occurring in nuclear research emulsions (photographic plates) which are placed beneath various thicknesses of absorbing material. These plates, covered with

lead, have been exposed to cosmic radiation at free balloon altitudes. Most of the plates have been examined and results will be given as to the variation in numbers of the various types of mesons and nuclear discriptions with thickness of absorber. Additional data are also available for plates exposed similarly but covered with paraffin and carbon.

M9. On the Decay Products of the μ-Meson. E. P. HINCKS AND B. PONTECORVO, *Chalk River Laboratories.*—With an arrangement previously described,[1] the penetration in carbon, aluminum, and lead, of the particles from the 2.2-μsec. meson decay has been investigated. A soft and a hard component can be clearly distinguished. The former is essentially absorbed by ~26 g/cm² carbon, a thickness equivalent to the maximum range of 50 Mev electrons. The latter is found with both high and low Z absorbers, and gives an observed rate of the order of 1/20 of the initial total intensity (without absorber), and about ten times the casual rate. In a new arrangement designed to investigate the "hard component" five counter trays are used, from top to bottom, A, B, C, D, E. Mesons are stopped between B and C, and the decay particle absorber between C and E is divided by the intermediate tray D. Experiments in which the absorber was 16.6+16.6 =33.2 g/cm² lead indicate that the delayed events $(CE)_{del}$ are rarely, if ever, accompanied by $(D)_{del}$. If we interpret this as a demonstration that the "hard component" is the result of bremsstrahlung by the particles of the "soft component" we can conclude that the latter have indeed a mass not greater than one electron mass. Further experiments on the "hard component" in the case of low Z absorbers are in progress.

[1] E. P. Hincks and B. Pontecorvo, Phys. Rev. 74, 697 (1948). See also, J. Steinberger, Phys. Rev. 74, 500 (1948).

M10. Diurnal and Seasonal Variation in Frequency of Occurrence of Small Cosmic-Ray Bursts.* R. M. WHALEY** AND V. A. LONG,*** *University of Colorado.*—Further analyses have been made of data taken during 18 months in 1938–1939 with a heavily shielded high pressure ionization chamber.[1] A total of 25,161 bursts were analyzed. An integral frequency-size plot parallels in general that calculated by Christy and Kusaka for spin zero mesons, thus agreeing with other burst data by Schein and Gill and analyses by Lapp. However, the small bursts produced by the order of 100 particles occur approximately four times more frequently than expected. Furthermore, they show marked seasonal variations, having a maximum frequency in winter over 2.5 times that observed in summer. They exhibit strong diurnal variations, being most frequent during the day; a diurnal amplitude of 30 percent of the mean value is observed in winter. Broxon[2] has shown that these small bursts have a large negative barometric pressure coefficient and are related to sunspot area.

* Preparation of paper assisted by contract with Office of Naval Research.
** Now at Purdue University.
*** Now at Colorado School of Mines.
[1] V. A. Long, R. M. Whaley, Phys. Rev. 59, 470 (1941).
[2] J. W. Broxon, Phys. Rev. 72, 1187 (1947).

M11. Relation of the Cosmic Radiation to Sunspot Magnetic Moments. JAMES W. BROXON, *University of Colorado.*—A function $(SS-MM)$ designed to represent the arithmetic sum of the magnetic moments of all visible sunspots has been compared statistically with the intensity of the cosmic radiation (C−R). Large pulses (20 to 30 percent) in $SS-MM$ were found to occur out of phase with primary pulses in C−R. $SS-MM$ pulses of comparable magnitude bore different phase relations to subsidiary pulses in C−R. For subsidiary pulses preceding the primaries, the C−R was generally high when the $SS-MM$ was increasing and low when it was decreasing. For subsidiary pulses following the primaries, the C−R was generally high when the $SS-MM$ was decreasing and low when it was increasing. The analysis was carried out for intervals of 60 days preceding and following the selected days of high or low C−R. Some consideration was given to the e.m.f. generated in connection with an imaginary but in some respects representative sunspot by electromagnetic induction. This work was supported in part by the Office of Naval Research.

Nuclear Scattering and Nuclear Resonance

N1. Some Calculations Concerning Neutron-Proton Scattering. J. M. BLATT AND J. D. JACKSON, *Massachusetts Institute of Technology.*—A Schwinger variational method gives an expansion of $k\cot\delta$ in powers of the energy (or k^2). A previous analysis[1] of available scattering data was made on the assumption that the third and higher terms of the expansion are negligible, in which case the experimental data give no information about the shape of the potential well. We have obtained approximate values of the third term $(-Tk^4)$ for square, Gaussian, exponential, and Yukawa well shapes for all relevant ranges and depths, neglecting the tensor force. $|T|$ is smaller than $0.15r^3$ for these wells (r=effective range), about three times to small to have been detected by experiments to date. If the tensor force does not increase T appreciably, the analysis of reference (1) is valid for these four well shapes. We also obtained a qualitative understanding of the shape dependence of T.

[1] J. M. Blatt, Phys. Rev. 74, 92 (1948).

N2. Electrostatic Scattering of Neutrons. S. M. DANCOFF AND S. D. DRELL, *University of Illinois.*—Recent experiments of Havens, Rabi, and Rainwater,[1] and of Fermi and Marshall[2] indicate a weak electron-thermal neutron interaction with a cross section not greater than 4×10^{-31} cm². According to meson theory this interaction may be interpreted as electrostatic scattering by the electron of the neutron, which exists part of the time as a proton plus negative meson. To calculate the cross section, the neutron and proton are treated as two charge states of a nucleon which obeys Dirac's equation and is coupled to a meson field of zero spin. A third order perturbation calculation is performed, a sample scheme of which has the neutron, by virtue of its interaction with the meson field,

become a proton and negative meson. Either proton or meson is then scattered in a fixed Coulomb potential before they recombine to form the scattered neutron. The calculated cross section is velocity independent for thermal neutrons, proportional to g^4, where g is the (dimensionless) coupling constant between the nucleon-meson fields, and is of the experimentally observed order of magnitude for $g^2 \sim \frac{3}{16}$ in a weak coupling approximation.

[1] Havens, Rabi, and Rainwater, Phys. Rev. 72, 634 (1947).
[2] Fermi and Marshall, Phys. Rev. 72, 1139 (1947).

N3. Angular Distribution of 14-Mev Neutrons Scattered by Protons. H. H. BARSCHALL AND R. F. TASCHEK, *Los Alamos Scientific Laboratory.*—Monoenergetic 14-Mev neutrons were produced by bombarding a tritium target with 200-kev deuterons. Proton recoils originating in a thin polythene radiator could pass through three proportional counters arranged in a direction perpendicular to the radiator, and coincidences in the three counters were observed. By rotating the foil and the counters about the center of the foil the angular distribution of the recoiling protons could be measured. The angular resolution was $\pm 10°$ in the center of mass system. Protons corresponding to neutrons scattered through 90°, 120°, 150°, and 180° in the CM system were observed. Within the statistical accuracy of five percent at each angle the angular distribution of the scattered neutrons appeared isotropic in the center of mass system.

N4. Consideration of Multiple Scattering in the Evaluation of Cloud-Chamber Tracks.* MARTIN BERGER AND GERHART GROETZINGER, *University of Chicago.*—H. A. Bethe analyzed the influence of multiple scattering on the curvature of cloud-chamber tracks as projected on a plane perpendicular to the magnetic field on the basis of approximating the entire track by a section of a circle.** A method will be described in which the track is divided into sections whose curvatures are determined individually. According to the theory of multiple scattering these curvatures constitute a sample of a normally distributed population.*** A function of the mean and a function of the variance are distributed according to a "Student t" and a "χ^2" distribution, respectively, which determine the probabilities for mean and variance to be within specified limits. These parameters, which are functions of the momentum, mass, and charge of the particle, provide an estimate of two of these quantities with an accuracy increasing with the number of sections into which the track can be reasonably divided.

* This work was supported in part by the Office of Naval Research.
** H. A. Bethe, Phys. Rev. 70, 821 (1946).
*** B. Rossi and K. Greisen, Rev. Mod. Phys. 13, 240 (1941).

N5. Cloud-Chamber Tracks of Positive Particles Branching from Beta-Rays.* GERHART GROETZINGER, FRED RIBE, AND LLOYD SMITH,** *University of Chicago.*—In four cases tracks of positive particles branching from tracks of negative beta-particles originating in a P_{32} source have been found. In none of these cases could a change in direction of the beta-ray at the branch point be detected, but in at least two cases a change of curvature. The positives emerge at angles of from 50° to 86° with the forward direction of the beta-ray. Their scattering and ionization are similar to that of positrons with tracks of the same curvature, and energies between 90 and 640 kev. The only known process in which branching of an electron track occurs is electron-electron scattering. The possibility of the "positive" tracks being tracks of multiply scattered electrons has been considered, using Bethe's criteria and a method described in the previous abstract. These considerations and considerations concerning the observed angles exclude the possibility of electron-electron scattering.

* This research was supported in part by the Office of Naval Research.
** Now at the Radiation Laboratory, University of California.

N6. Angular Distribution of 1- to 3.5-Mev Protons Scattered by He^4. GEORGE FREIER, EUGENE LAMPI, W. SLEATOR, AND J. H. WILLIAMS, *University of Minnesota.*—The angular distributions of protons scattered by He^4 have been measured in the energy range from 1 to 3.5 Mev with the scattering chamber previously described.[1] By counting both protons and recoil He^4, values of the cross section could be obtained over an angular range of 10° to 160°. The results of this experiment essentially confirm those of Heydenburg and Ramsey[2] in which the existence of a resonance due to an excited state of Li^5 was established.

* This work was supported in part by the Office of Naval Research.
[1] Blair, Freier, Lampi, Sleator, and Williams, Phys. Rev. 74, 553 (1948).
[2] N. P. Heydenburg and N. F. Ramsey, Phys. Rev. 60, 42 (1941).

N7. On the Scattering of Fast Neutrons. H. FESHBACH AND V. F. WEISSKOPF, *Massachusetts Institute of Technology.*—Measurements by Sherr[1] and Amaldi[2] of the total cross section σ_t of neutrons of 14 mev and 25 mev respectively were used by these authors to determine the nuclear radius R from $\sigma_t = 2\pi R^2$. This relation is valid only in the limit $\lambda \ll R$. A more accurate relation can be obtained only by defining the boundary conditions at the nuclear surface. We assumed that, inside the surface, the neutron wave function consists of an ingoing wave only, of a high wave number corresponding to nuclear kinetic energies. This is a formal expression of the usual assumption that the neutron, after entering into the nucleus, will surely form a compound system. It leads to values of σ_t 20 to 40 percent higher than $2\pi R^2$. The new values of R lie much closer to the conventional expression $1.5 \times A^{\frac{1}{3}} \times 10^{-13}$. This result is not very sensitive to the choice of boundary conditions.

[1] R. Sherr, Phys. Rev. 68, 240 (1945).
[2] Amaldi, Bocciarelli, Cacciapuoti, and Trabacchi, Nuovo Cimento 3, 203 (1946).

N8. Polarization of *d-d* Neutrons. LINCOLN WOLFENSTEIN, *Carnegie Institute of Technology.*—Procedures for polarizing fast neutrons by scattering have recently been suggested by Schwinger.[1] Since a second scattering is needed to detect the polarization the suggested experi-

ments are very difficult. However, it is possible that fast neutrons may be already polarized when they are produced with the consequence that a double-scattering experiment is not necessary. A recent analysis[2] of the *d-d* reactions near the the threshold indicates a large contribution to the cross section from incoming *p*-waves and also a large amount of spin-orbit coupling. These are the necessary (although not sufficient) conditions for the outgoing neutrons (or protons) to be polarized. If only incoming *s*-waves and *p*-waves are considered the polarization is proportional to $\sin\theta\cos\theta$, where θ is the outgoing angle. The direction of polarization is perpendicular to the plane of the reaction. For a deuteron energy of 500 kev, the polarization (for $\theta=45°$) may be anywhere between 0 and 50 percent, with the most likely value around 20 percent. The polarization might be detected by one of Schwinger's methods.[1]

[1] J. Schwinger, Phys. Rev. **69**, 681 (1946); **73**, 407 (1948).
[2] E. J. Konopinski and E. Teller, Phys. Rev. **73**, 822 (1948).

N9. Double Refraction and Polarization of Neutron Beams. OTTO HALPERN, *University of Southern California*.—The magnetic double-refraction[1] of neutrons can be utilized to obtain completely polarized neutron beams with an intensity loss of only 50 percent of the primary beam. For this purpose a well defined neutron beam of moderate spread in wave-length is allowed to fall on a sheet of iron which can be magnetized. To obtain a maximum effect the direction of magnetization should be chosen parallel to the projection of the beam on the iron sheet. Total reflection will then occur for the two spin states at different critical glancing angles which will be smaller and larger than the critical angle for unmagnetized iron. Theory leads in the case of iron to values of 12.5 minutes and 6 minutes, respectively. Variation of the direction of magnetization should permit a test of the assumed expression for the interaction energy of the magnetic moments of neutron and ion.

[1] Halpern, Hamermesh, and Johnson, Phys. Rev. **59**, 981 (1941). The formula preceding (5.1) suffers from misprints; the denominator obviously is k^2 and not k; furthermore $+1$ must be added to the right side.

N10. The Hyperfine Structure of Tritium. EDWARD B. NELSON AND JOHN E. NAFE, *Columbia University*.—The h.f.s. of the ground state of tritium was measured by the atomic beam magnetic resonance method. The apparatus previously used in the measurement of the h.f.s. of H and D was modified to permit the recirculation of a small sample of tritium. The frequency of the field independent, central Zeeman component of the transition $F=1\leftrightarrow F=0$ gives the h.f.s. almost exactly with a field correction of less than 0.001 Mc. The mean of three independent determinations of the h.f.s. in different weak magnetic fields is 1516.702 ± 0.010 Mc. The probable error is caused by the uncertainty in the Doppler correction and possible asymmetry in the resonance line causing a shift of the center of the line. The reproducibility of determining the center of the resonance line was ±0.002 Mc. The theoretical value of the h.f.s. based on the triton-proton moment ratio[1] and the value of the h.f.s.[2] of H is 1516.709 ± 0.015 Mc. The theoretical and experimental values agree within the probable error in the ratio of the moments, 1 part in 10^5. This close agreement is in accord with the calculations of Teller,[3] who has considered the detailed interaction of the electron with the elementary particles of the triton. We thank the Atomic Energy Commission for the loan of a sample of tritium gas.

[1] F. Bloch, A. C. Graves, M. Packard, and R. W. Spence, Phys. Rev. **71**, 551 (1947).
[2] J. E. Nafe and E. B. Nelson, Phys. Rev. **73**, 718 (1948).
[3] E. Teller, Pocono Conference, sponsored by the National Academy of Science, April 1, 1948.

Liquid and Solid States

P1. Studies on the Size and Shape of Tactoids.* W. HELLER AND W. WOJTOWICZ, *Wayne University*.—Colloidal solutions of orthorhombic rodlike crystals of V_2O_5 were used as model systems for studying the conditions for and the rate of formation of the anisotropic concentrated phase (tactoid phase), discovered by Zocher, which is in thermodynamic equilibrium with the dilute isotropic phase. Extensive distribution curves of size and shape of tactoids were compiled by means of photomicrography. Above a certain critical colloidal concentration, which depends on ionic strength, microscopic tactoids are formed. The rate of their formation increases with the colloid concentration and with the concentration of sensitizing electrolyte. The number average size of tactoids increases with the colloid concentration and it decreases, at constant colloid concentration, with increasing electrolyte concentration. The axial ratio of the tactoids increases with decreasing colloid concentration and it increases, at constant colloid concentration, with the concentration of sensitizing electrolyte. The extreme shapes of tactoids are represented by nearly spherical spindles and practically rodlike particles. The factors determining the size of tactoids are the rate of nucleus formation, and the rate of growth of the nuclei. The factors determining the shape appear to be the potential energy of the primary particles within the tactoid and the interfacial energy (anisotropy of the interfacial energy) of the tactoid with respect to the dilute phase.

* This work was supported by the Research Corporation.

P2. Undercooling and Nucleation of Liquid Metals. BEN H. ALEXANDER, *Sylvania Electric Products, Inc.*—The variations of undercooling with overheating for several high purity metals of different crystal structures have been determined. In confirmation of the previous limited amount of work on this subject, it was found that the undercooling increased rapidly with overheating, then more slowly, and finally was no longer affected by overheating 200–300°C above the melting point. Also the F.C.C. and H.C.P. metals exhibit small undercooling (2 to 5°C) even at high overheating. The metals of more complex structure, rhombohedral and tetragonal, show undercooling up to 50°C and more. The effect of overheating is explained by assuming the presence of foreign particles which serve as nuclei. These are either destroyed or de-

activated by overheating. The effect of crystal structure is explained by the variations in interfacial energy between the solid and liquid states, the relative values of which can be approximated. There appears to be a further effect caused by the thermal properties of the metal which also influences the undercooling.

P3. Magnetic Refraction of Neutrons at Domain Boundaries. D. J. HUGHES, M. T. BURGY, R. B. HELLER, AND J. W. WALLACE, *Argonne National Laboratory.*—In the course of experiments on the production of polarized neutrons, small angle scattering (or the order of one minute) of neutrons in unmagnetized iron was observed. Further detailed experiments on the angular distribution and variation with iron thickness of the scattering have been performed. The RMS scattering angle at a single domain boundary is 0.027 minute and the deviation is found to increase with the square root of the number of domains traversed. The results are compared with theory and are shown to be consistent with the hypothesis that the scattering is caused by magnetic refraction of the neutrons at domain boundaries. The index of refraction is expected to have two values in unmagnetized iron and refraction takes place at boundaries where the index changes.

P4. Some Simple Theorems on the Free Energies of Crystal Surfaces. CONYERS HERRING, *Bell Telephone Laboratories.*—An understanding of the effects of various kinds of heat treatment on the structure of crystal surfaces is important in many problems of electron emission, adsorption, etc. Though the changes involved generally occur under non-equilibrium conditions, it is helpful to know something about the relative free energies of different surface structures. Ideas similar to those used in Wulff's equilibrium polyhedron construction can be applied to the problem of thermal etching of a large plane surface. In order that it be possible to lower the free energy of an initially smooth surface by rearranging the atoms into a hill-and-valley structure, it turns out to be necessary and sufficient that the initial plane should fail to occur among the boundary planes of the equilibrium polyhedron. It is also easily shown that if the energy of the crystal can be written as a sum of pair interactions all of one sign and if the surface and interior lattice spacings are the same, the Wulff polyhedron is in a sense "degenerate" and the hill-and-valley structure is never favored. These results also have a bearing on the amount of rounding of edges and corners which is to be expected.

P5. Photoelectric Determination of the Fermi Level at Surfaces of Amorphous Arsenic. E. TAFT AND L. APKER, *General Electric Research Laboratory.*—Evaporated surfaces of amorphous As exhibit photoelectric emission that is characteristic of a semi-conductor. Spectral and energy distributions for electrons ejected from this material were obtained and interpreted by the methods previously applied to Te, Ge, and B.[1] The results indicated that the Fermi level lay above the top of the occupied band by an amount $\delta = 0.5$ ev. Effects due to this energy structure were more pronounced and clear-cut than those for the elements investigated before. Except for the relatively large value of δ, however, the distributions were similar to those for crystalline Te. In particular, the "stopping potential" corresponding to the edge of the filled band was as sharp for the amorphous As as for the Te. The estimated density of surface states was 10^{10} cm^{-2}, an unusually low value. The work function was 4.66 ev. Thermoelectric measurements showed that the deposits were *N*-type. The resistivity ($\sim 10^7$ ohm cm) decreased rapidly with increasing temperature.

[1] Apker, Taft, and Dickey, Phys. Rev., in press.

P6. Correlation of Geiger-Counter and Hall-Effect Measurements in Alloys Containing Germanium and Radioactive Antimony 124. G. L. PEARSON, J. D. STRUTHERS, AND H. C. THEUERER, *Bell Telephone Laboratories.*—Ingots of germanium-antimony alloys have been prepared from standard high back voltage germanium and radioactive antimony 124.[1] The amounts of antimony added were 0.054, 0.0081, and 0.00078 percent. Radioautographs indicate that the antimony concentration varies exponentially with the depth in the ingot, being greatest at the top which was the last to freeze. Geiger-counter measurements on specimens from various positions give a quantitative analysis of the antimony distribution. Hall-effect measurements on the same specimens show that in the saturation region of the impurity range each antimony atom produces one conduction electron. Having correlated the Geiger-counter and Hall-effect measurements, one can make accurate impurity atom counts in non-radioactive ingots. An *N*-type high back voltage germanium ingot to which no impurity had been deliberately added has an excess of 1.8×10^{14}/cc donor over defect impurity atoms at the bottom of the melt compared with 1×10^{15}/cc near the top of the melt.

[1] The antimony 124 used in this investigation was supplied by Clinton Laboratories and obtained on allocation from the U. S. Atomic Energy Commission.

P7. Sintering of Metallic Particles. G. C. KUCZYNSKI, *Sylvania Electric Products, Inc.*—Spherical copper powder 5μ–80μ in diameter was sintered to the flat copper blocks at temperatures ranging from 400°C to 1000°C for various periods of time. It was found that at given temperature $(x/a)^6 \sim t$ where x is the radius of the junction formed between the spherical particle and the crystal block, a the original radius of the particle and t the time of sintering. This relationship seems to disprove the theory of J. Frenkel* that the sintering is caused by the viscous flow under the action of surface tension. If this would be the case the square instead of fifth power relationship should be obtained. The analysis of the found relationship suggests that the sintering of metallic particles is caused by volume and surface diffusion with the latter one predominant for smaller particles and lower temperatures.

[* J. Frenkel, J. Phys. U.S.S.R. IX, 385–391 (1945).

P8. The Index of Refraction of Evaporated Films of LiF. L. G. SCHULZ, *University of Chicago.*—Thin films prepared by evaporating LiF in a vacuum on to glass substrates were examined with an Abbe refractometer. It was found that contact liquids entered and filled most of the voids in the porous structure of the films, thereby changing their optical density. From the variation of the index of refraction of a film with different contact liquids it was possible to calculate the extent of the voids accessible to the liquid, as well as those inaccessible. Films 70,000A thick contained 25 percent by volume of voids of which about 1 percent was inaccessible. The calculated index of refraction of such a film in air is 1.29. A similar value was obtained from measurements made with a Michelson interferometer. Thinner films were slightly more porous and accordingly had a lower index of refraction in air.

P9. Concerning the Work of Polarization in Ionic Crystals of the NaCl Type. I. Polarization Around a Single Charge in the Rigid Lattice.* E. S. RITTNER, R. A. HUTNER, AND F. K. DU PRÉ, *Philips Laboratories.*—Many problems dealing with ionic solids require quantitative calculations of the polarization work resulting from the removal of one or of two adjacent charges. The former problem reduces to finding the potential field at the origin due to all induced dipoles. The dipole-dipole interactions introduce such great difficulties that only approximate solutions have been obtained heretofore, the best of which is that of Mott and Littleton.[1] Examination of their method for the rigid lattice reveals extremely irregular variation of the dipole moments with distance as well as unexpected excellent agreement between the first and fourth order polarization work. To gain more insight we have carried out modified higher order approximations involving ten simultaneous linear equations. Solutions were obtained for us by the use of the R.C.A. "Electronic Simultaneous Equation Solver."[2] Rapid convergence of the numerical results occurs for the modified approximations of higher order than the third for the hypothetical monatomic crystal[1] and for NaCl. The excellence of the values obtained by the Mott-Littleton first order approximation is found to be somewhat fortuitous.

* This work was supported in part by the Air Materiel Command.
[1] Mott and Littleton, Trans. Faraday Soc. 34, 485 (1938).
[2] Goldberg and Brown, J. App. Phys. 19, 339 (1948).

P10. Concerning the Work of Polarization in Ionic Crystals of the NaCl Type. II. Polarization Around Two Adjacent Charges in the Rigid Lattice.* R. A. HUTNER, E. S. RITTNER, AND F. K. DU PRÉ, *Philips Laboratories.*—Previous polarization calculations for the removal of two adjacent charges are reviewed and extended. The method of Klemm[1] neglects dipole-dipole interactions and thus leads to values which are too high. The Mott-Littleton[2] method, employing zero and first order approximations, has been applied by us to this problem. The latter approximation led to two sets of four simultaneous linear equations, which were solved by the use of the R.C.A.[3] machine. Numerical results are given in Table I.

TABLE I. Polarization work in ev for different degrees of approximation.

	Klemm	Zero order	First order
NaCl	1.51	0.94	1.11
RbCl	1.20	0.77	0.92

* This work was supported in part by the Air Materiel Command.
[1] Klemm, Zeits. f. Physik 82, 529 (1933).
[2] Mott and Littleton, Trans. Faraday Soc. 34, 485 (1938).
[3] Goldberg and Brown, J. App. Phys. 19, 339 (1948).

P11. Relation Between Residual Strain Energy and the Elastic Moduli. CLARENCE ZENER, *The University of Chicago.*—It is shown from theoretical considerations that the presence of residual elastic strain energy will be associated with a reduction of the shear modulus and of the Young's modulus. A semi-quantitative theory is derived between the total residual elastic strain energy and the lowering of these moduli. This relation is seen to be consistent with the observations of Köster's upon the lowering of Young's modulus by the introduction of solute atoms of small solubility. This effect of strain energy in lowering the elastic moduli is shown to be of importance in the diffusion of interstitial atoms, such as in the diffusion of carbon in iron. As the solute atom passes over the potential energy barrier between two stable interstitial positions, the lattice acquires additional strain energy, which in turn is associated with a lowering of the elastic moduli, and hence, with an increase in the entropy of the system. This increase in entropy may be sufficiently large to result in a large increase in diffusion rate.

P12. A New Criterion of Slip in Thin Single Al Crystals. T. L. WU AND R. SMOLUCHOWSKI, *Carnegie Institute of Technology.*—Observations of slip in thin flat specimens of aluminum single crystals under tension show that the Boas and Schmidt criterion of maximum resolved shear stress $S(B.S.)=(F/A)\cos\phi\cos\lambda$ where F is the applied load, A the cross section, ϕ angle between direction of load and normal to the slip plane and λ angle between direction of load and the slip direction, does not apply in this case. Rather it appears that in such specimens slip occurs in the direction in which the resolved shear divided by the thickness of the specimens in that direction is maximum. A corresponding formula $S(S.W.)=(F/Ad)\cos^2\phi\cos\lambda/\sin\theta$, where d is the relative thickness of the specimen and θ angle between slip direction and the surface of the specimen measured in the slip plane, is derived and compared with experimental data which confirm it without exception. At higher elongations a new slip system sets in and this also complies with the new formula. In one case duplex slip has been observed corresponding to simultaneous slip in two directions both of which satisfy the new criterion. A possible reason for this dependence of slip mechanism on the thickness of specimens is suggested.

P13. Internal Friction and Slip in Thin Single Aluminum Crystals. R. SMOLUCHOWSKI AND T. L. WU, *Carnegie Institute of Technology.*—An apparatus for measuring internal friction of thin strips has been designed, and internal friction has been measured in single aluminum

crystals as a function of elongation. Specimens were etched out from the same crystal and electrolytically polished to the proper thickness. The original thickness was so adjusted that after elongation all had the same final thickness. The damping was measured at the resonant frequency of about 300 cycles, at the constant strain amplitude of 10^{-6} and at a pressure of $\frac{1}{10}$ mm Hg. The results indicate: (1) That the dependence of internal friction on elongation varies with the orientation of the crystal and the respective slip system; (2) A plot of this dependence for each specimen shows two maxima—the first maximum being related to the onset of a second slip system; (3) With increasing strain amplitude the second maximum becomes higher and shifts towards higher elongation; (4) Decrease of internal friction as a function of time (recovery) has been measured at room temperature; (5) Internal friction measured parallel to the slip lines is lower than perpendicular to them. The observations are interpreted in terms of theory of dislocations.

Papers Not Classed Elsewhere

Q1. Diffraction Patterns of Electromagnetic Waves Near Rods and Apertures. C. L. ANDREWS, *General Electric Company.*—The diffraction patterns of microwaves by rods and apertures have been measured on the sides toward and away from the source and in the planes of the apertures themselves. These patterns were most easily explained as the resultant of the direct geometrically propagated beam and reradiation from rods or edges of apertures. The interference pattern of a single rod parallel to the electric field of an incident plane wave was approximately a set of parabolas. The maximum intensities in the pattern of two rods or of a slit were at the intersections of the two sets of parabolas. The positions of maxima and minima of intensity and the relative intensities were checked with theory.

Q2. A Double Focusing Mass Spectrometer.* ALFRED O. NIER, T. R. ROBERTS, AND E. G. FRANKLIN, *University of Minnesota.*—A double focusing mass spectrometer has been constructed in which mass separation is accomplished by sending the ion beam through a 90° electric condenser followed by a 60° magnetic field. The use of different object and image distances in the magnetic analyzer serves to reduce the usual second-order aberration caused by the diverging ion beam. Although extremely stable electronic supplies are employed, even greater stability is insured by having an ordinary 60° mass spectrometer in the same magnetic field. Both spectrometers obtain their accelerating and deflection voltages from a common voltage divider across a high voltage supply. The auxiliary spectrometer employs a split ion collector. A change in either the magnetic field or high voltage supply sends a differential signal from the split ion collector through an amplifier into the high voltage supply. Because of the high gain in the inverse feed-back loop involved, the effect of the initial change is almost eliminated. Preliminary tests indicate than equivalent stability approaching one part in 10^6 may be reached. The resolution of one in several thousand will permit the precision determination of atomic masses or the analysis of gaseous mixtures where the gases have the same mass numbers but different packing fractions.

* Assisted by the joint program of the ONR and the AEC

Q3. Measurement of Electron Mobility by Means of Pulse Techniques.* F. F. RIEKE AND DARYL ERRETT, *Purdue University.*—Low energy electrons are set free in an ionization chamber by means of 0.5-microsecond pulses of 300-kilovolt electrons. A uniform electric field is produced within the chamber by plane parallel electrodes and intermediate potential-distributing rings. The central portion of one of the electrodes is insulated from the rim and serves as a collector. For measuring the collection time, the current to the collector is amplified and displayed on an oscilloscope having a calibrated driven sweep. Preliminary measurements, carried out primarily to test the method and apparatus, have been made with dry air for the pressure range 1–68 mm and with tank nitrogen for the range 2–344 mm. The range of applied electric fields was 5–275 volts/cm. With a chamber 15 cm long,measured collection times ranged from 3 to 40 micro-seconds. The electron mobility was found to rise with increasing field for low fields, and then to fall after going through a maximum. For the higher pressures the rise in mobility was more pronounced than for the lower pressures. For example, in tank nitrogen at 4 mm pressure the mobility is 70×10^3 cm²/volt. sec. at 5 volts/cm and rises to 110×10^3 units at 23 volts/cm.

* Assisted by ONR.

Q4. On the Characteristics of the Parallel Plate Spark Counter. LEON MADANSKY AND R. W. PIDD, *Johns Hopkins University.*—A parallel plate spark counter was constructed[1] to provide a uniformly sensitive avalance volume for detecting ionizing radiations. Further work has shown that the rise time and average delay error time is compatible with time interval measurements of 10^{-9} sec. The recovery time of the counter is critically dependent on the cathode material suggesting some sort of surface emission phenomena. However, recovery times of one millisecond are obtained with lead and ten cathodes. Quantitative results on all the characteristics of the counter will be given.

[1] L. Madansky and R. W. Pidd, Phys. Rev. 73, 1215 (1948).

Q5. Electrostatic Interaction in d.c. Discharges in Gases.* JULIUS H. CAHN,** *Yale University.****—The problem of electrostatic interaction in space-charge neutralized d.c. discharges has been dealt with by the classical methods of the Boltzmann transport equation. This work has been made possible following the work of Landau[1] in which the assumption was made that in the majority of electron-electron collisions a very small fraction of momentum is exchanged. The electronic velocity distribution function thus obtained has been examined for two specific electron-molecule cross sections for momentum transfer. In one, the cross section is assumed inversely proportional

to the electronic velocity. This leads to a Maxwellian velocity distribution which is independent of electron density until such densities are reached that the ions become important. In the other case, the cross section is assumed independent of the electronic energy, and the transition can then be shown from the Davydov to the Maxwellian distribution as the electron density increases.

* Part of a dissertation presented to the Faculty of the Graduate School of Yale University, in fulfillment of the requirements for the degree of Doctor of Philosophy.
** Now at the University of Nebraska, Lincoln, Nebraska.
*** This work was assisted by ONR.
[1] E. Landau, Physik Zeits. Sowjetunion, 10, 154 (1936).

Q6. The Effects of Various Barium Compounds with Respect to Cold Cathode Behavior as a Function of Life in a Glow Discharge.* HAROLD JACOBS AND ARMAND P. LAROCQUE, *Sylvania Electric Products, Inc.*—The effects of various barium compounds in glow discharge tubes are determined and compared with those of barium metal. The various barium compounds are shown to require different activation schedules in order to obtain the lowest initial regulation voltage. The regulating voltage, as a function of time, is determined for all the cathode surfaces. The composite surfaces are found to have greater stability than the metallic surface over a long period of time. The composite barium surfaces are shown to reach an asymptotic limit in their respective regulating voltages with these values being of the same order of magnitude as the original regulating voltage of the metallic barium surface.

* This work was undertaken in association with the Applied Physics Laboratory of the Johns Hopkins University and sponsored by the Bureau of Ordnance, U. S. Navy.

Q7. Oxide Cathode Interface and Coating Voltages.* A. EISENSTEIN AND J. R. YOUNG, *University of Missouri.*—A d.c. retarding potential method has been developed for determining the voltage drop across the oxide cathode interface and coating, V_{ic}, when emission current is drawn. This technique is similar to a pulse method previously used and involves a measurement of the energy of electrons arriving at the anode having fallen through the potential drop between the coating surface and the anode. Under d.c. emission conditions V_{ic} is of the same order of magnitude as the contact potential, c.p. The latter is determined and extracted from the measured voltage by extrapolating a plot of (V_{ic}+c.p.) *vs.* anode current to zero current. Over the range 950–1250°K the interfaceless cathode, (BaSr)O on pure nickel, shows a linear variation of V_{ic} with current which is interpreted as a coating voltage only. Coating conductivity values obtained from the slope are in agreement with previous measurements made using probes. The difference between the work function obtained from a Richardson plot and the conductivity activation energy indicates an electron affinity of 0.3ev. Similar d.c. measurements on the Ba_2SiO_4 interface cathode shows a non-linear variation of V_{ic} with anode current at low temperatures and a considerably higher total interface and coating voltage.

* This work was supported in part by ONR.

Q8. The Production of Free Alkaline Earth Metal in Simple Vacuum Tube Filaments. GEORGE E. MOORE, H. W. ALLISON, AND JAMES MORRISON, *Bell Telephone Laboratories.*—The production of free alkaline earth metal through reduction of the oxide in contact with tungsten was measured by two independent methods. The first method consists in exposing the experimental tube to water vapor and measuring the hydrogen evolved when the water vapor is decomposed by the metal, such as Sr. In the second method, the total Sr evaporated from a SrO coated tungsten filament is compared with that evaporated from a similar platinum filament, assuming that only SrO evaporates from the platinum. The use of radioactive isotopes made the second method practical. The results by both methods agree and indicate that approximately 100 atoms of Sr metal leave a tungsten support for every SrO molecule. The rate of reaction is apparently not limited by interphase diffusion. The observed reduction of MgO agrees with the rate computed by thermodynamics and kinetic theory. The agreement is less satisfactory for the reduction of SrO, probably because of uncertainty in the published data used for computation. The methods seem applicable to other reactions now being investigated between pure alkaline earth oxides and pure metallic supports. Photoelectric observations were employed to maintain constant reaction temperatures.

Q9. Electrical Phenomena Resulting from the Freezing of Dilute Aqueous Solutions. E. J. WORKMAN AND S. E. REYNOLDS,* *New Mexico School of Mines.*—Observations on the electrical potential and charge generated during the freezing of dilute aqueous solutions have been extended.[1] Solutions of a variety of chemical substances in concentrations from 10^{-6} to 10^{-3} normal have been frozen in bulk by contact with a refrigerating surface at about −15°C. The compounds used exemplify known types of chemical bonds. The electrical potential of the growing ice mass with respect to the remaining liquid ranged from −34 volts with CsF (3×10^{-5} normal) to +190 volts with relatively dilute NH_4OH (approximately 5×10^{-6} normal). Electrical charges in excess of 4×10^5 c.g.s. units per ccm frozen were observed in the case of NaF. In the series NaF, Cl, Br, and I the charge developed was progressively less corresponding to the decrease in degree of ionic bonding. Observed differences of potential between the growing ice and the liquid as a function of concentration in the case of very dilute solutions of NH_4OH suggest this effect as a possible method of detection and analysis.

* Supported by War Department Signal Corps.
[1] E. J. Workman and S. E. Reynolds, Phys. Rev. 74, 709 (1948).

Q10. Electrical Charge Separation Produced by Rapid Freezing of Rainwater. S. E. REYNOLDS AND E. J. WORKMAN,* *New Mexico School of Mines.*—The generation of electrical potential differences and relatively large charge separations as caused by rapid freezing of slightly contaminated water, has been suggested as a mechanism for the generation of thunderstorm electricity.[1] This subject has been further studied in the laboratory by freezing

numerous samples of rainwater collected at an elevation near the zero isotherm in actual thunderstorms. Also, samples of rainwater collected at the surface of the ground (5000 ft. and 10,000 ft. elevation) have been studied for contamination and electrical properties. The electrical conductivity of precipitation forms collected at the zero isotherm and measured without appreciable warming was approximately 10^5 ohm cm. Subsequent laboratory investigations on conductivity and freezing indicate that the application of this freezing effect to thunderstorm electricity may depend upon a sensitive but naturally controlled balance to contaminants including $CaCO_3$ and CO_2, the latter playing the additional role of holding Ca in solution as $Ca(HCO_3)_2$.

[1] E. J. Workman and S. E. Reynolds, Phys. Rev. **74**, 709 (1948).
* Supported by War Department Signal Corps.

Q11. Specificity of Interaction between Pairs of Identical Large Molecules.* HERBERT JEHLE, *University of Pennsylvania.*—In self-duplication of genes the original gene selects from the surrounding medium those macromolecules which happen to be identical with the macromolecules which constitute the gene. The accuracy of selection through generations and the versatility of this phenomenon working for all kinds of genes makes this problem interesting. Genes are built of nucleoproteins which from x-ray analysis are known to be rigid. Most of the thermal vibrations of the macromolecules can be treated classically. They are anharmonic which means that those "modes" of a molecule which have approximately commensurable frequencies will have a strong statistical preference for phase-related vibrations (synchronized, i.e., librational motion in subharmonic resonance). A pair of macromolecules will interact through their electric dipole and higher moments which accompany the thermal (paticularly the low frequency) vibrations. Phase relations in between the "modes" of each individual molecule have as a consequence that if the pair of fundamental "modes" of a pair of *identical* molecules are inphase, then also the pairs of other "modes" are mostly inphase. So the cumulative effect of coupling between the various pairs of thermally excited "modes" can become of the order of kT even while the two molecules are a considerable distance apart.

* Work done at the Institute for Advanced Study and at the Eldridge W. Johnson Foundation.

SUPPLEMENTARY PROGRAMME

SP1. Magnetic Scattering of Elementary Nucleons. JOSEPH W. WEINBERG, *University of Minnesota.**—Cross sections for electromagnetic *nn*, *np*, and *pp* scattering have been obtained following Møller's treatment[1] for the Dirac electron. Pauli corrections to the Dirac equation have been applied to describe magnetic interactions according to the phenomenological theory of fixed anomalous moments.[2] Though magnetic scattering increases rapidly with energy, the reaction upon internal meson currents that normally sustain anomalous nuclear moments would tend to limit magnetic forces as the meson production threshold is approached. Without a detailed mesonuclear theory, one must therefore confine predictions here to non-relativistic laboratory energies below 200 Mev. In the laboratory system, T = kinetic energy in units of Mc^2, θ = scattering angle, $g_p = 2.79$, $g_n = -1.91$, the gyromagnetic ratios

$$d\sigma_{pp}/d\Omega = [(e^2/Mc^2)^2(1+3T/2)/(T^2\sin^2\theta\cos\theta)] \times [\tan^2\theta + \cot^2\theta - 1 + (T/2) \times (\tan^2\theta - \cot^2\theta) + T g_p(g_p-1)];$$

$$d\sigma_{np}/d\Omega = [g_n^2(e^2/Mc^2)^2/16][\tan^2\theta/2 + \cot^2\theta/2 - 1 + 2g_p^2];$$

$$\sigma_{nn} = (5\pi/2)g_n^4(e^2/Mc^2)^2.$$

In $d\sigma_{pp}/d\Omega$, powers of T beyond the first have been neglected, and the new contribution given by the last term of the second bracket appears as part of the relativistic correction. It amounts to about 10 percent of the cross section at 15° and 200 Mev. In $d\sigma_{np}/d\Omega$ and σ_{nn} all relativistic effects have been dropped; for, except at small angles in the former, both cross sections are only of the order of microbarns.

* To be given after Session B if time permits.
[1] C. Møller, Ann. d. Physik **14**, 568 (1932).
[2] J. W. Weinberg, Bull. Am. Phys. Soc. **23**, No. 3 (1948).

SP2. The Masses of the Mesons. ENOS E. WITMER, *University of Pennsylvania.**—The writer[1] has presented evidence in support of the idea that the masses of all nuclei (or at least all stable nuclei) are integral multiples of a natural unit of mass designated the *prout*. The prout is defined to be the nuclear mass of O^{16} divided by 82012. The mass of the proton is 6×861 prouts. The number 861 is an important number in the writer's scheme. Although the masses of the mesons cannot be fitted into this scheme with any certainty as yet, the measured mass of the π mesons is close enough to 861 prouts to lead me to believe it is 861 prouts exactly. The masses of still heavier mesons which have supposedly been observed lead me to suggest that there are positive and negative mesons of masses 861 n, where n is any integer from one to five, possibly also six in the care of negative mesons. The measurements of the μ mesons suggest a mass of 574 prouts, one-ninth the proton mass. Nothing can be said about the neutral mesons or other positive and negative mesons yet.

* To be given after Session M if time permits.
[1] Enos E. Witmer, Proc. Nat. Acad. Sci. **32**, 283 (1946).

SP3. Difference in the *E–W* Asymmetry of the Hard Component of the Cosmic Radiation for Particles of Opposite Charge.* GERHART GROETZINGER AND GORDON W. MCCLURE, *University of Chicago.***—Two telescopes, each having a magnetic deflecting system selecting mesons of either charge with energies around 500 Mev, were used on the summit of Mt. Evans to determine the *E–W* asymmetry at a zenith angle of 24°. A small asymmetry of the total hard component has been observed there previously, which can be ascribed to the deflection of the mesons produced with a positive excess from isotropic primaries. Our experiment gave a difference of 18±7 percent for the asymmetries for each charge, which is consistent with the above assumption.[1] The positive excess was found to be 22±4 percent. A smaller difference in the asymmetry and a smaller positive excess seems to occur for mesons stopped and producing decay electrons in a carbon plate after leaving the telescopes. The described arrangement could at lower latitudes be used to check on the existence of negative meson producing primaries.

* This research was supported in part by the Office of Naval Research.
** To be given after Session M if time permits.
[1] Thomas H. Johnson, Phys. Rev. 59, 11 (1941).

SP4. Magnetic Moments of Sunspots. JAMES W. BROXON, *University of Colorado.*—Simple approximate representations of the magnetic fields of sunspots by dipoles or ring currents are considered, and expressions deduced for the magnetic moment of a sunspot in terms of its area and its maximum central magnetic field strength. These are extended to include sunspot groups, and a function ($SS-MM$) is defined as the arithmetic sum of the equivalent moments of all visible groups. Statistical treatment of Chree's method of superposed epochs provides some indication of a 27-day interval between recurrences of fluctuations in $SS-MM$. This work was supported in part by the Office of Naval Research.

TO BE READ BY TITLE

T1. Nuclear Magnetic Moments as Integral Multiples of a Natural Unit. ENOS E. WITMER, *University of Pennsylvania.*—The ratios of the g values of a number of nuclei to the g value of the proton have now been measured with great accuracy. Among these are the neutron and the nuclei of H^2, H^3, C^{13}, F^{19}, and Tl^{205}. The results for all these nuclei appear to support the conclusion that the magnetic moments of nuclei are integral multiples of $\mu_N/672$, where μ_N is the nuclear magneton. The magnetic moment of the proton is assumed to be 1876 of these units. The corresponding numbers for the neutron and other nuclei are 1285, 576, 2001, 472, 1766, and 1095 in the order given in the second sentence. These results are in accord with a previous statement by the writer.[1]

[1] Enos E. Witmer, Phys. Rev. 73, 1243(A) (1948). See also Enos. E. Witmer, Proc. Nat. Acad. Sci. 32, 283, (1946).

Author Index to Contributed Papers Presented at the Chicago Meeting.

Alexander, Ben H.—No. P2
Allen, K. W. and J. T. Dewan—No. J10
Alpher, R. A., R. C. Herman, and G. A. Gamow—No. B9
Andrews, C. L.—No. Q1
Band, William—No. K7
Barschall, H. H. and R. F. Taschek—No. N3
Beach, Louis A., Charles L. Peacock, and Roger G. Wilkinson—No. A10
Beck, Carl A.—No. C8
Belinfante, Frederik J.—No. K1
Berger, Martin and Gerhart Groetzinger—No. N4
Blatt, J. M. and J. D. Jackson—No. N1
Bockelman, C. K., R. K. Adair, H. H. Barschall, and O. Sala—No. J5
Borst, Lyle B.—No. B2
Broxon, James W.—No. M11, SP4
Cahn, Julius H.—No. Q5
Carney, Rose A. and Forrest F. Cleveland—No. C4
Claassen, R. S. and R. W. Boom—No. B5
Clark, Harold E.—No. C9
Clark, R. K. and G. Failla—No. A1
Cleveland, Forrest F., K. W. Greenlee, and E. E. Bell—No. C5
Coryell, C. D., L. E. Glendenin, and R. R. Edwards—No. J11
Dancoff, S. M. and S. D. Drell—No. N2
Drell, S. D.—No. K4
Eisenstein, A. and J. R. Young—No. Q7
Ellis, Cecil B.—No. B1
Fahy, E. F. and Marcel Schein—No. M5
Feenberg, Eugene and Kenyon C. Hammack—No. B11
Feldman, David and Julian Schwinger—No. K2
Feshbach, H. and V. F. Weisskopf—No. N7
Floyd, J. J., C. D. Coryell, and L. B. Borst—No. A5
Freier, George, Eugene Lampi, W. Sleator, and J. H. Williams—No. N6
Freier, P. S., E. J. Lofgren, E. P. Ney, and F. Oppenheimer—No. M4
French, J. B. and V. F. Weisskopf—No. K3
Gideon, D. N., W. C. Miller, and B. Waldman—No. A8
Glendenin, L. E.—No. J12
Goldhaber, Gerson—No. J6
Green, Alex E. S.—No. B12
Groetzinger, Gerhart and Gordon W. McClure—No. SP3
——**Fred Ribe, and Lloyd Smith**—No. N5
Hafner, E. M., W. F. Donoghue, and H. Snyder—No. B6
Halpern, Otto—No. N9
Hanna, G. C., B. Pontecorvo, and D. H. W. Kirkwood—No. B4
Harkins, William D. and Martin Popelka, Jr.—No. B10
Heller, W. and W. Wojtowicz—No. P1
Herring, Conyers—No. P4
Hincks, E. P. and B. Pontecorvo—No. M9
Hughes, D. J., M. T. Burgy, R. B. Heller, and J. W. Wallace—No. P3
Hunter, G. T. and H. T. Richards—No. J1
Hutner, R. A., E. S. Rittner, and F. K. du Pré—No. P10
Jacobs, Harold and Armand P. LaRocque—No. Q6
Jehle, Herbert—No. Q11
Kerst, D. W., G. D. Adams, H. W. Koch, and C. S. Robinson—No. B3
Kreusch, E., J. S. Ziomek, and Forrest F. Cleveland—No. C7
Krone, R. W., S. S. Hanna, and D. R. Inglis—No. J3
Kuczynski, G. C.—No. P7
Kundu, D. N. and M. L. Pool—No. J8
Kurbatov, D. and Donald Gideon—No. A6
Langer, Lawrence M.—No. A2
Leaf, Boris—No. K8
Longini, R. L.—No. C10
Longmire, C. and H. Brown—No. A3
Lord, Jere J. and Marcel Schein—No. M8
Madansky, Leon and R. W. Pidd—No. Q4
McClure, Gordon W. and Gerhart Groetzinger—No. M7
Mandeville, C. E., M. V. Scherb, and W. B. Keighton—No. A9
Meister, Arnold G.—No. C2
Miller, Edward E.—No. C11
Miller, Walter C. and Bernard Waldman—No. A7
Moore, George E., H. W. Allison, and James Morrison—No. Q8
Nelson, Edward B. and John E. Nafe—No. N10
Ney, E. P., P. Freier, E. J. Lofgren, and F. Oppenheimer—No. M3
Nier, Alfred O., T. R. Roberts, and E. G. Franklin—No. Q2
Osborne, M. F. M.—No. K6
Peacock, Charles L. and Roger G. Wilkinson—No. 11
Pearson, G. L., J. D. Struthers, and H. C. Theuerer—No. P6
Pool, M. L. and D. N. Kundu—No. J9
Reynolds, S. E. and E. J. Workman—No. Q10
Richards, H. T. and R. V. Smith—No. J7
Richards, J., J. Brown, F. Felber, and D. Saxon—No. B7
Rieke, F. F. and Daryl Errett—No. Q3
Rittner, E. S., R. A. Hutner, and F. K. du Pré—No. P9
Rosser, Shirley E. and Forrest F. Cleveland—No. C1
Saxon, D. and R. Heller—No. A12
Schein, Marcel, Victor H. Yngve, and Theodore Bowen—No. M2
Schulz, L. G.—No. P8
Shaw, A. E.—No. B8
Sherr, R., H. R. Muether, and M. G. White—No. A4
Shoupp, W. E., B. Jennings, W. Jones, and M. Garbuny—No. J4
Sitte, K.—No. M6
Smith, R. V. and H. T. Richards—No. J2
Smoluchowski, R. and T. L. Wu—No. P13
Symon, K. R.—No. B13
Taft, E. and L. Apker—No. P5
Weinberg, Joseph W.—No. K5, SP1
Wheley, R. M. and V. A. Long—No. M10
Witmer, Enos E.—No. SP2, T1
Wolfenstein, Lincoln—No. N8
Workman, E. J. and S. E. Reynolds—No. Q9
Wu, T. L. and R. Smoluchowski—No. P12
Yagoda, Herman and Nathan Kaplan—No. M1
Zeitlow, James P., Forrest F. Cleveland, and Arnold G. Meister—No. C3
Zener, Clarence—No. P11
Ziomek, Joseph S. and Forrest F. Cleveland—No. C6

CONTENTS

THE PHYSICAL REVIEW SECOND SERIES, VOL. 75, NO. 2 JANUARY 15, 1949

Effect of Crystal Orientation on the Scattering of Slow Neutrons . . . . . G. P. ARNOLD, V. W. MYERS, AND A. H. WEBER 217

Radiations from Cd^{115}, In^{115}, and Hf^{175} . . . . . C. E. MANDEVILLE, M. V. SCHEER, AND W. B. KEIGHTON 221

Radiations from Hf^{181} . . . . . K. Y. CHU AND M. L. WIEDENBECK 226

Evidence for a New Isotope of Potassium . . . . . ROY OVERSTREET, LOUIS JACOBSON, AND P. R. STOUT 231

Space Charge Effects in Bombardment Conductivity through Diamond . ROBERT R. NEWTON 234

Absolute Voltage Determination of Three Nuclear Reactions . . . . . R. G. HERB, S. C. SNOWDON, AND O. SALA 240

Microwave Spectroscopy in the Region of Three to Five Millimeters . . . . . ALEX G. SMITH, WALTER GORDY, JAMES W. SIMMONS, AND WILLIAM V. SMITH 248

Screening and Relativistic Effects on Beta-Spectra . . . . . C. LONGMIRE AND H. BROWN 254

Rotational Absorption Spectrum of OCS . . . . . M. W. P. STRANDBERG, T. WENTINK, JR., AND R. L. KYHL 270

Grain Density in Photographic Tracks of Heavy Particles . . . . . M. BLAU 279

Radioactivity of C^{10} and O^{14} . . . . . R. SHERR, H. R. MUETHER, AND M. G. WHITE 282

Electronic Interaction in Electrical Discharges in Gases . . . . . JULIUS H. CHEM 293

Remarks on the Determination of a Central Field of Force from the Elastic Scattering Phase Shifts . . . . . V. BARGMANN 301

Condensation of Pure He^3 and Its Vapor Pressures between 1.2° and Its Critical Point . . . . . S. G. SYDORIAK, E. R. GRILLY, AND E. F. HAMMEL 303

On the Experimental Value of the Fine Structure Constant . H. A. BETHE AND C. LONGMIRE 309

Letters to the Editor:

On the Mesic Charge . . . . . TAIZUKE OKAYASHA 308
Note on Dirac's Theory of Magnetic Poles . . . . . H. A. WILSON 309
Magnetic Moments of the Neutron and Proton . . . . . J. M. LUTTINGER 309
Interpretation of Dependence of Resistivity of Germanium on Electric Field . . . . . E. J. RYDER AND W. SHOCKLEY 310
Influence of Order on the Saturation Magnetic Moment . . J. E. GOLDMAN AND R. SMOLUCHOWSKI 310
Multiple Scattering with Energy Loss . . . . . LESLIE L. FOLDY 311
On the Definition of the "Effective Range" of Nuclear Forces . . F. C. BARKER AND R. E. PEIERLS 313
Mass Spectrographic Assignment of Rubidium Isotopes . . . . . FREDERICK L. REYNDERS, D. G. KARRAKER, AND D. H. TEMPLETON 313
Three Additional Collateral Alpha-Decay Chains . W. W. MEINKE, A. GHIORSO, AND G. T. SEABORG 314
Correction and Addendum: Scattering of Particles by the Gas in a Synchrotron . . . . . NELSON M. BLACHMAN AND ERNEST D. COURANT 315
Beta-Ray Spectra of Cu^{64} . . . . . C. S. WU AND R. D. ALBERT 315
Additional Ferromagnetic Resonance Absorption Measurements on Supermalloy . . W. A. YAGER 316
Ferromagnetic Resonance Absorption in Heusler Alloy . . . . W. A. YAGER AND F. R. MERRITT 316
Disintegration of Hg^{203} . . . . . HILDING SLÄTIS AND KAI SIEGBAHN 316
Single Crystal Growth of Selenium . . . . . S. BERGLUND, L. R. JOHNSON, AND O. IRENE 320
Nuclear Shell Structure and Ionization . . . . . EUGENE FEENBERG 320
Comparison of Atmospheric Methane Content above Flagstaff, Arizona, and Columbus, Ohio . . . . . ARTHUR ADEL 322
Isotopic Constitution of Ytterbium . . . . . RICHARD J. HAYDEN, DAVID C. HESS, JR., AND MARK G. INGHRAM 322
Measurement of the Half-Life of Double Beta-Decay from $a^{50}n^{124}$ . . . . . E. L. FIREMAN 323
Internal Conversion Electrons from Metastable Te^{125} . . . . . R. D. HILL, G. SCHARFF-GOLDHABER, AND G. FRIEDLANDER 324

Proceedings of the American Physical Society:

Minutes of the Meeting at Chicago on November 26–27, 1948 325

LANCASTER PRESS, INC., LANCASTER, PA.